Novel nanocomposite forward osmosis membranes for treating highly saline and oily wastewater with low fouling, high water flux and high selectivity

Qin, Detao

2016

Qin, D. (2016). Novel nanocomposite forward osmosis membranes for treating highly saline and oily wastewater with low fouling, high water flux and high selectivity. Doctoral thesis, Nanyang Technological University, Singapore.

http://hdl.handle.net/10356/68799

https://doi.org/10.32657/10356/68799

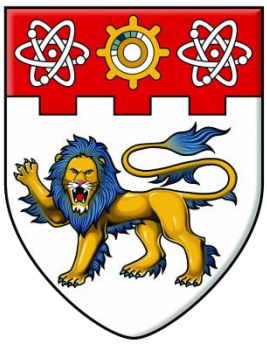

NANYANG TECHNOLOGICAL UNIVERSITY

NOVEL NANOCOMPOSITE FORWARD OSMOSIS MEMBRANES FOR TREATING HIGHLY SALINE AND OILY WASTEWATER WITH LOW FOULING, HIGH WATER FLUX AND HIGH SELECTIVITY

QIN DETAO

INTERDISCIPLINARY GRADUATE SCHOOL

ENERGY RESEARCH INSTITUTE @ NTU (ERI@N)

2016

NOVEL NANOCOMPOSITE FORWARD OSMOSIS MEMBRANES FOR TREATING HIGHLY SALINE AND OILY WASTEWATER WITH LOW FOULING, HIGH WATER FLUX AND HIGH SELECTIVITY

QIN DETAO

Interdisciplinary Graduate School

Energy Research Institute @ NTU (ERI@N)

A thesis submitted to the Nanyang Technological University in partial fulfillment of the requirement for the degree of Doctor of Philosophy

2016

ACKNOWLEDGEMENTS

Foremost, I would like to express my deepest gratitude to my main supervisor Associate Professor Darren Delai Sun for his wise guidance, whole-hearted support, and ever-lasting amiability. I have always held Prof. Sun in high esteem as the most important leader throughout my Ph.D. journey. Prof. Sun tirelessly imparts me not only the great ideas of research but also the valuable philosophy about life. Prof. Sun would like to utilize his foresighted vision to help his students grasp the significant direction on research. Particularly, he puts a lot of efforts in training me to become a good writer, speaker, researcher, and time-manager in professional filed. Every time I meet any difficulty, Prof. Sun can direct me to view that difficulty in a positive way. It's Prof. Sun's highly informative instructions and energetic encouragements that support me to persevere in my studies. Meanwhile, Prof. Sun takes his students really as friends. He always maintains a kind and approachable style to his students, bridging the gap between students and teachers through his good communication. I cannot forget the active time Prof. Sun shares his own experiences with me and other students in the lab and office. In short, it's my highest honor to conduct the Ph.D. study under Prof. Sun.

Furthermore, I would like to sincerely thank my co-supervisor Dr. Liu Zhaoyang. Dr. Liu is an inspired scientist who always imparts many valuable research ideas to me. Dr. Liu's dedication into science greatly encourages me to become a conscientious researcher. He gives me professional instructions on research design, experimental work, and paper writing. His wisdom guides me to explore the most important directions of my research and summarize the most significant outcomes for publication. More importantly, he enthusiastically teaches me the way to improve the quality of my research article. Besides, he also takes me truly as a friend. He would like to discuss with me in the fullest detail and listen patiently to my voice. I will always cherish the time I work under his guide in the lab to strive together for our research goals.

Meanwhile, I deeply appreciate the warm-hearted assistances from my group members. Particularly, I would like to thank my mentor Dr. Bai Hongwei for his informative advice and suggestions. I am also grateful for Dr. Song Xiaoxiao's enthusiastic assistance to my lab work. Additionally, Dr. Tai Minghang, Dr. Lee Siewsiang, Dr. Gao

Peng and other group members give me lots of help. I treasure the contributions from every member of our group to the creation of a friendly and helpful study environment. I wish we will be a family forever that shares our feelings and opinions in research and daily life.

I also would like to express my sincere gratitude to my research institute ERI@N and my school IGS for providing me the full Ph.D. scholarship. My joining in IGS-ERI@N is really a life fortune to me, for I have met and made many friends from other disciplines. IGS-ERI@N not only broadens my scope but also makes my Ph.D. journey colorful. Particularly, I would like to thank school staffs Ms. Lim Seok Kim Lily and Ms. Heng Yuxuan Ellen for their excellent managements that greatly facilitate my study.

In addition, I am grateful to the assistances from Ms. Lim-Tay Chew Wang, Mr. Tan Han Khiang, Ms. Chong Ai Shing Maria, Mr. Ong Chee Yung, Ms. See Shen Yen Pearlyn and other Environmental Lab staffs of CEE school. They help me to acquire the skills on the operation of many advanced instruments for chemical analysis. Besides, they are always willing to share their knowledge on technical details to me.

Finally, the encouragements and supports from my family members and my girlfriend motivate me to move forward. I would like to dedicate this achievement to all of them.

ABSTRACT

This study focuses on the design and synthesis of a new nanocomposite forward osmosis (FO) membrane that is able to separate highly saline and oily wastewater with low fouling, high water flux and high selectivity, in order to battle against global freshwater scarcity. A new design rationale of FO membrane is developed, which highlights that a genuine FO membrane must possess high antifouling capability as the requisite besides high water flux and high selectivity. Guided by this rationale, as-designed new nanocomposite FO membrane consists of a novel antifouling selective layer on top of a three-dimensionally (3D) interconnected porous support layer. Particularly, graphene oxide (GO) nanosheets assisted phase inversion technology is developed to fabricate the 3D interconnected porous support layer, on top of which dip-coating technique is employed to further construct the hydrogel selective layer in ultrathin thickness (~100 nm).

The structures and properties of hydrogel selective layer are finely tuned towards both high antifouling capability and high selectivity, wherein the key role of chemical crosslinking is revealed. The best crosslinking agent is identified as glutaraldehyde; the optimum molecular weight of hydrogel is found to be 93 kDa; the optimum concentration of hydrogel solution is 0.25 wt%; the optimum coating time is 20 min; and more importantly, the optimum crosslinking degree is determined as 30%. Based upon all these optimized results, as-synthesized hydrogel FO membrane even with conventional phase inversion constructed support layer can already demonstrate the evident advantages in high selectivity and high antifouling capability, with its water flux/reverse salt flux ratio (J_W/J_S) 2.4 times higher than that of commercial HTI FO membrane (cellulose triacetate, woven).

Furthermore, the support layer is optimized through introducing GO nanosheets to finely adjust the phase inversion process. Here, support layer in highly interconnected porous structure is the key to minimize FO's intrinsic limitation on water flux *i.e.* internal concentration polarization (ICP) problem. For the first time, hydrophilic 2D graphitic nanomaterial is demonstrated able to transform the interior pore structure of the support layer from 1D connected to 3D interconnected. Based upon systematic

optimization of GO assisted phase inversion process, an entirely new support layer structure with its interior pores highly interconnected in all three dimensions at micrometer scale is created. The formation mechanism of this 3D interconnected porous support layer is attributed to GO induced viscosity difference. Compared with conventional 1D pore connected support layer, this 3D pore interconnected support layer can reduce FO membrane structural parameter (S) by as much as 41.4%, leading to the enhancement in FO water flux (J_W) by 72%. Meanwhile, the J_W of as-synthesized nanocomposite membrane arrives at 30.5 L m^{-2} h^{-1} at FO mode with draw solution of 1.5 M Na_2SO_4, which is 3.1 times higher than that of HTI membrane under identical operational conditions. Therefore, for the first time, micrometer-scale 3D interconnected porous support layer that is able to break the ICP bottleneck and thus achieve high FO water flux is successfully synthesized with dominant membrane manufacture process (*i.e.* phase inversion).

Most importantly, as-synthesized nanocomposite FO membrane is systematically investigated for its ability to accomplish simultaneous desalination and oil/water separation of highly saline and oily wastewater. FO separation results indicate that this nanocomposite membrane can simultaneously desalinate and deoil hypersaline oil-in-water emulsion with more than three times higher water flux, higher removal efficiencies of both oil and salts (>99.9% for oil and >99.7% for multivalent salt ions), and significantly lower membrane fouling (>80% lower water flux reduction ratio) compared with HTI membrane. The further operation results reveal that this new FO membrane is remarkably superior to HTI membrane in both resistance to salinity induced fouling aggravation and long term antifouling durability.

In summary, this is the first study that explores and optimizes the capability of hydrogel macromolecule as a new selective layer for FO membrane. Furthermore, it creates a micrometer-scale 3D interconnected porous nanocomposite support layer to break ICP bottleneck with dominant membrane manufacture process (*i.e.* phase inversion). Moreover, it also achieves simultaneous desalination and oil/water separation of highly saline and oily wastewater by as-synthesized new FO membrane with low fouling, high water flux and high selectivity. This study points out a new direction for the development of genuine FO membrane and makes a significant

impetus to the industrialization of FO technology in order to address global freshwater scarcity.

LIST OF PUBLICATIONS

Journals

1. **Qin, D.T.**, Liu, Z.Y., Sun, D.D., Song, X.X. and Bai, H.W. (2015). "A new nanocomposite forward osmosis membrane custom-designed for treating shale gas wastewater", Scientific Reports, **5**, 14530.

2. **Qin, D.T.**, Liu, Z.Y., Bai, H.W., Sun, D.D. and Song, X.X. (2016). "A new nano-engineered hierarchical membrane for concurrent removal of surfactant and oil from oil-in-water nanoemulsion", Scientific Reports, **6**, 24365.

3. **Qin, D.T.**, Liu, Z.Y., Zhang, J. and Sun, D.D. (2016). "A new approach for fabricating composite FO membranes towards low fouling, high selectivity and high permeability for water treatment", Desalination, (***Under review***).

4. **Qin, D.T.**, Liu, Z.Y., Bai, H.W. and Sun, D.D. (2016) "From 1D to 3D: the key role of graphene oxide nanosheets in minimizing internal concentration polarization towards high water flux forward osmosis membranes", (***Submitted***).

5. **Qin, D.T.**, Liu, Z.Y., Bai, H.W. and Sun, D.D. (2016) "A highly antifouling forward osmosis membrane with hydrogel selective layer", (***In preparation***).

Conferences

1. Tan, B.Z., **Qin, D.T.**, Tai, M.H., Sun, D.D. and Liu, Z.Y. "Ultra high flux oil-water separation using anti-fouling electrospun polyvinyl alcohol nanofibers", IWA Water and Industry 2015 Conference on innovation and solutions for industrial water and wastewater, Vasteras, Sweden, 18-20 June 2015. (**Best Paper Award**).

2. Liu, Z.Y., **Qin, D.T.** and Sun, D.D. "Synthesis of new thin film composite forward osmosis membrane for improved fouling resistance", 2nd International conference on desalination using membrane technology, Singapore, 26-29 July 2015.

3. **Qin, D.T.**, Liu, Z.Y. and Sun, D.D. "A new nanocomposite membrane for separating oil-in-water nanoemulsion with low fouling and high flux", 15th Network Young Membrains, Aachen, Germany, 04-05 September 2015.

4. **Qin, D.T.**, Liu, Z.Y. and Sun, D.D. "A novel nanocomposite ultrafiltration membrane for highly efficient separation of nanosized oil-in-water emulsions", Euromembrane 2015, Aachen, Germany, 06-10 September 2015.

5. Liu, Z.Y., **Qin, D.T.** and Sun, D.D. "New generation of nanocomposite forward osmosis membrane for concurrent oil and salt removals", Euromembrane 2015, Aachen, Germany, 06-10 September 2015.

TABLE OF CONTENTS

LIST OF FIGURES

LIST OF TABLES

LIST OF SYMBOLS

Symbol	***Description***
A	Water permeability of FO membrane (L m^{-2} h^{-1} bar^{-1})
A_m	Effective membrane area (m^2)
B	Salt permeability of FO membrane (L m^{-2} h^{-1})
C	Molar concentration of draw solute in draw solution (mole L^{-1})
C_{FS}	Molar concentration of draw solute in feed solution (mole L^{-1})
D	Diffusion coefficient of draw solute (m^2 s^{-1})
d_p	Membrane or support layer pore diameter (nm)
FRR	Average flux reduction ratio (%)
FRR_f	Average flux reduction ratios of "oil-fouling stage" (%)
FRR_c	Average flux reduction ratios of "post-cleaning stage" (%)
J_S	FO reverse salt flux (g m^{-2} h^{-1})
J_W	FO water flux (L m^{-2} h^{-1})
J_W/J_S	The ratio of FO water flux to reverse salt flux (L g^{-1})
K	Solute resistivity of FO membrane (s m^{-1})
k	Mass transfer coefficient (L m^{-2} h^{-1})
l	FO membrane thickness (m)
m_{DS}	Mass of draw solution (g)
M_W	Weight averaged molecular weight (g $mole^{-1}$)
R	Rejection of draw solute by FO membrane under RO mode (%)
R_a	Average roughness of membrane or support layer surface (nm)
$Removal$	Removal ratio of oil and salt by membrane under FO process (%)
R_g	Universal gas constant (8.314 Joule mol^{-1} K^{-1})
R_q	Root-mean-square roughness of membrane or support layer surface (nm)
S	FO membrane structure parameter (m)
T	thermodynamic temperature (K)
$TCLD$	Theoretical crosslinking degree (dimensionless, %)
V_{DS}	Volume of draw solution (L)
W	Power density of PRO process (watt m^{-2})
β	van't Hoff factor (dimensionless)

ΔP	Transmembrane hydrostatic pressure difference (bar)
Δt	Time interval (min)
$\Delta\pi$	Osmotic pressure difference (bar)
$\Delta\pi_{bulk}$	Osmotic pressure difference between draw solution and feed solution bulks (bar)
$\Delta\pi_{eff}$	Osmotic pressure difference across the selective layer of FO membrane (bar)
$\Delta\pi_m$	Osmotic pressure difference across FO membrane (bar)
ε	FO membrane porosity (dimensionless, %)
π	Osmotic pressure (bar)
$\pi_{D,b}$	Osmotic pressure of draw solution bulk (bar)
$\pi_{D,eff}$	Osmotic pressure of draw solution at the interface between support layer and selective layer (bar)
$\pi_{D,m}$	Osmotic pressure of draw solution at membrane surface (bar)
$\pi_{F,b}$	Osmotic pressure of feed solution bulk (bar)
$\pi_{F,m}$	Osmotic pressure of feed solution at membrane surface (bar)
ρ	Density of feed solution (kg m^{-3})
σ	Membrane reflection coefficient (dimensionless, $0 \leq \sigma \leq 1$)
τ	FO membrane tortuosity (dimensionless)

LIST OF ABBREVIATIONS

Abbreviation	*Description*
AFM	Atomic force microscopy
ATR-FTIR	Attenuated total reflection-Fourier transform infrared spectroscopy
AFO	Pressure assisted forward osmosis
BSA	Bovine serum albumin
CEOP	Cake enhanced osmotic pressure
CP	Concentration polarization
CTA	Cellulose triacetate
DI	Deionized
DLS	Dynamic light scattering
DMAc	*N*,*N*-Dimethylacetamide
DMF	*N*,*N*-dimethylformamide
ECP	External concentration polarization
EDX	Energy dispersive x-ray spectroscopy
FESEM	Field emission scanning electron microscopy
FO	Forward osmosis
FO mode	Membrane orientation of selective layer facing feed solution
GO	Graphene oxide
GO\P	GO assisted phase inversion constructed nanocomposite support layer
GO\P-H	Hydrogel FO membrane with GO\P support layer
HTI	Hydration Technologies Incorporation
ICP	Internal concentration polarization
IP	Interfacial polymerization
MBR	Membrane bioreactor
MDC	Microbial desalination cell
MF	Microfiltration
MFC	Microbial fuel cell
NF	Nanofiltration
NMP	1-methyl-2-pyrrolidone
OMBR	Osmotic membrane bioreactor
OMFC	Osmotic microbial fuel cell

P	Conventional phase inversion constructed support layer
PBI	Polybenzimidazole
PEG	Polyethylene glycol
PEI	Polyethyleneimine
PEO	Polyethylene oxide
PES	Polyethersulfone
P-H	Hydrogel FO membrane with P support layer
PRO	Pressure retarded osmosis
PRO mode	Membrane orientation of selective layer facing draw solution
PSf	Polysulfone
PVA	Polyvinyl alcohol
PWP	Pure water permeability (bar)
RO	Reverse osmosis
RMS	Root-mean-square
SDS	Sodium dodecyl sulfate
SEM	Scanning electron microscopy
TDS	Total dissolved salts (g L^{-1})
TEM	Transmission electron microscopy
TFC	Thin film composite
TFNC	Thin film nanocomposite
TGA	Thermogravimetric analysis
UF	Ultrafiltration
WAS	Waste activated sludge
XRD	X-ray diffraction
“3 high”	High antifouling capability, high water flux, and high selectivity

CHAPTER 1 INTRODUCTION

1.1. Background

More than 70% of the earth is covered by the deep blue ocean, displaying the unintended illusion that life on this planet is at ease with water. However, the cruel truth is that scarcity of clean freshwater has been one of the biggest problems that afflict human beings throughout the world. According to the reports, 1 billion people do not have access to safe drinking water; 2.3 billion people suffer from water-stress with this number estimated to approach 3.5 billion by 2025; 2.6 billion people lack for improved sanitation; and millions of people died annually due to water-related diseases (Service, 2006; Montgomery & Elimelech, 2007). What's even worse, rapid population growth, environmental pollution, and climate change are conspiring to exacerbate this situation, with the average freshwater supply per capita estimated to decrease by one third in the next two decades (Aldhous, 2003). Mankind's demand for water to meet basic needs such as health and hygiene can already threaten the integrity of natural ecosystems and also harbour the risk for serious international conflicts even over war (Barnaby, 2009). In the foreword of 1st world water development report (WWDR1) entitled "Water for People, Water for Life", the former Secretary-General of United Nations Kofi Annan highlighted that "*The centrality of freshwater in our lives cannot be overestimated. Water has been a major factor in the rise and fall of civilizations… And its quality reveals everything, right or wrong, that we do in safeguarding the global environment*" (United Nations World Water Assessment Program, 2003).

Moreover, in modern time water is inextricably linked with energy that is another global scarce resource valued as the lifeblood of technological and economic development (Chow *et al.*, 2003). For example, thermoelectric power production consumes a large quantity of clean freshwater (Feeley *et al.*, 2008), though electricity can be used for water treatment (*e.g.* pumping water from deep aquifer, purifying and transporting water, *etc.*). The problem is that currently there exists no form of energy that can be utilized to sustainably increase freshwater supply (McGinnis & Elimelech, 2008). This protrudes the ever fiercer competition relationship between energy generation and other water usage purposes (*e.g.* domestic usage, agricultural irrigation, and other industrial usages *etc.*). While energy consumption is estimated to increase by

50% by 2030 worldwide, this trend will squeeze the already scarce freshwater resources (Hightower & Pierce, 2008). What's even worse, the overdependence of global energy on fossil fuels has accelerated its depletion, brought forth huge impacts upon global climate due to anthropogenic emission of greenhouse gases (*e.g.* CO_2), and inevitably resulted in environmental deterioration during the mining processes (Hook & Tang, 2013). Climate change as well as environmental pollution drives further freshwater shortage and hence more energy expenditure to obtain safe drinking water, so on and so forth, forming the unsustainable "downward spiral" (McGinnis & Elimelech, 2008). By further taking account of the intrinsic relationships between water/energy and food production, industrial development, medical care, ecological balance and other global issues (Schiermeier, 2008a; Bourzac, 2013), it's not difficult to understand that life on the earth is under water-related multiple crises.

These crises motivated scientists and researchers to seek innovative technologies for sustainable production of clean freshwater and energy. And the major efforts to battle against global freshwater scarcity should be made in two ways. One way is to preserve the limited existing freshwater resources including reinforcing environmental protection, restricting discharge standards, employing water-saving equipment, improving water distribution efficiency and so on. The other way, which is recognized as the only method to increase water supply beyond directly tapping the continental hydrosphere, is to reclaim non-traditional water resources including wastewater treatment and reuse, water purification and recycle, brackish water and seawater desalination *etc.* (Elimelech & Phillip, 2011). For example, municipal wastewater, saline lake water, extracted mine water *etc.* can be utilized as the alternative supplies after sufficient treatment so as to meet water demands that do not require drinking qualities (*e.g.* cooling water, landscape irrigation *etc.*); and this will increase the total usable water amount while prioritizing the pristine freshwater resources for health and hygiene purposes. Similarly, if low grade energy (*e.g.* waste heat) can be utilized for water/wastewater treatment, high grade energy (*e.g.* electricity) can be saved for other prime objectives. Considering that the current water/wastewater treatment processes are still far from their natural law limits in terms of efficiencies, tremendous research activities need to be focused on the exploration of new technologies that can accomplish the treatment at lower cost, less energy consumption and smaller

environmental impacts (Shannon *et al.*, 2008; Subramani *et al.*, 2011).

Among all sorts of water/wastewater treatment processes, membrane technology is expected to continue the dominant role owing to its high removal efficiency and exemption from secondary pollution (Geise *et al.*, 2010). Particularly, pressure-driven membrane processes *e.g.* microfiltration (MF), ultrafiltration (UF), nanofiltration (NF) and reverse osmosis (RO) offer a wide continuum of rejection capability covering from micrometer-sized particles to subnanometer-sized salt ions (Karakulski *et al.*, 2002). However, the major drawbacks of pressure-driven membrane process are (1) the intensive consumption of high grade energy (*e.g.* electricity) and (2) severe membrane fouling especially for NF and RO associated with their high hydraulic working pressure. Started with the expectation to overcome these two intrinsic problems, researchers have found a new way to operate membrane process using the driving force other than hydrostatic pressure while maintain its high removal efficiency, that is, forward osmosis (FO).

FO employs the osmotic gradient as the driving force to draw water molecules from a less concentrated solution (feed solution) through a semipermeable membrane to a more concentrated solution (draw solution) (Schiermeier, 2008b; Liu *et al.*, 2011). Compared with pressure-driven salt-rejecting membrane processes (*e.g.* RO and NF), FO has several distinctive attributes. Firstly, FO can be operated under very low hydraulic pressure (Elimelech, 2007), while reach the same pollutant removal efficiency as RO or NF. Secondly, the use of thermolytic draw solute in FO process can employ low grade energy (*e.g.* waste heat) to regenerate the draw solution, thus reducing the dependence of FO on high grade energy (McCutcheon *et al.*, 2006). Thirdly, FO holds the potential to achieve high water recovery of seawater desalination, which may address the environmental concern on the discharge of seawater RO concentrated brine (McCutcheon *et al.*, 2005). Fourthly, the special form of FO *i.e.* pressure retarded osmosis (PRO) can be utilized to generate electricity from saline gradient (Chung *et al.*, 2012). These attributes stimulate the renaissance of FO in scientific world during last decade, wherein FO has been investigated for its wide applications including seawater/brackish water desalination, water purification, wastewater treatment, clean power generation, controlled drug delivery *in vivo*,

pharmaceutical/food dehydration, and other processes (York *et al.*, 1999; Verma *et al.*, 2000; McGinnis, 2002; Cath *et al.*, 2005c; Dova *et al.*, 2007; Nayak & Rastogi, 2010; Phuntsho *et al.*, 2011; Zhao *et al.*, 2012; Butler *et al.*, 2013; Song *et al.*, 2013). These extensive studies come to the expectation that FO technology may become a potential solution to global scarcity of freshwater and energy (Klaysom *et al.*, 2013).

Despite these promises, FO is not widely embraced by water/wastewater industry primarily for two interrelated reasons. The first reason is that the long-term misunderstanding on FO's capability especially in seawater desalination and power generation. Although FO process without draw solution regeneration is a low energy process, FO-draw solution regeneration process, which is virtually used for large-scale freshwater and energy production, is not. And it's only very recently that FO-draw solution regeneration process is clarified to be much less competitive than the standalone RO process (even with UF pretreatment) in energy consumption for seawater/brackish water desalination (McGovern & Lienhard, 2014). Noteworthily, the choice of draw solute may influence the form of energy for draw solution regeneration but cannot reduce the minimum energy of separation for the entire process (Shaffer *et al.*, 2015). Regarding osmotic power generation, river water/seawater pairing has been proved unrealistic for net energy output due to its small osmotic gradient; while seawater RO concentrated brine/impaired river water pairing has also been revealed to be economically unfeasible (Straub *et al.*, 2016). These recently published clarifications indicate that it's pressing to rectify those misguiding notions on FO technology.

The second reason is that the long-term overestimation on FO's capability misdirects the development in FO membrane. As a result, to date there is no genuine FO membrane that can advance FO technology to seize the foothold in mainstream water/wastewater industry. In order to understand what a genuine FO membrane is, the first step is to make clear where the true future is for FO. The last and only beauty of FO is that a salt-rejecting membrane may directly handle challenging wastewaters which are high in either salinity or fouling potential or both, owning to the promise associated with FO's low hydraulic pressure working manner. And to excel with these challenging wastewaters, a genuine FO membrane must simultaneously possess the

following three requisites: (1) high antifouling capability, (2) high water flux and (3) high selectivity. Particularly, antifouling capability and selectivity are determined by the selective layer of FO membrane, while FO water flux (J_W) is determined by both the water permeability of selective layer and the pore structure of the support layer. In retrospect, the overestimation of FO's capability results in the negligence on the development of antifouling selective layer for FO membrane. The studies on FO membrane follow the trend for many years to use polyamide selective layer that is directly copied from RO technology (Chou *et al.*, 2010; Yip *et al.*, 2010; Sukitpaneenit & Chung, 2012; Luo *et al.*, 2014; Liu & Ng, 2015). However, polyamide membrane is prone to fouling due to its inherent hydrophobic (oleophilic) property and rough topography (Vrijenhoek *et al.*, 2001; Castrillon *et al.*, 2014), which makes itself not able to cope with those challenging wastewaters. For example, during the treatment of oil-polluted wastewater, oil droplets will easily foul polyamide surface and thus cause the significant reduction of FO water flux. Therefore, the top priority should be given to the search of a new selective layer with high antifouling capability specially for FO membrane. In addition, the J_W of FO technology is intrinsically bottlenecked by the internal concentration polarization (ICP) problem. The key to solve this problem is to construct the support layer with its interior pores highly interconnected in all three dimensions (3D). Although lots of endeavors have been made by worldwide researchers (Song *et al.*, 2011; Bui & McCutcheon, 2013), there still lacks for an uncomplex and effective technology which can be compatible with currently dominant membrane manufacture processes (*e.g.* phase inversion) to fabricate such 3D interconnected porous support layer for FO membrane.

In short, it's crucial to arrive at the precise understanding of FO's advantages and limitations, thoroughly cast off those confines on membrane design from pressure-driven membrane processes, and further establish an entirely new design rationale for FO membrane on both the selective layer and the support layer. Within this mind, this thesis takes up the challenge to design and synthesize a genuine FO membrane in order to advance FO technology towards recycling useful resources (water or energy) from highly saline/fouling wastewaters with low fouling, high water flux and high selectivity. In particular, a unique hydrogel macromolecule (*i.e.* polyvinyl alcohol in this study) is systematically optimized as a new FO membrane

selective layer for high antifouling capability, high water permeability and high selectivity; and GO assisted phase inversion technology is developed to construct the 3D interconnected porous nanocomposite support layer to minimize the ICP problem for high FO water flux. As-demonstrated combination of cutting-edge nanotechnology with dominant membrane manufacture process is expected to make a significant impetus to push the practical applications of FO technology.

1.2. Scope and objective

This study aims to direct the research and development on FO technology to the correct track, in order to advance its industrialization for the battle against global freshwater scarcity. Towards this goal, this study analyzes the specialties of FO technology, explores the design principles of a genuine FO membrane, further synthesizes such membrane and eventually utilizes this new membrane to demonstrate the unparalleled advantage of FO technology over existing pressure-driven salt-rejecting membrane processes (*e.g.* NF and RO) for the treatment of challenging wastewaters (*e.g.* highly saline and oily wastewater).

The objectives of this study include:

(1) To elucidate the design rationale for a genuine FO membrane in order to guide the synthesis of FO membrane.

(2) To investigate the potentiality of hydrogel macromolecule as the antifouling selective layer for FO membrane, if applicable to further optimize its capability.

(3) To search out an entirely new support layer structure in terms of pore interconnectivity with current membrane manufacture technique by the leverage of frontier nanotechnology, for the purpose of breaking the ICP bottleneck on FO technology.

(4) To explore the membrane technology able to simultaneously desalinate and deoil highly saline and oily wastewater, while further verifying this proposal with as-synthesized new nanocomposite membrane through FO process.

1.3. Innovations of this study

The major innovative contributions of this study are summarized as follows in brief.

For the first time, the design rationale is developed for a genuine FO membrane that is able to excel with highly saline and oily wastewater.

For the first time, the capability of hydrogel macromolecule as the selective layer of FO membrane is systematically investigated and further optimized.

For the first time, a new nanocomposite support layer with its interior pores highly interconnected in all three dimensions at micrometer-scale is created using dominant membrane manufacture technique (phase inversion), in order to break the ICP bottleneck on FO. Moreover, it's also the first time to demonstrate that hydrophilic 2D graphitic nanomaterial can direct the transformation of pore structure from 1D connected to 3D interconnected during support layer formation process.

For the first time, FO technology is purposely developed towards the challenge of treating highly saline and oily wastewater, in order to ascertain the exceptional advantage of FO technology herein over existing pressure-driven salt-rejecting membrane processes (*e.g.* NF and RO). Accordingly, as-synthesized nanocomposite FO membrane (hydrogel selective layer + 3D pore interconnected support layer) is systematically verified for its ability to achieve simultaneous desalination and oil/water separation of hypersaline oil-in-water emulsion with low fouling, high water flux and high selectivity.

1.4. Organization of study

Seven chapters constitute this thesis.

Chapter 1 introduces the background, scope, objective, innovations, and organization of this study.

Chapter 2 reviews the history, concept, proposed applications, critical challenges, and recent developments of FO technology. It's explained in detail that FO technology

should be directed to the correct track *i.e.* to cope with challenging wastewaters (*e.g.* highly saline and/or oily wastewaters), and hence high antifouling capability is a requisite for a genuine FO membrane. Furthermore, the techniques to improve membrane antifouling capability are discussed with the emphasis on recently developed underwater superoleophobic membrane technology. Most importantly, the design rationale for an ideal FO membrane to treat highly saline and highly oily wastewater with low fouling, high water flux and high selectivity is summarized.

Chapter 3 presents the materials and methods employed in the experimental work of this study.

Chapter 4 to Chapter 6 focuses on the results and discussion of this study. Particularly, Chapter 4 investigates the potentiality of hydrogel macromolecule as the selective layer for FO membrane, and further reveals the key role of crosslinking to optimize the structure and property of as-synthesized hydrogel selective layer for FO applications.

Chapter 5 integrates dominant membrane manufacture process (phase inversion) with cutting-edge nanotechnology to search out a new support layer *i.e.* micrometer-scale 3D interconnected porous support layer, for the purpose of breaking the ICP bottleneck on FO technology.

Chapter 6 challenges as-synthesized nanocomposite FO membrane (hydrogel selective + 3D pore interconnected support layer) on the treatment of highly saline and oily wastewater, and systematically verifies that this new nanocomposite membrane can simultaneously desalinate and deoil hypersaline oil-in-water emulsion through FO process with low fouling, high water flux and high selectivity.

Finally, Chapter 7 draws the conclusions carefully and provides valuable recommendations for the further studies.

CHAPTER 2 LITERATURE REVIEW

2.1. Introduction

This chapter presents a comprehensive review on FO technology in the following storyline. Firstly, the concept, history, classification, and potential advantages of FO technology are introduced to provide an overview. Secondly, the modernly proposed applications of FO process are examined with the highlight to clarify two usual misunderstandings about FO technology. Accordingly, this thesis clearly declares that (1) FO-draw solution regeneration technology is not a low energy process, and (2) the true future for FO technology is to cope with challenging wastewaters (*e.g.* highly saline and/or fouling wastewaters). Thirdly, the critical challenges confronted by FO technology are analyzed, wherein high antifouling capability is ascertained as the requisite of a genuine FO membrane. Fourthly, the recent developments of FO membrane are discussed, wherein it is pointed out that no membrane up to now can meet high antifouling ability, high water flux and high selectivity ("3 high") requirements of genuine FO membrane. Fifthly, the techniques to improve membrane antifouling ability are elaborated. Sixthly, the recently developed underwater superoleophobic membrane technique and the potentiality of hydrogel macromolecule as the antifouling selective layer for FO membrane are emphasized in detail. Finally, the correct direction to advance FO technology is summarized. More importantly, the design rationale on an ideal FO membrane to treat challenging wastewater (*e.g.* highly saline and highly oily wastewater) with low fouling, high water flux and high selectivity is proposed.

2.2. Overview on osmotically-driven membrane processes (ODMPs)

2.2.1. Concept and history

Osmosis is the phenomenon that solvent molecules spontaneously move through a semipermeable membrane from less concentrated solution (feed solution) to more concentrated solution (draw solution). The mechanism viewed in thermodynamics is that less concentrated solution contains more free energy that drives its solvent molecules to diffuse to a region of lower free energy (more concentrated solution) in order to reach energy equalization. Ideally, this semipermeable membrane retains all the solute molecules while allowing the solvent molecules to pass through it.

Consequently, a net transportation of solvent from hypotonic solution to hypertonic solution is built. This net solvent flow can be countered through applying external hydrostatic pressure at the hypertonic side. Osmotic pressure (π) is defined as the value equaling to the external pressure required to reach the dynamic equilibrium wherein the net solvent flow becomes zero (Kramer & Myers, 2013). Noteworthily, osmotic pressure is a colligative property that depends upon the concentration of solute rather than the type of solute (Parsegian *et al.*, 2000).

In nature, osmosis occurs almost everywhere. The exploitations of this phenomenon can be traced back to the early days of mankind. One example handed down to the present is the tradition to utilize saline environments to preserve food. Microbes, including those potentially pathogenic ones can be dehydrated by osmosis for inactivation, because biological membranes are impermeable to certain large molecules (*e.g.* polysaccharides, proteins, *etc.*) while permeable to many small molecules (*e.g.* water, carbon dioxide, oxygen, etc.) (Parisi *et al.*, 2007).

The earliest report pertaining to osmosis is documented in 1780, as quoted indirectly from (Yokozeki, 2006). But the term "osmose", now "osmosis" is not used until 1854 introduced by British chemist Thomas Graham. According to *Encyclopedia Britannica online*, the first relatively systematic investigation on osmosis was conducted by a German plant physiologist Wilhelm Pfeffer in 1877. Ten years later, van't Hoff published the theoretical study on osmotic pressure (van't Hoff, 1995), based on which in 1914 American chemist Harmon Northrop Morse presented the equation in simplified form as:

$$\pi = \beta \times C \times R_g \times T \tag{2.1}$$

where β is the van't Hoff factor (dimensionless), C is the molar concentration, R_g is the universal gas constant (8.314 Joule mol^{-1} K^{-1}) and T is the thermodynamic temperature. The validity of this equation is limited with dilute solutions (Wilson & Stewart, 2013).

From that time onwards, the development of osmotic technology experiences four stages in history, demonstrating that membrane is the core of this technology. (1) Early scientists investigated osmosis with goldbeaters' skin, porcelain, nitrocellulose

collodion, rubber, animal bladders *etc.* as the membrane and thus their experimental results are less accurate. (2) The breakthroughs made in polymeric membrane from 1950s to 1980s, *i.e.* the inventions of phase inversion technique in 1950s (Loeb & Sourirajan, 1962) and interfacial polymerization technique in 1980s (Cadotte *et al.*, 1980), pushed the research on osmotically-driven membrane processes (ODMPs). For example, in 1975 Kravath *et al.* tried to desalinate seawater by osmosis with cellulose acetate membrane (Kravath & Davis, 1975). In 1976, Kessler *et al.* investigated the extraction of drinking water from seawater through osmotic process (Kessler & Moody, 1976; Moody & Kessler, 1976). And also in 1976 Loeb initiated the study on harvesting energy from saline gradient (Loeb, 1976). However, most of the studies at this stage were proof of concept and their results were much lower than expectations, because the membranes employed were manufactured for pressure-driven membrane processes (*e.g.* NF or RO). (3) In 1990s, Osmotek Inc., currently Hydration Technologies Incorporation (HTI) commercialized the membrane specially for osmotic process. This proprietary membrane is considered to be made of cellulose triacetate (CTA). Different from typical RO membranes which use a thick fabric to reinforce mechanical strength, a polyester mesh is embedded in HTI membrane to provide mechanical support. As a result, the overall thickness of membrane is reduced to be around 50 μm, which is much thinner than that of traditional NF or RO membranes (typically ~150 μm). HTI membrane has been proven to be superior to any conventional NF or RO membrane in osmotic processes. HTI membrane has already been used for small-scale supply of drinkable water under emergency, recreational and military circumstances (Biberdorf, 2004). The availability of HTI membrane provides the studies on ODMPs with relatively reliable basis. (4) Since 2005, the renaissance of ODMPs has been initiated by Menachem group at Yale University who proposed ammonium bicarbonate (NH_4HCO_3) as the draw solute to desalinate seawater through FO process (McCutcheon *et al.*, 2005). From that time onwards, ODMPs has become a hot topic that is intensively investigated for its potentialities to recover water and energy from seawater or wastewaters.

2.2.2. Classification of osmotically-driven membrane processes (ODMPs)

The net solvent flow in osmotic processes is illustrated in Figure 2.1, which is redrawn with significant improvements based upon (Cath *et al.*, 2006). Here, external

hydrostatic pressure is applied at the side of draw solution. So a positive value of transmembrane hydrostatic pressure difference (ΔP) means osmotic diffusion of water molecules from feed solution (hypotonic) to draw solution (hypertonic) is retarded. When transmembrane hydrostatic pressure difference is bigger than osmotic pressure difference ($\Delta P > \Delta\pi$), water molecules are pushed backwards through the semipermeable membrane from the draw solution to the feed solution. This is RO process that can be used to directly produce fresh water. When transmembrane hydrostatic pressure difference is zero ($\Delta P = 0$), water diffuses naturally across the membrane from feed solution to draw solution. This is FO process. When transmembrane hydrostatic pressure difference is bigger than zero but smaller than osmotic pressure difference ($0 < \Delta P < \Delta\pi$), water molecules diffuse through the membrane in the same direction with FO but with smaller flux than that of FO. This is PRO process wherein the net water flow makes work as it overcomes ΔP during the transportation. Therefore, PRO process can be used to recover energy from the osmotic gradient. When the value of transmembrane hydrostatic pressure difference is smaller than zero ($\Delta P < 0$ *i.e.* virtually hydrostatic pressure is applied at the side of feed solution), forward diffusion of water molecules takes place in the bigger flux than that of FO. This process is termed as pressure assisted forward osmosis (AFO) (Blandin *et al.*, 2013), which receives attention just recently.

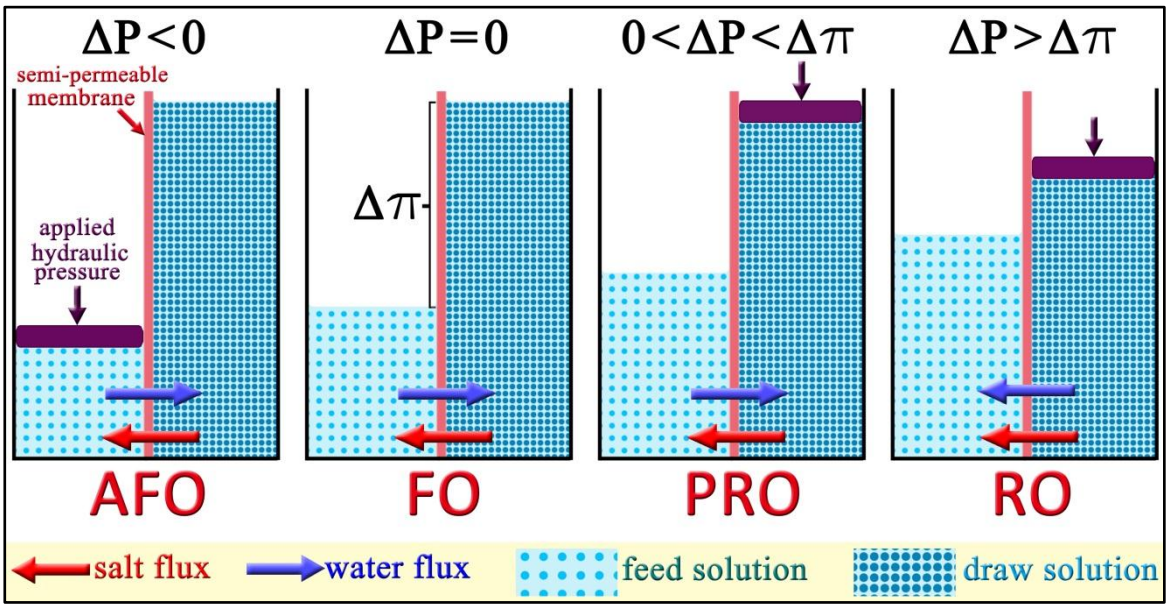

Figure 2.1 The solvent flow in AFO, FO, PRO and RO. The figure is redrawn with significant improvements based upon (Cath *et al.*, 2006). Feed solution is less concentrated (hypotonic) while draw solution is more concentrated (hypertonic). A semi-permeable membrane is used to separate the feed solution from draw solution.

Except RO, osmotic pressure difference across the membrane ($\Delta\pi$) serves as the driving force in the other three membrane processes. Hence FO, PRO, AFO are all osmotically driven membrane processes (ODMPs). Taking account of the fact that both PRO and AFO can be regarded as a special form of FO, FO is focused primarily by this thesis in the following investigations.

The formula governing water flux (J_W) across the semipermeable membrane as a function of transmembrane hydrostatic pressure difference is summarized in equation 2.2 (Loeb, 1976).

$$J_W = A \times (\Delta\pi - \Delta P) \tag{2.2}$$

where A is water permeability coefficient that is an intrinsic property of the membrane. In reality, the osmotic pressure difference is less than the theoretical value because of the leakage of solutes. So this governing formula could be modified as equation 3 (Cath *et al.*, 2006).

$$J_W = A \times (\sigma \times \Delta\pi - \Delta P) = A \times (\Delta\pi_{eff} - \Delta P) \tag{2.3}$$

where A is water permeability coefficient; σ is the reflection coefficient, symbolizing the solute rejection by the membrane ($0 \leq \sigma \leq 1$); $\Delta\pi_{eff}$ is effective osmotic pressure difference across membrane. Both equation 2.2 and equation 2.3 indicate the positive correlation between J_W and A value.

2.2.3. The potential advantages of FO technology

Compared with traditional pressure-driven salt-rejecting membrane processes (*e.g.* RO and NF), FO can achieve similar or even better rejection of contaminants. Meanwhile, FO process has several potential advantages over NF or RO. Firstly, FO can be operated at low or nearly zero applied hydraulic pressure, because the only pressure needed in FO is to circulate water flow in membrane system (usually $\leq$ 1 bar) (Elimelech, 2007). This has significant implications for the construction of non-thermally-driven salt-rejecting membrane processes (*i.e.* RO and NF): high-pressure pumps can be dispensable. Secondly, low grade energy (*e.g.* waste heat) can be utilized to recycle certain draw solute (*e.g.* NH_4HCO_3). The top two merits are the beauty of FO, which means FO is more independent on high grade energy (*i.e.* electricity) than RO or NF. Thirdly, PRO can be used to produce electricity from

salinity gradients, which is regarded as a potential approach to realize clean power generation. Fourthly, FO process can attain high water flux and high water recovery, and thus holds the potential to accomplish zero liquid discharge in desalination processes, which will address the environmental concerns on the concentrated brine generated from seawater RO desalination plants (McCutcheon *et al.*, 2005; Elimelech, 2007). Last but not least, because the applied hydrostatic pressure in FO is considerably smaller than that in RO or NF, the fouling propensity of FO is usually thought to be lower than that of RO or NF.

However, four points should be further emphasized on the issue of FO fouling. Firstly, it is "low fouling propensity" but not "no fouling propensity" in FO. Secondly, the fouling propensity of FO is merely "relatively low" compared to RO or NF under the same feed solution, which does not necessarily mean the "absolute fouling" cannot be severe in FO. Thirdly, more and more studies reveal that remarkable or even severe fouling does exist in FO process depending on the operational conditions. Some peer studies point out that the fouling mechanism in FO can be even more complicated than that in RO or NF due to the coupled effects of ICP and fouling (Tang *et al.*, 2010; She *et al.*, 2016). Last and most importantly, because of the "low fouling propensity", FO is frequently designated as ("doomed to be") the pretreatment process that works in harsh environment (*e.g.* high foulant concentrations) rather than the terminal process like RO or NF that generates the final water product. Therefore, good antifouling property becomes an obliged attribute for a genuine FO membrane.

2.3. Modernly proposed applications of FO technology

Stimulated by the promising benefits of FO process, lots of attention has been paid to the potential applications of FO in a wide scope including water, energy and life science *etc*. Here, the research on modern applications of FO is systematically reviewed in the following seven aspects.

2.3.1. Desalination

2.3.1.1. The development of FO desalination technology

The concept of removing salts from saline water through FO process was first documented in several U.S.A. patents half a century ago. However, few of them

matured into full-scale applications (Batchelder, 1965; Frank, 1972). The utilization of FO technology as a continuous process for large-scale desalination did not receive lively interest until the commercial FO membrane (HTI membranes) became available in late 1900 s.

In order to produce fresh water from saline sources, two steps are required in FO desalination technology: (1) osmotic extraction of water from saline feed solution to more concentrated draw solution, and (2) the separation of draw solute from water in diluted draw solution (*i.e.* the reconcentration of draw solution). And based upon whether the second step employs membrane process, FO desalination technology can be further classified into two categories. The first category utilizes the method other than membrane process (*e.g.* thermal decomposition, magnetic separation *etc.*) to recycle draw solute. In 2002, a U.S.A. patent from McGinnis recorded the utilization of KNO_3 and SO_2 aqueous solution (recycled by cooling and heating) for FO desalination of seawater (McGinnis, 2002). In 2005, a milestone was achieved by McCutcheon *et al.* from Menachem group at Yale University, who investigated FO desalination of synthetic seawater (0.5 M NaCl) with 6.0 M NH_4HCO_3 as the draw solution. Besides, the J_W of HTI membrane (CTA, nonwoven) reached as high as 23.0 L m^{-2} h^{-1} in their lab-scale FO module (McCutcheon *et al.*, 2005). The significance of this study lies in the wise selection of draw solute: the solubility of NH_4HCO_3 is highly temperature-dependent. At low temperature the solubility of NH_4HCO_3 is high, which can yield the maximum π value >200 bar; while at temperature ~60℃ most of NH_4HCO_3 is decomposed into CO_2 and NH_3 and released from draw solution in gas form. In addition, their further work reported that approximately 70% water recovery can be attained by their ammonia-carbon dioxide draw solute technology (McCutcheon *et al.*, 2006). However, there is still a large room for the improvement since their "maximum performance ratio" (defined as the experimental J_W value divided by the theoretical J_W value) is as low as only 20%.

The second category employs an additional membrane process (*e.g.* RO, NF, MD *etc.*) to separate draw solute from fresh water. Here, FO can be regarded as a pretreatment unit while the downstream membrane process can be regarded as the terminal unit. The selection of membrane in the terminal unit depends on the difficulty to retain the

specific draw solute. For example, RO process was proposed when monovalent ionic salts *e.g.* NaCl were used as draw solute (Bamaga *et al.*, 2011; Yangali-Quintanilla *et al.*, 2011), while NF process was recommended when divalent ionic salts *e.g.* $MgCl_2$, Na_2SO_4, $MgSO_4$ *etc.* (Tan & Ng, 2010; Zhao *et al.*, 2012) or small organic molecules *e.g.* sucrose, glucose *etc.* (Su *et al.*, 2012) were used as the draw solute. Recently, the employment of UF process for draw solution reconcentration has been proposed with hydrophilic nanoparticles used as draw solute (Ling & Chung, 2011). However, there is a major limitation on this FO-UF process. The FO membrane must have very high rejection of salt ions otherwise these salt ions will diffuse through feed solution to draw solution in considerable flux. Under this situation, the leaked salt ions cannot be separated by the downstream UF membrane and thus will eventually contaminate the product water. This implies that FO-UF process may be less suitable to desalinate seawater compared to brackish water.

2.3.1.2. Where can FO truly outmaneuver other desalination technologies?

More importantly, there exists a misguided notion that FO-draw solution regeneration process could be more energy efficient than a standalone RO process for brackish water/seawater desalination. It's imperative to emphasize that this notion is wrong! In 2014, McGovern *et al.* carefully compared FO-RO process with a standalone RO process in terms of energy efficiency, which included theoretical minimum energy of separation, the energy for cross-flow circulation, the energy required by pretreatment (*e.g.* UF process) for standalone RO process and other factors. They concluded that a standalone RO process even with UF pretreatment is significantly more energy-efficient than FO-RO process. And they further attributed the inefficiency of FO technology to its draw solution regeneration step that increases the theoretical and actual energy requirements regardless of the specific draw solute employed (McGovern & Lienhard, 2014). Noteworthily, the use of thermolytic salt as draw solute only means waste heat if available can be used to replace electricity for the recycle of draw solute but does not mean that the total energy required for the FO-draw solution regeneration technology can be reduced lower than that of standalone RO process. This recent assertion that FO-RO desalination technology is less energy efficient than standalone RO process for brackish water/seawater desalination is also support by Shaffer *et al.* from Menachem group at Yale University (Shaffer *et al.*,

2015).

But this does not mean FO desalination technology is always inferior to RO process under all circumstances. On the contrary, the author of this thesis believes that FO-draw solution regeneration technology can outperform a standalone RO process principally for the treatment of three kinds of wastewaters: (1) high fouling potential, (2) high salinity, and (3) the most challenging one *i.e.* both high fouling potential and high salinity. This viewpoint is virtually in good agreement with the recently published critical review on FO technology by Shaffer *et al.* (Shaffer *et al.*, 2015).

Most importantly, this newly readjusted vision on FO technology tolls the alarm bell on the design of FO membrane. Merely high water permeability and/or good selectivity are not enough for the survival of FO membrane in water/wastewater industries, because some commercial RO membranes already acquire these attributes. Therefore, a genuine FO membrane must possess outstanding antifouling ability so as to fully take advantage of its low pressure working manner and thus reduce fouling-caused flux decline to the minimum extent. Only through this way can FO membrane excel with highly fouling/saline wastewater and thus outmaneuver pressure-driven salt-rejecting membranes (RO/NF membranes). Under this guideline, this thesis endeavors to direct the design and synthesis of FO membrane towards the "correct track": to develop a highly antifouling FO membrane that can treat hypersaline wastewater of high fouling potential with low fouling, high water flux and high selectivity.

2.3.2. Water purification

In this thesis, only those technologies that aim at supplying drinkable water are labeled as water purification. Usually the contamination of water source is not heavy and potable water can be produced at affordable cost. The use of FO technology for water purification can be also sorted into two categories based upon whether FO serves as the terminal process unit.

In the first category, FO serves as the terminal process unit and the osmotically diluted FO draw solution is consumed directly as the drinkable liquid without further

treatment. The example is the portable HTI hydration package, which is commercialized to meet recreational, military, and emergency relief purposes (Biberdorf, 2004; Butler *et al.*, 2013).The HTI hydration package contains two bags: (1) the internal bag, which is made of CTA FO membrane, is filled with edible draw solution (*e.g.* flavored sucrose, or beverage powder etc.); and (2) the external bag, which is the sealed plastic cover that can hold certain volume of raw water inside. This design provides more flexibility of usage, because the user can either take out the internal bag and submerge it in the source water (*e.g.* a pond or a river) or fill the external bag with source water and take along the entire package. The draw solution is finally diluted into a beverage that also contains nutrients and minerals. The merits of this hydration bag are that (1) no power is required and (2) emergent drinking from undefined or lightly polluted water source (*e.g.* river water, muddy ponds *etc.*) becomes much safer. However, there are several drawbacks of this technology: (1) the process is slow due to low water flux (it takes 3 ~ 4 hours to completely hydrate a 12 oz beverage); (2) it can be operated only at batch mode; and (3) it only provides drinkable water in small-scale.

In the other category, FO serves as the pretreatment technology and a downstream process unit is added to produce drinking water from the diluted draw solution. One example is the membrane contactor technology that produces fresh water from humidity condensate, urine and hygiene wastewater on space craft, which is also termed as direct osmotic concentration (DOC) system by the proposers (Cath *et al.*, 2005b). As illustrated in the flow diagram on their paper (Cath *et al.*, 2005c), DOC system consists of three units: (1) one FO unit, (2) one FO+OD (osmotic distillation) unit, and (3) one RO unit. The FO unit was used to reclaim water from hygiene wastewater and humidity condensate; and the FO+OD was used to extract water from wastewater and urine (the OD here aims at approximately complete rejection of small organic compounds *e.g.* urea and ions); while RO was used as the terminal process to produce drinking water from the diluted draw solution (Cath, 2010). Interestingly, the draw solution of the FO and FO+OD units was cycled in one close loop: the draw solution was diluted by the FO unit, concentrated by RO unit, diluted by FO+OD unit and then pumped back to FO unit again (Cath *et al.*, 2005a).

It's worthy to note that as discussed previously in section 2.3.1.2., FO-draw solution regeneration technology is also less energy-efficient compared to a standalone RO for water purification. The merits by employing FO unit as a pretreatment process to replace conventional pressure-driven pore-flow membrane process (*e.g.* MF and UF) for water purification are: (1) membrane fouling can be relatively less severe compared to MF/UF owing to the low hydraulic pressure working manner of FO, and (2) FO provides an additional barrier besides RO to reject tiny pollutants (*e.g.* salt ions, hardness, small organic molecules and other specific contaminants that cannot be retained by pore-flow membrane) and thus improves the quality of product water.

2.3.3. Wastewater treatment

The overarching goal for wastewater treatment is to remove the pollutants or reduce the concentrations of pollutants to certain levels in order to protect the receiving environments and comply with the discharge requirements. Because the low hydraulic pressure working manner of FO process promises itself to achieve relatively low fouling extent compared with conventional pressure-driven membrane processes, FO technology does have the opportunity to directly tackle wastewaters even those heavily polluted ones. This section provides a comprehensive review on the recent proposals to treat wastewater with FO technology. Noteworthily, under some situations the difficulty to treat the wastewater is not because the concentration of certain pollutant is high, on the contrary, but because the concentration of certain pollutant is too low to make the existing technology cost-effective. That motivates the utilization of FO to reclaim water (or even energy) directly from wastewater and thus facilitate the downstream treatment of concentrated wastewater (FO). This kind of application is also included in the below review.

2.3.3.1. Landfill leachate treatment

Sanitary landfilling is the most common way to deal with municipal solid wastes. Landfill leachate, which is generated by excess rainwater percolating through the waste layers, contains four types of pollutants in general: dissolved organic matter, inorganic components, heavy metals and xenobiotic organic compounds (Kjeldsen *et al.*, 2002). Due to the ever stricter pollution control in many countries, conventional biological or physic-chemical treatments are usually not enough to meet the newly

established discharge standards. Membrane process has come into view as the advanced technology for the treatment of landfill leachate. In late 1990s, York *et al.* investigated the use of FO technology to concentrate landfill leachate with HTI FO membrane. Their pilot-scale experiment observed 30% ~ 50% decline of J_W due to the membrane fouling, quoted indirectly from (Cath *et al.*, 2006). Besides, their full-scale FO-RO hybrid system obtained average 91.9% water recovery and >90% rejection of most pollutants (York *et al.*, 1999). This work demonstrates the pronounced benefits of FO for the treatment of landfill leachate: (1) high water recovery, and (2) nearly zero liquid discharge (the concentrated leachate can be solidified before discharge).

2.3.3.2. Concentration of activated sludge

Waste activated sludge (WAS) is the one of the most troublesome issues confronted by conventional activated sludge processes, because the treatment of WAS accounts for up to 60% of the total cost of wastewater treatment. It's desirable to explore novel strategies for the minimization of excess biological sludge (Wei *et al.*, 2003), wherein FO may serve as a good choice. And the combination of FO with sludge digestion (the mature process unit to stabilize, detoxicate, and minimize WAS) has been investigated in the following two ways. One way is to use FO technology to concentrate the raw sludge with digestion unit worked simultaneously or subsequently. For example, Zhu *et al.* studied the use of concentrated brine to concentrate the raw sludge with digestion and thickening operated concurrently. And their bench-scale experiment found that raw sludge can be concentrated by >4 times (MLSS concentration increased from 7 g/L to 39 g/L) (Zhu *et al.*, 2012). The other way is to use FO technology to dewater the digester centrate. For instance, Holloway *et al.* reported that their bench-scale FO-RO hybrid system should be operated at 70% water recovery to reach energy optimization for the dewatering of digester centrate (Holloway *et al.*, 2007).

2.3.3.3. Osmotic membrane bioreactor (OMBR)

Membrane bioreactor (MBR) offers many advantages over traditional biological wastewater treatment process chain (*i.e.* activated sludge process plus secondary sedimentation tank) including smaller footprint, relatively higher effluent quality, higher volumetric loading and less WAS production (Visvanathan *et al.*, 2000). In an OMBR, the pressure-driven pore flow membrane (*i.e.* MF or UF) of MBR is replaced

with a FO membrane. The earliest study on OMBR was documented in 2008 (Cornelissen *et al.*, 2008). And in 2009, the study from Achilli *et al.* on OMBR demonstrated that FO membrane could be superior to MF/UF membrane in bioreactor because FO membrane was able to achieve higher removal of TOC as well as nutrients (Achilli *et al.*, 2009b). These two studies stimulated more attentions on OMBR in the following years (Xiao *et al.*, 2011; Alturki *et al.*, 2012). However, there are some technical hurdles on the industrialization of OMBR: (1) the FO membrane must possess high anti-biofouling capability because microbes can colonize on membrane surface to form the biofilm, (2) the draw solute should not impair the microbial activities with its reverse solute leakage, and (3) novel strategy should be developed to overcome the negative impacts induced by salinity accumulation in bioreactor (Yap *et al.*, 2012; Wang *et al.*, 2016).

2.3.3.4. Osmotic Microbial Fuel Cell (OMFC)

Osmotic microbial fuel cell (OMFC) is an emerging technology that aims at biological wastewater treatment, clean water extraction and electricity generation in an integrated system. In an OMFC, FO membrane replaces the ion-exchange membrane in microbial fuel cell (MFC) to separate the two electrode chambers. The catholyte (*e.g.* synthetic seawater, hypertonic) works as the draw solution to extract water molecules from the anolyte that is the mixture of microbes and wastewater (hypotonic). Zhang *et al.* reported that OMFC can generate more electricity than traditional MFC in both batch-type operation and continuous operation based upon their bench-scale experiment. They thought that this was possibly because the convective transportation of ions got enhanced along with forward diffusion of water molecules (Zhang *et al.*, 2011). Werner *et al.* proposed to use an air-cathode to further enhance the energy recovery of OMFC (Werner *et al.*, 2013).

As a modified form of MFC, microbial desalination cell (MDC) consists of three chambers: an anion exchange membrane (AEM) adjacent to the anode, a cation exchange membrane (CEM) adjacent to the cathode, and a middle chamber sandwiched between the membranes filled with saline water that is to be desalinated (Cao *et al.*, 2009; Akther *et al.*, 2015). In the recently proposed osmotic microbial desalination cell (OMDC), the AEM was replaced with a FO membrane to induce

active osmosis of water from anolyte to the saline feed solution (Ge *et al.*, 2013). It should be noted that OMFC and OMDC are in the infant stage of development (Ge & He, 2012), and a lot of work needs to be conducted in future in order to examine their feasibility.

2.3.3.5. Oily wastewater treatment

During the same time with the author's Ph.D. research on the development of a special FO membrane to separate highly saline and oily wastewater, FO technology is just proposed for the treatment of oily wastewaters including emulsified oil/water mixtures (Duong & Chung, 2014; Duong *et al.*, 2014). However, these works merely focused on the separation of salinity-free oil-in-water emulsions, which is much less challenging. Few study touches on the separation of hypersaline oil/water emulsions through FO process. To the best knowledge of the author, there is no special FO membrane designed and synthesized purposely for the separation of hypersaline oil/water mixture (*e.g.* shale gas wastewater, onshore oil and gas produced water). Even at the time when the author's first manuscript (entitled "A new nanocomposite membrane custom-designed for shale gas wastewater treatment", *Scientific Reports* 2015, **5**, 14530) has been submitted to research journal for review, parallel studies still relied on HTI membrane to treat saline oily wastewater and observed severe fouling of HTI membrane during the separation process (Altaee & Hilal, 2014; Coday & Cath, 2014; Li *et al.*, 2014). These results also reflect the urgency to develop a special membrane for the separation of hypersaline oil/water emulsion and thus justify the importance of this thesis.

2.3.4. Clean power generation

Human being's overdependence on fossil energy causes the quick depletion of natural resources and considerable environmental deterioration. A wise way to protect this planet from energy crisis is to explore clean and renewable energy sources, among which osmotic power may hold the potential. Optimistic estimation stated that global electricity production by PRO could be on the potential of 2000 TWh per year (Aaberg, 2003), which accounts for approximately one fifth of the global energy demand presently (Post *et al.*, 2007). The concept of harvesting energy from mixing solutions of different chemical potentials had been proposed six decades ago (Pattle, 1954).

Around 1975, Loeb *et al.* made the earliest endeavor in PRO experiments with Dead Sea brine used as draw solution (Loeb, 1975; Loeb *et al.*, 1976). Since then the development of PRO has experienced a struggling journey with the details recorded in a published review from Achilli *et al.* (Achilli & Childress, 2010).

The schematic diagram of PRO power plant is illustrated in the figure on the research article from Achilli *et al.* (Achilli *et al.*, 2009a). It can be seen that PRO equipment consists of two important components: the pressure exchanger and the membrane module. Inside the module, draw solution (*e.g.* RO concentrated brine) and feed solution (*e.g.* river water) are separated by a semi-permeable membrane *i.e.* PRO membrane. Because osmotic pressure difference is bigger than transmembrane hydrostatic pressure difference ($0 < \Delta P < \Delta\pi$), water molecules diffuses from feed solution to draw solution. Then the pressurized draw solution is split into two streams: one passes through the pressure exchanger to facilitate the continuous intake of draw solution and the other (net water flux) is used to drive a hydro turbine for electricity generation.

The most important parameter to evaluate PRO performance is power density (W), which is defined as the power generated per unit membrane area (Lee *et al.*, 1981a).

$$W = J_W \times \Delta P \tag{2.4}$$

Equation 2.5 is obtained through combining equation 2.2 and 2.4.

$$W = A(\Delta\pi - \Delta P)\Delta P = -A\left(\Delta P - \frac{\Delta\pi}{2}\right)^2 + A\frac{\Delta\pi^2}{4} \tag{2.5}$$

Therefore, the maximum power density W_{max} is obtained when ΔP is set as $\Delta\pi/2$.

$$W_{max} = \frac{1}{4} \times A \times \Delta\pi^2 \tag{2.6}$$

Equation 2.6 shows that the W_{max} is positively correlated with A and $\Delta\pi$. Since $\Delta\pi$ can be considered as a constant for the specific PRO plant because both feed and draw solutions of a PRO plant have fixed quality parameters (*e.g.* $\Delta\pi$ is about 27 bar using seawater-river water pairing). Therefore, the improvement in A value of a PRO membrane is an important way to enhance W_{max}. It's generally accepted that the threshold of W_{max} is 4 ~ 6 W m^{-2}, below which the engineering of PRO plant would not be theoretically feasible (Skilhagen *et al.*, 2008). The earliest PRO research using conventional RO membrane only obtained the W_{max} value <1 W m^{-2} (Lee *et al.*, 1981a; Loeb, 1998). The availability of HTI FO membrane enhanced this W_{max} value to 5.1 W

m^{-2} (draw solution is 60 g L^{-1} NaCl and feed solution is deionized water) at coupon test (Achilli *et al.*, 2009a). Yip *et al.* reported that W_{max} of 10 W m^{-2} could be achieved with their lab-fabricated thin film composite (TFC) PRO membrane that consisted of a polyamide selective layer and a phase inversion fabricated polysulfone support layer (Yip *et al.*, 2011). And in 2013, Song *et al.* achieved a new record of W_{max} as high as 21.3 W m^{-2} with their thin film nanocomposite (TFNC) PRO membrane that consisted of a polyamide selective layer and a electrospun nanofiber structured support layer (Song *et al.*, 2013).

It's worthy to emphasize that very recently (Nov. 2015), Straub *et al.* from Menachem group at Yale University published a critical review on *Energy & Environmental Science* to discuss the economic feasibility of power generation from PRO process. They argued that the pairings of (impaired) river water with seawater or RO concentrated brine are not effective to recover energy from saline gradient, because practical energetic inputs for pretreatment and membrane fouling cannot be neglected. Furthermore, they concluded that the only viable way to generate power from osmotic energy is to choose hypersaline source (*e.g.* hypersaline lakes *e.g.* Dead Sea, or hypersaline wastewater *e.g.* oil & gas exploration produced water *etc.*) as the draw solution (Straub *et al.*, 2016). Their work also justifies the significance of this thesis that is to develop a highly antifouling FO membrane specially for the treatment of hypersaline oil/water mixtures.

2.3.5. Medical industry

FO technology has been proposed in medical industry primarily for two kinds of applications: (1) osmotically controlled drug delivery *in vivo* and (2) osmotic enrichment of pharmaceuticals.

2.3.5.1. Osmotically controlled drug delivery

Traditional drug delivery through oral ingestion is inferior in the control of drug release, which often causes poor therapeutic activity and considerable side effects (Verma *et al.*, 2000). Novel controlled drug release technologies enable the drug concentration to be maintained at optimum level in the target region over a long period, among which osmotically controlled drug delivery system (also named as osmotic

pump) becomes a very successful approach (Zhu *et al.*, 2010; Herrlich *et al.*, 2012). The remarkable advantages of osmotic drug delivery technology over other rate-controlled drug release systems are (1) the independence on electric energy and (2) accurate adjustment of mass transport (Verma *et al.*, 2002). Although the specific configuration varies among different types, four components are indispensable in an osmotic pump: (1) drug reservoir, (2) FO membrane, (3) osmotic agent (draw solute), and (4) a microactuator (Sareen *et al.*, 2012).

When the osmotic pump is brought into contact with blood or tissue fluid, osmotic gradient drives the water to diffuse through the FO membrane. Thereby, the draw solution expands and thus pushes the microactuator to adjust the process (Su *et al.*, 2002). Along with the pressure buildup in reservoir, drug is released through the delivery channel towards the target area *in vivo*. Ideally, the osmotic pressure difference can be kept nearly as a constant during drug release period, so the liquid drug is pushed out at a steady rate (Singer, 2004).

2.3.5.2. Enrichment of pharmaceuticals

Non-thermal concentration is an important process during the manufacture of pharmaceuticals especially for those heat-sensitive products. Therefore, FO could serve as a competent option for the enrichment of pharmaceuticals. In 2009, Yang *et al.* investigated the use of FO technology to concentrate lysozyme with $MgCl_2$ as the draw solute (Yang *et al.*, 2009b). In 2010, Nayak proposed to concentrate anthocyanin through FO process (Nayak & Rastogi, 2010). In 2011, Wang *et al.* conducted lab-scale experiments on the concentration of protein solutions by a FO-MD hybrid system and reported that their system was stable in continuous operation when dehydration rate equaled to the distillation rate (Wang *et al.*, 2011). All the above studies imply that FO is promising to achieve the enrichment without generating denaturing effect on the pharmaceuticals.

2.3.6. Food dehydration

Conventional food dehydration processes based on evaporation or pressure-driven membrane technique cause severe quality deterioration in color, taste, aroma, nutritional values *etc.* (Dalla Rosa & Giroux, 2001; Petrotos & Lazarides, 2001). FO

technology shows promises to outperform these conventional processes owing to its low hydraulic pressure working manner. The investigations on the utilization of FO technology to concentrate liquid food (*e.g.* fruit juices, vegetable juices, *etc.*) were initiated in late 1990s. And the availability of HTI membrane helped push ahead the research on this topic (Dova *et al.*, 2007; Petrotos *et al.*, 2010). The review published by Jiao *et al.* on recent progress of food treatment is recommended for more details (Jiao *et al.*, 2004).

Different from desalination or water purification through FO process as discussed previously, the final product in food/pharmaceutical dehydration is the concentrated feed solution. In order to avoid the deterioration of feed solution quality by reverse salt leakage (J_S), edible draw solute is usually employed to run the FO process. For example, Beaudry *et al.* proposed Brix sugar as the draw solute for the concentration of fruit juice through FO process (Beaudry & Lampi, 1990). Wrolstad *et al.* investigated the use of fructose corn syrup as the draw solution to dehydrate raspberry juice through FO process and they reported that the flavor of the product was preserved (Wrolstad *et al.*, 1993).

2.3.7. Draw solution regeneration-free applications

Generally speaking, FO technology does not have to recycle the draw solute under two situations. The first situation is that the diluted draw solution is consumed directly as the final product, such as HTI hydration package mentioned in section 2.3.2. The second situation is that the diluted draw solution can be discharged safely without further treatment in order to save cost. In the second situation, the draw solution is usually cheap or abundant, *e.g.* seawater or RO concentrated brine. Hoover *et al.* argued that draw solution regeneration-free applications of FO technology could enhance the environmental sustainability under certain scenarios (Hoover *et al.*, 2011). Draw solution regeneration-free FO process is a truly low energy technology, because no energy is spent on the recovery of draw solute. This section enumerates some notable examples of draw solution regeneration-free FO technology as follows.

2.3.7.1. Direct fertigation

Phuntsho *et al.* proposed to employ fertilizers as the draw solute to reclaim water from

seawater with the diluted draw solution used directly for irrigation (Phuntsho *et al.*, 2011). However, more works are needed to examine whether this approach will be harmful to the plants.

2.3.7.2. Osmotic backwashing

FO process was proposed as a membrane friendly technique to clean RO/NF membranes (Ramon *et al.*, 2010), in order to avoid membrane deterioration and secondary pollution caused by chemical cleaning (Sagiv & Semiat, 2005). Qin *et al.* reported that osmotic backwashing could be effective to clean RO membrane with municipal secondary effluent based upon their pilot scale tests (Qin *et al.*, 2010).

2.3.7.3. Osmotic dilution of RO concentrated brine

Concentrated brine of seawater RO plants arouses environmental concerns because it will impair coastal water quality and endanger marine life when discharged into the sea without any treatments (Lattemann & Hopner, 2008). Hoover *et al.* proposed to mitigate the detriments of RO concentrated brine through osmotic dilution (Hoover *et al.*, 2011).

2.3.7.4. Concentration of oil-producing algae

Microalgae have been suggested as the good candidates other than terrestrial crops for the production of biodiesel, owing to their higher photosynthetic efficiency and no occupation of land (Miao & Wu, 2006; Wiley *et al.*, 2011). However, the major obstacle here is the lack of economical way to dewater the algae broth for further process. NASA investigated the use of seawater as the draw solution to dewater algae culture through FO process. This process is termed as offshore membrane enclosure for growing algae (OMEGA) technology, with its more details found at the indirect citation source (Hoover *et al.*, 2011).

2.4. Critical challenges confronted by FO technology

Although FO technology has tremendous potential in many areas as discussed in section 2.3, it is not widely embraced by the industry up to now. Noteworthily, many of the above lab-scale proposals have to go a long expedition before they can be transformed into full-scale applications. This is because there are three critical

challenges to overcome for the industrialization of FO technologies: (1) the lack of a highly antifouling selective layer, (2) the lack of a highly interconnected porous support layer, and (3) the lack of a suitable draw solute.

2.4.1. The lack of highly antifouling selective layer

The selective layer determines the antifouling and salt-rejecting capabilities of FO membrane while influences membrane water permeability (*A* value) and FO water flux (J_W) to a considerable extent. The ideal FO selective layer should simultaneously possess high antifouling ability, high water permeability and high selectivity ("3 high" selective layer). However, there is a long march to achieve this goal. This is partially because it's already very difficult to balance high water permeability with high salt rejection. Therefore, when antifouling capability is also taken into account, the goal of "3 high" selective layer becomes even more challenging especially when principally relying on one material to synthesize it.

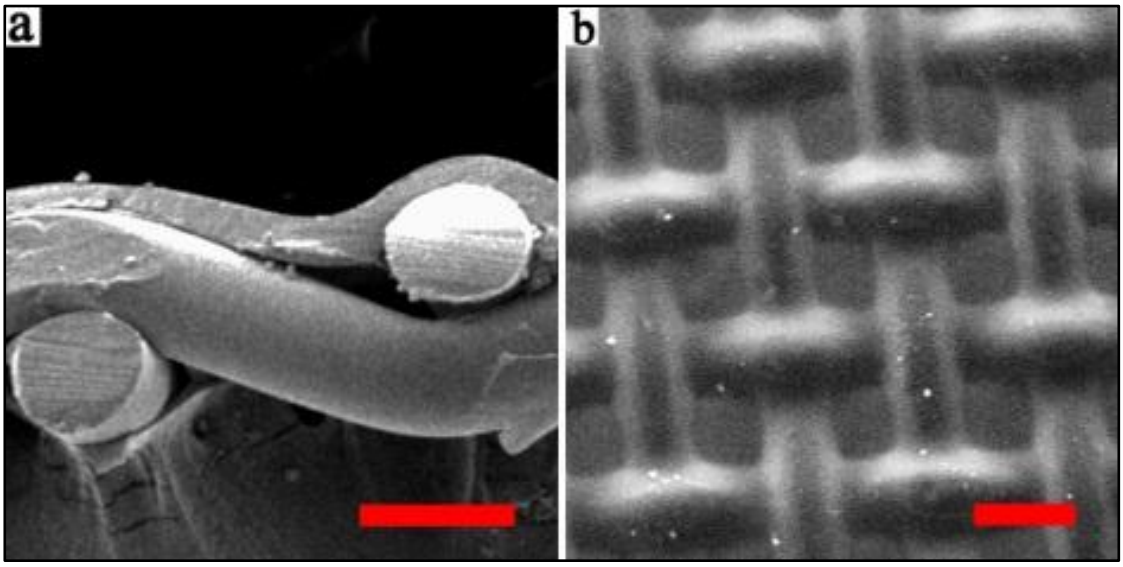

Figure 2.2 HTI FO membrane structure characterized by FESEM. The membrane is CTA woven. (**a**) Membrane cross-section, scale bar, 50 μm. (**b**) Membrane top surface, scale bar, 100 μm.

Currently, no FO membrane selective layer can meet the "3 high" requirements to the best knowledge of the author. The only commercially available HTI FO membrane (CTA) has low water permeability due to its thick selective layer (~1 μm) and low selectivity. This results in the low J_W and poor J_W/J_S of HTI membrane as observed from many previous peer studies. For example, Lay *et al.* reported that the water flux

of OMBR using HTI FO membrane with 0.5 M NaCl as draw solution is only around 5 L m^{-2} h^{-1} (Lay *et al.*, 2012). And Ge *et al.* reported that the water flux of OMFC using HTI FO membrane is as low as 2 ~ 3 L m^{-2} h^{-1} (Ge & He, 2012). The low J_W drawback of HTI membrane will cause lots of problems for the engineering of FO process such as large membrane area, big reactor size, high capital cost *etc.*, and thus render the corresponding FO technology economically less competitive. Meanwhile, the antifouling property of HTI membrane is also poor. Previous peer studies have observed considerable fouling extents of HTI membrane in various FO processes (Mi & Elimelech, 2010; Zhang *et al.*, 2012a; Zou *et al.*, 2013). Taking account of that the material to fabricate HTI membrane (*i.e.* CTA) is relatively hydrophilic, this thesis attributes the poor antifouling capability of HTI membrane to its uneven topography. As displayed in Figure 2.2a, the embedded woven polyester mesh enables the total thickness of HTI membrane to be reduced to ≤ 50 μm. But under this architecture, membrane surface region on top of mesh fiber forms the convex parts while the surface region in-between mesh fibers forms the concave parts, as shown in Figure 2.2b. This makes the topography roughness of HTI membrane as high as tens of micrometers. As a result, foulants can easily deposit and accumulate in clog the concave parts of HTI membrane surface. This viewpoint will be verified by the experimental results of this thesis (Chapter 6).

Moreover, recent developments in FO membrane usually ignore the issue that a genuine FO membrane must possess good antifouling capability and their FO membranes cannot meet the "3 high" requirements either. This is because most of the proposed TFC FO membranes choose aromatic polyamide as the selective layer (Wei *et al.*, 2011; Widjojo *et al.*, 2011; Bui & McCutcheon, 2013; Setiawan *et al.*, 2013; Huang & McCutcheon, 2015). Polyamide selective layer outperforms its predecessors owing to is high rejection of monovalent salt ions (~99% rejection of NaCl) (Service, 2006) and has dominated RO membrane technology for more than 30 years (Geise *et al.*, 2010), though it is not good in all the three properties (*i.e.* antifouling capability, water permeability, and salt rejection). In fact, RO membrane with polyamide selective layer is prone to severe fouling due to its hydrophobic property (Gilron *et al.*, 2001; Hurwitz *et al.*, 2010) and rough topography (Elimelech *et al.*, 1997; Zhu & Elimelech, 1997). Despite its inferiority in antifouling ability, polyamide RO membrane seizes the

foothold in desalination and water purification technologies because RO process is usually designated as the terminal process to provide freshwater product and the upstream pretreatment unit (*e.g.* MF or UF) helps to protect RO membrane from severe fouling.

However, the copy of existing RO membrane selective layer (*i.e.* polyamide) directly to FO membrane is not a "shortcut" but virtually a "*cul-de-sac*". As discussed previously, only through tackling a tough job *e.g.* to treat highly fouling/saline wastewater can FO-draw solution regeneration technology compensate its low energy-efficiency. Noteworthily, the inherent hydrophobicity and rough surface of polyamide will result in severe flux decline, more frequent cleaning and shorter membrane life during the treatment of those challenging wastewater, which will deprive FO process of its true value (*i.e.* low fouling potential). For example, Zhang *et al.* used the lab-prepared polyamide hollow fiber FO membrane in OMBR experiments and observed that fouling caused more than 45% decline of water flux (Zhang *et al.*, 2012b). Lu *et al.* reported as high as ~30% water flux decline at 500 mL cumulative permeate (water) volume of polyamide FO membrane (the draw solution is 2 M $MgCl_2$) under only 250 mg/L alginate concentration during their bench-scale test (Lu *et al.*, 2015). Therefore, it's urgent to develop a new selective layer for FO membrane that possesses excellent antifouling capability besides high water permeability and high selectivity, in order to advance FO technology especially towards the treatment of highly saline/fouling wastewater.

2.4.2. The lack of highly interconnected porous support layer

In history, significant improvements were first achieved in pressure-driven salt-rejecting membrane processes (*e.g.* RO and NF). But this also leaves a confine on the initial design and synthesis of membrane for FO applications. A typical TFC RO membrane consists of a thin and dense selective layer (thickness ~ 100 nm) on top of a polymeric support layer (thickness ~ 50 μm) which is further supported by a thick fabric (~90 μm) to reinforce mechanical strength (Lee *et al.*, 2011). These RO membranes suffer a significantly lower J_W than expectation when they are used in FO process (Loeb *et al.*, 1976; McCutcheon *et al.*, 2005). Their thick and tortuous support layer causes severe ICP problem that results in their poor FO performances (Mehta &

Loeb, 1978). Therefore, it's essential to explore the mechanism on ICP in order to innovate membrane design and synthesis.

2.4.2.1. Concentration polarization

Concentration polarization (CP) is a ubiquitous phenomenon that exists in almost all membrane processes. This thesis focuses on the CP in RO and FO processes for detailed comparison.

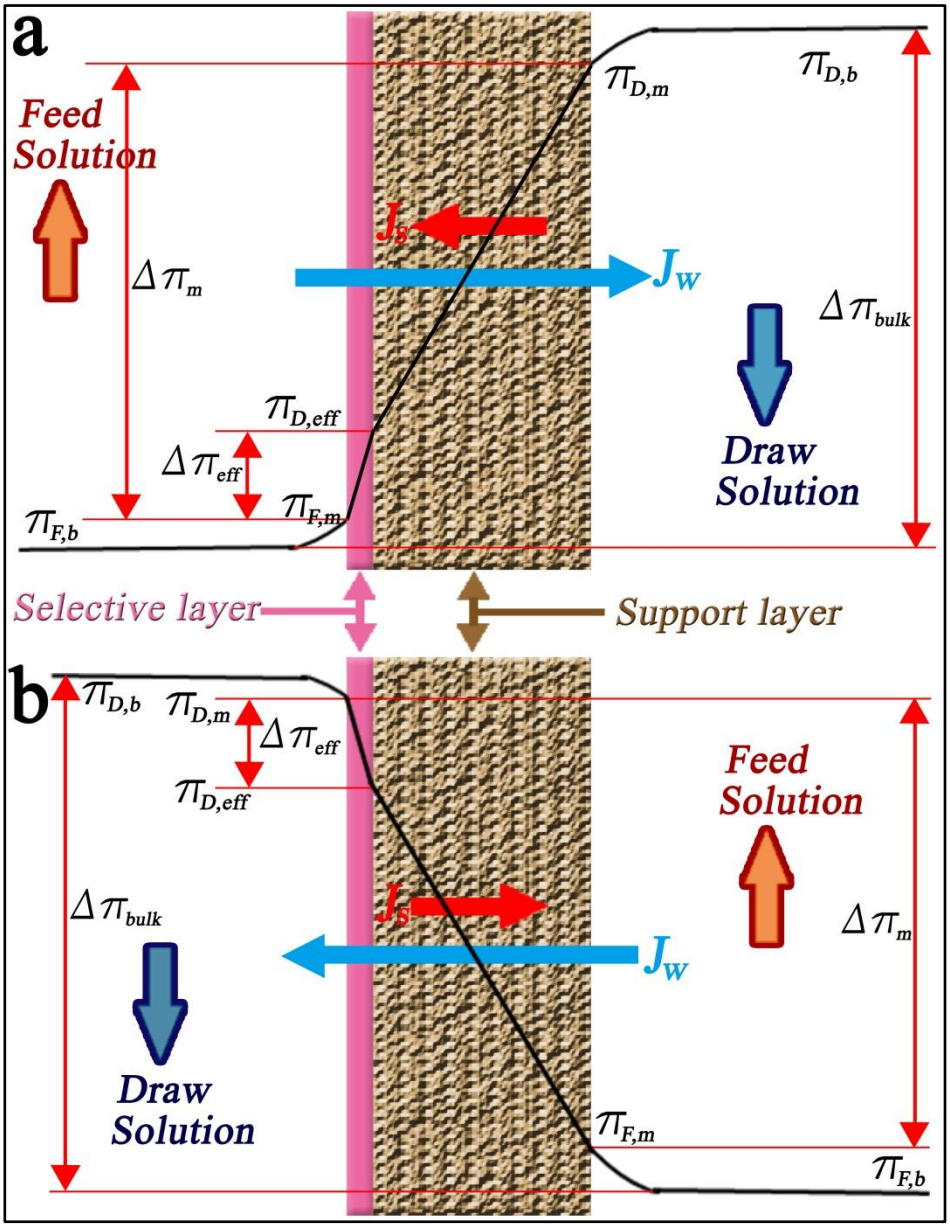

Figure 2.3 Illustration of dilutive (a) and concentrative (b) ICP across a composite or asymmetric membrane in FO process. This figure is redrawn with significant improvements based upon (Cath *et al.*, 2006).

In RO process, the convective water flow drags the solute from feed solution bulk to membrane surface, wherein membrane selective layer allows water molecules to pass through but retains the solute molecules. As result, the solute concentration on the surface of membrane becomes much higher than that in the bulk of feed solution, which increases the osmotic pressure difference ($\Delta\pi$) across membrane. As a result, a higher hydrostatic pressure needs to be applied in order to buffer against the decrease in virtual driving force (ΔP-$\Delta\pi$). This phenomenon is termed as external concentration polarization (ECP) (Goosen *et al.*, 2004), for it occurs outside the membrane. Particularly, water flux and salt flux of RO process are in the same direction and hence water flux helps to bring the penetrated salt solute out of membrane. Therefore, there is no accumulation of solute inside the membrane. In short, CP occurs only in one form *i.e.* ECP (concentrative ECP) in pressure-driven membrane processes.

Differently, CP becomes much complex in FO process because the water flux (J_W) and salt flux (J_S) of FO process are in opposite directions. As illustrated in Figure 2.3 which is redrawn from (Cath *et al.*, 2006), ECP takes place at both top and bottom surfaces of membrane simultaneously in each membrane orientation: concentrative ECP occurs on the membrane surface facing feed solution while dilutive ECP occurs on the membrane surface facing draw solution. Both concentrative and dilutive ECP bring down the osmotic pressure difference across the membrane ($\Delta\pi_m$). Fortunately, the adverse effect of ECP can be mitigated by increasing crossflow velocity or turbulence on membrane surface (Mulder, 1996).

In addition to ECP, CP also takes place inside asymmetric membrane in FO process, because the support layer of membrane functions as an unstirrable barrier to the diffusion of draw solute. This phenomenon is termed as internal concentration polarization (ICP), which is unique because it only occurs in osmotically-driven membrane processes (Mehta & Loeb, 1978; Lee *et al.*, 1981a; McCutcheon *et al.*, 2006). What is worse, unlike ECP the adverse effect of ICP cannot be mitigated through increasing crossflow velocity or turbulence on membrane surface.

Based upon the specific membrane orientation, ICP takes place in the form of either concentrative or dilutive, as displayed in Figure 2.3. In detail, when selective layer is

set facing feed solution (*i.e.* FO mode), as water molecules permeates through selective layer into support layer, the draw solution within the support layer is being diluted. The osmotic pressure of draw solution at the interface between selective layer and support layer ($\pi_{D,eff}$) becomes considerably lower than that at the bottom surface of membrane ($\pi_{D,m}$). As a result, the effective driving force (*i.e.* effective osmotic gradient across membrane selective layer, $\Delta\pi_{eff}$) turns to be significantly lower than $\Delta\pi_m$ ($\Delta\pi_m \leq$ osmotic difference between draw and feed solution bulks $\Delta\pi_{bulk}$). This is specified as dilutive ICP (Figure 2.3a). When selective layer is set facing draw solution (*i.e.* PRO mode), as water molecules permeates through membrane selective layer out of support layer, the draw solution within the support layer is being concentrated. $\pi_{D,eff}$ becomes considerably higher than $\pi_{D,m}$. As a result, $\Delta\pi_{eff}$ also turns to be significantly lower than $\Delta\pi_m$ ($\Delta\pi_m \leq \Delta\pi_{bulk}$). This is specified as concentrative ICP (Figure 2.3b). Both dilutive and concentrative ICP works to bring down $\Delta\pi_{eff}$. Moreover, recent studies reveal that ICP is principally responsible for the much smaller FO J_W than theoretical expectation (McCutcheon & Elimelech, 2006; Zhang *et al.*, 2010; Puguan *et al.*, 2014; Yasukawa *et al.*, 2015; Yang *et al.*, 2016). Besides, ICP can couple with ECP to worsen FO performances.

2.4.2.2. Mathematical modeling of ECP in FO process

Mathematical modeling is discussed in FO process in order to reach the deep understanding of CP effects. The ECP effect in FO has been modeled using boundary layer theory by previous peer studies. The modulus of concentrative ECP is defined as equation 2.7 (McCutcheon & Elimelech, 2006).

$$\frac{\pi_{F,m}}{\pi_{F,b}} = exp\ (\frac{J_W}{k}) \tag{2.7}$$

where $\pi_{F,m}$ is the osmotic pressure of feed solution at membrane surface and $\pi_{F,b}$ is the osmotic pressure of the feed solution bulk, respectively; J_W is the experimental water flux; and k is the mass transfer coefficient. Particularly, the definition of k is given by equation 2.8.

$$k = \frac{Sh \times D}{d_h} \tag{2.8}$$

where D is the solute diffusion coefficient; d_h is the hydraulic diameter, and Sh is Sherwood number that can be calculated from Reynolds number (Re) and Schmidt number (Sc).

Similarly, the dilutive ECP can be defined as equation 2.9.

$$\frac{\pi_{D,m}}{\pi_{D,b}} = exp\ (-\frac{J_W}{k}) \tag{2.9}$$

where $\pi_{D,m}$ is the osmotic pressure of draw solution at membrane surface and $\pi_{D,b}$ is osmotic pressure of draw solution bulk, respectively; the minus sign indicates $\pi_{D,m}$ is smaller than $\pi_{D,b}$.

According to equation 2.3, the FO J_W can be expressed as equation 2.10 where the reflection coefficient σ is assumed as 1.

$$J_W = A \times (\pi_{D,m} - \pi_{F,m}) \tag{2.10}$$

Therefore, ECP effect can be modeled as equation 2.11 by substituting equation 2.7 and 2.9 into 2.10 (McCutcheon & Elimelech, 2007).

$$J_W = A[\pi_{D,b} exp\ \left(-\frac{J_w}{k}\right) - \pi_{F,b} exp\ \left(\frac{J_w}{k}\right)] \tag{2.11}$$

Equation 2.11 indicates both concentrative ECP and dilutive ECP contribute to reduce $\Delta\pi_m$ across membrane in FO process. It's worthy to note that equation 2.11 is only valid for symmetric membrane and thus the applicability of this equation is limited.

2.4.2.3. Mathematical modeling of ICP in FO process

Lee *et al.* derived the modeling for the ICP effect in PRO mode by adopting the solution-diffusion theory (Lee *et al.*, 1981b). Based on Lee's work, Loeb *et al.* developed the modeling for the ICP effect in FO mode (Loeb *et al.*, 1997). The formulae of ICP modeling are given in equation 2.12 (PRO mode) and 2.13 (FO mode).

$$J_W = \frac{1}{K}\ ln\frac{B+A\pi_{D,m}-J_W}{B+A\pi_{F,b}} \tag{2.12}$$

$$J_W = \frac{1}{K}\ ln\frac{B+A\pi_{D,b}}{B+J_W+A\pi_{F,m}} \tag{2.13}$$

where B is the solute permeability coefficient of the selective layer; and K is the solute resistivity that symbolizes the solute's ability to diffuse through FO membrane support layer. The definition of K is further introduced in equation 2.14 (Gray *et al.*, 2006; Phillip *et al.*, 2010).

$$K = \frac{S}{D} = \frac{t\times\tau}{\varepsilon} \times \frac{1}{D} \tag{2.14}$$

where D is the solute diffusion coefficient; and S is the FO membrane structural parameter that characterizes the average distance for a solute molecule to travel when

diffusing through the support layer; t is support layer thickness, τ is support layer tortuosity (dimensionless, $\tau \geq 1$; ideal support layer has τ value equaling to 1), and ε is support layer porosity (dimensionless, $0 \leq \varepsilon < 1$).

Equation 2.12 and equation 2.13 only take account of ICP effect. However, ICP and ECP occur simultaneously. Therefore, the governing formulae of J_W that takes both ICP and ECP into account are presented in equation 2.14 (PRO mode) and 2.15 (FO mode).

$$J_W = A[\pi_{D,b}\, exp\left(-\frac{J_w}{k}\right) - \pi_{F,b}\, exp(J_w K)] \quad (2.14)$$

$$J_W = A[\pi_{D,b}\, exp(-J_w K) - \pi_{F,b}\, exp\left(\frac{J_w}{k}\right)] \quad (2.15)$$

2.4.2.4. The bottleneck of ICP on FO technology

Previous studies found that the experimental results of FO J_W match well with the ICP modeling aforementioned in last section and thus confirmed that ICP modulus dominates the diminution in effective osmotic driving force (McCutcheon & Elimelech, 2006; McCutcheon & Elimelech, 2007). What's even worse, the negative impact of ICP on J_W is aggravated exponentially along with the increase of J_W. This is defined as self-limiting phenomenon of FO J_W which signifies the bottleneck of ICP on FO performance (McCutcheon & Elimelech, 2006). Therefore, the increase in FO J_W as the return of the increase in draw solution osmotic pressure ($\pi_{D,b}$) becomes gradually smaller especially at high $\pi_{D,b}$ values.

The primary method to break this ICP bottleneck is through innovating support layer structure *i.e.* reducing S value. As indicated by equation 2.14, three parameters *i.e.* t, τ and ε constitute S. In theory, the decrease in t or τ, or the increase in ε will all lead to the decrease of S. However, the decrease in t and the over increase in ε would adversely affect the mechanical strength of FO membrane. Therefore, the smartest way to reduce S value is to reduce the tortuosity (τ) of support layer. Traditional RO membranes have the S value as high as 9600 μm, explaining their extremely poor performance in FO processes. Yip *et al.* reduced the S value of RO membrane from 9583 μm to 2155 μm through peeling off its nonwoven fabric (Yip *et al.*, 2010). However, the S value is still too high. HTI membrane has an S value of ~600 μm. TFC polyamide FO membrane with conventional phase inversion constructed support layer

(with certain adjustment on the composition of conventional polymer dope solution) is reported to reduce the *S* value to ~400 μm (Tiraferri *et al.*, 2011; Wang *et al.*, 2012a). And the main reason for the relatively high *S* value of FO membrane with conventional phase inversion constructed support layer is its high τ value ($\geq$ 3.0). Therefore, there is still a large room to further reduce τ value so as to bring down *S* value, for the purpose of battling against ICP problem.

In 2011, a breakthrough has been made by Song *et al.*, who utilized electrospun nanofiber to construct FO membrane support layer and as-fabricated support layer has scaffold-like structure with ultrahigh pore interconnectivity in all three dimensions at micrometer scale (Song *et al.*, 2011). This scaffold-like support layer has the τ value as low as 1.26, which endows its FO membrane (selective layer is polyamide) with remarkable advantages of small ICP limitation and high water flux. However, the low productivity and high cost of electrospun nanofiber impede the practical applications of this kind of FO membrane. Therefore, it's still in high demand that the support layer with highly interconnected pore structure can be constructed through affordable membrane manufacture processes (*e.g.* phase inversion).

2.4.3. The lack of suitable draw solute

Draw solute is another indispensable part besides membrane in FO technology. Although the selection of draw solute cannot reduce the total energy input for FO-draw solution regeneration process, it does determine the form of input energy (high grade or low grade) and also define the specific configuration and operation of process. Both the physicochemical properties of draw solute and the end use purpose of FO process will influence the selection of draw solute. Therefore, the specific requirements on draw solute vary from case to case. In particular, desalination or water purification for drinking purpose requires that the draw solute should be nontoxic. FO enrichment of pharmaceuticals demands reverse solute leakage to be as small as possible in order to maintain high purity of final product. Edible draw solute is favorable in FO dehydration of food and its reverse leakage should not impair the flavor. Draw solution for clean power production should generate high osmotic pressure and hence hypersaline wastewater (*i.e.* oil & gas exploration produced wastewater) may be a good candidate. Draw solution generation-free technology require the draw solute to

be inexpensive or abundant, which after osmotic dilution can be consumed directly or discharged without further treatment.

But in general, there are some common criteria on FO draw solute which is still far to fulfill. Firstly, the draw solute is able to generate sufficient osmotic pressure that can be used as the driving force. Secondly, the draw solute will not foul or damage FO membrane. Last but not least, inevitable adverse effects *i.e.* ICP and reverse solute leakage should be carefully examined (Zhao & Zou, 2011). Detailed information can be found in the following interesting studies on FO draw solute (McCormick *et al.*, 2008; Achilli *et al.*, 2010; Ling *et al.*, 2010; Yen *et al.*, 2010; Bai *et al.*, 2011; Li *et al.*, 2011; Liu *et al.*, 2011; Kim *et al.*, 2014; Lee & Lee, 2014).

2.5. Recent development of FO membrane

The potential benefits of FO technology, the unsatisfactory FO performances of existing membranes, and the extremely limited FO membrane availability in both industry and research fields drive the boom in FO membrane development during last decade. The research aim of these studies varies significantly; some of them did achieve improvements in certain areas that are worthy to note. However, it's only recent 1~2 years the voice comes out in scientific world to declare that the true future for FO technology is to tackle those highly fouling/saline wastewaters (McGovern & Lienhard, 2014; Shaffer *et al.*, 2015; Straub *et al.*, 2016). And the highly antifouling capability is a requisite of genuine FO membrane that should not but actually frequently be dodged by existing studies. Therefore, the current stage is still far from offering a genuine FO membrane that enable FO technology to seize the foothold in mainstream water/wastewater industry. This section carefully reviews the studies on the development of FO membrane, with the emphasis on the strong and weak points of previous peer works.

2.5.1. Integral asymmetric FO membranes

FO membranes can be classed into two groups based upon membrane structure: (1) integral asymmetric and (2) thin film composite (TFC). "Integral" means both selective layer and support layer are made from the same material while "asymmetric" means the selective layer is different from (more compact than) support layer in

structure. Integral asymmetric membrane is usually fabricated by phase inversion technique. So its synthetic process is relatively simple. But it's quite difficult to accomplish a good balance between high water permeability and high salt rejection for the integral asymmetric membrane. For example, high salt rejection requires the selective layer to be compact, which usually makes the support layer to be less porous since selective layer and support layer are formed in one process. As a result, the improvement in salt rejection usually brings forth the decrease in FO J_W and undefined result on membrane selectivity (J_W/J_S).

HTI FO membrane (CTA) is an integral asymmetric membrane that is far from the requirements on a genuine FO membrane *i.e.* high antifouling capability, high water flux and high selectivity ("3 high") as discussed previously. Some other research articles to verify this standpoint can be found elsewhere (Tang & Ng, 2008; Jin *et al.*, 2011; Li *et al.*, 2012b). Recently, scientists tend to use HTI membrane to compare with their lab-fabricated FO membrane rather than reply on HTI membrane to demonstrate a FO application.

Other efforts that tried to develop integral asymmetric FO membrane include the studies on cellulose acetate FO membrane (Su *et al.*, 2010; Wang *et al.*, 2010a; Sairam *et al.*, 2011) and polybenzimidazole (PBI) (Wang *et al.*, 2009; Yang *et al.*, 2009a; Flanagan & Escobar, 2013) FO membrane. However, their membrane performances in terms of FO J_W and J_S are generally inferior to TFC FO membrane, which is principally ascribed to the intrinsic structure limitation of integral membrane.

2.5.2. Thin film composite FO membranes

For TFC membrane, "Thin film" means the overall thickness of membrane is in the scale of 100 micrometer (typically < 150 μm) while "composite" means the selective layer and support layer are from different materials. Usually, the selective layer is ultrathin in thickness (< 1 μm, and typically < 300 nm) and compact in structure. Particularly, salt-rejecting selective layer is non-porous in at least nanometer scale. Meanwhile, the support layer has a porous structure with its thickness dominating the overall thickness of membrane. The support layer, which is not able to retain draw solute, is primarily used to provide mechanical strength for TFC membrane (Ismail *et*

al., 2015). Viewed in membrane synthetic process, the support layer and selective layer are fabricated in separate processes: support layer is prepared first and following this the selective layer is constructed on top of as-fabricated support layer. This allows selective layer and support layer to be tailored separately towards each optimum structure and property. Therefore, it's not surprising that TFC FO membrane is often reported to be superior to integral asymmetric FO membrane in both water flux and salt rejection. The recent developments in TFC FO membrane are discussed as follows. It's worthy to note that these works on TFC FO membrane are at the early stage and none of them meet the "3 high" requirements (high antifouling capability, high water flux, and high selectivity).

2.5.2.1. The development in the selective layer for TFC FO membrane

From 2010 to date, the studies on the selective layer of TFC FO membrane are mainly involved with two kinds of polymeric material: polyelectrolyte and polyamide.

Polyelectrolytes are polymers with charged groups in the repeat monomer units whereby the ion pair can dissociate in polar solvent (*e.g.* water) releasing the ion in solution and leaving the counter charge on polymer (Joseph *et al.*, 2014). Particularly, polycation has positively charged monomer units and polyanion has negatively charged monomer units, both of which have been investigated as TFC FO membrane selective layer. In 2011, polyethyleneimine (PEI, polycation) was proposed as the selective layer of TFC FO membrane with polyamide-imide (PAI) as the support layer (Setiawan *et al.*, 2011). At the same year, layer-by-layer (LbL) assembly method, which makes use of the electrostatic attraction between polycation (*e.g.* polyallylamine hydrochloride, PAH) and polyanion (*e.g.* polystyrenesulfonate, PSS) to fabricate NF membrane selective layer, was applied for the synthesis of FO membrane selective layer (Qi *et al.*, 2011). Other efforts on TFC FO membrane with polyelectrolyte as selective layer can be found elsewhere (Qiu *et al.*, 2011; Qi *et al.*, 2012; Duong *et al.*, 2013; Liu *et al.*, 2013; Lee *et al.*, 2015), with support layer in both flat-sheet and hollow-fiber forms included.

However, it's important to emphasize that they are several drawbacks of polyelectrolyte selective layer. Firstly, the TFC FO membrane with polyelectrolyte as

selective layer even after additional chemical crosslinking only arrives at NF level selectivity. So the rejection of monovalent ions (especially Cl^-) by polyelectrolyte selective layer is poor, which result in severe reverse salt flux (J_S) when monovalent ionic salt is used as draw solute. Secondly, the selective layer of FO membrane is electrically charged (either positively or negatively). This will enhance the electrostatic attractions between selective layer and oppositely charged foulants and thus exacerbate membrane fouling. This issue is particularly critical when polycation is layered on the upmost surface of FO membrane because many foulants in aqueous environment are reported to be negatively charged. Last but not least, the complex fabrication procedure (especially for LbL assembly) and high material cost of polyelectrolyte obstruct the mass production of this kind selective layer.

Polyamide is formed through the polymerization of polyfunctional amine monomer (*e.g. m*-phenylenediamine, MPD) that is dissolved in water and polyfunctional acid chloride monomer (*e.g.* trimesoyl chloride, TMC) that is dissolved in organic solvent at the interface of the two immiscible solvents (*i.e.* interfacial polymerization, IP) (Ghosh *et al.*, 2008). The first study on the synthesis of polyamide as the selective layer of TFC FO membrane was reported by Yip *et al.* in 2011. And their hand-cast polyamide membrane attained >18 L m^{-2} h^{-1} J_W using 1.5 M NaCl as draw solution with the salt rejection around 97% (Yip *et al.*, 2010). The other works on the use of polyamide as FO membrane selective layer can be found elsewhere (Chou *et al.*, 2010; Wang *et al.*, 2010b; Han *et al.*, 2012a; Li *et al.*, 2012a; Sukitpaneenit & Chung, 2012; Luo *et al.*, 2014; Ong *et al.*, 2015).

As mentioned in section 2.4.1., the drawbacks of TFC FO membrane with polyamide selective layer include hydrophobic (oleophilic) property and rough topography. For example, Castrillon *et al.* observed that the water contact angle of their fabricated TFC polyamide FO membrane is ~100 °, confirming the hydrophobicity of polyamide selective layer (Castrillon *et al.*, 2014). Membrane hydrophobicity has been verified to induce more irreversible fouling via hydrophobic adsorption of foulants on membrane surface since many foulants have hydrophobic properties (Yamagiwa *et al.*, 1993; Shen *et al.*, 2010). Han *et al.* reported that the TFC polyamide FO membrane has typical ridge-and-valley surface structure, which is the same type topography with that of TFC

polyamide RO membrane. And the root-mean-square (RMS) roughness of their hand-fabricated FO membrane topography is as high as 116.4 nm (Han *et al.*, 2012b). The intrinsic rough topography of interfacially polymerized polyamide selective layer has been revealed as an important reason for colloidal fouling of TFC membrane: foulants preferentially deposit on and further clog the valley regions (Elimelech *et al.*, 1997) on membrane surface.

Interestingly, the embedment of nanoparticle (*e.g.* zeolite, TiO_2, alumina, *etc.*) or other substance (*e.g.* aquaporin *etc.*) into the polyamide selective layer of TFC RO membrane via IP step has been investigated for the purpose of improving the water permeability of RO membrane (Xu *et al.*, 2013). Similarly, this method has also been applied to synthesize the polyamide selective layer of TFC FO membrane, with the relevant studies found elsewhere (Ma *et al.*, 2012; Amini *et al.*, 2013; Wang *et al.*, 2013; Niksefat *et al.*, 2014; Ghanbari *et al.*, 2015). However, there are several drawbacks of the embedment of nanoparticles or other substance in polyamide selective layer. Firstly, since polyamide selective layer is as thin as ~100 nanometers, the embedment of nanoparticle/substance can easily cause the formation of heterogeneous defects that will exacerbate reverse salt leakage. Secondly and more importantly, the embedment of nanoparticle/substance cannot effectively smoothen the ridge-and-valley rough topography of polyamide selective layer. Thirdly, the improvement in membrane surface hydrophilicity by such embedment varies remarkably from case to case among different nanoparticles/substances due to the uncertainty on the ratio of filler exposed at the upmost surface to that enclosed inside polyamide layer. Last but not least, the filler embedded polyamide selective layer should be examined carefully under long term FO operation because draw solution usually provides a highly saline environment (the salinity of draw solution can be similar with or even several times higher than that of seawater) that may undermine the stability and effectiveness of the embedded filler especially aquaporins.

In short, it’s urgent to develop a new selective layer other than polyelectrolyte and polyamide in order to endow as-synthesized TFC FO membrane with highly antifouling capability, high water permeability, and high selectivity.

2.5.2.2. The development in the support layer for TFC FO membrane

As aforementioned, FO membrane structure parameter (S) has positive linear correlation with porosity (ε) and negative linear correlation with tortuosity (τ) as well as thickness (t). The decrease in t and over-increase in ε impairs membrane mechanical strength, which will adversely affect the practical application of membrane. Therefore, a suitable support layer for FO membrane should have minimized τ besides reasonably thin t (50~100 μm) and high ε (70%~90%). Here, the difficulty is how to minimize the tortuosity of support layer. In other words, the challenge is how to construct a support layer with its interior pores highly interconnected in all three dimensions at micrometer scale, because this highly interconnected pore structure can facilitate the water molecules to find and take the shortest path from top surface to bottom surface inside support layer with smallest resistance.

As introduced in section 2.4.2.4., Song *et al.* in 2011 demonstrated that support layer in scaffold-like structure with ultrahigh pore interconnectivity at micrometer scale in all three dimensions can break the bottleneck of ICP (Song *et al.*, 2011). The scaffold-like structure support layer of ultrahigh interior pore interconnectivity endows their synthesized TFNC FO membrane with ultralow tortuosity (as low as 1.26), which is nearly one third as that of TFC FO membrane with conventional phase inversion constructed support layer (3.65), and one fourth as that of HTI CTA non-woven FO membrane (4.96). As a result, TFNC FO membrane with support layer in scaffold-like structure attains the J_W of 37 L m^{-2} h^{-1}, outclassing that of TFC membrane with conventional phase inversion constructed support layer (11 L m^{-2} h^{-1}) and that of HTI membrane (5.5 L m^{-2} h^{-1}) under identical experimental condition (draw solution is 0.5 M NaCl and feed solution is deionized water). Stimulated by this work, some other scientists also put effort into TFC FO membrane with support layer in scaffold-like structure via the same technical route (Bui & McCutcheon, 2013; Hoover *et al.*, 2013; Puguan *et al.*, 2014; Tian *et al.*, 2014).

However, this scaffold-like structure is obtained through the deposition of electrospun polymeric nanofibers while the low productivity, high cost, and less environmentally-benign fabrication manner (*i.e.* the organic solvent is evaporated into gas form during the electrospinning process that needs sufficient treatment before

discharge into environment) of electrospinning make it hardly affordable for scale-up production. Therefore, it's necessary to explore other cost-effective methods to synthesize the support layer in highly interconnected pore structure.

The other pioneering direction on the development of TFC FO membrane support layer is to modify support layer structure and property by the leverage of nanotechnology. Usually, the nanomaterial is mixed as an additional ingredient in polymer dope solution that is used to fabricate the support layer. This technique is relatively uncomplex and compatible with prevailed membrane manufacture process (*e.g.* phase inversion). For example, Ma *et al.* in 2013 proposed to add commercial zeolite nanoparticles (40-150 nm, Sigma-Aldrich) into PSf polymer dope solution for the fabrication of TFC FO membrane support layer. And they observed that the optimum zeolite loading is 0.5 wt% in entire dope solution and the increase of zeolite loading to 1.0 wt% will lead to considerable decrease in both FO membrane salt rejection and support layer porosity (Ma *et al.*, 2013). Emadzadeh *et al.* in 2014 proposed to use commercially available TiO_2 nanoparticle (Degussa P25, Evonik) as the additional ingredient to prepare the support layer of TFC FO membrane via phase inversion technique. And they found the introduction of TiO_2 nanoparticle can lead to the enhancement of FO membrane water permeability owing to the increase in support layer porosity and hydrophilicity (Emadzadeh *et al.*, 2014b). Furthermore, they reported that their TFC FO membrane with PSf-TiO_2 support layer has better water flux recovery from fouling decline compared to that with virgin PSf support layer at PRO operation mode possibly owing to the improvement in support layer hydrophilicity (Emadzadeh *et al.*, 2014a). In 2015, Liu *et al.* proposed to add commercial fumed silica (SiO_2, Sigma-Aldrich) nanoparticle into polysulfone (PSf) dope solution for the fabrication of TFC FO membrane support layer. They reported that the addition of SiO_2 nanoparticle improves the water flux of as-fabricated TFC FO membrane and their best FO membrane with PSf/SiO_2 support layer attains 31.0 L m^{-2} h^{-1} water flux at FO mode using 1.0 M NaCl as draw solution and deionized water as feed solution. Noteworthily, because SiO_2 nanoparticle has the tendency to agglomerate and precipitate from the organic solvent of dope solution, they highlighted that a step including 30 min sonication followed by 30 min mechanical stirring was repeated five times to minimize the aggregation of SiO_2 nanoparticle (Liu & Ng, 2015).

Interestingly, all these studies did not synthesize the nanomaterial in lab but purchased the commercially available one and used it as the additional ingredient in polymer dope solution. In other words, they skip the nanomaterial synthesis step that virtually can be utilized to finely adjust the structure and property of the blended nanomaterial in order to reach a deep study leveraging membrane fabrication by nanotechnology.

Among all the material candidates that can be used as the additional ingredient in polymer dope solution for the synthesis of TFC FO membrane support layer, a special nanomaterial that is worthy to highlight is graphene oxide (GO) nanosheet as well as its derivatives. This is because graphene-based material derived from GO can be mass-produced in ton quantities at low cost via chemical route (Segal, 2009), which guarantees the scale-up manufacture of GO embedded support layer for TFC FO membrane. Furthermore, GO nanosheet and its derivative nanomaterial possess the unique properties such as extremely high lateral size to thickness ratio, high surface area, strong attraction of water molecules (*i.e.* superhydrophilicity), excellent compatibility with polymeric host, outstanding chemical and thermal stabilities, and advantageous solution processibility *etc.* (Geim & Novoselov, 2007; Zhu *et al.*, 2010; Han *et al.*, 2013; Dreyer *et al.*, 2014). These properties are expected to hold great potential to engineer phase inversion process and thus can be utilized to innovate support layer structure. And from 2012 to date, GO nanosheet has been investigated as an additional ingredient in polymer dope solution to modify pore-flow membrane (especially UF membrane) for pressure-driven usages. The following research articles are recommended on the topic of GO embedded pressure-driven pore-flow membrane (Wang *et al.*, 2012b; Ganesh *et al.*, 2013; Lee *et al.*, 2013; Zhao *et al.*, 2013; Xu *et al.*, 2014; Zinadini *et al.*, 2014).

This thesis, together with several other peer works, pioneers to investigate the use of GO nanosheet as the additional ingredient in dope solution to fabricate the nanocomposite support layer for TFC FO membrane. Only very recently in 2015, Wang *et al.* proposed to employ graphene oxide modified graphitic carbon nitride (CN/rGO) as the nanofiller to synthesize the support layer for TFC FO membrane (Wang *et al.*, 2015). Besides, Park *et al.* proposed to use GO nanosheet as the filler in dope solution to fabricate the support layer for TFC FO membrane (Park *et al.*, 2015).

These two studies observed that the embedment of GO nanosheet or its derivative can modify the support layer to be more hydrophilic and thus improve FO water flux. However, none of the two studies arrives at the broad horizon on the genuine potentialities of GO, that is (1) to search and construct an entirely new support layer structure in terms of pore interconnectivity specially suitable for FO membrane, or (2) to go further to reveal the mechanism on the engineering of phase inversion process by 2D hydrophilic nanomaterial.

In fact, all those published articles on the use of GO or its derivative as nanofiller to fabricate pressure-driven pore-flow membrane do not accomplish the above two goals either. But this thesis is designed to take up these two challenges with the aim of constructing a GO incorporated support layer in entirely new pore structure specially for the suppression of ICP problem. Furthermore, unlike the studies from (Park *et al.*, 2015; Wang *et al.*, 2015) that reply on polyamide as FO membrane selective layer, this thesis explores a new selective layer that endows as-synthesized nanocomposite FO membrane with strong antifouling ability besides high water flux and high selectivity.

In short, it's highly desirable to synthesize a support layer with highly interconnected porous structure that can effectively reduce ICP problem through dominant membrane manufacture process (*e.g.* phase inversion).

2.6. The techniques to improve membrane antifouling ability

The fouling of membrane is the result of combined effects including membrane antifouling capability, foulant type and concentration, pretreatment, membrane operating conditions (*e.g.* crossflow velocity), cleaning and so on (Flemming, 2002; Seidel & Elimelech, 2002). In this thesis, the techniques to endow the membrane with better antifouling fouling property for water/wastewater treatment will be discussed. In theory, any measure that can minimize the intermolecular attraction force between membrane surface and foulant can enhance membrane antifouling capability. Viewed in the structure and property of membrane surface, there are three major characters to be controlled: (1) surface hydrophilicity, (2) topography (surface roughness), and (3) surface electric-charge. This section will review the control of each character to enhance membrane antifouling property in detail. Because the studies on FO fouling

are at the early stage, the examples in this section cover both osmotically-driven and pressure-driven membrane processes.

2.6.1. The control of membrane surface hydrophilicity

Wetting is the ability of solid surface to maintain contact with a liquid that is governed by interfacial interactions (Bonn *et al.*, 2009). Particularly, the ability of membrane to be wetted by water is hydrophilicity, which is commonly indicated by water contact angle. Hydrophilicity is a useful information to predict the fouling behavior of water/wastewater treatment membranes. It's generally acknowledged that the membrane with hydrophilic surface is less susceptible to nonspecific adhesion of foulants and the fouling is relatively more reversible (Marshall *et al.*, 1993).

The fundamental mechanism here is that the interfacial energy of membrane (selective layer) surface with water has a profound effect on fouling behavior. In particular, hydrophobic surface is high in surface energy and thus favorable for the adsorption of foulant in order to lower down its surface energy. On the contrary, hydrophilic surface is low in surface energy and thus inert or even repulsive to the adhesion of macromolecule or colloid (Rosenhahn *et al.*, 2010). Lots of experiments revealed that minimal fouling can be achieved at superhydrophilic condition with surface energy as low as 20~30 mJ m^{-2} (Baier, 2006). Surface hydrophilic modification can be realized through various techniques. And the most often used three techniques *i.e.* (1) hybrid with nanoparticle, (2) coating and (3) grafting are reviewed in this section.

2.6.1.1. Hybrid with nanoparticle

Nanoparticles (*e.g.* TiO_2, SiO_2, zeolite, *etc.*) can be used for hydrophilic modification of membrane surface in two ways: (1) incorporated into selective layer as aforementioned in section 2.5.2.1. (2) deposited onto membrane surface. For example, Ghanbari *et al.* embedded superhydrophilic TiO_2/Halloysite nanotube (HNT) nanocomposites into polyamide selective layer by IP and found the incorporation of TiO_2/HNT nanocomposite can remarkably increase the hydrophilicity of as-fabricated FO membrane and thus improve membrane's capability to resist the fouling by bovine serum albumin (BSA) (Ghanbari *et al.*, 2015). A concern on this technical route is that some nanoparticles are encapsulated within the polyamide thin films thus reducing

their efficiency to be exposed at the upmost surface (Kang & Cao, 2012).

2.6.1.2. Coating

Coating is a convenient and efficient technique to tailor the chemical property and physical structure of membrane surface (Kang & Cao, 2012). For example, Nunes *et al.* used polyether-block-polyamide copolymer to coat asymmetric porous polyvinylidene fluoride (PVDF) membrane and found as-coated composite membrane has lower susceptibility to fouling compared to commercial Amicon YM30 cellulose membrane (Nunes *et al.*, 1995). Sarkar *et al.* coated the commercial RO membranes (XLE, FilmTec. Inc.) with *in situ* crosslinked dendrimers and found the coating was able to reduce water contact angle from 60 ° to 35 ° (Sarkar *et al.*, 2010). And the example for FO membrane synthesis is that Huang *et al.* coated titanium dioxide (TiO_2) particle on the polyamide selective layer and found water contact angle was decreased from 37 ° to 27 ° after such modification (Huang *et al.*, 2015).

2.6.1.3. Grafting

Grafting is to anchor the hydrophilic species onto the membrane surface through establishing new covalent bonds (Ulbricht & Riedel, 1998). One explanation for the improved antifouling capability is that the grafted polymer chains on the membrane surface prevent the deposition of macromolecules through steric repulsion effect (Jeon *et al.*, 1991). Grafting can be classified into several different categories based on different reaction route: (1) reduction-oxidation (redox) initiated grafting (Belfer *et al.*, 2004), (2) photo induced grafting (Hilal *et al.*, 2003), (3) plasma induced grafting (Yu *et al.*, 2005; Zou *et al.*, 2011), and so on. The examples of hydrophilic surface modification through grafting technique for the synthesis of FO membrane are enumerated as follows. Tiraferri *et al.* grafted functionalized silica nanoparticles to polyamide selective layer and found the modification was able to mitigate fouling induced by alginate and BSA during FO operation (Tiraferri *et al.*, 2012). Castrillon *et al.* grafted polyethylene glycol diglycidyl ether (PEGDE) on polyamide selective layer through the bridging of ethylenediamine (EDA) and found the modified FO membrane has smaller intermolecular interactions with foulants (Castrillon *et al.*, 2014). Similarly, Lu *et al.* grafted Jeffamine (an amine-terminated polyethylene glycol derivative) to dangling chloride groups on the polyamide selective layer and found the modification

significantly improved surface hydrophilicity of FO membrane with water contact angle reduced from 94.2 ±2.5 °to 24.8 ±2.7 °(Lu *et al.*, 2013). However, it's worthy to note that the complicated fabrication procedure, time-consuming fabrication process, and high fabrication cost are the three big drawbacks that obstruct the industrialization of grafting techniques.

Moreover, it should also be noted that the coating or grafting hydrophilic species on existing selective layer surface will cause considerable decrease in membrane water permeability, because the coated/grafted substance also has its own resistance to water diffusion (Shaffer *et al.*, 2015). Noteworthily, the counterproductive result does exist as improved flux restoration after modification cannot compensate the loss in pure water permeability (Louie *et al.*, 2006). Therefore, the trade-off of "water permeability-antifouling capability" should be examined carefully in order to validate this kind of surface hydrophilic modification.

2.6.2. The control of membrane surface roughness

Membrane topography will influence foulant settlement to a large extent (Howell & Behrends, 2006). As aforementioned, rough topography suffers from severer fouling compared to smooth topography, because the valley regions of rough topography are easier to be clogged by foulants. Zhu *et al.* compared colloidal fouling behavior of TFC polyamide RO membrane with cellulose acetate RO membrane and found that interfacially polymerized selective layer had inherently higher surface roughness which resulted in the heavier fouling of polyamide RO membrane under the same operating conditions (Zhu & Elimelech, 1997). Vrijenhoek *et al.* in 2001 reported that colloidal fouling of polyamide RO and NF membranes was almost perfectly correlated with membrane surface roughness, regardless of physical and chemical operating conditions. Moreover, AFM results revealed the "valley clogging" phenomenon: colloidal particles preferentially accumulate in the "valleys" regions of membrane surface which causes severe decline of water flux (Vrijenhoek *et al.*, 2001).

Generally, there are three technical routes to smoothen membrane topography in order to enhance its antifouling capability. The first measure is to deposit an additional layer on membrane surface. For example, Wilbert *et al.* deposited polyethylene oxide (PEO)

macromolecules on the surface of commercial RO and NF membranes. And they found that after the deposition the membranes had smaller surface roughness and demonstrated better flux stability during the filtration of vegetable broth solution (Wilbert *et al.*, 1998). Louie *et al.* investigated the coating of various commercial polyamide RO membranes by polyether-polyamide block copolymer. They found that while membrane surfaces become smoother, the coating resulted in considerable decrease in pure water permeability of membrane. As a result, different water flux behaviors existed between SWC4 RO membrane (low water flux) and ESPA RO membrane (high water flux). For SWC4 RO membrane, long-term operation result indicated that the improvement in antifouling capability compensated for the decrease in pure water permeability. However, for ESPA RO membrane, the severe decrease in pure water permeability made the investment on antifouling property to be rewardless. Therefore, they inferred that the decrease of pure water permeability was because the copolymer not only covered the upmost surface of polyamide selective layer but also penetrated into the porous part of ridge-and-valley structure (Louie *et al.*, 2006). This example clearly demonstrates that the trade-off exists between antifouling capability and pure water permeability for additional coating. And the reward of additional coating varies from case to case. In order to minimize the decrease in membrane water permeability, the additional layer of coating should be sufficiently thin and inherently low in the resistance for water molecules to pass through.

The second measure is to adjust the structure of support layer especially support layer top surface. This is because selective layer is built on the top surface of support layer and hence the structure of support layer top surface has certain influences on the formation of selective layer. Han *et al.* employed oxidant induced dopamine polymerization to modify the top surface of polysulfone (PSf) support layer. Afterwards, the polyamide selective layer was built on this polydopamine modified support layer through IP to synthesize TFC FO membrane. They found that average roughness of polyamide selective layer is reduced from 94.7 nm to 60.1 nm and RMS roughness is reduced from 116.4 nm to 77.4 nm, respectively (Han *et al.*, 2012b). Unfortunately, no experimental data can be found on the impact on membrane fouling behavior by such modification of support layer top surface because they did not explore further in membrane fouling behavior. Moreover, it’s necessary to highlight

that one critical limitation of this measure is that surface chemistry of selective layer will not be changed by such support layer modification.

The third measure is to incorporate an additional ingredient during the formation of selective layer. For example, An *et al.* immobilized the polyvinyl alcohol (PVA) into the NF membrane selective layer through IP of piperazine (PIP) with trimesoyl chloride (TMC). They reported that the RMS roughness decreased proportionally from 110.7 nm to 41.6 nm along with the increase in the ratio of PVA over PIP from 0% to 16%. Besides, filtration tests indicated that the antifouling performance of as-modified NF membrane got improved (An *et al.*, 2011).

2.6.3. The control of membrane surface charge

Membrane antifouling characteristic is also related with the density and type of its surface electric-charge (Ostuni *et al.*, 2001). In aqueous environment foulant can carry electric charge through two ways: (1) the ionization of its inherent functional groups (*e.g.* –COOH, -NH_2, *etc.*), or (2) the adsorption of ions in water by the formation of electric double layer at its colloidal surface. Under some special situations where all foulants are known to carry negative charges, stable water flux may be obtained with negatively charged membrane owing to the strong electrostatic repulsion effect (Norberg *et al.*, 2007). However, taking account of the fact that wastewater usually can contain both negatively charged and positively charged foulants (Jin *et al.*, 2009), electroneutral membrane surface or surface with small electric-charge amount shall be a better way to minimize the electrostatic interactions between foulants and membrane under general scenarios.

To date, at least two methods have been investigated to modify membrane surface towards electroneutrality. One method is to use electroneutral polymer that does not have any charged or ionizable group for surface modification. For example, Zhang *et al.* proposed to use PVA to modify the surface of polypropylene non-woven fabric and found the antifouling property of modified fabric was significantly enhanced (Zhang *et al.*, 2008). Lee *et al.* also observed that the PVA coated commercial polyamide RO membrane SW30HR exhibited better antifouling property during the filtration test (Lee *et al.*, 2010b).

The other way is to employ zwitterionic polymer for the enhancement of surface electroneutrality. Zwitterionic polymer has both positive and negative groups in repeated monomer unit, but the charge amount of positive group equals to that of negative group so the polymer remains electrically neutral as a whole (Magin *et al.*, 2010). Zwitterionic polymers *e.g.* polysulfobetaine methacrylate (pSBMA), polycarboxybetaine methacrylate (pCBMA) *etc.* have been revealed to possess high resistance to non-specific protein adsorption (Li *et al.*, 2008; Vaisocherova *et al.*, 2008). The ultralow fouling mechanism of zwitterionic polymer lies in two aspects. Firstly, its charged moieties can bond water molecules tightly via electrically induced hydration and thus form a stable water barrier to resist the adhesion of foulants. Secondly, its polymer chain can be grafted on membrane surface that will block the deposition of macromolecules (*e.g.* protein) as a steric prefilter.

Zhao *et al.* demonstrated the grafting of zwitterionic polymer (pSBMA) on polypropylene MF membrane surface and as-modified membrane has significantly better hydrophilicity and resistance to protein fouling (Zhao *et al.*, 2010). In recent two years zwitterionic polymer has also been applied in the surface modification of FO membrane. For example, Nguyen *et al.* proposed to use zwitterionic amino acid (L-DOPA) to coat the bottom surface of HTI CTA FO membrane and they found that as-modified HTI membrane exhibited less organic fouling in PRO mode (bottom surface facing feed solution) (Nguyen *et al.*, 2013). Yu *et al.* proposed to graft polyzwitterions on polyamide TFC FO membrane by click chemistry and nucleophilic substitution on nitrogen and they reported that as-grafted polyamide membrane showed improved resistance to humic acid fouling during FO operation (Yu *et al.*, 2014). However, it's worthy to note that the high material cost of zwitterionic polymers makes it less competitive in scale-up applications.

In short, wise selection of material candidate for hydrophilic surface modification should take material cost and the "antifouling property-water permeability" tradeoff into account. More importantly, it's extremely valuable to explore an uncomplex method to effectively synthesize the FO membrane selective layer in one step that possesses integrated anti-fouling capabilities (hydrophilicity and underwater oleophobicity, smooth topography, and electroneutrality) besides high water

permeability and high selectivity.

2.7. Underwater superoleophobic membrane and hydrogel

2.7.1. Underwater superoleophobic membrane

From 2011 to date, the modification of pore-flow mesh or membrane surface to be underwater superoleophobic has enabled a novel technology for oil/water separation. The chemical employed for such surface modification is usually a superhydrophilic nanomaterial or hydrogel macromolecule. These underwater superoleophobic meshes or membranes have aroused remarkable attention, for they are able to achieve relatively low oil-fouling of membrane and ultrahigh separation performance (*i.e.* high water flux and high oil rejection) during the treatment of oil-polluted wastewater. For example, Xue *et al.* used the superhydrophilic hydrogel macromolecule polyacrylamide (PAM) to coat commercial stainless steel mesh (average pore diameter ~50 μm). Their as-modified mesh possessed superoleophobicity under water (underwater oil contact angle 155.3° ±1.8°) and >99.0% separation efficiency when fed by oil-in-water dispersions (Xue *et al.*, 2011). Zhang *et al.* prepared all-inorganic underwater superoleophobic mesh through surface oxidation of commercial copper mesh (average pore diameter ~60 μm) in alkaline solution with $(NH_4)S_2O_8$. The oxidation formed $Cu(OH)_2$ nanowires in diameter of 200~500 nm on mesh surface and as-modified mesh under water exhibited >150° oil contact angle and < 1 μN oil adhesion force (Zhang *et al.*, 2013). Chen *et al.* coated $CaCO_3$-based mineral on top surface of commercial polypropylene MF membrane (porosity 75%, Membrana GmbH, Germany) by an alternate soaking process. Their as-modified membrane displayed >150° underwater oil contact angle with ~4° underwater oil sliding angle. Besides, their as-modified membrane attained >99% rejection of oil with >40% loss of water flux during 30 min filtration of oil-in-water microemulsion (Chen & Xu, 2013). Zhang *et al.* fabricated PVDF membrane through phase inversion technique and further grafted the hydrogel macromolecule polyacrylic acid (PAA) on their PVDF membrane surface. Their as-modified membrane possessed underwater superoleophobicity (>160° underwater oil contact angle) and could separate oil-in-water microemulsion with water flux of ~130 L m^{-2} h^{-1} and 23% loss of water flux in-between filtration cycles (Zhang *et al.*, 2014). Zeng *et al.* coated zeolite onto commercial stainless steel wire (100 or 150 mesh) by seed growth hydrothermal

synthesis. And their as-modified steel wire exhibited >146 ° oil contact angle under water and up to 96% oil removal efficiency for the separation of oil-in-water dispersion (Zeng & Guo, 2014). And in 2015 Liu *et al.* coated graphene oxide (GO) nanosheets on commercial stainless steel wire (from 50 to 1000 mesh) and further employed O_2 plasma to treat as-coated steel wire from the back side. Their as-prepared steel wire exhibited underwater superoleophobicity (underwater oil contact angle ~150 °) and the separation of oil-in-water dispersion indicated that residual oil of ~0.02 wt% left in water permeate (Liu *et al.*, 2015b).

These studies indicated that underwater superoleophobic modification of membrane surface enable as-modified membrane to resist the fouling of oily pollutants during filtration process. However, up to now there is no study showing that these pressure-driven meshes or membranes with underwater superoleophobicity are capable of removing salts from water. Therefore, this thesis demonstrates the remarkable values to explore membrane selective layer with simultaneous high salt rejection and high underwater oleophobicity purposely for the treatment of highly saline and oily wastewater through FO process.

2.7.2. Polyvinyl Alcohol: a unique hydrogel macromolecule

Although both hydrogel macromolecule and nanomaterial can endorse membrane with underwater oleophobicity that is promising to treat the wastewater of high fouling potential (*e.g.* highly oily wastewater) with low membrane fouling and high oil rejection, only certain kind of hydrogel macromolecule hold the potential to form the matrix of functional layer that is able to simultaneously reject salt ions. And these special hydrogel macromolecules may be utilized to construct the selective layer for FO membrane. This section reviews a very unique hydrogel macromolecule *i.e.* polyvinyl alcohol (PVA). PVA has linear structure with the product commercially available from 2,000 Da to 200,000 Da in molecular weight. It has semi-crystalline morphology with one hydroxyl group (-OH) repeated in its monomer unit.

PVA is a promising candidate for membrane selective layer because it possesses many special properties. Firstly, PVA has excellent film-forming property (Lang *et al.*, 1996), which means it holds the potential to construct a selective layer in ultrathin thickness.

Secondly, PVA is electroneutral (Liu *et al.*, 2015a), which means it will minimize the electrostatic interactions between itself and foulants. Thirdly, PVA is solution processable and the temperature required to dissolve PVA in water can be as high as 90 ℃ for certain PVA molecules (*e.g.* PVA of 93 kDa molecular weight and 99% hydrolysis degree), which means it can possess high stability at normal temperature for filtration process. Fourthly, PVA is insoluble in most organic solvents, which is associated with its superiority of high resistivity to chemical erosion (*e.g.* Cl_2) over polyamide (Lang *et al.*, 1994). This indicates PVA membrane is more suitable for the process that couples membrane separation with chlorine disinfection. Fifthly, PVA is also an environmentally benign material owing to its biodegradability and biocompatibility. On one hand, PVA can be biodegraded into acetic acid by a combination of hydrolase and oxidase enzymatic processes. This means biological process could be utilized to treat the PVA wastes. However, it should be noted that only in the presence of selected microorganisms, whose presence in natural environments is relatively uncommon, can PVA be efficiently degraded (Chiellini *et al.*, 2003). On the other hand, PVA has been identified to be biosafe. PVA is neither carcinogenic nor mutagenic. In addition, the acute toxicity of PVA is very low, because orally administered PVA do not accumulate in the body owing to its poor gastrointestinal absorption (DeMerlis & Schoneker, 2003). Finally, PVA is a cheap polymer that can be manufactured through uncomplex synthetic procedure.

Moreover, PVA is valued for its hydrophilicity and oleophobicity (Bolto *et al.*, 2009). PVA can swell in aqueous environment due to the large amount of water uptake. Interestingly, recent studies have revealed that while surface energy is an important antifouling indicator, the stable hydration of the surfaces is an even more important prerequisite to prevent irreversible fouling (Chen *et al.*, 2010). The hydroxyl group of PVA can build hydrogen bond tightly with water molecules to form an ultrathin bonded water layer on PVA surface. The deposition of proteins or colloids onto PVA membrane has to expulse the bonded water molecules, which is thermodynamically unfavorable due to the entropic effect (Herrwerth *et al.*, 2003). Therefore the bonded water layer functions as a physical and energetic barrier to resist fouling.

Most importantly, PVA is crosslinkable and the physicochemical properties of PVA can

be finely tuned through crosslinking. Particularly, after crosslinking PVA develops into a three-dimensional network that can have both high hydrophilicity and structural stability. The degree of crosslinking determines the polarity, viscoelasticity, melting point, refractive index, diffusional, biological and other properties for PVA (Slaughter *et al.*, 2009). For example, high crosslinking degree forms stiff hydrogels which consists of 40% ~ 50% amount of water while low crosslinking degree forms soft hydrogels contains as high as 90% amount of water (Baker *et al.*, 2012). PVA has been proposed in broad applications including medical devices, food package, textile manufacturing and membrane technology. The applications of PVA in membrane technology are specialized as follows.

2.7.2.1. PVA for antifouling modification

The mechanism on hydrophilic modification by PVA is that the hydrophobic solid irreversibly adsorb PVA molecules from aqueous environment onto its surface to displace original water molecules so as to lower down its surface energy. As a result, PVA concentrates at the interface, exceeds its "kinetic solubility" and undergoes the crystallization to generate a hydrophilic layer (Kozlov *et al.*, 2003; Weis *et al.*, 2004). One example is Ma *et al.* used PVA to modify polyethersulfone UF membrane through adsorption-crosslinking technique. And they found that the total and irreversible fouling ratios of as-modified membrane were 0.38 and 0.22, respectively, much lower than that of control PES membrane (0.61and 0.47, respectively) (Ma *et al.*, 2007). Another example is Liu *et al.* grafted PVA onto the surface of polyamide TFC RO membrane and reported that as-modified membrane exhibited an improved antifouling property with better chlorine resistance when investigated with model foulants included BSA, sodium dodecyl sulfate (SDS) and dodecyltrimethyl ammonium bromide (DTAB) (Liu *et al.*, 2015a).

2.7.2.2. PVA as membrane selective layer

PVA has also been proposed as the selective layer for pressure-driven membrane processes (*e.g.* UF, NF and RO). For example, Wei *et al.* fabricated composite hollow fiber membrane with PVA as the selective layer for the separation of ethanol/water mixture through pervaporation process (Wei *et al.*, 2005). Gohil *et al.* used maleic acid crosslinked PVA as the selective layer of NF membrane and reported their TFC NF

(PSf-PVA) membrane attained ~90% rejection of $MgSO_4$ (Gohil & Ray, 2009). Peng *et al.* coated succinic acid crosslinked PVA onto the top surface of commercial PSf UF membrane (NanoH_2O Inc., CA, USA) to fabricate the selective layer for NF membrane and reported as-fabricated TFC NF (PSf-PVA) membrane had 90% rejection of Na_2SO_4 (Peng *et al.*, 2010). Immelman used potassium peroxydisulfate crosslinked PVA as the selective layer of RO membrane and reported their TFC RO (PES-PVA) membrane reached ~60% rejection of NaCl at 4 MPa transmembrane hydrostatic pressure (Immelman *et al.*, 1993).

However, the permeability of PVA selective layer may be undermined in pressure-driven membrane processes, because the high applied hydraulic pressure could compact the hydrogel architecture and thus increase the frictional resistance for water molecules to pass through (Bolto *et al.*, 2009). This problem can be solved by FO technology to achieve "win-win" effect, owing to the low hydraulic pressure working manner of FO process. At the time of this thesis, there is no systematic study to investigate the capability of crosslinkable hydrogel macromolecule (*e.g.* PVA) as the selective layer for FO membrane. Noteworthily, this thesis takes up this challenge in order to explore a new FO membrane with high antifouling capability, high water flux, and high selectivity.

2.8. Summary

2.8.1. The true future of FO technology

The literature review of this thesis clearly reveals that FO technology is doomed to treat challenging wastewaters (*e.g.* highly saline wastewater, highly oily wastewater, and the wastewater contaminated heavily by both oil and salt, *etc.*). And only through excelling with these challenging wastewaters can FO technology thrive with an undoubted advantage over existing pressure-driven membrane processes (*e.g.* UF, NF and RO *etc.*). Therefore, the development of FO membrane should be directed to the correct track that is to place a top priority on membrane antifouling capability. Noteworthily, this thesis purposely chooses the most challenging wastewater *i.e.* highly saline and highly oily wastewater (*e.g.* shale gas wastewater, onshore oil & gas exploration produced water, *etc.*) to test the new FO membrane developed by this study.

2.8.2. The ideal FO membrane to excel with challenging wastewater

The ideal FO membrane should demonstrate high antifouling capability, high water flux, and high selectivity for the treatment of highly saline and oily wastewater. This membrane is designed in thin-film composite structure. There are at least three requirements on its selective layer. Firstly, its selective layer should be able to reject salt ions with high efficiency, leading to the small reverse salt leakage (low J_S) during FO operation. Secondly, its selective layer should be constructed in an ultrathin thickness which favors high water permeability (A value). Thirdly and most importantly, its selective layer should simultaneously possess high antifouling ability. Hence the selective layer is synthesized towards superhydrophilic as well as underwater superoleophobic, ultrasmooth and electroneutral in order to minimize the interactions between itself and foulants. Meanwhile, its support layer should have highly interconnected interior pore structure in all three dimensions at micrometer scale that can minimize the ICP problem and thus endorse this membrane with high water flux (J_W). Towards these goals, this study strives for the new membrane that is able to simultaneously desalt and deoil hypersaline oil-in-water emulsion with low fouling, high water flux, and high selectivity through FO process.

CHAPTER 3 MATERIALS AND METHODS

3.1. Introduction

This chapter elucidates all the experimental details that lead to the findings of this study. Firstly, the chemicals used in this study are introduced. Secondly, the syntheses of GO nanosheets and nanocomposite FO membrane are elaborated. Thirdly, the equipment pertaining to characterization is presented. Finally, the methods to evaluate the separation performance and antifouling capability of as-synthesized nanocomposite membrane are explained clearly.

3.2. Chemicals

Unless stated otherwise, all chemicals were in analytical grade and used as received. 18 MΩ cm deionized (DI) water was obtained from a Millipore ultrapure water system. Figure 3.1 illustrates the molecular structure of the key chemicals utilized in this thesis.

3.2.1. The chemical for the synthesis of GO nanosheets.

Flake graphite (SP1, Bay carbon, USA) was used as the parent material to synthesize GO nanosheets. Sodium nitrate (anhydrous, $NaNO_3$, >99.0% Sigma-Aldrich), potassium permanganate (anhydrous, $KMnO_4$, >99%, Sigma-Aldrich), concentrated sulfuric acid (H_2SO_4, >98%, Sigma-Aldrich), and hydrogen peroxide (H_2O_2, 35% w/w aqueous solution, Alfa Aesar) were also involved in the synthetic process.

3.2.2. The chemicals for the synthesis of nanocomposite FO membrane

3.2.2.1. The chemicals for the fabrication of nanocomposite support layer

Polyethersulfone (PES, weight averaged molecular weight $M_W \approx 63$ kDa, Solvay) was used as the polymer to prepare the dope solution. Pure liquid of *N*,*N*-dimethylformamide (DMF, ≥99.8%, Sigma-Aldrich), or *N*,*N*-Dimethylacetamide (DMAc, ≥99.8%, Sigma-Aldrich), or 1-methyl-2-pyrrolidone (NMP, ≥99.9%, Sigma-Aldrich) was used as solvent of the dope solution, separately. Polyvinyl pyrrolidone (PVP, $M_W \approx 40.5$ kDa, Sigma-Aldrich) was used as the polymeric additive in some conventional polymer dope solutions (absence of GO nanosheet).

3.2.2.2. The chemicals for the synthesis of hydrogel selective layer

Polyvinyl alcohol (PVA, >98% hydrolyzed, Sigma-Aldrich) with M_W varied from 15.5 ~ 166 kDa was used as the hydrogel macromolecule to synthesize the selective layer. Glutaraldehyde (>99.8%, 25 wt% aqueous solution, Sigma-Aldrich), or succinic acid (>99%, Alfa Aesar), or DL-malic acid (≥99%, Sigma-Aldrich) was used as the crosslinking agent, separately. Dilute sulfuric acid aqueous solution was used to catalyze the crosslinking reaction.

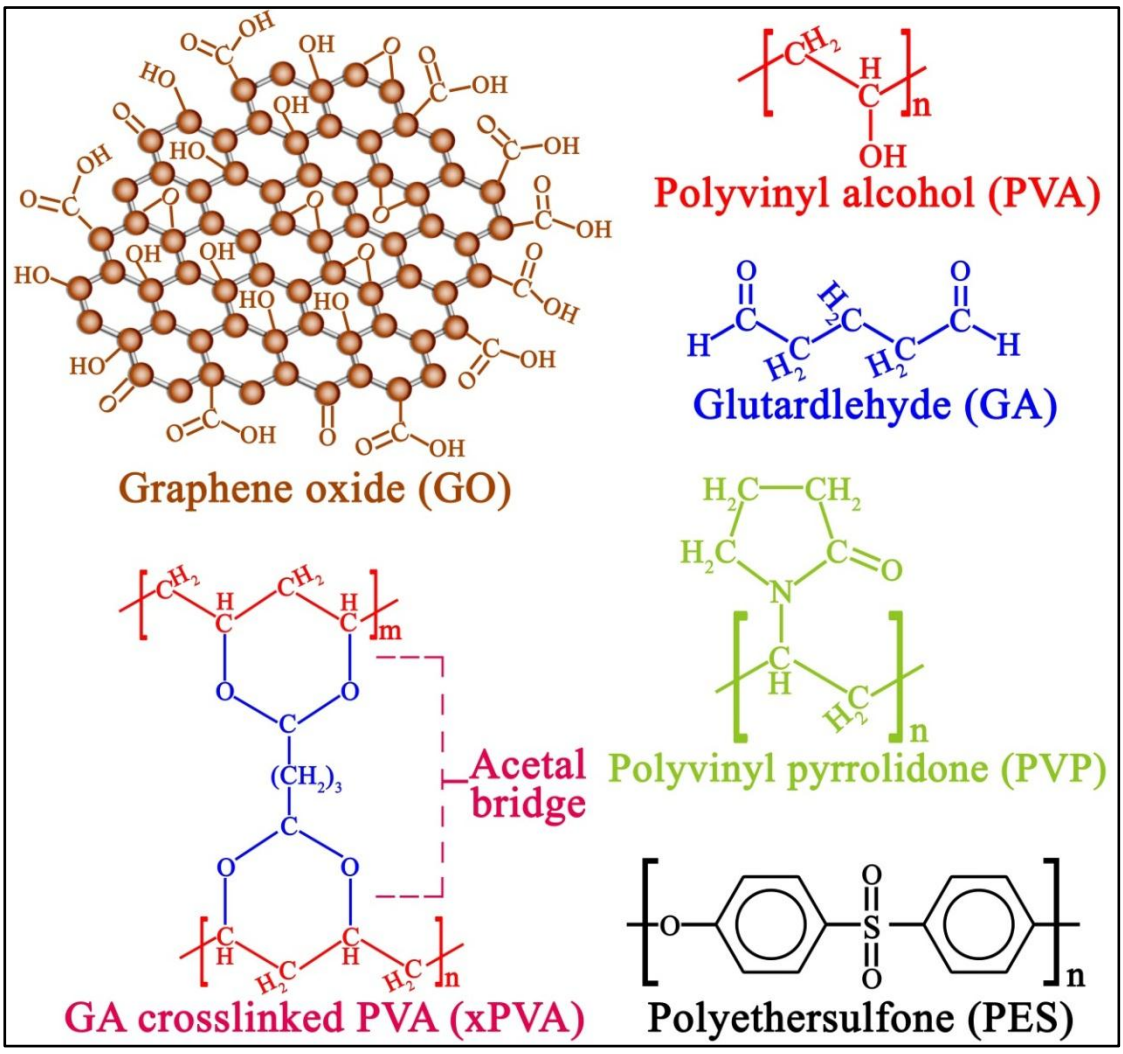

Figure 3.1 Molecular structure of the key chemicals used in this study.

3.2.3. The chemicals for the evaluation of support layer selectivity

Different M_W (10 ~ 600 kDa) of polyethylene glycol (PEG, Sigma-Aldrich) and polyethylene oxide (PEO, Sigma-Aldrich) were used to evaluate the selectivity of support layer on neutrally charged polymeric solutes.

3.2.4. The chemicals for the evaluation of FO membrane performances

3.2.4.1. The chemicals for the evaluation of FO water flux and reverse salt flux

DI water was used as feed solution. Sodium chloride (anhydrous, NaCl, >99.5%, Merck) was used as the draw solute with monovalent cation and monovalent anion. Magnesium chloride (magnesium chloride hexahydrate, $MgCl_2 \cdot 6H_2O$, >99%, Merck) was used as the draw solute with divalent cation and monovalent anion. Sodium sulfate (sodium sulfate decahydrate, $Na_2SO_4 \cdot 10H_2O$, >99.0%, Sigma-Aldrich) was used as the draw solute with monovalent cation and divalent anion.

3.2.4.2. The chemicals for the evaluation of FO membrane antifouling capability

Oil, surfactant and inorganic salts were used to prepare saline oil-in-water emulsion. In particular, vegetable oil (Brand name: "*Sunflower & Olive Oil*"; producer: DFI Brands Limited Hong Kong) was obtained from a local supermarket ("*Giant*"). Petroleum oils with different carbon atoms in molecule were selected based upon the rationales as follows: (1) *n*-hexane (C_6H_{14}, Sigma-Aldrich) is the alkane that is in stable liquid form at room temperature (boiling point ~69 ℃) with the fewest carbon atoms in molecule. (2) 2,2,4-trimethylpentane (iso-octane, $(CH_3)_3CCH_2CH(CH_3)_2$, Sigma-Aldrich) is an important component of gasoline. This particular octane isomer is set as the standard 100 point on the 'octane number' rating scale. Noteworthily, it can be used in large proportions to increase the knock resistance of gasoline (Dabelstein *et al.*, 2007). (3) Isopar-G (Univar, China) is a typical isoparaffin to represent branched aliphatic hydrocarbons. It is produced through distilling crude oil at temperature 161~173 ℃ and has 10~11 carbon atoms in one molecule (Bowen & Balster, 1998). (4) *n*-Hexadecane ($C_{16}H_{34}$) is an important component of diesel fuel. This particular alkane hydrocarbon ignites very easily under compression. So it is assigned as the standard 100 point on the 'cetane number' rating scale, which is used to evaluate the detonation of diesel fuel (Dabelstein *et al.*, 2007). (5) Mineral oil is a mixture of hydrocarbons with 15~40 carbon atoms in one molecule, which is produced as the byproduct of petroleum distillation. The mineral oil used here is a commercially available pump lubricating oil produced from Vacuubrand, Wertheim Germany.

Triton X-100 (Polyethylene glycol *tert*-octylphenyl ether, $M_W \approx 625$ Da, Sigma-Aldrich) was used as the non-ionic surfactant.

Sodium chloride, magnesium sulfate (magnesium sulfate heptahydrate, $MgSO_4 \cdot 7H_2O$, >99.0%, Merck), aluminum sulfate (aluminum sulfate hexadecahydrate, $Al_2(SO_4)_3 \cdot 16H_2O$, >95%, Sigma-Aldrich) were used as the monovalent, divalent and trivalent inorganic salts in saline oil-in-water emulsion, respectively.

3.3. Synthesis of GO nanosheets

GO nanosheets were prepared through a modified Hummers' method as follows (Hummers & Offeman, 1958). Firstly, concentrated H_2SO_4 (14 mL) was added into the mixture of graphite (0.5 g) and $NaNO_3$ (2.0 g). This mixture was stirred for 30 min while being cooled at 0 ℃ in an ice-water bath. Secondly, $KMnO_4$ (3.0 g) was added into the mixture slowly. Afterwards, the mixture was stirred at 0 ℃ for another 2 hours. Thirdly, external heating was introduced to warm the reaction to 35 ℃ for 30 min. Fourthly, DI water (40 mL) was added into the mixture, and the reaction temperature was further increased to 100 ℃ for 15 min. Fifthly, the slurry was cooled down to room temperature and diluted with additional 70 ml DI water. Sixthly, H_2O_2 (10 mL) was added into the diluted suspension, triggering the immediate change of suspension color from dark red to bright yellow. Seventhly, the resultant suspension was centrifuged and resuspended in 10% HCl for three times to remove impurities, followed by washed with DI water several times to adjust pH value. Eighthly, the precipitates were freeze-dried for at least 2 days to obtain the dry graphite oxide. Finally, graphene oxide nanosheets were produced by the exfoliation of as-synthesized graphite oxide through sonication.

3.4. Synthesis of nanocomposite FO membrane

3.4.1. GO assisted phase inversion to fabricate nanocomposite support layer

Hierarchically structured nanocomposite support layer was fabricated by GO assisted phase inversion technique. Noteworthily, weight fraction wt% refers to the proportion of entire dope solution. Several arrays of nanocomposite dope solutions were prepared through varying the weight fraction of GO (from 0.10 wt% to 1.00 wt%) as well as polymer (from 15 wt% to 20 wt%) or using different solvent, with the specific composition of each dope solution listed in the following chapters. The experiment was conducted as the following procedure. Firstly, as-synthesized graphite oxide was

sonicated in solvent (*e.g.* DMF) to obtain a homogenous GO solution. Secondly, PES was added into this GO solution under mechanical stirring. After heated at 55 ℃ for 12 hours, the mixture became a homogenous solution. Thirdly, as-prepared nanocomposite dope solution was cooled down to room temperature and degassed in vacuum desiccator. Fourthly, the nanocomposite dope solution was spread on a clean glass plate and instantly cast into a thin film by applicator (Elcometer, Belgium) with gate height of cast knife set as 150 μm. Finally, the cast film was immediately immersed in DI water to initialize phase inversion at room temperature. The formed support layer was stocked in 4 ℃ DI water before usage. Conventional phase inversion fabricated PES membrane was cast through the same procedure except that the GO wt% was zero.

3.4.2. Dip-coating in crosslinked hydrogel solution to synthesize selective layer

Chemically crosslinked PVA was coated onto the top surface of as-fabricated support layer to synthesize the hydrogel selective layer. Firstly, PVA powder was dissolved in DI water at 90 ℃ under mechanical stirring to obtain the hydrogel solution. The concentration of PVA was varied from 0.125 wt% ~ 1.00 wt%. Secondly, crosslinking agent (*e.g.* glutaraldehyde) was added into the hydrogel solution with theoretical crosslinking degree (*TCLD*) varied from 0% to 100%. Equation 3.1 demonstrates the calculation of *TCLD* (Peng *et al.*, 2011). Thirdly, 1 wt% 2M H_2SO_4 was introduced as the catalyst, and the reaction was heated at 60 ℃ for 15 min to obtain the crosslinked hydrogel solution. Fourthly, as-fabricated support layer was dip-coated in the crosslinked hydrogel solution with only top surface in contact with the solution. Fifthly, the coating time was varied from 10 ~ 40 min, after which the excess crosslinked hydrogel solution was drained off. Sixthly, the nascent FO membrane was cured in oven at 100 ℃ with curing time varied from 5 ~ 40 min. Finally, as-synthesized FO membrane was stocked in 4 ℃ DI water before usage.

$$\boldsymbol{TCLD} = \left(\frac{\boldsymbol{W_{CL}} \times \boldsymbol{MW_{PVA\ Unit}} \times \mathbf{2}}{\boldsymbol{W_{PVA}} \times \boldsymbol{MW_{CL}}}\right) \times \mathbf{100}\% \qquad (3.1)$$

where *TCLD* is theoretical crosslinking degree, W_{CL} is the weight of crosslinking agent, $MW_{PVA\ Unit}$ is the molecular weight of one PVA unit (CH_2CHOH, 40 g $mole^{-1}$), W_{PVA} is the weight of PVA, and MW_{CL} is molecular weight of crosslinking agent.

3.5. Characterization

3.5.1. Transmission electron microscopy (TEM)

The morphology of as-synthesized GO nanosheet was characterized by transmission electron microscopy (TEM, JEOL JSM 2010-H) under the accelerated voltage of 200 kV. Prior to the measurement, sonicated GO solution was dripped onto 400-mesh carbon coated copper grids and dried at 45 ℃ in windless oven for the evaporation of solvent.

3.5.2. Atomic force microscopy (AFM)

The topographies of as-synthesized membranes and GO nanosheet were probed by atomic force microscopy (AFM, Park XE-100) in non-contact mode. For the preparation of GO sample, sonicated GO solution was dripped onto silicon wafer and dried at room temperature to evaporate the solvent.

3.5.3. Field emission scanning electron microscopy (FESEM)

The structures of as-synthesized membranes and graphite oxide were characterized by field emission scanning electronic microscopy (FESEM, JEOL JSM 7600F) under the accelerated voltage of 5 kV. All samples were coated by gold for 30 s using an EMITECH SC 7620 sputter coater. Membrane cross-sections were acquired by fracturing the samples immediately after flash-frozen in liquid nitrogen.

3.5.4. Energy dispersive x-ray spectroscopy (EDX)

Energy dispersive x-ray (EDX) detector that is attached to the FESEM equipment was utilized to provide element mapping in order to differentiate the architecture between polymeric support layer and hydrogel selective layer.

3.5.5. X-ray diffraction (XRD)

X-ray diffraction (XRD) patterns of graphite, as-synthesized GO nanosheet and membranes were recorded using a Bruker AXS D8 Advance diffractormeter equipped with a Cu Kα radiation source.

3.5.6. Fourier transform infrared spectroscopy (FTIR)

Attenuated total reflection-Fourier transform infrared spectroscopy (ATR-FTIR, Perkin

Elmer 2000, ZnSe crystal method) was used to analyze the surface functional groups of as-synthesized membranes. The samples were freeze-dried for 2 days before scanned.

3.5.7. Measurement of membrane surface charge

Surface charge of as-synthesized membranes were determined using streaming potential in the pH range 2~11 by a SurPASS electrokinetic analyzer (Anton Paar GmbH, Austria).

3.5.8. Contact angle

Contact angles were determined on an optical goniometric equipment (AST VCA Optima) using sessile drop technique. Two types of contact angle were tested, namely water contact angle in air and underwater oil contact angle, with 3 μl DI water in air or 10 μl 1,2-dichloromethane under water used as the probe liquid, respectively. All the contact angle data were recorded at the initial moment when probe liquid fully wet the solid surface. Noteworthily, the contact angle result was reported as the average of at least 9 random measurements for each sample.

3.5.9. Thermogravimetric analysis (TGA)

Thermogravimetric analysis (TGA) of as-synthesized GO nanosheets and membranes are conducted using Perkin Elmer TGA 7 analyzer equipped with thermal analysis controller TAC 7/DX. The samples were heated from 30 ℃ to 900 ℃ at the temperature ramp of 10 ℃/min under either dry air or nitrogen gas.

3.5.10. Measurement of oil droplet size distribution

The droplet size distribution of as-synthetic oil-in-water emulsion was characterized by both dynamic laser light scattering (DLS, Mastersizer 2000) and optical microscopy (Olympus IX 71) at room temperature.

3.5.11. Measurement of organic concentration

The total concentration of organic pollutants in emulsion (including both oil and surfactant) was determined by both total organic carbon (TOC, Shimadzu TOC-VCSH) analyzer and chemical oxygen demand (COD, HACH method 8000 HR and ULR)

method.

3.5.12. Measurement of ion concentration

Inductively coupled plasma-optical emission spectroscopy (ICP-OES, Perkin Elmer Optima 2000 DV) was utilized to analyze the concentration for cations *i.e.* Mg^{2+} and Al^{3+} in this study (total Mg and total Al have been measured by ICP-OES); while ion chromatography (DIONEX ICS-1000) was utilized to analyze the concentration of anion *i.e.* Cl^- in this study.

3.6. Pore size distribution of support layer based on solute transport method

Solute transport method is employed to determine pore size distribution of support layer top surface, with the procedure of this method following the published paper (Singh *et al.*, 1998). Firstly, 200 ppm PEG (or PEO) was used as the feed solution. A custom-built cross-flow filtration module was employed to circulate the feed solution on support layer top surface at transmembrane hydrostatic pressure (ΔP) of 1 bar under 23 ± 2 ℃. The cross flow rate was kept as 1.0 L min^{-1}. Besides, plastic spacer (SEPA CF spacer, 17 mil) was placed in the module to generate flow turbulence on top of support layer. Rejection was calculated by measuring the concentration of PEG (or PEO) in permeate and retentate via total organic carbon (TOC) analysis. Generally, a linear correlation can be established between rejection and natural logarithm of solute diameter (ln d_S) (Michaels, 1980). From this linear fitting on log-normal probability paper, mean solute diameter (μ_S) can be determined as d_S at rejection = 50%, while σ_S can be determined from the ratio of d_S at rejection = 84.13% and d_S at rejection = 50%. By ignoring the dependence of solute rejection on the hydrodynamic interaction between solute and pore sizes (Cooper & Vanderveer, 1979), the mean pore diameter (μ_P) can be considered to be the same as solute mean pore diameter (μ_S), and geometric standard deviation (σ_P) of membrane can be considered to be the same as solute geometric standard deviation (σ_S). Therefore, the pore size distribution of a pore-flow membrane (*i.e.* as-fabricated support layer here) can be expressed as the following probability density function.

$$\frac{df(d_p)}{dd_p} = \frac{1}{d_p ln\sigma_p\sqrt{2\pi}} \exp\left[-\frac{(lnd_p - ln\mu_p)^2}{2(ln\sigma_p)^2}\right] \quad (3.2)$$

where d_P is the pore diameter of membrane (as-fabricated support layer), σ_P is geometric standard deviation of membrane pore diameter, μ_P is membrane mean pore

diameter.

3.7. Measurement of FO water flux (J_W) and reverse salt flux (J_S)

FO performance was tested by a custom-built crossflow module wherein the hydrostatic pressure difference across membrane is kept as 0 bar (Figure 3.2). Gear pumps (Cole-Parmer) were used to circulate both feed and draw solutions at the flow rate of 1.0 L min^{-1} (flow velocity of 21.4 cm s^{-1}) under 23 ± 2 ℃. Plastic spacers (SEPA CF spacer, 17 mil) were placed on both sides in the module to increase flow turbulence. It's worthy to note that under this crossflow condition the effect of ECP was rendered negligible. Membrane orientations in both FO mode (*i.e.* selective layer facing feed solution) and PRO mode (*i.e.* selective layer facing draw solution) were tested. The feed solution was DI water and typical draw solution was 0.5 M Na_2SO_4. Water flux (J_W) was determined from the weight increment of draw solution using a digital balance (equation 3.3).

$$J_W = \frac{\Delta V_{DS}}{A_m \times \Delta t} = \frac{\Delta m_{DS}}{\rho \times A_m \times \Delta t} \quad (3.3)$$

where Δt is the time interval (2 min), A_m is the effective membrane area (23.8 cm^2), V_{DS} is the volume of draw solution, m_{DS} is the mass of draw solution, and ρ is the density of feed solution. Meanwhile, reverse salt flux (J_S) was measured by calculating the increment of draw solute concentration in feed solution (equation 3.4).

$$J_S = \frac{(V_t C_t - V_0 C_0) \times MW}{A_m \times \Delta t} \quad (3.4)$$

where V_0 and V_t are volumes of feed solution at time 0 and t, respectively; C_0 and C_t are molar concentrations of draw solute (converted from calibrated conductivity, COND610, Eutech) in feed solution at time 0 and t, respectively; MW is the molecular weight of draw solute. Noteworthily, commercial HTI FO membrane (cellulose triacetate, woven) was tested in the same condition for the comparison purpose.

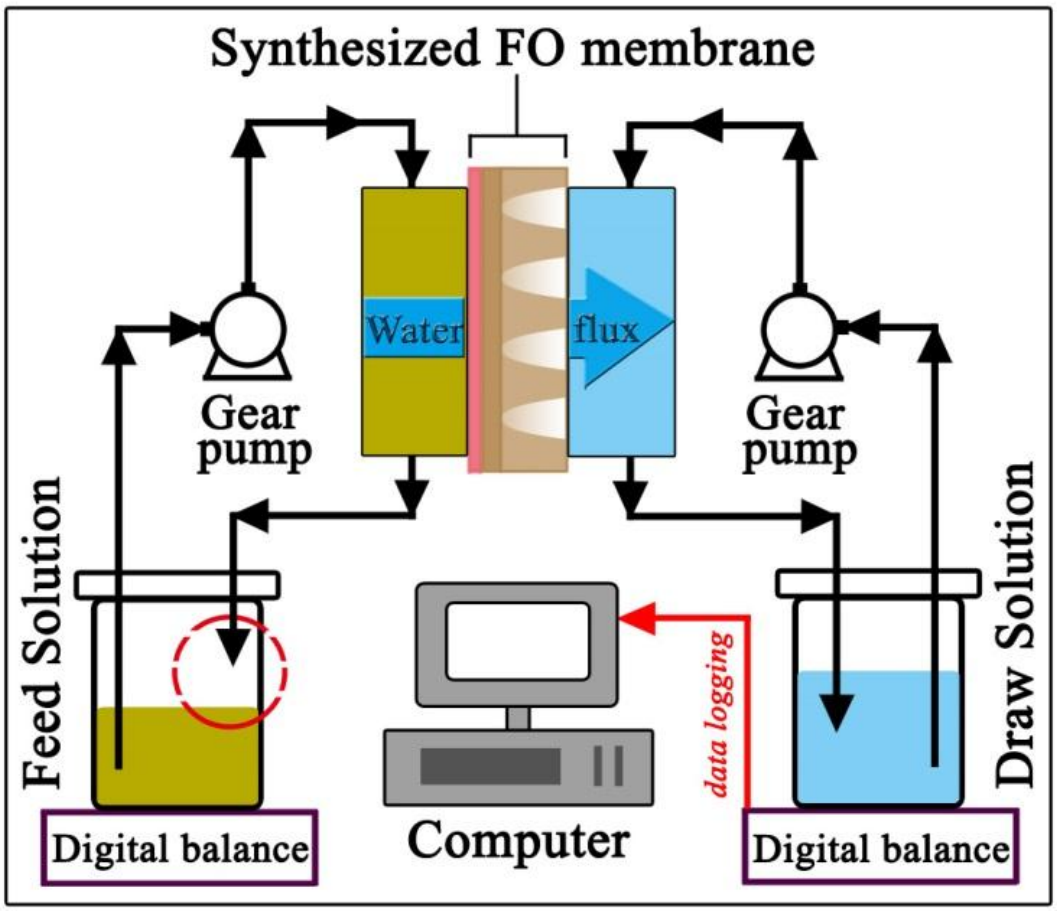

Figure 3.2 Schematic diagram of the custom-built FO setup. Note that in the feed tank the returning tubing tip of concentrate was placed 3 cm higher than water level (as marked by the dash-line circle).

3.8. Determination of FO membrane structural parameter (*S*)

FO membrane structural parameter (*S*), which represents the average distance a draw solute molecule must take when traveling through the support layer (Phillip *et al.*, 2010), is determined by ICP modeling as shown in equation 3.5 (McCutcheon & Elimelech, 2007):

$$S = K \times D = \frac{t \times \tau}{\varepsilon} \tag{3.5}$$

where t, τ and ε are membrane thickness, tortuosity and porosity, respectively; D is the diffusion coefficient of draw solute, and K is solute resistivity of FO membrane. Particularly, K can be determined by equation 3.6 (Lee *et al.*, 1981b; Loeb *et al.*, 1997):

$$K = \frac{1}{J_W} ln \frac{B + A \times \pi_{D,b}}{B + J_v + A \times \pi_{F,m}} \tag{3.6}$$

where J_W is water flux at FO mode, $\pi_{D,b}$ is osmotic pressure of draw solution bulk, $\pi_{F,m}$ is osmotic pressure of feed solution at membrane surface, A is intrinsic water

permeability of FO membrane, *B* is solute permeability of selective layer. Particularly, *B* can be determined by equation 3.7 (Zhang *et al.*, 2010):

$$B = \frac{(1-R)A(\Delta P-\Delta\pi)}{R} \quad (3.7)$$

where *R* is the rejection of draw solute under RO mode, *A* is intrinsic water permeability of FO membrane, ΔP is the transmembrane hydrostatic pressure difference, $\Delta\pi$ is transmembrane osmotic pressure difference. Additionally, *A* and *R* of FO membranes were determined by a lab-scale cross-flow RO test unit (Sterlitech, effective area 33.6 cm^2) under ΔP of 5 bar.

3.9. Evaluation of membrane's antifouling capability

3.9.1. Preparation of saline oil-in-water emulsion

Various oil-in-water emulsions were used as FO feed solution to evaluate membrane's antifouling capability. Different kinds of oil were involved in the preparation with oil concentration ranged from 2.5 to 100 g/L (g oil/L water) and surfactant/oil ratio ranged from 0.00 to 0.20, respectively. In order to simulate shale gas wastewater (a typical hypersaline oil-in-water emulsion), hexadecane-in-water emulsions of different salinity (0~256 g/L total dissolved salts) were prepared according to the following procedure. Firstly, NaCl, $MgSO_4$ and $Al_2(SO_4)_3$ were dissolved in DI water with their molar concentration ratio equalling to 1:1:1. Secondly, certain amounts of surfactant and hexadecane were added into the salt solution sequentially under mechanical stirring. Thirdly, the mixture was sonicated under 100 W at 20 ℃ for 3 hours to obtain a homogenous milky emulsion. Fresh emulsions were immediately used in the subsequent fouling tests.

3.9.2. Evaluation of flux reduction ratio (*FRR*)

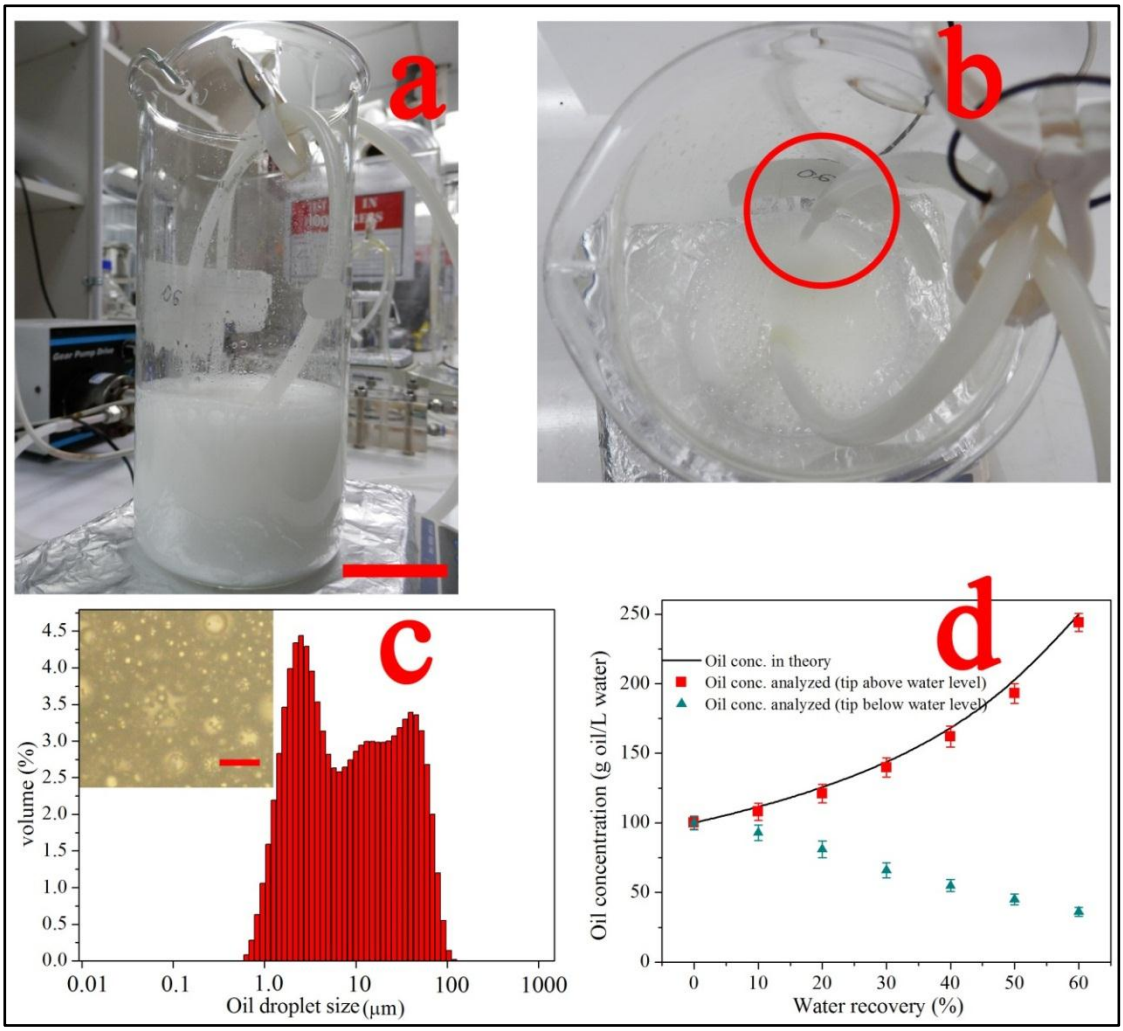

Figure 3.3 Placing the returning tubing tip of concentrate above water level in feed tank to eliminate oil/water stratification. Surfactant concentration is zero. (**a**, **b**) Optical photos of 100 g/L oil-in-water emulsion, wherein the scale bar on subfigure (a) is 5 cm and the red circle on subfigure (b) highlights that the returning tubing tip of concentrate is placed 3 cm above water level. These two photos substantiate that the feed solution is kept as a homogenous emulsion during fouling test period. (**c**) Optical microscopy image (inserted, the scale bar is 50 μm) and dynamic light scattering (DLS) analysis of 100 g/L oil-in-water emulsion, showing that the oil droplet sizes are ranged from 1.0 to 100 μm. (**d**) Oil concentration measurement results along with FO operation period, verifying that the membrane confronts the oil concentration truly as high as designated.

For any particular oil-in-water emulsion, J_W decrease resulted from oil-fouling was reported as the average based upon parallel testing results of three pieces of membrane. For a particular piece of membrane, the testing consisted of a "baseline running" followed by a "oil-fouling running", with separate batch of 500 mL 1.5 M Na_2SO_4 used as draw solution for each running. The protocol of testing is further elaborated as follows. Firstly, DI water (500 ml) was used as the feed solution to record a J_W baseline of 440 min, wherein the J_W value would drop gradually due to the osmotic

dilution of draw solution. Secondly, "oil-fouling running" was performed in three sequential stages: "precondition" (40 min), "oil-fouling" (360 min) and "post-cleaning" (40 min). In "precondition" stage, the feed solution is still DI water. Oil-in-water emulsion was used as feed solution from 41th min to 400th min to investigate membrane fouling. After that, the membrane was *in situ* washed three times through flushing DI water in the feed side. Data recording was stopped during cleaning and resumed for another 40 min (designated as 401th min to 440th min) wherein DI water was reused as feed solution to investigate flux restoration after *in situ* cleaning.

Noteworthily, the returning tubing tip of concentrate in the feed tank was placed 3 cm higher than water level in order to generate sufficient hydraulic mixing of feed solution, as highlighted by the red circle in Figure 3.3. This setting of tubing can ensure membrane to confront the oil concentration truly as high as designated through eliminating any stratification of oil/water mixture during testing period, thus designed as the worst-scenario with respect to membrane fouling.

Average flux reduction ratio *(FRR*), which indicates the loss of membrane permeability due to additional resistance induced by fouling for water molecule to overcome when passing through membrane, was calculated for both "oil-fouling stage" and "post-cleaning stage" according to the following equation 3.8~3.9:

$$FRR_f(\%) = 1 - \frac{\int_{t_1}^{t_2} J_{w,fouling} dt}{\int_{t_1}^{t_2} J_{w,baseline} dt} \quad (3.8)$$

$$FRR_c(\%) = 1 - \frac{\int_{t_3}^{t_4} J_{w,fouling} dt}{\int_{t_3}^{t_4} J_{w,baseline} dt} \quad (3.9)$$

where t_1 is 41th min, t_2 is 400th min, t_3 is 401th min, t_4 is 440th min; $J_{W,\ baseline}$ and $J_{W,\ ,fouling}$ are average J_W value of "baseline running" and "oil-fouling running", respectively; FRR_f and FRR_c are average flux reduction ratio of "oil-fouling stage" and "post-cleaning stage", respectively. Note $\int J_W dt$ bears the physical meaning of FO throughput during a given period for 1 m^2 membrane (L m^{-2}).

3.9.3. Simultaneous removal of oil and salts

Simultaneous removal ratios of oil and salts by FO process were determined by equation 3.10:

$$Removal(\%) = 1 - \frac{C_{DS,t2}}{C_{FS,t2}} \times \frac{V_{DS,t2}}{V_{DS,t2} - V_{DS,t1}} \quad (3.10)$$

where *Removal* is the removal ratio of oil or salt, t_1 is 41th min, t_2 is 400th min, $C_{DS,t2}$ is the pollutant (oil and salt) concentration in draw solution at t_2, $C_{FS,t2}$ is the pollutant concentration in feed solution at t_2, $V_{DS,t1}$ and $V_{DS,\,t2}$ are volume of draw solution at t_1 and t_2, respectively. Note that the calculation of removal ratios by FO process should consider the dilution of permeates in draw solution.

3.10. Summary

This chapter shares the technical details on the experimental work of this thesis, which is expected to provide the readers all the useful information for pursuing further research on this topic.

CHAPTER 4 OPTIMIZATION OF HYDROGEL SELECTIVE LAYER: THE KEY ROLE OF CROSSLINKING IN ENHANCING SELECTIVITY

4.1. Introduction

Towards the final goal of a new FO membrane that can simultaneously desalt and deoil highly saline and oily wastewater with low fouling, high water flux, and high selectivity, the potentiality of hydrogel macromolecule as the selective layer for FO membrane is explored as the first step, with specific investigations carried out according to the deliberate research design as follows.

Firstly, the structures of as-synthesized TFC FO membrane with hydrogel as selective layer are investigated by diverse characterization techniques.

Secondly, the factors that influence the formation of hydrogel selective layer as well as the performance of as-synthesized TFC FO membrane, including different crosslinking agents, molecular weight of hydrogel macromolecule, hydrogel concentration, crosslinking degree, and coating time *etc.*, are systematically discussed from the perspective of adsorption process, in order to optimize the structures and properties of as-crosslinked hydrogel selective layer. The investigation on these factors proceeds step by step, with each step focused on one factor and the obtained optimum value utilized for the next step. And for the specific investigation on each factor, the significance to study this factor is introduced at first, followed by the discussion on its effect upon FO membrane's water flux (J_W) and reverse salt flux (J_S). Moreover, the indictor J_W/J_S, which stands for how many liters of clean water to be obtained at the cost of one gram draw solute, is employed to judge the optimum value from a comprehensive perspective. Besides, the J_W, J_S, and J_W/J_S of as-synthesized TFC FO membrane are compared with the commercial FO membrane (HTI, cellulose triacetate, nonwoven) under exactly the same operating conditions in order to evaluate the economic feasibility. In addition, the results are further compared with relevant research articles published recently to conduct a deep analysis on the mechanism.

Thirdly, all the above results are summarized to draw an informative conclusion on the

potentiality of hydrogel macromolecule as FO membrane's selective layer, within the scope of the final goal that is to synthesize a new FO membrane able to treat challenging wastewater (*e.g.* highly saline and oily wastewater) with low fouling, high water flux, and high selectivity.

To the best knowledge of the author, this is the first study that systematically explores and further optimizes the capability of hydrogel macromolecule (PVA) as the selective layer for FO membrane.

Noteworthily, the support layer in this chapter is purposely fabricated from conventional phase inversion process (GO concentration is 0.00 wt%) in order to exclude the interference from nanomaterial incorporation. And this TFC FO membrane is denoted as P-H FO membrane, wherein "P" stands for conventional phase inversion constructed support layer while "H" stands for hydrogel selective layer, respectively. For clarification purpose, the nanocomposite FO membrane synthesized with GO assisted phase inversion constructed support layer is denoted as GO\P-H FO membrane, wherein "GO\P" stands for GO assisted phase inversion constructed nanocomposite support layer and "H" stands for hydrogel selective layer. GO\P-H nanocomposite FO membrane will be introduced in the next chapter (Chapter 5).

4.2. Structures of as-synthesized FO membranes with hydrogel as selective layer

As introduced in Chapter 3, the flat-sheet support layer is fabricated by conventional nonsolvent induced phase inversion technology and hydrogel selective layer is synthesized through dip-coating technology. Table 4.1 lists the specific composition of conventional dope solution employed in this chapter. The structures of as-synthesized TFC P-H FO membrane are elucidated as follows.

Table 4.1 The composition of the traditional dope solution used in this chapter.

Dope solution (100 wt%)	Polymer wt% (Polyethersulfone)	PVP wt%	Solvent	Solvent wt%
Traditional	15.0	1.0	dimethylformamide	84.0

4.2.1. Surface structure and properties

The surface morpholgies of as-fabricated P support layer and P-H FO membrane are

compared in Figure 4.1. The top surface of support layer is worth careful investigation because it functions as the interface between support layer and selective layer. Figure 4.1a shows that the pores of P support layer top surface are 13.5 ± 5 nm in diameter. Therefore, conventional phase inversion constructed P support layer can be regarded as a typical ultrafiltration membrane (UF, a pore-flow membrane) that has surface pore size ranged from 1 nm to 100 nm (Zeman & Zydney, 1996). The water contact angle in air of P support layer top surface is 71 ° ± 3.9 °, indicating its poor hydrophilicity. Figure 4.1b shows that the bottom surface of P support layer has relatively uniform pores with diameter of 0.51 ± 0.10 μm.

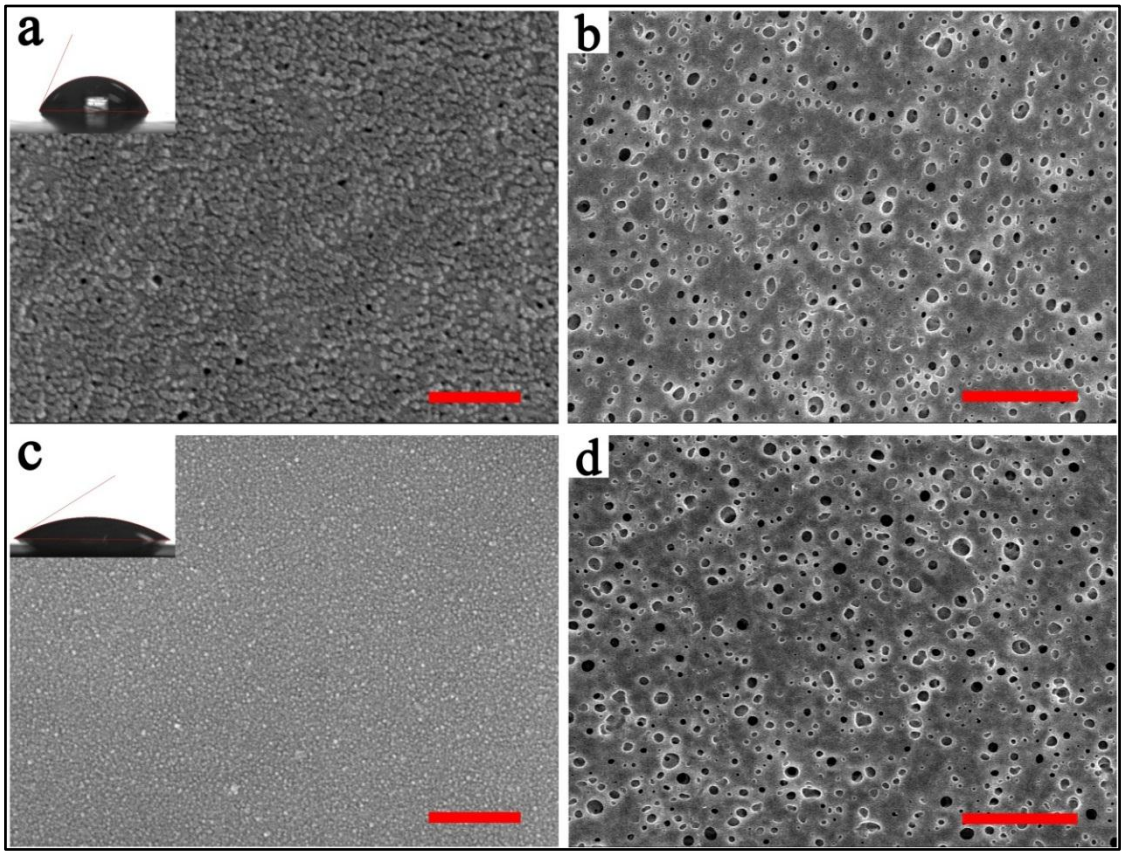

Figure 4.1 Surface structure of as-synthesized P support layer and P-H FO membrane. (**a**) Top surface of P support layer, scale bar, 200 nm, wherein the inserted graph is water contact angle of P support layer. (**b**) Bottom surface of P support layer, scale bar, 5 μm. (**c**) Top surface of P-H FO membrane, scale bar, 200 nm, wherein the inserted graph is water contact angle of P-H FO membrane (theorectical crosslinking degree is 30%). (**d**) Bottom surface of P-H FO membrane, scale bar, 5 μm.

In contrast, Figure 4.1c shows that PVA nanograins with diameter of ~8 nm are assembled into the orderly arrays, forming the upmost surface of hydrogel selective layer. As-built hydrogel upmost surface is nonporous, compact and defect-free at

nanometer scale, which demonstrates the promise in effective rejection of common inorganic ions that are generally in sub-nanometer scale. Moreover, this surface architecture also enables as-synthesized hydrogel selective layer to possess ultrasmooth topography, as average roughness (R_a) reduced from 16.5 ± 3.0 nm of P support layer to 5.1 ± 1.3 nm of P-H FO membrane. Meanwhile, this hydrogel selective layer is highly hydrophilic, with its water contact angle as lows as 31 ° ± 2.8 °. Therefore, as-synthesized hydrogel selective layer possesses integrated properties of (1) ultrasmooth topography that avoids the clogging of foulants in otherwise valley regions of rough surface, and (2) high hydrophilicity that can resist the adsorption of hydrophobic foulants. Noteworthily, these integrated properties of hydrogel selective layer are advantageous to the mitigation of membrane fouling under harsh operating conditions (*e.g.* filtering wastewater of high foulant concentration). Besides, Figure 4.1d shows that the synthesis of hydrogel selective layer using dip-coating technology does not alter the morphology of support layer bottom surface.

4.2.2. Cross-sectional structure

Figure 4.2 compares the cross-sectional structure between as-synthesized P support layer and P-H FO membrane. Figure 4.2a provides the overview of P support layer cross-section, which shows that the overall thickness of P support layer is 84 ± 6 μm. The enlarged FESEM image (Figure 4.2b) reveals that the cross-section of P support layer is hierarchical in structure: it is composed of a relatively thin nanoporous sponge-like sublayer (with pores of 50 ~ 150 nm in diameter) sitting on the thick microporous finger-like channels. Noteworthily, these finger-like channels gradually grow bigger in channel width (*i.e.* inner diameter) along with the direction from top surface to bottom surface (here the interior pores are connected in only one dimension), with their channel widths increased from ~1.0 μm near top surface to as large as 21.5 μm near the bottom surface.

Figure 4.3c shows that the finger-like channels in P-H FO membrane maintains the same structure (connected in only one dimension from top surface to bottom surface) with that of P support layer. While the enlarged FESEM image (Figure 4.2d) demonstrates that as-synthesized hydrogel selective layer is immobilized on the top of P support layer at a uniform thickness of 119 ± 10 nm. The super-uniform thickness of

as-synthesized selective layer is an advantageous attribute for salt-rejecting membranes, which ensures the separation performances among different membrane surface regions are consistent in terms of water permeability and salt rejection. Moreover, the sponge-like sublayer beneath the hydrogel selective layer maintains its nanoporous structure characteristic with its pore size ranged in the same scale with that of P support layer. This means most of the crosslinked hydrogel macromolecules are coated onto the upmost surface of P support layer without penetrating P support layer to alter its inner pore structure. In short, Figure 4.2d exhibits that the entire cross-section of P-H support layer consists of an ultrathin hydrogel selective layer on top of a hierarchically structured PES support layer (including a sponge-like sublayer on top of finger-like channels that are connected in only one dimension).

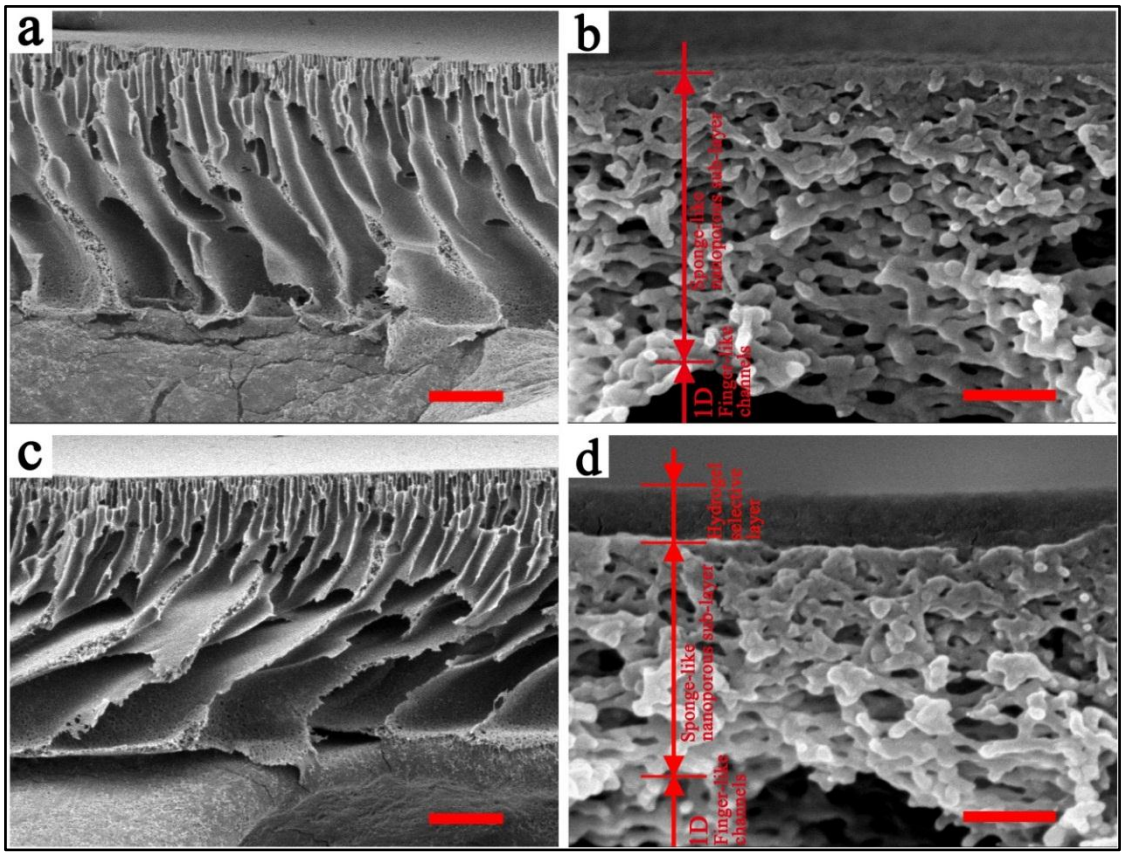

Figure 4.2 Cross-section of as-synthesized P support layer and P-H FO membrane. (**a**) Cross-sectional overview of P support layer, scale bar, 20 μm. (**b**) Enlarged cross-sectional image of P support layer, scale bar, 200 nm. (**c**) Cross-sectional overview of P-H FO membrane, scale bar, 20 μm. (**d**) Enlarged cross-sectional image of P-H FO membrane, scale bar, 200 nm (theoretical crosslinking degree is 30%).

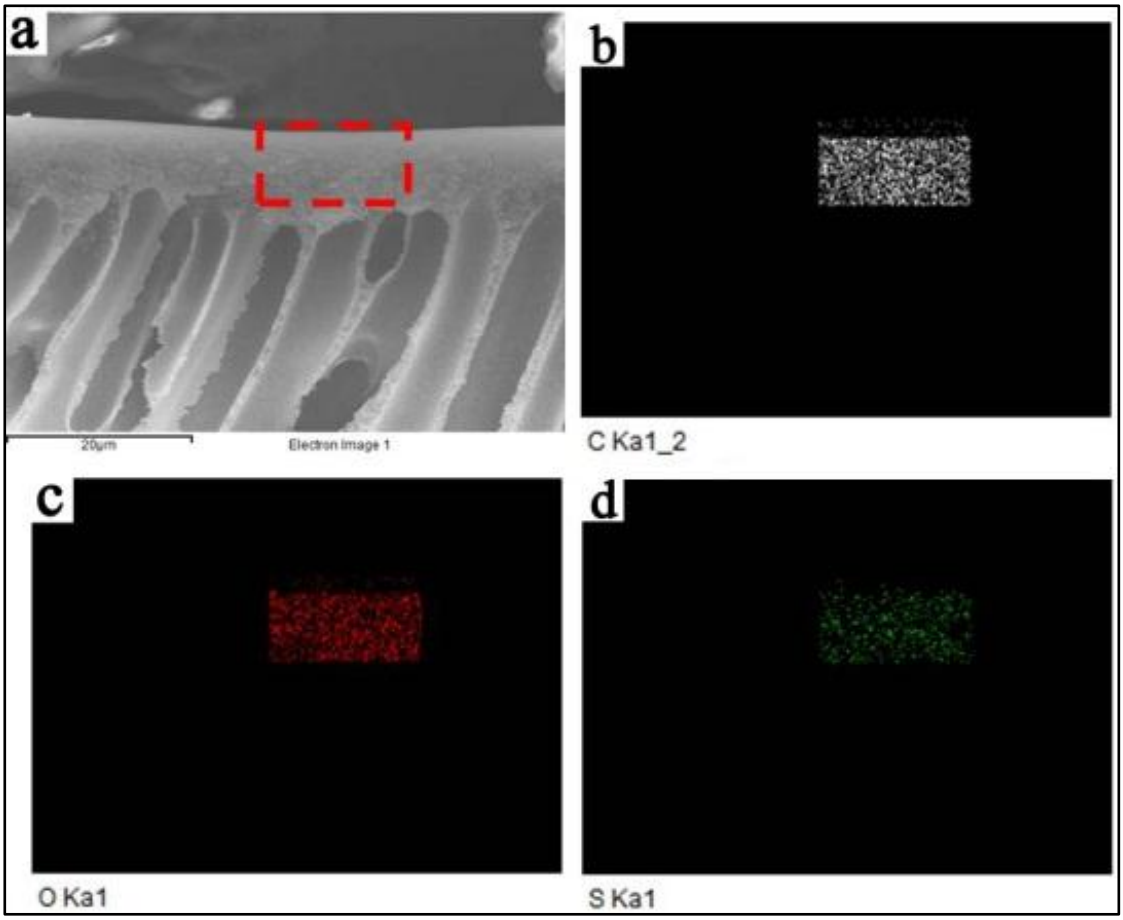

Figure 4.3 Energy dispersive x-ray spectroscopy (EDX) result of P-H FO membrane. (**a**) Enlarged FESEM image on the cross-section of P-H FO membrane, scale bar, 20 μm. (**b**) Element mapping of carbon. (**c**) Element mapping of oxygen. (**d**) Elment mapping of sulfur.

The cross-section of as-synthesized P-H FO membrane is also probed by EDX element mapping, which substantiates the difference in chemical composition between support layer made of PES and selective layer made of crosslinked hydrogel macromolecule (Figure 4.3). In particular, the EDX results demonstrate that P support layer contains ~4 wt% sulfur element, which is displayed by the distribution of green dots in P support layer cross-section as shown in Figure 4.3d. In contrast, this green dot is absent at the spatial position corresponding to the cross-section of hydrogel selective layer, which verifies that the selective layer is different from support layer in chemical compositions. Furthermore, although both selective layer and support layer contain the elements of carbon and oxygen, the spatial distribution of which forms evident stratification architecture: the upper layer is loose in elemental distribution while the below layer is dense, with the horizontal borderline indicating the interface between selective layer and support layer. In short, EDX analysis reveals that the selective layer

and support layer of P-H FO membrane are from different materials.

4.3. Optimization of hydrogel selective layer

As introduced in Chapter 2, the mechanism for the immobilization of hydrogel macromolecule onto polymeric support layer is irreversible adsorption (Kozlov *et al.*, 2003). This means crosslinking plays a crucial role in the adsorption process because it determines the physicochemical properties of adsorbate (crosslinked hydrogel macromolecule). Therefore, the factors influencing crosslinking reaction are investigated systematically, for the purpose of optimizing the structures and properties of as-synthesized hydrogel selective layer towards high J_W, low J_S, and most importantly high J_W/J_S. In particular, the effects of different crosslinking agents, hydrogel (PVA) molecular weight, hydrogel concentration, crosslinking degree are carefully investigated. Besides, the effect of coating time (time for adsorption process) and different draw solutes are also examined in the FO operation. The relevant results are presented as follows.

4.3.1. Effect of different cross-linking agents on hydrogel selective layer

Figure 4.4a-1 and Figure 4.4a-2 present J_W of P-H membrane prepared by different crosslinking agents under PRO mode and FO mode, respectively, with HTI FO membrane used as the comparison. The J_W of P-H membrane among different crosslinking agents are ranged from 5.0 ~ 6.9 L m^{-2} h^{-1}. Under PRO mode, the J_W of succinic acid as crosslinking agent is 6.9 ± 1.3 L m^{-2} h^{-1}, which is higher than that of glutaraldehyde as crosslinking agent (5.8 ± 0.9 L m^{-2} h^{-1}); while the J_W of malic acid as crosslinking agent is the smallest (5.0 ± 1.6 L m^{-2} h^{-1}). The J_W under FO mode follows the same trend as that of PRO mode. Interestingly, the J_W of hydrogel membrane without any chemical crosslinking is only 5.2 ± 1.5 L m^{-2} h^{-1} under PRO mode and 3.1 ± 0.7 L m^{-2} h^{-1} under FO mode, which is even smaller than that of glutaraldehyde as the crosslinking agent, respectively.

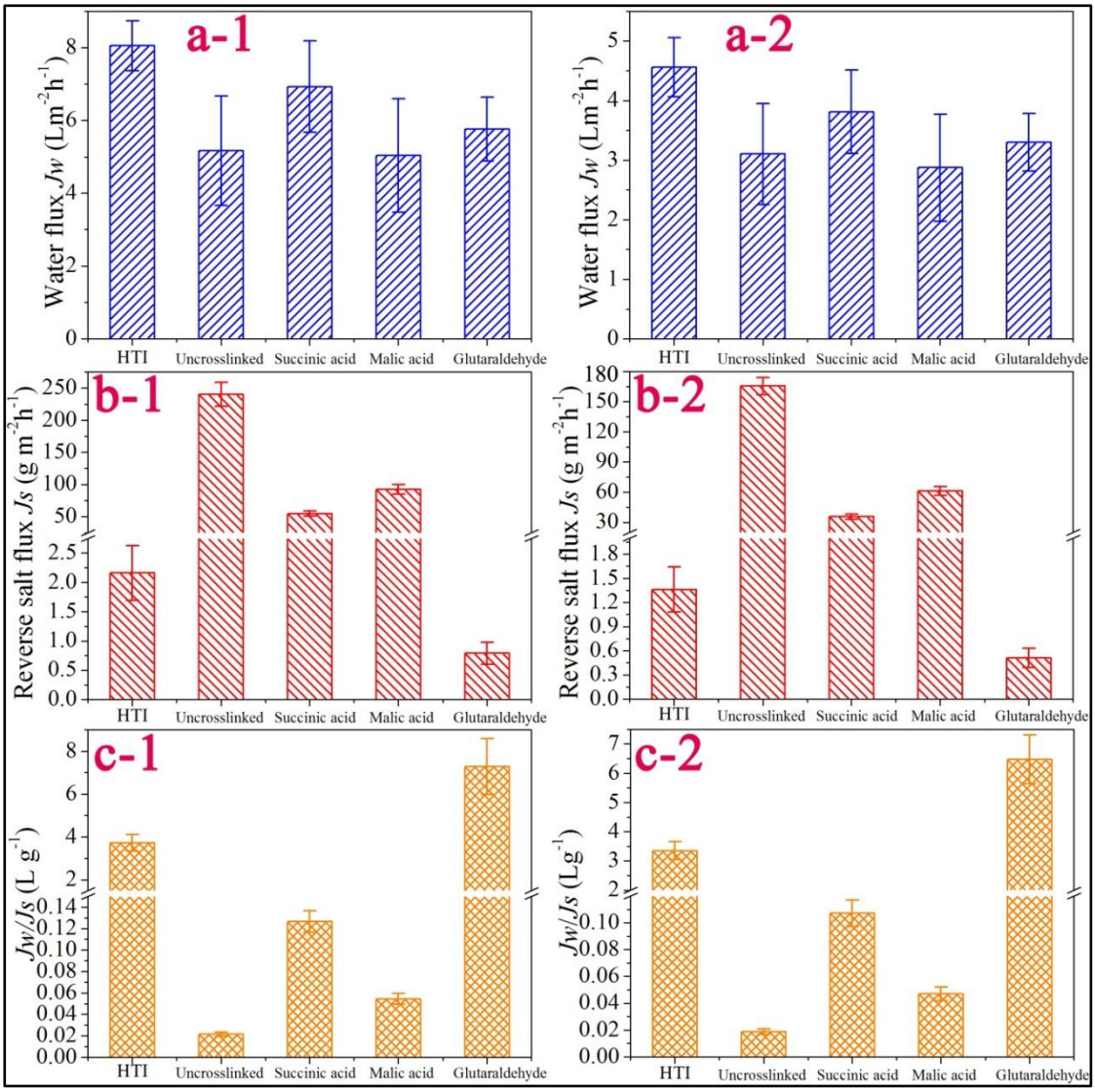

Figure 4.4 Effect of different crosslinking agents on hydrogel selective layer. (**a-1**) Water flux at PRO mode. (**a-2**) Water flux at FO mode. (**b-1**) Reverse salt flux at PRO mode, wherein the J_S axis is broken from 2.75 g m^{-2} h^{-1} to 25 g m^{-2} h^{-1}. (**b-2**) Reverse salt flux at FO mode, wherein the J_S axis is broken from 2 g m^{-2} h^{-1} to 20 g m^{-2} h^{-1}. (**c-1**) J_W/J_S at PRO mode, wherein the J_W/J_S axis is broken from 0.15 L g^{-1} to 1.5 L g^{-1}. (**c-2**) J_W/J_S at FO mode, wherein the J_W/J_S axis is broken from 0.12 L g^{-1} to 2.0 L g^{-1}. All the results are tested under DI water as feed solution and 0.5 M Na_2SO_4 as draw solution. Hydrogel (PVA) concentration and molecular weight are 1.0 wt% and 40.5 kDa, respectively. Besides, the theorectical crosslinking degree is 60%.

Noteworthily, distinct results in terms of reverse salt flux are found among different crosslinking agents (Figure 4.4b-1 ~ 4.4 b-2). The uncrosslinked hydrogel membrane suffers the severest reverse salt leakage, with its J_S as high as 240 ± 19 g m^{-2} h^{-1} under PRO mode and 166 ± 9 g m^{-2} h^{-1} under FO mode. This indicates uncrosslinked hydrogel is not suitable to be used as the selective layer of FO membrane due to its poor rejection of ionic draw solute (Na_2SO_4). The use of malic acid as crosslinking

agent can reduce J_S to 93 ± 8 g m^{-2} h^{-1} under PRO mode and 61 ± 5 g m^{-2} h^{-1} under FO mode, respectively. And the employment of succinic acid as crosslinking agent can reduce J_S to 55 ± 4 g m^{-2} h^{-1} under PRO mode and 36 ± 3 g m^{-2} h^{-1} under FO mode, respectively. However, the J_S values of malic acid or succinic acid are still too high to afford for practical applications. Besides, it's necessary to mention that although many attempts on the crosslinking reaction have been tried including different reaction temperature, reaction time, crosslinking degree *etc*., considerable decrease in J_S has not been found for either malic acid or succinic acid.

A qualitative improvement in the decrease of reverse salt leakage is achieved through using glutaraldehyde as the crosslinking agent, which can further reduce the J_S by nearly two orders of magnitude to as low as 0.79 ± 0.19 g m^{-2} h^{-1} under PRO mode and 0.51 ± 0.12 g m^{-2} h^{-1} under FO mode. These J_S values of glutaraldehyde are even smaller than that of HTI FO membrane (2.2 ± 0.5 g m^{-2} h^{-1} under PRO mode and 1.4 ± 0.3 g m^{-2} h^{-1} under FO mode). The above results indicate that glutaraldehyde crosslinked hydrogel macromolecule (PVA) is most effective in the rejection of ionic draw solute.

Most importantly, the FO performance of P-H membranes with hydrogel selective layer crosslinked by different agents are evaluated from the comprehensive perspective by the indicator J_W/J_S, which signifies membrane's apparent selectivity on water permeability (A) over draw solute permeability (B) during FO operation. Therefore, the higher J_W/J_S, the higher membrane selectivity is. As shown in Figure 4c-1 ~ 4c-2, the J_W/J_S values of different crosslinking agents are grouped into two clusters: one cluster with ultralow J_W/J_S value ≤ 0.2 L g^{-1} (uncrosslinked, malic acid and succinic acid) and the other cluster with relatively much higher J_W/J_S value that are above 3 L g^{-1} (glutaraldehyde; HTI membrane). In detail, the J_W/J_S of uncrosslinked hydrogel is as low as 0.022 ± 0.002 L g^{-1} under PRO mode and 0.019 ± 0.002 L g^{-1} under FO mode, which discloses its invalidity for the selective layer of FO membrane. Furthermore, the J_W/J_S of malic acid is 0.054 ± 0.005 L g^{-1} under PRO mode and 0.047 ± 0.004 L g^{-1} under FO mode, respectively. And the J_W/J_S of succinic acid is 0.13 ± 0.02 L g^{-1} under PRO mode and 0.11 ± 0.01 L g^{-1} under FO mode, respectively. These J_W/J_S values are still far lower than the J_W/J_S values of commercial FO membrane (*i.e.* HTI membrane)

that are 3.7 ± 0.4 L g^{-1} under PRO mode and 3.4 ± 0.3 L g^{-1} under FO mode, respectively. This means it's not economical to use malic acid or succinic acid to crosslink hydrogel macromolecule (PVA) as the selective layer of FO membrane. Fortunately, the J_W/J_S of glutaraldehyde is 7.3 ± 1.3 L g^{-1} at PRO mode and 6.5 ± 0.8 L g^{-1} at FO mode, which are higher than that of HTI membrane, respectively. Although at this initial trying stage, the J_W of glutaraldehyde is not higher than that of HTI membrane, its evidently higher J_W/J_S value demonstrates the promise for the further optimization of hydrogel selective layer.

In addition, the viewpoint that glutaraldehyde outclasses succinic acid and malic acid as the crosslinker to synthesize high selectivity salt-rejecting layer differentiates from the findings by previous work on pressure-driven salt-rejecting membranes (*e.g.* NF or RO). For example, Peng *et al.* reported that the NF membrane with PVA selective layer crosslinked by glutaraldehyde has 97% rejection of Na_2SO_4 while crosslinked by succinic has 91% rejection of Na_2SO_4 (Peng *et al.*, 2011). Lang *et al.* reported that RO membrane with PVA selective layer crosslinked by glutaraldehyde has 90% rejection of NaCl while crosslinked by malic acid has 89% rejection of NaCl (Lang *et al.*, 1995; Lang *et al.*, 1996). In their reports, succinic acid or malic acid can attain the salt rejection comparable to glutaraldehyde. This is possibly because these reports tested membrane rejection under much lower salt concentration that is 2 g/L Na_2SO_4 or 2 g/L NaCl, while in this study the draw solution used is much more concentrated that is 71 g/L Na_2SO_4. And it's the much higher salt concentration that clearly reveals the superiority of glutaraldehyde over succinic acid or malic acid in membrane selectivity (rejection) otherwise the difference among them may be ambiguous.

In short, glutaraldehyde is found to be the best crosslinker that overwhelms other crosslinking agents studied and thus is employed for the following investigations.

4.3.2. Effect of hydrogel molecular weight on hydrogel selective layer

The molecular weight (M_W) of hydrogel macromolecule (PVA) is worth careful examination because it can influence both crosslinking reaction process and the size of as-crosslinked macromolecular adsorbate to a considerable extent. Therefore, FO performances are systematically investigated for P-H membranes with selective layer

synthesized from different molecular weights of hydrogel macromolecule. Accordingly, the J_W and J_W/J_S are presented in Figure 4.5a and Figure 4.5b, respectively.

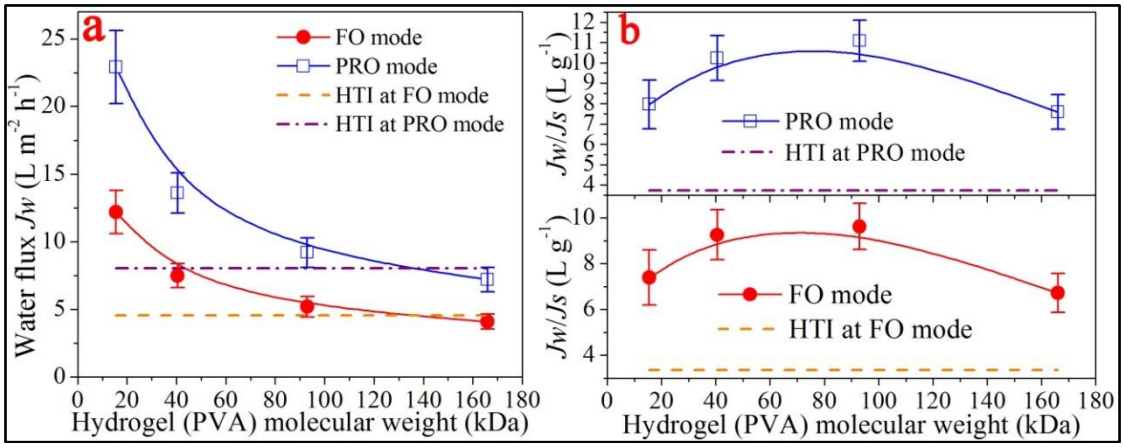

Figure 4.5 Effect of hydrogel molecular weight on hydrogel selective layer. (**a**) Water flux J_W. (**b**) J_W/J_S. All the results are tested under DI water as feed solution and 0.5 M Na_2SO_4 as draw solution. Hydrogel (PVA) concentration is 1.0 wt%. Crosslinking agent is glutaraldehyde. Besides, the theorectical crosslinking degree is 60%.

As shown in Figure 4.5a, the J_W of as-synthesized P-H FO membrane is decreased monotonously from 22.9 ± 2.7 L m^{-2} h^{-1} to 7.2 ± 0.9 L m^{-2} h^{-1} under PRO mode and from 12.2 ± 1.6 L m^{-2} h^{-1} to 4.1 ± 0.6 L m^{-2} h^{-1} under FO mode, respectively, along with the increase of hydrogel M_W from 15.5 kDa to 166 kDa. This result indicates that hydrogel selective layer crosslinked from higher molecular weight macromolecule generally has bigger resistance to water diffusion. Specifically, HTI membrane has the J_W of 8.1 ± 0.8 L m^{-2} h^{-1} under PRO mode and 4.7 ± 0.5 L m^{-2} h^{-1} under FO mode. So P-H membranes with hydrogel selective layer made of macromolecule ≤ 93 kDa outperform HTI membrane in terms of J_W.

More importantly, as hydrogel M_W increased from 15.5 kDa to 166 kDa, the J_S of as-synthesized P-H FO membrane is reduced from 2.88 ± 0.32 g m^{-2} h^{-1} to 0.95 ± 0.1 g m^{-2} h^{-1} under PRO mode and from 1.65 ± 0.22 g m^{-2} h^{-1} to 0.61 ± 0.11 g m^{-2} h^{-1} under FO mode, respectively. These results indicate that hydrogel selective layer crosslinked from higher molecular weight macromolecule can have better rejection of ionic salts. This is because only the hydrogel macromolecules (after crosslinking) with size big enough can effectively cover the top surface pores of polymeric support layer to construct a compact and defect-free selective layer that is able to retain the diffusion of

subnanometer-sized salt ions. Additionally, a turning point on the J_S – M_W curve is found at 93 kDa for both PRO mode and FO mode, exceeding which the decrease in J_S arised from the increase of hydrogel M_W is not significant.

Figure 4.5b shows that as hydrogel M_W increased from 15.5 kDa to 93 kDa, the J_W/J_S of as-synthesized P-H FO membrane is increased from 8.0 ± 1.2 L g^{-1} to 11.1 ± 1.1 L g^{-1} under PRO mode and from 7.4 ± 1.1 L g^{-1} to 9.6 ± 1.0 L g^{-1} under FO mode, respectively. However, the further increase of hydrogel M_W to 166 kDa leads to the considerable decrease in J_W/J_S to 7.6 L g^{-1} under PRO mode and 6.7 L g^{-1} under FO mode, respectively. Undoubtedly, the optimum hydrogel M_W is 93 kDa because the selective layer made from this hydrogel macromolecule can achieve the highest J_W/J_S at this stage, which is almost two times higher than that of HTI membrane (3.7 ± 0.4 L g^{-1} under PRO mode and 3.4 ± 0.3 L g^{-1} under FO mode, respectively).

In short, the molecular weight of hydrogel macromolecule (PVA) for the synthesis of selective layer has been optimized to be 93 kDa, which is employed for the following investigations.

4.3.3. Effect of hydrogel concentration on hydrogel selective layer

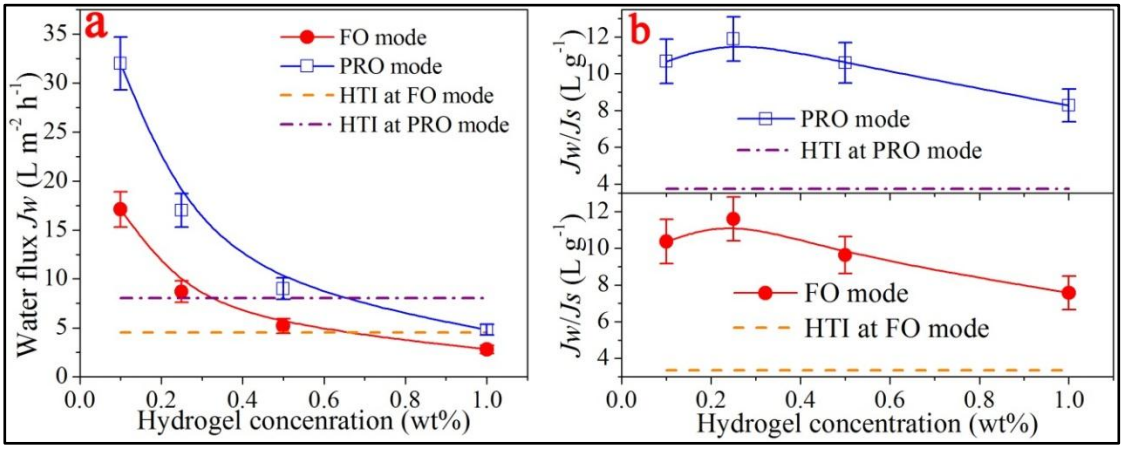

Figure 4.6 Effect of hydrogel concentration on hydrogel selective layer. (**a**) Water flux J_W. (**b**) J_W/J_S. All the results are tested under DI water as feed solution and 0.5 M Na_2SO_4 as draw solution. Hydrogel (PVA) molecular weight is 93 kDa. Crosslinking agent is glutaraldehyde. Besides, the the theorectical crosslinking degree is 60%.

The effect of hydrogel concentration has also been systematically studied because it plays an important role in the morphology of hydrogel selective layer and the

performance of as-synthesized P-H FO membrane, with relevant results presented in Figure 4.6 ~ Figure 4.8. Figure 4.6a shows that as the hydrogel concentration increased from 0.10 wt% to 1.00 wt%, the J_W of as-synthesized P-H membranes is decreased by nearly one order of magnitude from 32 ± 2.8 L m^{-2} h^{-1} to 4.8 ± 0.6 L m^{-2} h^{-1} under PRO mode and from 17.2 ± 1.8 L m^{-2} h^{-1} to 2.8 ± 0.4 L m^{-2} h^{-1} under FO mode, respectively. At hydrogel concentration ≤ 0.25 wt%, P-H membrane demonstrates an evident advantage in J_W over HTI membrane under both PRO and FO operation modes.

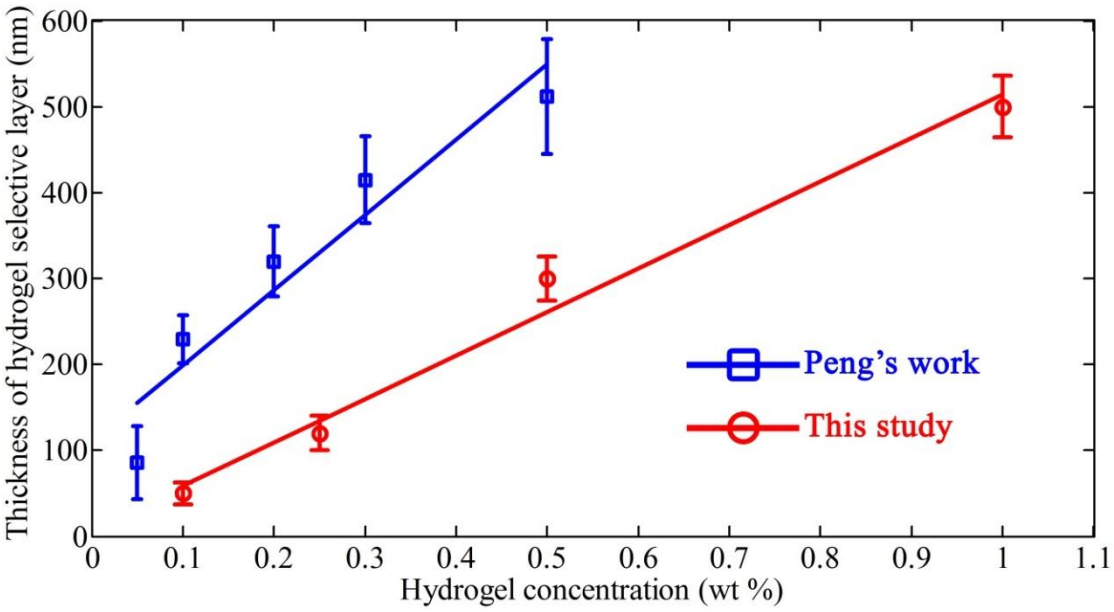

Figure 4.7 The regression analysis between hydrogel concentration and thickness of as-synthesized hydrogel selective layer.

$$\text{HSthickness} = 506 \times \text{conc.} + 8.3, \qquad R^2 = 0.983 \tag{4.1}$$

$$\text{HSthickness} = 877 \times \text{conc.} + 110.8, \qquad R^2 = 0.908 \tag{4.2}$$

where HSthickness is the thickness of as-synthesized hydrogel selective layer, conc. is the hydrogel concentration, and R^2 is the coefficient of determination.

Enlarged FESEM image on P-H membrane cross-section reveals the positive relationship between hydrogel concentration and hydrogel selective layer thickness. Furthermore, the regression analysis indicates that a linear correlation exists between the two factors, as displayed in Figure 4.7. As hydrogel selective layer becomes thicker along with the increase of hydrogel concentration, water molecules need to overcome more frictional resistance induced by additional selective layer thickness when diffusing through P-H membrane. Consequently, J_W exhibits a negative response to the

increase of hydrogel concentration as discussed in Figure 4.6a.

Furthermore, Figure 4.7 compares the regression analysis results between this study (equation 4.1) and previous work by Peng *et al.* on TFC NF membrane with PVA as the selective layer (equation 4.2) (Peng *et al.*, 2010). Noteworthily, the hydrogel selective layer obtained in this study is significantly thinner that of Peng's work at the same hydrogel concentration; and generally thinner selective layer is more favorable for water diffusion. The reasons are in the following four aspects. Firstly, the molecular weight of hydrogel is 93 kDa in this study while 47 kDa in Peng's work. Secondly, the crosslinking agent is glutaraldehyde in this study while succinic acid in Peng's work. The first two aspects will affect the physicochemical properties of as-crosslinked adsorbate. Thirdly, the support layer (*i.e.* the adsorbent here), upon which the selective layer is constructed, is from different polymers: polyethersulfone (PES) in this study while polysulfone (PSf) in Peng's work. The third aspect leads to the difference in adsorption capacity. Last but not least, coating is carried out only once in this study while three times in Peng's work; and more times of coating can produce thicker selective layer.

In addition, AFM results indicate that as-synthesized P-H FO membrane becomes smoother in topography along with the increase of hydrogel concentration, as shown in Figure 4.8. In particular, an evident decrease in topography average roughness (R_a) of P-H membrane from 16.5 ± 2.8 nm to 5 ± 1.3 nm is witnessed as hydrogel concentration increased from 0.00 wt% to 0.25 wt%. As hydrogel concentration further increased to 1.00 wt%, R_a of P-H membrane is as low as 2.0 ± 0.35 nm with root-mean-square (RMS) roughness (R_q) as low as 2.0 ± 0.42 nm, respectively. This means hydrogel selective layer with ultrasmooth topography can be synthesized through adjusting the concentration of hydrogel solution.

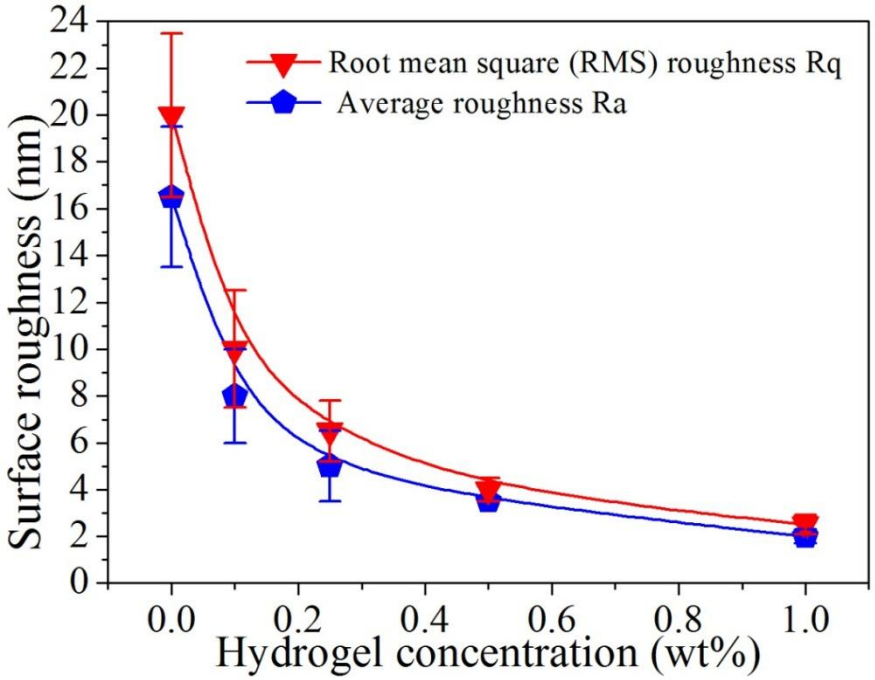

Figure 4.8 Topography roughness of as-synthesized P-H membrane as a function of hydrogel concentration.

Meanwhile, the concentration of hydrogel solution that is used for dip-coating also brings forth significant impacts on salt-rejecting capability of as-synthesized hydrogel selective layer. As hydrogel concentration increased from 0.10 wt% to 0.25 wt%, J_S is reduced by 52.3% from 3.05 ± 0.26 g m^{-2} L^{-1} to 1.43 ± 0.16 g m^{-2} L^{-1} under PRO mode and by 54.5% from 1.66 ± 0.20 g m^{-2} L^{-1} to 0.75 ± 0.11 g m^{-2} L^{-1} under FO mode, respectively. However, as hydrogel concentration further quadrupled to 1.00 wt%, J_S is merely decreased by 59.4% to 0.58 ± 0.08 g m^{-2} L^{-1} under PRO mode and to 0.37 ± 0.05 g m^{-2} L^{-1} under FO mode, respectively. Noteworthily, the J_S of 0.25 wt% hydrogel concentration is 34% lower than that of HTI membrane under PRO mode and 45% lower than that of HTI membrane under FO mode. This means it's already economical in terms of reverse salt leakage to choose 0.25 wt% hydrogel concentration for the synthesis of hydrogel selective layer.

Most importantly, the indicator J_W/J_S verifies that 0.25 wt% is the optimum hydrogel concentration for the synthesis of hydrogel selective through dip-coating process. As hydrogel solution concentrated from 0.10 wt% to 0.25 wt%, the J_W/J_S of as-synthesized P-H FO membrane is elevated from 10.6 ± 1.3 L g^{-1} to 11.9 ± 1.4 L g^{-1} under PRO mode and from 10.4 ± 1.2 L g^{-1} to 11.6 ± 1.2 L g^{-1} under FO mode, respectively. However, the J_W/J_S value turns to decrease from 11.9 ± 1.4 L g^{-1} to 8.3 ±

0.9 L g^{-1} under PRO mode and from 11.6 ± 1.2 L g^{-1} to 7.6 ± 0.9 L g^{-1} under FO mode, respectively, along with the increase of hydrogel concentration from 0.25 wt% to 1.00 wt%. Taking account of the fact that as-synthesized selective layer becomes thicker along with the increase of hydrogel concentration, it's deduced that there exists an optimum thickness for selective layer above which the tradeoff between the decrease in water permeability and the decrease in salt permeability is not favorable for membrane selectivity.

In short, hydrogel concentration is optimized to be 0.25 wt% and employed for the following investigations. And at this stage, the best J_W/J_S attained (at 0.25% hydrogel concentration) is 2.2 times higher than that of HTI under PRO mode and 2.5 times higher than that of HTI membrane under FO mode.

4.3.4. Effect of different draw solutes on FO membrane performance

As introduced in Chapter 2, the selection of draw solute is important to the implementation and operation of FO system. Therefore, the effect of different draw solutes on this P-H FO membrane performance has been elaborately studied, in order to (1) improve the economic feasibility of this FO system, and (2) explore P-H membrane's selectivity on different draw solutes.

Figure 4.9 presents the J_W and J_W/J_S of as-synthesized P-H FO membrane under different draw solutions including 0.5 M NaCl, or 0.5 M $MgCl_2$, or 0.5 M Na_2SO_4 separately. Figure 4.9a-1 shows that under PRO mode, the J_W values under different draw solutions follow the order of 0.5 M $MgCl_2$ (20.5 ± 2.1 L m^{-2} h^{-1}) > 0.5 M Na_2SO_4 (17.1 ± 1.7 L m^{-2} h^{-1}) > 0.5 M NaCl (11.3 ± 1.7 L m^{-2} h^{-1}). These results are further compared with that of HTI FO membrane under exactly the same operation conditions. The use of 0.5 M $MgCl_2$ as draw solution demonstrates the biggest advantage under PRO mode for P-H membrane, with its J_W 118% higher than that of HTI membrane (9.4 ± 0.8 L m^{-2} h^{-1}). The use of 0.5 M Na_2SO_4 as draw solution can attain similar advantage for P-H membrane with its J_W 111% higher than that of HTI membrane (8.1 ± 0.7 L m^{-2} h^{-1}). However, the use of 0.5 M NaCl as draw solution only reaches 62% higher J_W than that of HTI membrane (7.0 ± 0.7 L m^{-2} h^{-1}).

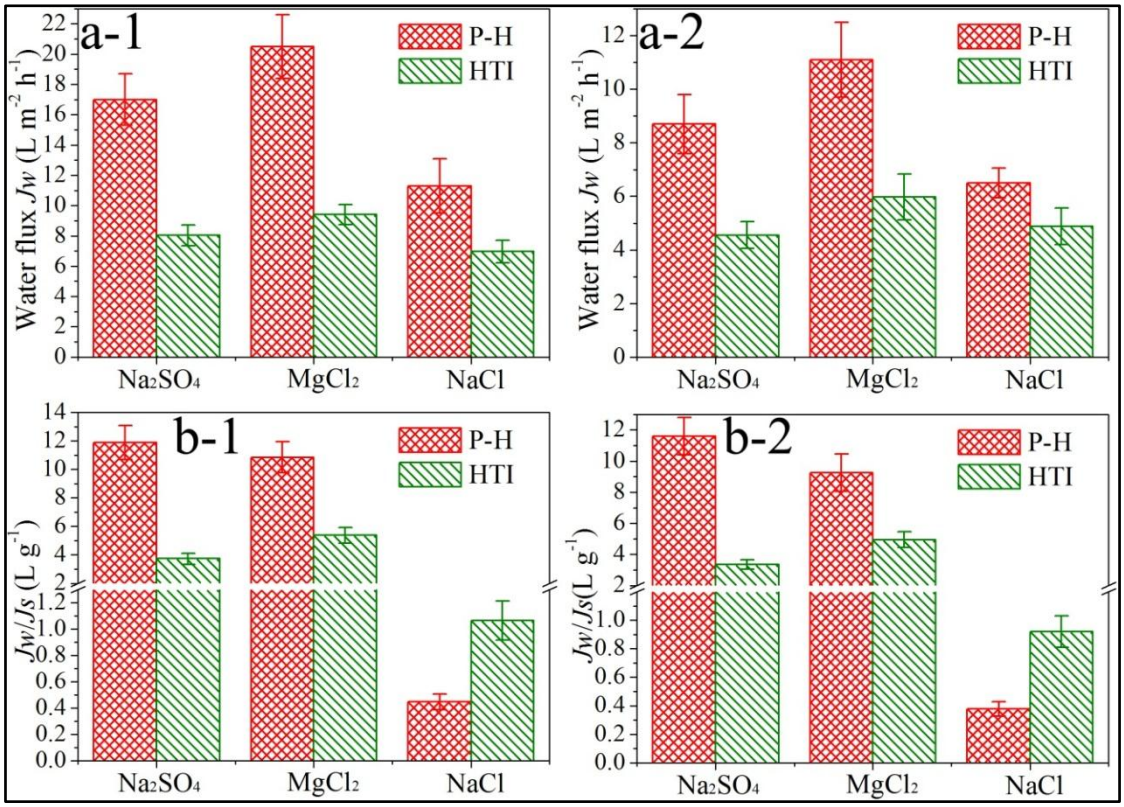

Figure 4.9 Effect of different draw solutes on FO membrane performance. (**a-1**) Water flux J_W under PRO mode. (**a-2**) Water flux J_W under FO mode. (**b-1**) J_W/J_S under PRO mode, wherein the axis of J_W/J_S is broken from 1.3 L g^{-1} to 2.0 L g^{-1}. (**b-2**) J_W/J_S under FO mode, wherein the axis of J_W/J_S is broken from 1.2 L g^{-1} to 2.0 L g^{-1}. All the results are tested under DI water as feed solution. The molar concentration of draw solute is 0.5 M. Hydrogel (PVA) molecular weight and concentration is 93 kDa and 0.25 wt%, respectively. Crosslinking agent is glutaraldehyde with the theorectical crosslinking degree is 60%.

Figure 4.9a-2 shows that under FO mode, the J_W values under different draw solutions follow the same order as that of PRO mode, which is 0.5 M $MgCl_2$ (11.1 ± 1.5 L m^{-2} h^{-1}) > 0.5 M Na_2SO_4 (8.7 ± 1.1 L m^{-2} h^{-1}) > 0.5 M NaCl (6.5 ± 0.6 L m^{-2} h^{-1}). But there are certain differences when comparing these J_W values with that of HTI membrane. The use of 0.5 M Na_2SO_4 as draw solution demonstrates the biggest advantage for P-H membrane under FO mode with its J_W 91% higher than that of HTI membrane (4.6 ± 0.5 L m^{-2} h^{-1}). The use of 0.5 M $MgCl_2$ as draw solution attains the 86% higher J_W than that of HTI membrane (6.0 ± 0.9 L m^{-2} h^{-1}). And the use of 0.5 M NaCl as draw solution reaches merely 33% higher J_W than that of HTI membrane (4.9 ± 0.7 L m^{-2} h^{-1}).

Meanwhile, there exist remarkable differences in terms of *Js* among different ionic salts as the draw solute. Under PRO mode, the *Js* with 0.5 M Na_2SO_4 as draw solution

is the lowest, which is as low as 1.43 ± 0.17 g m^{-2} h^{-1} (equaling to 10.07 ± 1.20 mM m^{-2} h^{-1}). The *Js* with 0.5 M $MgCl_2$ as draw solution is a little higher *i.e.* 1.89 ± 0.41 g m^{-2} h^{-1} (equaling to 19.89 ± 4.3 mM m^{-2} h^{-1}). However, the *Js* with 0.5 M NaCl as draw solution is more than one order of magnitude higher *i.e.* as high as 25.3 ± 4.8 g m^{-2} h^{-1} (equaling to 432.5 ± 82.1 mM m^{-2} h^{-1}). Under FO mode, the *Js* of different draw solutions follows the same order as that of PRO mode: 0.5 M Na_2SO_4 (0.75 ± 0.11 g m^{-2} h^{-1}, equaling to 5.28 ± 0.77 mM m^{-2} h^{-1}) < 0.5 M $MgCl_2$ (1.2 ± 0.13 g m^{-2} h^{-1}, equaling to 12.63 ± 1.37 mM m^{-2} h^{-1}) << 0.5 M NaCl (17.2 ± 3.1 g m^{-2} h^{-1},equaling to 294.0 ± 53.0 mM m^{-2} h^{-1}). These *Js* values are further compared with that of HTI membrane under the same opearting conditions. Firstly, the *Js* of P-H membrane with 0.5 M Na_2SO_4 as draw solution is 34% lower than that of HTI membrane under PRO mode and 45% lower than that of HTI membrane under FO mode, respectively. Secondly, the *Js* of P-H membrane with 0.5 M $MgCl_2$ as draw solution is comparable to that of HTI membrane under both PRO mode and FO mode (difference within 8%). Thirdly, the *Js* of P-H membrane with 0.5 M NaCl as draw solution is >2 times higher than that of HTI membrane (6.56 ± 0.86 g m^{-2} h^{-1}, equaling to 112.1 ± 14.7 mM m^{-2} h^{-1} under FO mode; 5.31 ± 0.71 g m^{-2} h^{-1}, equaling to 90.8 ± 12.1 mM m^{-2} h^{-1} under FO mode, respectively) under both operation modes. These *Js* results indicate that as-synthesized P-H membrane has exceptionally high rejection of divalent draw solutes (*e.g.* Na_2SO_4) but medium to high rejection of monovalent draw solutes (*e.g.* NaCl). This is because in aqueous environment the diameter of monovalent anion Cl^- (0.3 nm) is much smaller than that of divalent anion SO_4^{2-} (0.4 nm) (Achilli *et al.*, 2010). Hence monovalent anion is much more difficult to be rejected by salt-rejecting membranes. These results also substantiate that as-synthesized P-H FO membrane possesses the salt-rejecting capability that exceeds NF level and approaches RO level. The other point to be noted is that the reverse salt leakage of as-synthesized hydrogel selective layer with $MgCl_2$ as draw solution is one order of magnitude lower than the best (lowest) *Js* value achieved by the layer-by-layer formed polyelectrolyte selective layer published by Qi *et al.* (Qi *et al.*, 2011), which is 150 mM m^{-2} h^{-1} under PRO mode and 70 mM m^{-2} h^{-1} under FO mode for their membranes. This result demonstrates the remarkable advantage of as-synthesized hydrogel FO membrane over the layer-by-layer polyelectrolyte FO membrane (Qi *et al.*, 2011) in salt-rejecting capability.

More importantly, Figure 4.9b-1 ~ 4.9b-2 displays the significant difference in terms of J_W/J_S among different draw solutes. As-synthesized P-H membrane attains highest J_W/J_S values using Na_2SO_4 as draw solute, which are 11.9 ± 1.3 L g^{-1} (corresponding to the J_S/J_W of 0.60 ± 0.06 mM) under PRO mode and 11.6 ± 1.2 L g^{-1} (corresponding to the J_S/J_W of 0.61 ± 0.06 mM) under FO mode, respectively. And the J_W/J_S of P-H membrane using Na_2SO_4 as draw solute is 2.2 times higher than that of HTI membrane under PRO mode and 2.5 times higher than that of HTI membrane under FO mode, respectively. Using $MgCl_2$ as draw solute, P-H membrane attains the J_W/J_S of 10.8 ± 1.1 L g^{-1} (corresponding to the J_S/J_W of 0.97 ± 0.10 mM) under PRO mode and 9.3 ± 1.2 L g^{-1} (corresponding to the J_S/J_W of 1.13 ± 0.11 mM) under FO mode, respectively. And the J_W/J_S of P-H membrane using $MgCl_2$ as draw solute is 1.0 times higher than that of HTI membrane under PRO mode and 0.9 times higher than that of HTI membrane under FO mode, respectively. However, using NaCl as draw solute, P-H membrane attains the J_W/J_S of only 0.45 ± 0.06 L g^{-1} (corresponding to the J_S/J_W of 38.3 ± 5.1 mM) under PRO mode and 0.38 ± 0.05 L g^{-1} (corresponding to the J_S/J_W of 45.2 ± 5.9 mM) under FO mode, respectively. And the J_W/J_S of P-H membrane using NaCl as draw solute is 58% lower than that of HTI membrane under PRO mode and 59% lower than that of HTI membrane under FO mode, respectively. One point to be noted here is the lowest J_S/J_W of layer-by-layer polyelectrolyte FO membrane from Qi *et al.* using $MgCl_2$ as draw solute is 6.0 mM under PRO mode and 3.2 mM under FO mode, which is 5 time higher (worse) than as-synthesized hydrogel FO membrane under PRO mode and 2 times higher (worse) than as-synthesized hydrogel FO membrane under FO mode, respectively. These results further demonstrate the undoubted superiority of as-synthesized P-H FO membrane over the layer-by-layer polyelectrolyte FO membrane (Qi *et al.*, 2011) in membrane selectivity.

In short, among various ionic draw solutes investigated, the use of Na_2SO_4 as draw solute can achieve the lowest *Js*, second highest J_W, and consequently highest J_W/Js (*i.e.* lowest J_S/J_W). Therefore, Na_2SO_4 is found to be the best draw solute and selected for the following experiments.

4.3.5. Effect of crosslinking degree on hydrogel selective layer

Crosslinking degree is regarded as the decisive factor for the synthesis of hydrogel selective layer, because it determines the molecular structure as well as chemical properties (*e.g.* hydrophilicity and oleophobicity, *etc.*) of as-crosslinked hydrogel and thus influences the separation capabilities (*e.g.* salt-rejecting capability and water permeability, *etc.*) of as-synthesized FO membrane to a large extent. Therefore, the effect of theoretical crosslinking degree (*TCLD*) has been systematically investigated with the relevant results shown in Figure 4.10 ~ Figure 4.11.

Figure 4.10a shows that the J_W of as-syntheiszed P-H membrane undergoes the monotonous decrease from 31.8 ± 3.4 L m^{-2} h^{-1} to 17.0 ± 1.6 L m^{-2} h^{-1} under PRO mode and from 16.8 ± 1.9 L m^{-2} h^{-1} to 8.0 ± 1.6 L m^{-2} h^{-1} under FO mode, respectively, along with the increase of *TCLD* from 10% to 60%. As *TCLD* further increased to 100%, the J_W of as-syntheiszed P-H membrane experiences a much slower decrease with the value stabilized around 15 L m^{-2} h^{-1} under PRO mode and 7 L m^{-2} h^{-1} under FO mode, respectively. Noteworthily, as-syntheiszed P-H membrane maintains the advantage of high water flux over HTI membrane under both PRO and FO operation modes throughout the increase of *TCLD* from 10% to 100%, based upon the optimization of other crosslinking factors as discussed previously.

The corresponding changes in J_S are shown in Figure 4.10b, wherein the decrease of J_S along with the increase of *TCLD* can be divided into three stages. Firstly, the J_S of as-syntheiszed P-H membrane undergoes a rapid decrease from 3.40 ± 0.39 g m^{-2} h^{-1} to 1.90 ± 0.22 g m^{-2} h^{-1} under PRO mode and from 1.92 ± 0.23 g m^{-2} h^{-1} to 1.05 ± 0.14 g m^{-2} h^{-1} under FO mode, respectively, as *TCLD* increased from 10% to 30%. Secondly, the J_S experiences a slow decrease from 1.90 ± 0.22 g m^{-2} h^{-1} to 1.43 ± 0.16 g m^{-2} h^{-1} under PRO mode and from 1.05 ± 0.14 g m^{-2} h^{-1} to 0.75 ± 0.11 g m^{-2} h^{-1} under FO mode, respectively, along with the further increase of *TCLD* from 30% to 60%. Thirdly, the J_S turns to be stabilized around 1.35 g m^{-2} h^{-1} under PRO mode and 0.65 g m^{-2} h^{-1} under FO mode, respectively, as *TCLD* further increased to 100%. These results substantiate that it's effective to control reverse salt leakage of as-synthesized P-H FO membrane through adjusting the crosslinking extent of hydrogel macromolecule especially within the region of 10% ~ 60% *TCLD*, owning to as-demonstrated sensitive

response of J_S to *TCLD*. Besides, it's also worthy to note that ≥ *TCLD* of 30%, the J_S of as-synthesized P-H FO membrane is smaller than that of HTI FO membrane under each operation mode. This confirms the economical feasiblility of as-synthesized P-H FO membrane in terms of draw solute cost.

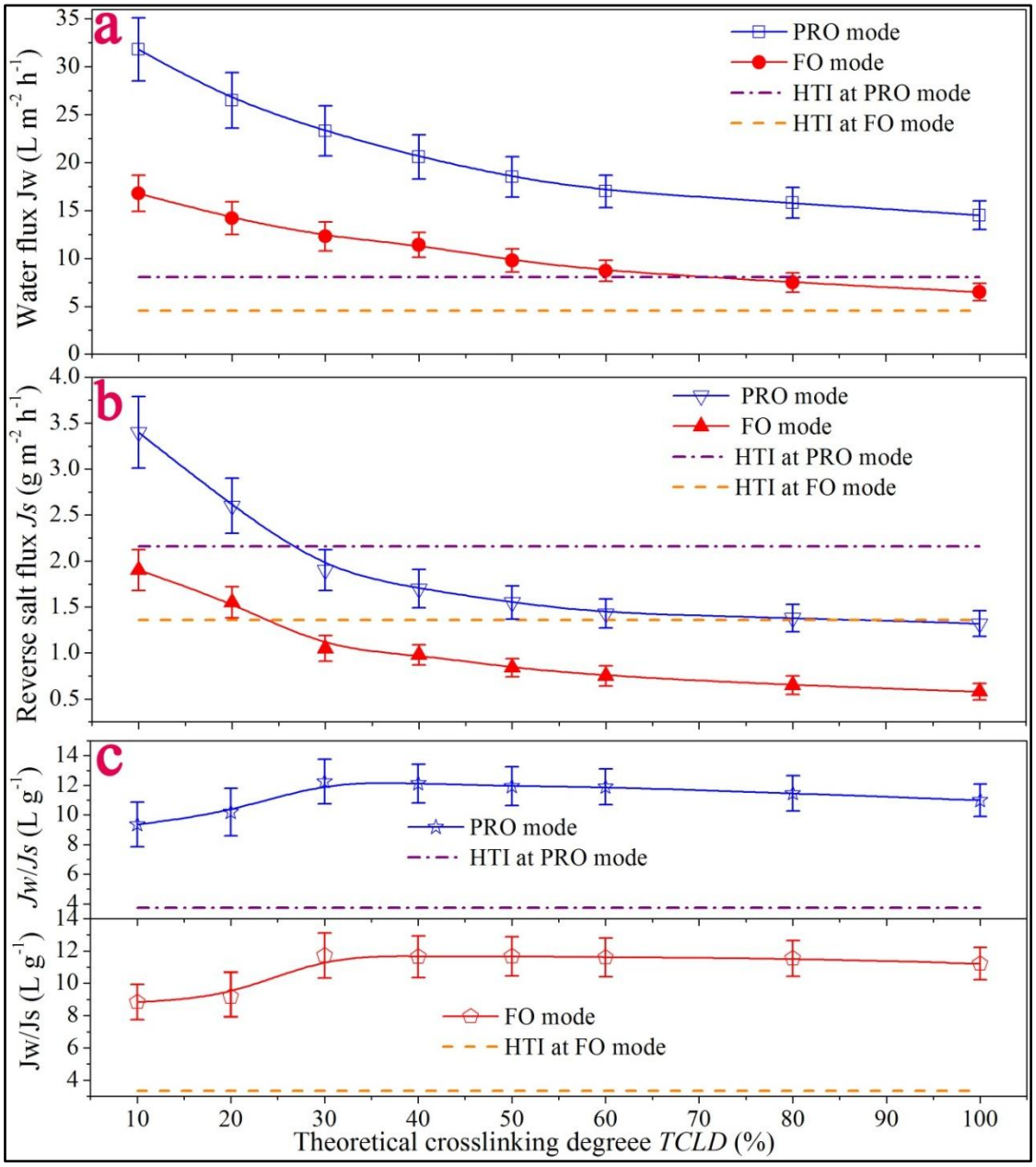

Figure 4.10 Effect of different crosslinking degree on hydrogel selective layer. (**a**) Water flux J_W. (**b**) Reverse salt flux J_S. (**c**) J_W/J_S. All the results are tested under DI water as feed solution and 0.5 M Na_2SO_4 as draw solution. Hydrogel (PVA) molecular weight and concentration is 93 kDa and 0.25 wt%, respectively. Besides, the crosslinking agent is glutaraldehyde.

Furthermore, taking the J_W and J_S together into acount, the operation results under

PRO mode reveal that the instrinsic water permeability (*A*) is gradually tuned down along with the increase of hydrogel crosslinking degree, with relevant analysis elucidated as follows. The J_W of P-H FO membrane is determined by four factors *i.e.* water permeability (*A*), osmotic pressure difference ($\Delta\pi$), ECP modulus and ICP modulus (McCutcheon & Elimelech, 2007). The ECP modulus here can be negelected on account of the employed vigrous cross-flow setting as introduced in Chapter 3. Moreover, because J_S from draw solution to feed solution (DI water) is in the ultralow level (< 20 mM m^{-2} h^{-1}), the draw solute concentration in the feed solution due to reverse salt leakage is neglibile. Therefore, the ICP modulus at the initial filtration period (the first several hours) can also be neglected. As a result, J_W under PRO mode can be simplified as *A* times $\Delta\pi$. And because $\Delta\pi$ is a constant (draw solution is 0.5 M Na_2SO_4 for all *TCLD* testing), the decrease in J_W indicates the decrease in *A* value, which means the instrinsic water permeability of as-synthesized P-H FO membrane can be finely tuned through controlling the crosslinking extent of hydrogel macromolecule.

Most importantly, Figure 4.10c presents the changes in J_W/Js along with the increase of *TCLD*, which can be divided into three stages. Firstly, as *TCLD* increased from 10% to 30%, the J_W/Js of as-synthesized P-H membrane is increased from 9.4 ± 1.4 L g^{-1} to 12.3 ± 1.5 L g^{-1} under PRO mode and from 8.8 ± 1.3 L g^{-1} to 11.7 ± 1.4 L g^{-1} under FO mode, respectively. Secondly, as *TCLD* continued the increase from 30% to 60%, the J_W/Js of P-H membrane is stabilized around 11.9 L g^{-1} under PRO mode and 11.6 L g^{-1} under FO mode, respectively. Thirdly, as *TCLD* further increased from 60% to 100%, the J_W/Js of P-H membrane turns to be reduced gradually from 11.9 ± 1.3 L g^{-1} to 11.0 ± 1.1 L g^{-1}under PRO mode and from 11.6 ± 1.2 L g^{-1} to 11.2 ± 1.0 L g^{-1}under FO mode, respectively. The plateau on the J_W/Js – *TCLD* curve located from 30% *TCLD* to 60% *TCLD* is the optimum crosslinking region wherein the J_W/Js can be maintained in the highest level regardless of the change in *TCLD*. Meanwhile, *TCLD* < 30% is regarded as insufficient crosslinking extent which induces severe draw solute leakage while *TCLD* > 30% is excessive crosslinking extent which results in significantly smaller J_W. It's necessary to note that the relatively wide region between 30% to 60% (border included) in terms of *TCLD* offers a large room to finely tune the physicochemical properties of hydrogel selective layer without compromising

membrane selectivity (J_W/J_S). Besides, this also means the use of as-crosslinked hydrogel as FO selective layer is a robust technology that can provide stable J_W/Js with a high tolerance on the change of *TCLD* which is possibly encountered in the practical synthetic processes, and thus is favorable for scale-up membrane manufacture. Besides, the other point to be noted is that throughout the change in *TCLD*, P-H membrane maintains the evident advantage over HTI membrane with its J_W/Js 1.5 ~ 2.3 times higher than that of HTI membrane under PRO mode and 1.6 ~ 2.5 times higher than that of HTI membrane under FO mode, respectively.

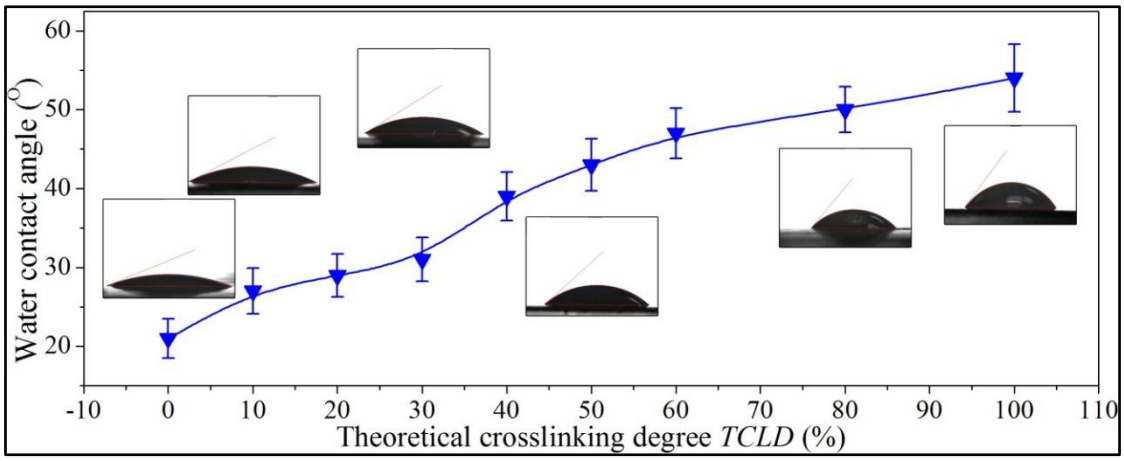

Figure 4.11 Water contact angle of P-H membrane top surface as a function of theoretical crosslinking degree (*TCLD*).

Besides the effect of *TCLD* upon FO performances, the impacts of *TCLD* on chemical properties of as-synthesized hydrogel selective layer have also been investigated for a comprehensive evaluation of optimum crosslinking degree. Figure 4.11 exhibits that water contact angle is increased monotonously from $21° \pm 2.5°$ to $54° \pm 4.3°$ as *TCLD* increased from 0% to 100%. Particularly, a turning point is found at *TCLD* of 30%, exceeding which the slope of water contact angle – *TCLD* turns to be steeper especially in the *TCLD* region from 30% to 60%. These results indicate that the hydrophilicity of as-synthesized selective layer is reduced along with the increase of hydrogel crosslinking extent. This is probably because the crosslinked region of hydrogel macromolecule is relatively hydrophobic while the uncrosslinked region of hydrogel is hydrophilic. Along with the increase of *TCLD*, less uncrosslinked hydroxyl groups is left, which renders as-synthesized hydrogel selective layer less hydrophilic. More importantly, hydrophilicity is one of the key indicators that promise the selective layer with high anti-fouling capability as discussed previously in Chapter 2.

As-synthesized FO membrane with hydrogel selective layer is designated to treat wastewater of high fouling potential (*e.g.* oil heavily polluted wastewater). Therefore, 30% is selected as the best *TCLD* value because it possesses the highest hydrophilicity within the optimum crosslinking region that guarantees simultaneous high membrane selectivity (J_W/J_S) and high water permeability (A).

In short, 30% is revealed as the optimum *TCLD* and selected for the following investigations. This outcome is acquired based upon the comprehensive optimizations of both FO performances and membrane physicochemical properties, thus expected to offer long-term stable FO operations with low fouling, high water flux, and high selectivity for the treatment of challenging wastewater (*e.g.* highly oily wastewater).

4.3.6. Effect of coating time on hydrogel selective layer

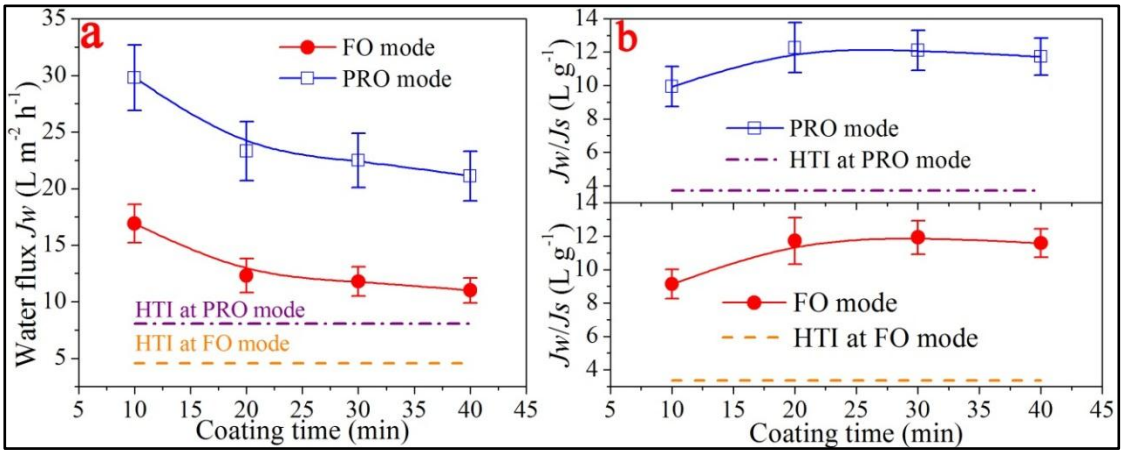

Figure 4.12 Effect of coating time on hydrogel selective layer. (**a**) Water flux J_W. (**b**) J_W/J_S. All the results are tested under DI water as feed solution and 0.5 M Na_2SO_4 as draw solution. Hydrogel (PVA) molecular weight and concentration is 93 kDa and 0.25 wt%, respectively. Besides, crosslinking agent is glutaraldehyde with *TCLD* of 30%.

It has been proposed that the adsorption of polymer with polar groups (*e.g.* hydroxyl group) generally undergoes two steps: adhesion and reconfiguration (McAloney & Goh, 1999). Firstly, polymer molecules diffuse from the bulk solution and get adsorbed onto the surface of solid substrate (*e.g.* support layer). This adhesion process is usually very fast (*e.g.* within 10 seconds). As a result, the original alignment of water molecules on the substrate surface is disrupted, leading to a temporarily metastable interfacial system. Secondly, the adhered macromolecules take a slow relaxation process, resulting in the realignment of water molecules and the minimization of

interfacial energy. Therefore, the control of coating time can be a useful way to finely tune the architecture and property of as-built hydrogel selective layer, with relevant investigation presented in Figure 4.12.

Figure 4.12a shows that along with the increase in coating time from 10 min to 40 min, the J_W of as-syntheiszed P-H membrane is decreased from 29.8 ± 2.9 L m^{-2} h^{-1} to 21.1 ± 2.2 L m^{-2} h^{-1} under PRO mode and from 16.9 ± 1.7 L m^{-2} h^{-1} to 11.0 ± 1.1 L m^{-2} h^{-1} under FO mode, respectively. Throughout the increase in coating time, P-H membrane maintains its superority over HTI membrane in J_W under both PRO and FO modes. Noteworthily, the negative correlation between J_W and coating time is different from that reported by Duong *et al.* on layer-by-layer polyelectrolyte FO membrane. Specifically, Duong *et al.* reported that as coating time increased, the J_W value is increased until a plateau is reached at 20 min (Duong *et al.*, 2013). The difference on the trends of J_W along with the increase of coating time may be ascribed to distinct chemical properties between the macromolecules to be adsorbed *i.e.* PVA in this study and poly(allylamine hydrochloride) (PAH)/poly(sodium 4-styrenesulfonate) (PSS) in their work.

Moreover, the J_S of as-syntheiszed P-H membrane undergoes a remarkable decrease from 3.05 ± 0.28 g m^{-2} h^{-1} to 1.90 ± 0.22 g m^{-2} h^{-1} under PRO mode and from 1.85 ± 0.25 g m^{-2} h^{-1} to 1.05 ± 0.16 g m^{-2} h^{-1} under FO mode, respectively, along with the increase in coating time from 10 min to 20 min. As coating time further increased from 20 min to 40 min, the J_S of P-H membrane is merely reduced by less than 10% from 1.90 ± 0.22 g m^{-2} h^{-1} to 1.80 ± 0.19 g m^{-2} h^{-1} under PRO mode and from 1.05 ± 0.16 g m^{-2} h^{-1} to 0.95 ± 0.17 g m^{-2} h^{-1} under FO mode, respectively. This result indicates that 20 min is sufficient for the adsorbed hydrogel macrmolecules (PVA) to conduct the reorientation and reconfiguration, which enables the alignment of adsorbed macromolecule chains to be more orderly in arrangement. As a result, some defects due to original irregular packing of macromolecule chains are repaired, which forms the hydrogel selective layer of less defects thus favorable for the minimization of reverse salt leakage.

Most importantly, Figure 4.12b shows that the maximum J_W/J_S is obtained at coating

time of 20 min. As coating time increased from 10 min to 20 min, the J_W/J_S of P-H membrane is enhanced from 9.9 ± 1.2 L g^{-1} to 12.3 ± 1.5 L g^{-1} under PRO mode and from 9.1 ± 0.9 L g^{-1} to 11.7 ± 1.4 L g^{-1} under FO mode, respectively. However, as coating time undergoes further increase from 20 min to 40 min, the J_W/J_S of P-H membrane is reduced from 12.3 ± 1.5 L g^{-1} to 11.7 ± 1. L g^{-1} under PRO mode and from 11.7 ± 1.4 L g^{-1} to 11.5 ± 0.9 L g^{-1} under FO mode, respectively. This result indicates that overlong coating time can be counterproductive, because the amount of adsorbed hydrogel macromolecule can be increased along with the extention of coating time. As a result, a relatively thicker selective layer is produced, which will compromise the intrinsic water permeability of as-synthesized P-H membrnae.

In short, 20 min is found to be the optimum coating time and selected for the following investigations. And at coating time of 20 min, as-synthesized P-H FO membrane can achieve ~1.8 times higher J_W, ~15% lower J_S, and ~2.4 times higher J_W/J_S than that of HTI FO membrane under both PRO and FO operation modes.

4.4. Summary

For the first time, the potentiality of hydrogel macromolecule as the selective layer of FO membrane is systematically studied, with relevant optimization results on the structures and properties of as-synthesized hydrogel selective layer summarized in Table 4.2. These optimum values are kept for the following investigations in this study. Important points are noted as follows.

Table 4.2 Optimizations on hydrogel selective layer of P-H FO membrane.

Parameters that have been investigated	Optimum value
Chemical crosslinking agent	Glutaraldehyde
Hydrogel (PVA) molecular weight	93 kDa
Hydrogel concentration	0.25 wt%
Crosslinking degree	*TCLD* of 30%
Coating time	20 min
Draw solutes	Na_2SO_4

Firstly, a variety of characterization results substantiate that an ultrathin selective layer (thickness of 119 ± 7 nm) made of hydrogel macromolecule (PVA) is successfully

constructed onto PES support layer top surface through dip-coating technology.

Secondly, FO performance test results further reveal that uncrosslinked hydrogel is not suitable to be used as the selective layer of FO membrane due to its poor rejections of ionic draw solutes. And the best chemical agent to crosslink hydrogel towards high selectivity FO membrane is found to be glutaraldehyde.

Thirdly, many other factors that influence the formation of hydrogel selective layer have been carefully optimized step by step, with an elaborate analysis carried out from the perspective of adsorption process. Among these factors, crosslinking degree plays a key role in fine-tuning both physical structure and chemical property of hydrogel selective layer. And the optimum crosslinking degree is found to be 30%, at which as-synthesized P-H FO membrane maintains both high hydrophilicity and high separation performances.

Last but not least, based upon all these optimized results, as-synthesized P-H FO membrane can accomplish ~1.8 times higher J_W, ~15% lower J_S, and ~2.4 times higher J_W/J_S than that of HTI FO membrane under both PRO and FO operation modes. These outstanding FO performances validate the feasibility of using chemically crosslinked hydrogel as the selective layer for FO membrane. By achiving so, the way to further explore the optimization of FO membrane's support layer towards the final goal of treating challenging wastewater (*e.g.* highly saline and oily wastewater) with low fouling, high water flux, and high selectivity is paved.

CHAPTER 5 OPTIMIZATION OF NANOCOMPOSITE SUPPORT LAYER: THE KEY ROLE OF GO NANOSHEETS IN MINIMIZING ICP TOWARDS HIGH WATER FLUX

5.1. Introduction

In Chapter 4, the utilization of hydrogel as the selective layer of FO membrane has demonstrated the ability to achieve high rejections of tiny inorganic ions (high selectivity) and the promise in resisting fouling owning to its high hydrophilicity and smooth topography (low fouling). Based upon these achievements, this chapter moves forward as the second step to clear another technique hurdle on the way to the final goal of this thesis, that is, high water flux FO membrane.

As introduced in section 2.4.2 of Chapter 2, FO technology suffers from the intrinsic bottleneck of internal concentration polarization (ICP) problem that limits FO water flux in the level much lower than theoretical expectation. Noteworthily, the membrane structure (support layer structure) that can break ICP bottleneck remains exceedingly desirable especially for the dominant membrane manufacture processes *e.g.* phase inversion technology. This chapter investigates the potentiality to utilize hydrophilic 2D nanomaterial (*e.g.* GO nanosheet) to explore the structure of support layer for the purpose of high water flux FO membrane. It's extremely worthy to note that distinct from the two published articles by peer researchers on modifying FO membrane support layer through the incorporation of GO nanosheet or its derivative (Park *et al.*, 2015; Wang *et al.*, 2015), this study arrives at a much higher horizon that is to search the potentiality of GO nanosheet to create an entirely new support layer structure in terms of pore interconnectivity and to further explore the mechanism on the engineering of phase inversion process with 2D hydrophilic nanomaterial. This is because this study fully understands that support layer with highly interconnected interior pores at micrometer scale is the key to solve the ICP problem.

Motivated by the target to create a support layer of highly interconnected pore structure for FO membrane support layer, systematic investigations have been conducted based upon the deliberate design of research as follows. Firstly, the structures and properties of as-synthesized GO nanosheets are studied. Secondly, the

GO nanosheets are incorporated into support layer through phase inversion technique and the embedment of GO nanosheets in as-synthesized nanocomposite support layer is verified by various characterization techniques. Thirdly, the influences on the chemical properties of as-synthesized support layer by the incorporation of GO nanosheets are investigated. Fourthly, the impacts on the surface structures of as-synthesized support layer by incorporating GO nanosheets are examined. Fifthly and most importantly, the impacts on the interior pore structure of as-synthesized support layer are investigated and emphasized, wherein a brand new support layer structure *i.e.* interior pores highly interconnected in all three dimensions at micrometer scale (3D interconnected porous support layer) is created for the first time based upon systematic optimizations of phase inversion parameters including GO concentration, polymer concentration, different solvents *etc*. Sixthly, the formation mechanism of this 3D interconnected porous support layer is explored from the perspective of GO induced viscous fingering. Seventhly, the impacts on FO membrane performance (water flux J_W and reverse salt flux J_S) and FO membrane structural parameter (S) by the formation of this 3D interconnected porous support layer are studied. Finally, the significances and implications of this newly built 3D interconnected porous support layer on FO technology are carefully summarized.

To the best knowledge of the author, this is the first study that demonstrates GO's ability to direct the construction of 3D interconnected porous structure for the synthesis of polymeric membrane. More importantly, this micrometer-scaled pore interconnectivity in all three dimensions is achieved through prevailed membrane manufacture process *i.e.* phase inversion at normal operation conditions. This guarantees its superiority in economic feasibility for scale-up applications.

In addition, for the clarification purpose, the nanocomposite FO membrane with GO assisted phase inversion constructed support layer (GO\P support layer) is coded as GO\P-H FO membrane, while the FO membrane with conventional phase inversion constructed support layer (P support layer) is coded as P-H FO membrane (H stands for hydrogel selective layer), as introduced previously in Chapter 4.

5.2. The structures and properties of as-synthesized GO nanosheets

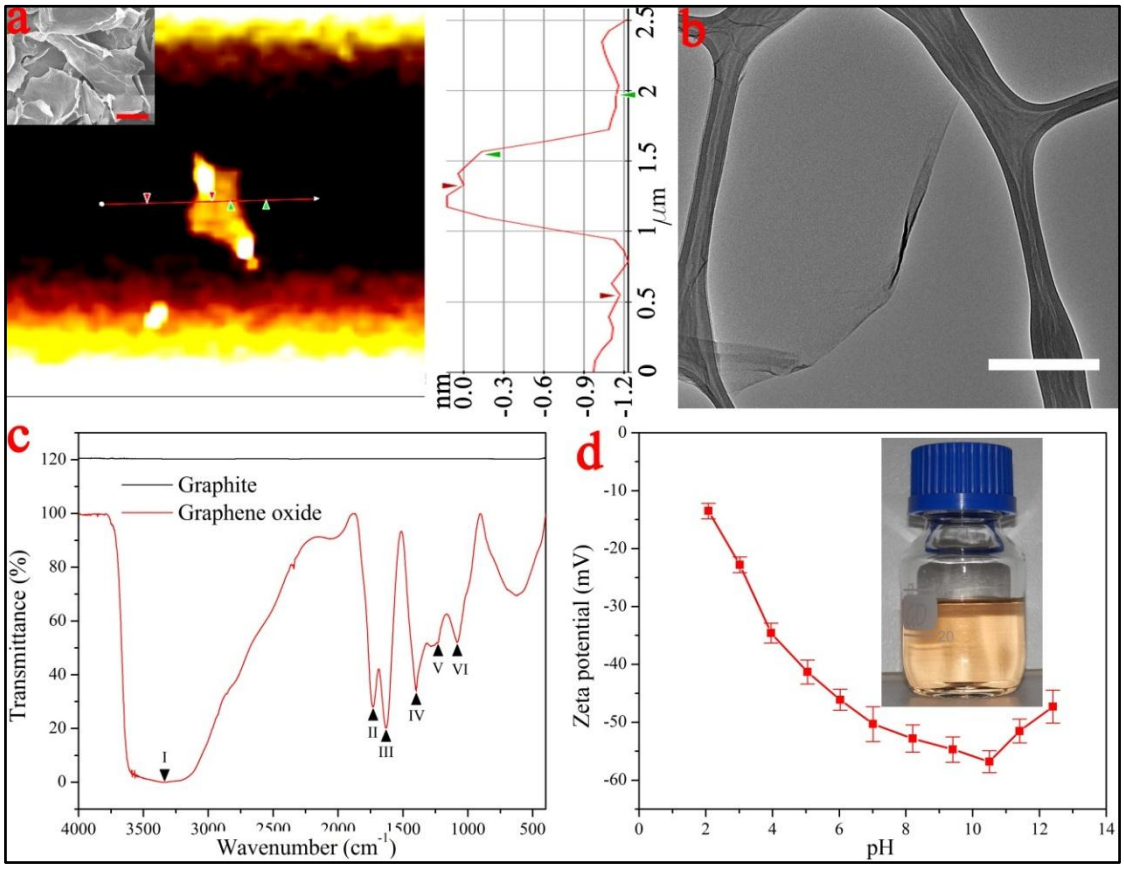

Figure 5.1 The structures and properties of as-synthesized GO nanosheets. (**a**) AFM image of a single graphene oxide sheet, scale bar, 1 μm. The inserted subfigure is the FESEM micrograph of as-synthesized graphite oxide sheets, scale bar 10 μm. (**b**) TEM image of a single graphene oxide sheet (scale bar, 400 nm). (**c**) The black curve is the FTIR spectrum of graphite, which is featureless while the red curve below is the FTIR spectrum of as-synthesized GO, which has several characteristic IR bands as listed in Table 5.1. (**d**) Zeta-potential of as-synthesized GO nanosheets at different pH values. The inserted subfigure is the optical photograph of GO aqueous solution (100 mg L^{-1}).

The structures and properties of as-synthesized GO nanosheets are characterized by various techniques and presented in Figure 5.1. Graphene oxide sheets in nanometer (nm) scale thickness are successfully prepared through exfoliating as-synthesized graphite oxide (inserted subfigure of Figure 5.1a) via a sonication process. AFM results indicate that a single GO sheet is ~1.2 nm in thickness (Figure 5.1a), which is slightly thicker than graphene monolayer (Novoselov *et al.*, 2005). The two-dimensional (2D) structure of graphene oxide nanosheets is also displayed by TEM result, which demonstrates that the nanometer-scale thickness renders GO monolayer approximately transparent in TEM image, though its lateral sizes are in

micrometer scale (Figure 5.1b).

Moreover, Figure 5.1c compares the infrared (IR) spectra between graphite and GO, with the characteristic IR bands of GO listed in Table 5.1. The FTIR results confirm the existences of various oxygen-containing functional groups on GO nanosheet, including hydroxyl (IR band 3333 cm^{-1} and 1398 cm^{-1}), carboxyl (IR band 1732 cm^{-1}) and epoxy (IR band 1232 cm^{-1}) groups, *etc*., which indicates that the parent material graphite has been successfully oxidized via as-selected chemical route. In addition, zeta-potential analysis reveal that the surface charge of GO nanosheet is highly pH sensitive: the increase of OH^- concentration from $10^{-11.9}$ M to $10^{-3.5}$ M leads to the decrease of its zeta-potential by 42 mV, which is mainly ascribed to the deprotonation of carboxylic and phenolic hydroxyl groups on GO nanosheets (Figure 5.1d). And the negatively charged GO surface due to ionization of the oxygen-containing functional groups is essential to maintain GO solution stable by electrostatic repulsion effect, as shown in the optical photo inserted in Figure 5.1d.

Table 5.1 The band assignments of FTIR spectra for graphite and GO.

IR band position (cm^{-1})	Marker	Assignments
3333	I	broad band from 3050 cm^{-1} to 3550 cm^{-1} indicating O-H stretching vibrations arisen from -OH groups of GO nanosheets and occluded/absorbed water molecules in GO layers
1732	II	the C=O stretching vibrations of –COOH groups
1630	III	the vibration resonance of adsorbed hydroxyl groups and unoxidized sp^2 C-C bonding in the carbon lattice
1398	IV	the –OH deformation of C-OH groups
1232	V	the stretching vibrations of C-O on epoxides (C-O-C)
1083	VI	the C-O stretching vibrations of –COOH groups

5.3. The confirmation of GO's embedment in GO\P nanocomposite support layer

Several arrays of dope solutions are prepared in this chapter, with their specific compositions listed in Table 5.2. Particularly, a traditional dope solution without GO nanosheets is included as the control group for each array. Besides, unlike the dope solution used in Chapter 4, the dope solutions studied in this chapter purposely exclude polyvinyl pyrrolidone (PVP) in order to ensure all outcomes can be directly attributed to the introduction of GO nanosheets. The effects on the structures and properties of as-synthesized support layer by the incorporation of GO nanosheets are systematically discussed as follows.

Table 5.2 The composition of dope solutions prepared in this chapter.

Dope solution (100 wt%)	Polymer wt% (Polyethersulfone)	GO nanosheet wt%	Solvent wt%	GO:PES (%)	Research aims
Traditional	15	0.00	85 (DMF)	0.00	To investigate the effect of GO concentration in dope solution
Nanocomposite	15	0.05	84.95 (DMF)	0.33	
	15	0.10	84.90 (DMF)	0.67	
	15	0.15	84.85 (DMF)	1.00	
	15	0.20	84.80 (DMF)	1.33	
	15	0.30	84.70 (DMF)	2.00	
	15	0.50	85.50 (DMF)	3.33	
	15	0.75	84.25 (DMF)	5.00	
	15	1.00	84.00 (DMF)	6.67	
Traditional	17.5	0.00	82.5 (DMF)	0.00	To investigate the effect of polymer concentration
Nanocomposite	17.5	0.50	82.0 (DMF)	2.86	
Traditional	20	0.00	80 (DMF)	0.00	
Nanocomposite	20	0.50	79.5 (DMF)	2.50	
Traditional	17.5	0.00	82.5 (DMAc)	0.00	To investigate the effect of different solvents
Nanocomposite	17.5	0.50	82.0 (DMAc)	2.86	
Traditional	17.5	0.00	82.5 (NMP)	0.00	
Nanocomposite	17.5	0.50	82.0 (NMP)	2.86	

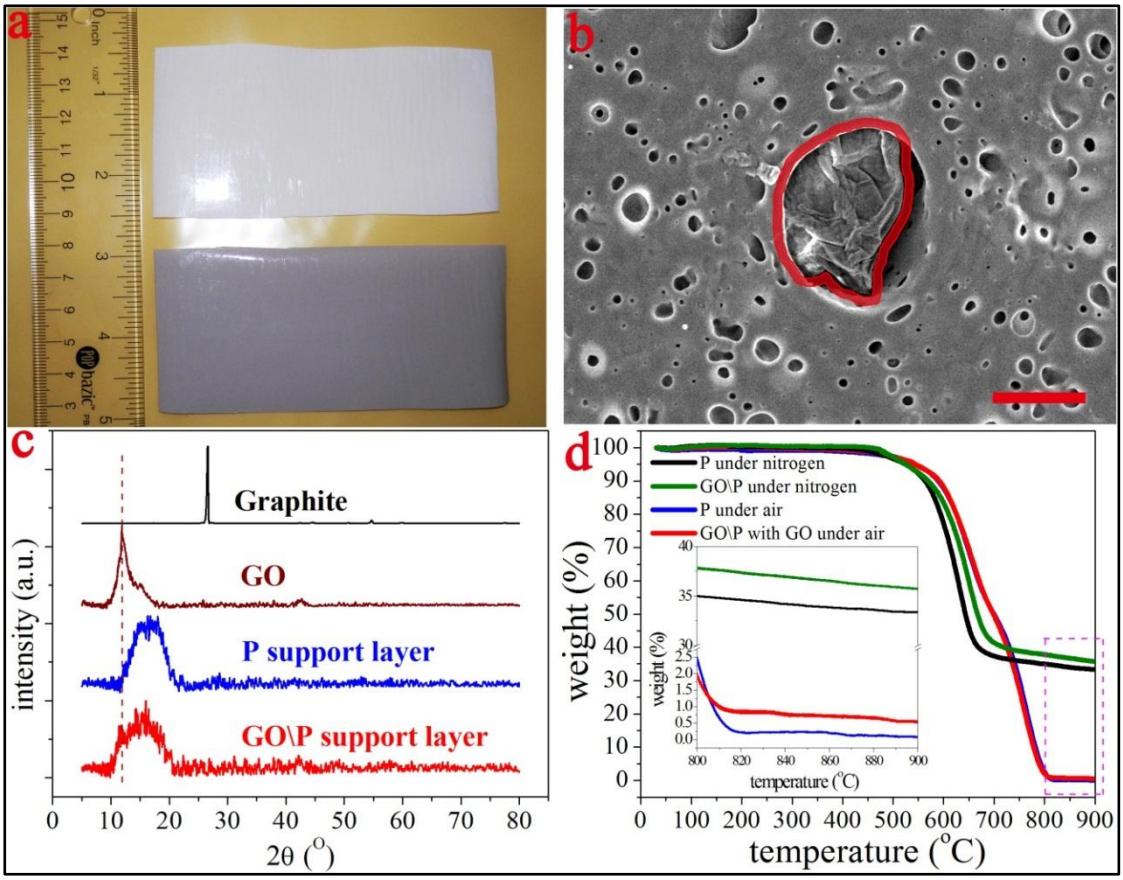

Figure 5.2 Confirmation of the existence of GO nanosheets in GO\P nanocomposite support layers. (**a**) Optical photograph of GO\P nanocomposite (below, dark grey piece) support layer and P polymeric support layer (upper, white piece). (**b**) Enlarged FESEM image on GO\P nanocomposite support layer (bottom surface, scale bar, 2 μm). The red circle highlights the embedded GO nanosheets (multi-layered). (**c**) XRD patterns of graphite, GO, GO\P nanocomposite support layer and P polymeric support layer, respectively. Graphite has a characteristic diffraction peak at 2θ of 26.5 °, corresponding to an interlayer spacing of 3.4 Å (Krishnamoorthy *et al.*, 2013). In contrast, as-synthesized GO has a different diffraction peak at 2θ of 11.6 °, corresponding to an interlayer spacing of 7.5 Å (Marcano *et al.*, 2010). As indicated by the purple dashed line, this 2θ peak of 11.6° is absent from the XRD pattern of P polymeric support layer but present on the XRD pattern of GO\P nanocomposite support layer. (**d**) Thermogravimetric analysis (TGA) results of GO\P nanocomposite support layer and P polymeric support layer. For (**a-d**), the nanocomposite dope solution contains 0.50 wt% GO, 15 wt% PES, 84.5 wt% solvent.

The evidences that confirm the successful embedment of GO nanosheets into as-fabricated nanocomposite support layer are summarized in Figure 5.2. Firstly, Figure 5.2a provides the optical photograph as the eye-visible evidence, which displays that the color of as-fabricated support layer is changed from pure white to dark grey due to the incorporation of GO nanosheets.

Secondly, the undoubted proof of GO nanosheets' existence in as-fabricated GO\P

support layer is obtained by FESEM scanning at high magnification folds, as highlighted by the red circle on Figure 5.2b. Interestingly, multi-layered GO nanosheets are frequently found to be embedded near the big pores (diameter ≥2 μm) at bottom surface inside as-fabricated support layer, which reveals the possible link between GO nanosheets and the formation of such big pores at support layer bottom surface.

Thirdly, on the XRD pattern of GO\P support layer, a 2θ peak at 11.6° is observed, which is the characteristic diffraction peak of GO. This XRD result not only confirms the presence of GO nanosheets in as-fabricated GO\P support layer, but also reveals that the embedded GO nanosheets maintain their 2D structure characteristics in the polymeric host (polyethersulfone).

Last but not least, TGA analysis provides an additional proof for the incorporation of GO nanosheets into GO\P support layer, as shown in Figure 5.2d. Generally, GO\P support layer possesses a slightly higher thermal stability compared with P support layer. Under nitrogen gas, the thermal decomposition of both support layers is started at ~460 ℃, and the weight loss rate of P support layer is constantly higher than that of GO\P support layer. At 900 ℃, the weight left is 33% for P support layer and 36% for GO\P support layer. The 3% higher weight left is attributed to the incorporated GO nanosheets. Interestingly, the concentration of GO in dope solution to synthesize the GO\P support layer for TGA analysis is 0.5 wt%, which is equaling to the ratio of GO : (GO+PES) of 3%. Under dry air, weight loss slope turns to be steep as temperature exceeding 580 ℃ for both P and GO\P support layers due to the oxidation and lysis of polymer chains. At 900 ℃, 0.0% weight is left for P support layer while 0.7% weight is left for GO\P support layer. The higher weight fraction left for GO\P support layer is also ascribed to the embedment of GO nanosheets in polymer matrix.

In short, GO nanosheets are confirmed to be embedded into as-synthesized GO\P support layer by a variety of evidences.

5.4. The amelioration in support layer's chemical properties by the incorporation of GO nanosheets

The amelioration in chemical properties of as-synthesized support layer owning to the incorporation of GO nanosheets have been investigated by diverse techniques, with the relevant results exhibited in Figure 5.3 ~Figure 5.4.

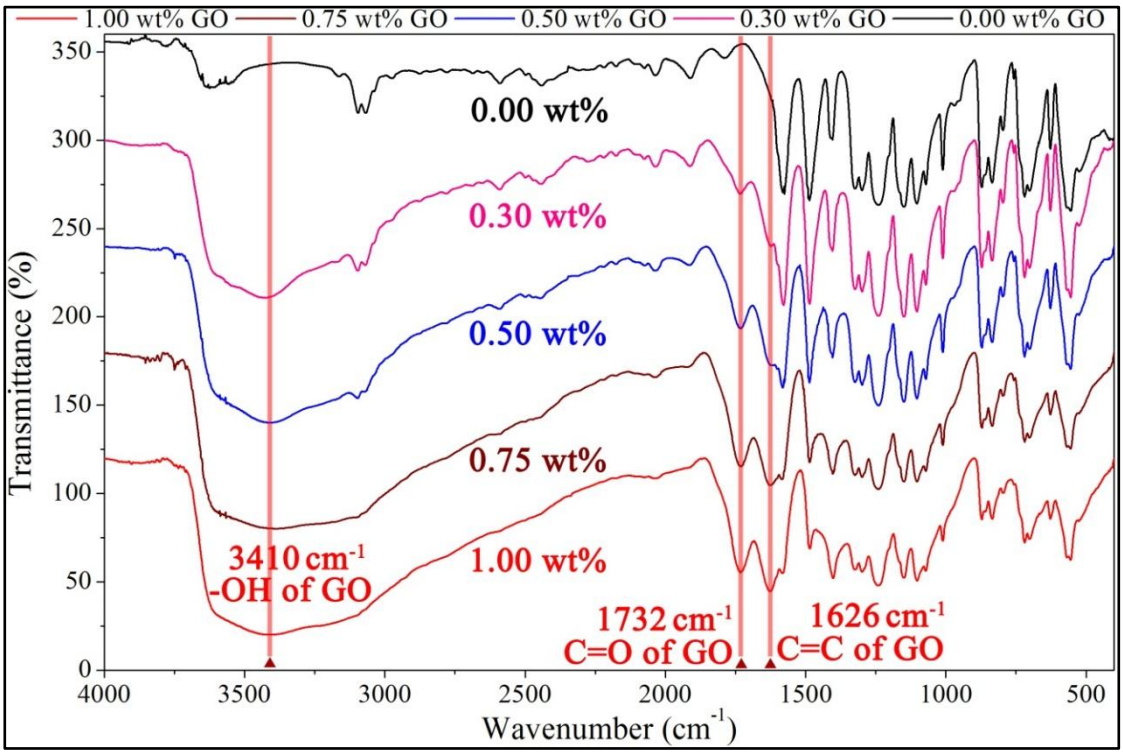

Figure 5.3 ATR-FTIR spectra of as-synthesized GO\P nanocomposite support layers under different GO concentrations. The PES concentration is kept as 15 wt% in nanocomposite dope solution.

As shown in Figure 5.3, ATR-FTIR results indicate that P support layer has several characteristic IR bands: 1578 cm^{-1} (C-C bond in benzene ring of PES), 1487 cm^{-1} (C=C bond in benzene ring of PES), 1325 cm^{-1} (asymmetric stretching of CSO_2C group), 1300 cm^{-1} (asymmetric stretching of O=S=O groups), 1244 cm^{-1} (C-O vibrations of the aromatic ether bond), 1153 cm^{-1} (symmetric stretching of O=S=O groups), and 1107 cm^{-1} (C-O vibrations of the aromatic ether bond). Besides these IR bands, another three new IR bands are observed on GO\P support layer: 3400 cm^{-1} (O-H stretching of hydroxyl groups on GO nanosheet), 1733 cm^{-1} (C=O stretching of carboxyl groups on GO nanosheet), 1627 cm^{-1} (C=C stretching of unoxidized graphitic carbon or the vibration of absorbed water molecules), which prove that the incorporation of GO nanosheets equips as-synthesized support layer with various

oxygen-containing functional groups.

Zeta-potential characterization results reveal that GO\P support layer carries more negative electric charges on the top surface compared with P support layer in a broad pH range (3~9), with the isoelectric point decreased from pH 5.5 to pH 3.0 as GO concentration increased from 0.00 wt% to 1.00 wt% (Figure 5.4a). This is because the oxygen-containing functional groups especially the carboxylic and phenolic hydroxyl groups that are equipped by the incorporation of GO nanosheets can take deprotonation process along with the increase of proton acceptor (OH^-) concentration in environment. Moreover, these functional groups equipped by the incorporation of GO nanosheets are expected to improve the electrostatic interactions between support layer top surface and subsequently coated hydrogel selective layer, and thus facilitate the immobilization and stabilization of hydrogel selective layer.

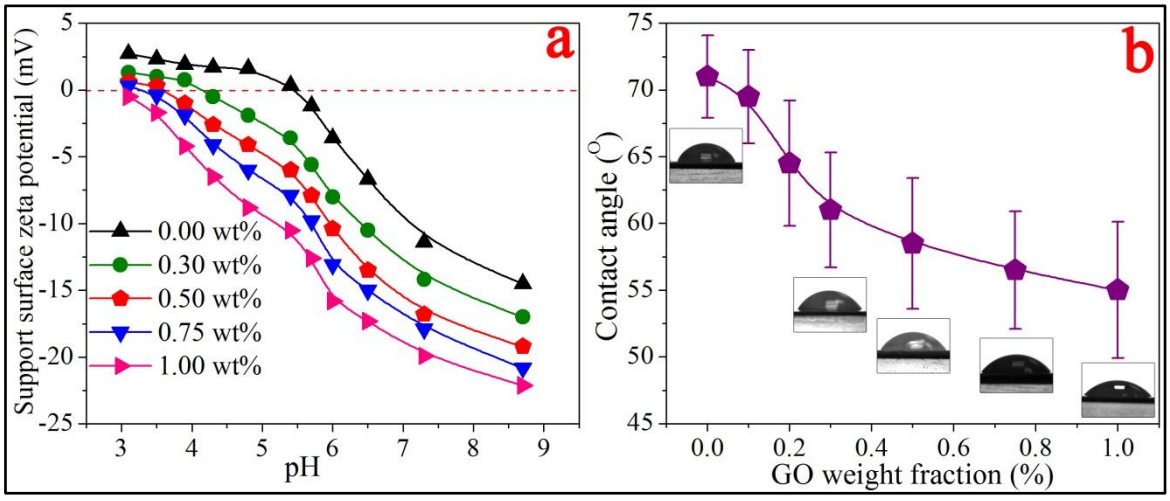

Figure 5.4 (a) Surface charges and (b) water contact angles of as-synthesized GO\P support layers under different GO concentrations. The PES concentration is kept as 15 wt% in nanocomposite dope solution.

And also because these oxygen-containing functional groups equipped by GO nanosheets have better affinity with water molecules, GO\P support layer demonstrates remarkably improved surface hydrophilicity compared to P support layer, with water contact angle decreased monotonously from $71° \pm 3.1°$ to $55° \pm 4.8°$ along with the increase in GO concentration from 0.00 wt% to 1.00 wt% (Figure 5.4b).

In short, the incorporation of GO nanosheets is able to modify the chemical properties of as-synthesized support layer to be more hydrophilic and negatively charged.

5.5. More porous and water permeable support layer surface structure

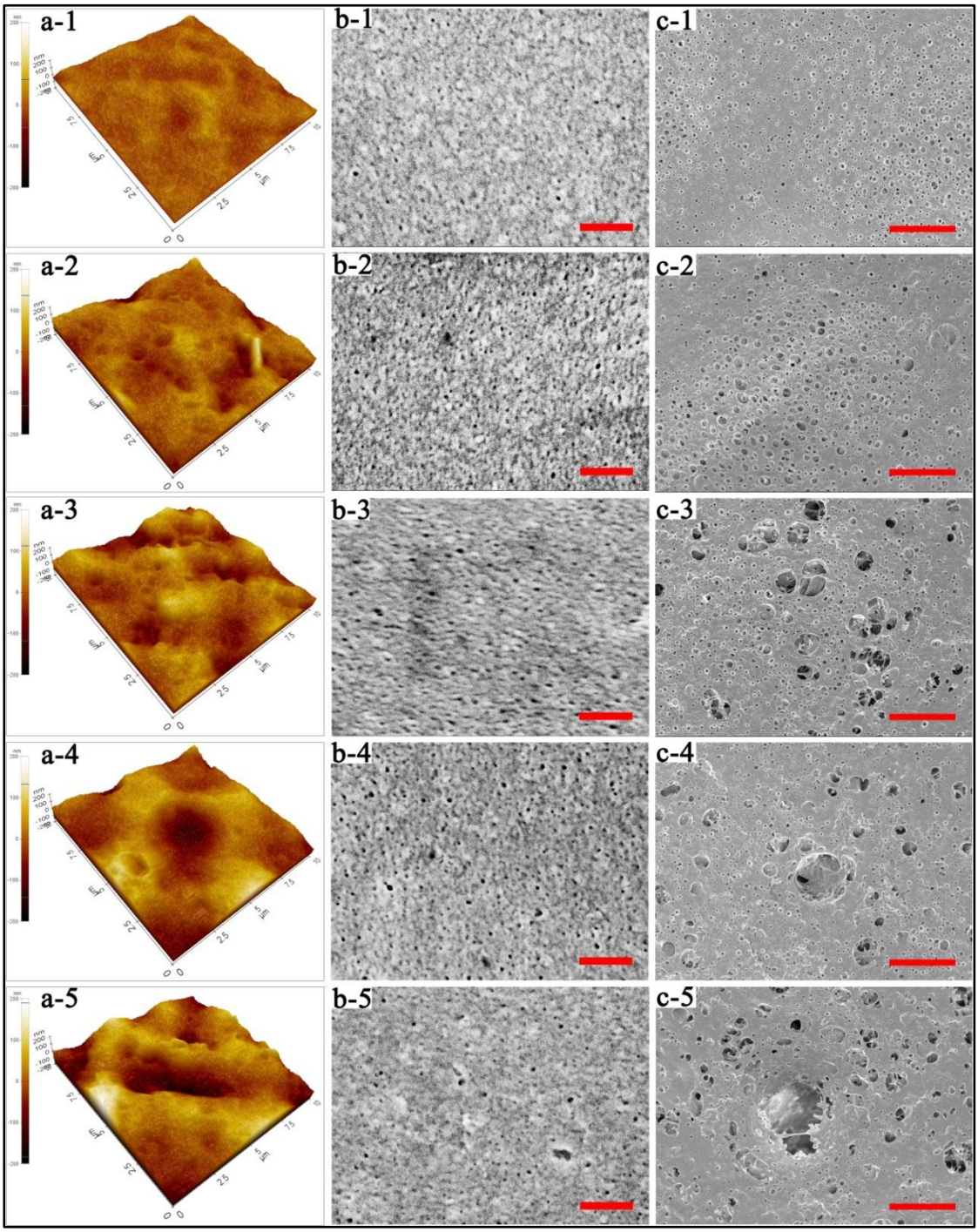

Figure 5.5 Surface structures of as-synthesized GO\P nanocomposite support layers under different GO concentrations. (**a**) Topography roughness of as-synthesized support layers. (**b**) FESEM image of support layer top surface, scale bar, 200 nm. (**c**) FESEM image of support layer bottom surface, scale bar, 10 μm. Subfigure 1 refers to 0.00 wt% GO, subfigure 2 refers to 0.30 wt% GO, subfigure 3 refers to 0.50 wt% GO, subfigure 4 refers to 0.75 wt% and subfigure 5 refers to 1.00 wt% GO, respectively. PES concentration is kept as 15 wt% in nanocomposite dope solution.

The top surface structures of GO\P support layer need to be carefully examined because it functions as the interface between hydrogel selective layer and nanocomposite support layer in as-synthesized hydrogel FO membrane. Particularly, Figure 5.5a indicates that the topography roughness of as-synthesized support layer is increased from 12 nm to 42 nm along with the increase of GO concentration in dope solution from 0.00 wt% to 1.00 wt%. The increase in support layer topography roughness to certain extent is thought to be favorable to the immobilization of selective layer.

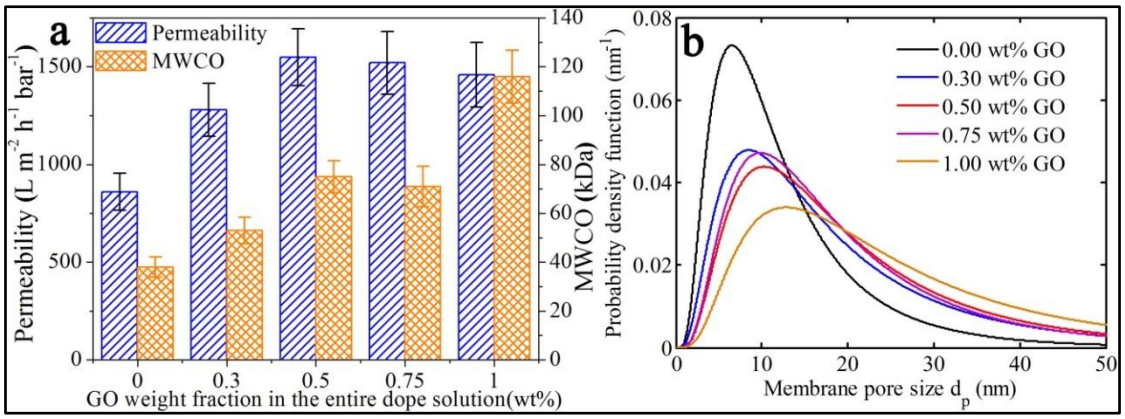

Figure 5.6 (a) Pure water permeability (PWP) and molecular weight cutoff (MWCO) of GO\P nanocomposite support layers under different GO concentrations. (b) Pore size distribution of GO\P nanocomposite support layers' top surface under different GO concentrations. The PES concentration is kept as 15 wt% in nanocomposite dope solution. PWP and MWCO are tested under 1 bar transmembrane hydrostatic pressure difference at 23 ±2 ℃ under 1.0 L/min crossflow mode.

More importantly, the incorporation of GO nanosheets can shape support layer top surface to be more porous, with both pore number density and pore size increased (Figure 5.5b). These FESEM observations are further confirmed by the analysis on pore size distribution (Figure 5.6), which indicate that (1) the increase of GO concentration from 0.00 wt% to 0.50 wt% leads to the monotonous enlargement in average pore size of support layer top surface from 10.2 nm to 16.7 nm (Figure 5.5b-1~Figure 5.5b-3), (2) the increase of GO concentration from 0.50 wt% to 0.75 wt% does not generate any considerable change in pore size distribution with average pore size slightly decreased from 16.7 nm to 15.7 nm (Figure 5.5b-4), and (3) the further increase of GO concentration to 1.00 wt% significantly flattens pore size distribution curve with average pore size enlarged to 21.3 nm (Figure 5.5b-5). In addition,

molecular weight cutoff (MWCO) of as-synthesized support layer is basically increased from 38 kDa to 116 kDa along with the increase of GO concentration from 0.00 wt% to 1.00 wt% (Figure 5.6a). This MWCO result is also consistent with FESEM observations on support layer top surface as aforementioned.

Meanwhile, GO assisted phase inversion process also produces bigger pores on bottom surface of support layer compared with conventional phase inversion process (Figure 5.5c). As shown in Figure 5.5c-1 ~ Figure 5.5c-3, the pores on support layer bottom surface are grown from ~0.5 μm to ~3.7 μm in diameter along with the increase of GO concentration from 0.00 wt% to 0.50 wt%. Particularly, Figure 5.5c-3 also suggests that the pore interconnectivity in cross-sectional direction (perpendicular to surface plane) gets significantly improved. Figure 5.5c-4 shows that super big pores with diameter larger than 5 μm are formed as GO concentration exceeding 0.50 wt%, possibly due to the mergence of original adjacent pores on bottom surface. And Figure 5.5c-5 shows that such super big pores can further grow up to as big as 10 μm in diameter as GO concentration increased to 1.00 wt%.

In addition, Figure 5.6a demonstrates that the pure water permeability (PWP) of as-synthesized support layers gets enhanced from 860 ± 95 L m^{-2} h^{-1} bar^{-1} to 1550 ± 140 L m^{-2} h^{-1} bar^{-1} along with the increase in GO concentration from 0.00 wt% to 0.50 wt%. However, as GO concentration further increased from 0.50 wt% to 1.00 wt%, the PWP of as-synthesized nanocomposite support layer is slightly reduced from 1550 ± 140 L m^{-2} h^{-1} bar^{-1} to 1460 ± 160 L m^{-2} h^{-1} bar^{-1}. Compared with P support layer, GO\P support layers possess higher water permeability that is mainly attributed to their more porous surface structures as discussed in this section.

In short, GO assisted phase inversion enables as-synthesized nanocomposite support layer to have more porous surface structures and thus higher water permeability.

5.6. 3D interconnected porous support layer structure

More importantly, the incorporation of GO nanosheets can bring forth a qualitative improvement in the interconnectivity of interior pore structure upon as-synthesized support layer, which will be presented based on the systematic investigations including

the effect of GO concentration, the effect of polymer concentration, and the effect of different solvents as follows. In order to facilitate the discussion, all the support layers are set in three dimensional Cartesian coordinate system (xyz coordinate system) with top-to-bottom direction set along z axis and cross-section plane (facing towards readers) set in xz plane, as demonstrated in Figure 5.7.

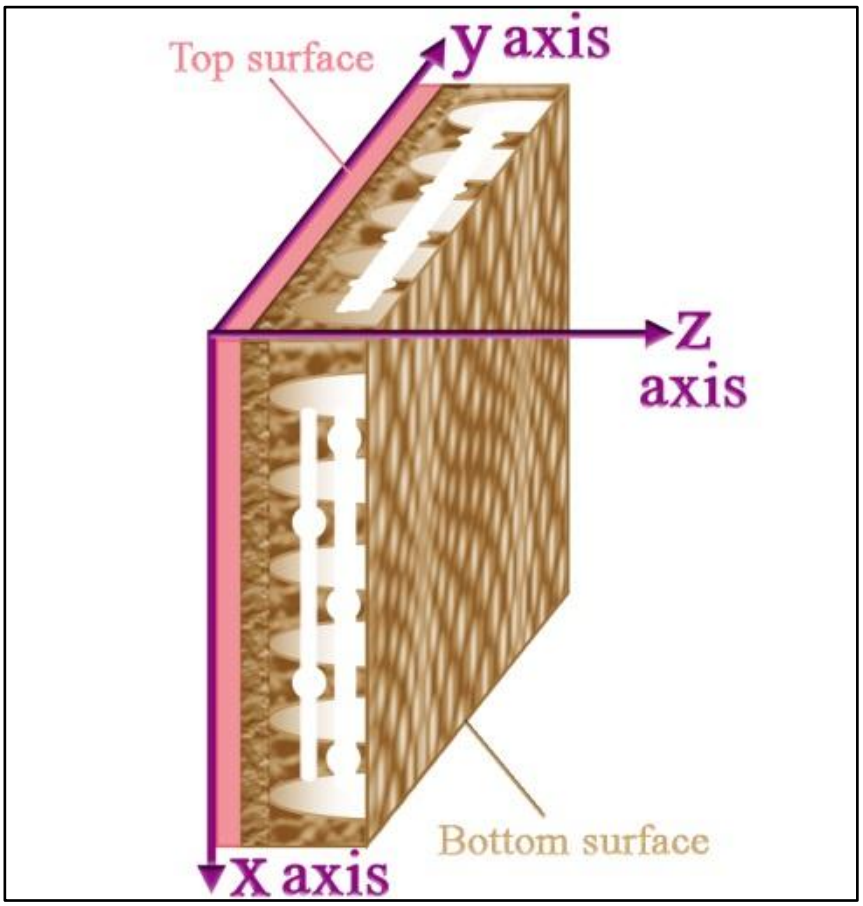

Figure 5.7 Demonstration of the three dimensional Cartesian coordinate system for the setting of as-synthesized support layers. The top-to-bottom direction is set along z axis and cross-section plane (facing towards readers) is in xz plane.

5.6.1. Effect of GO concentration (GO/Polymer ratio)

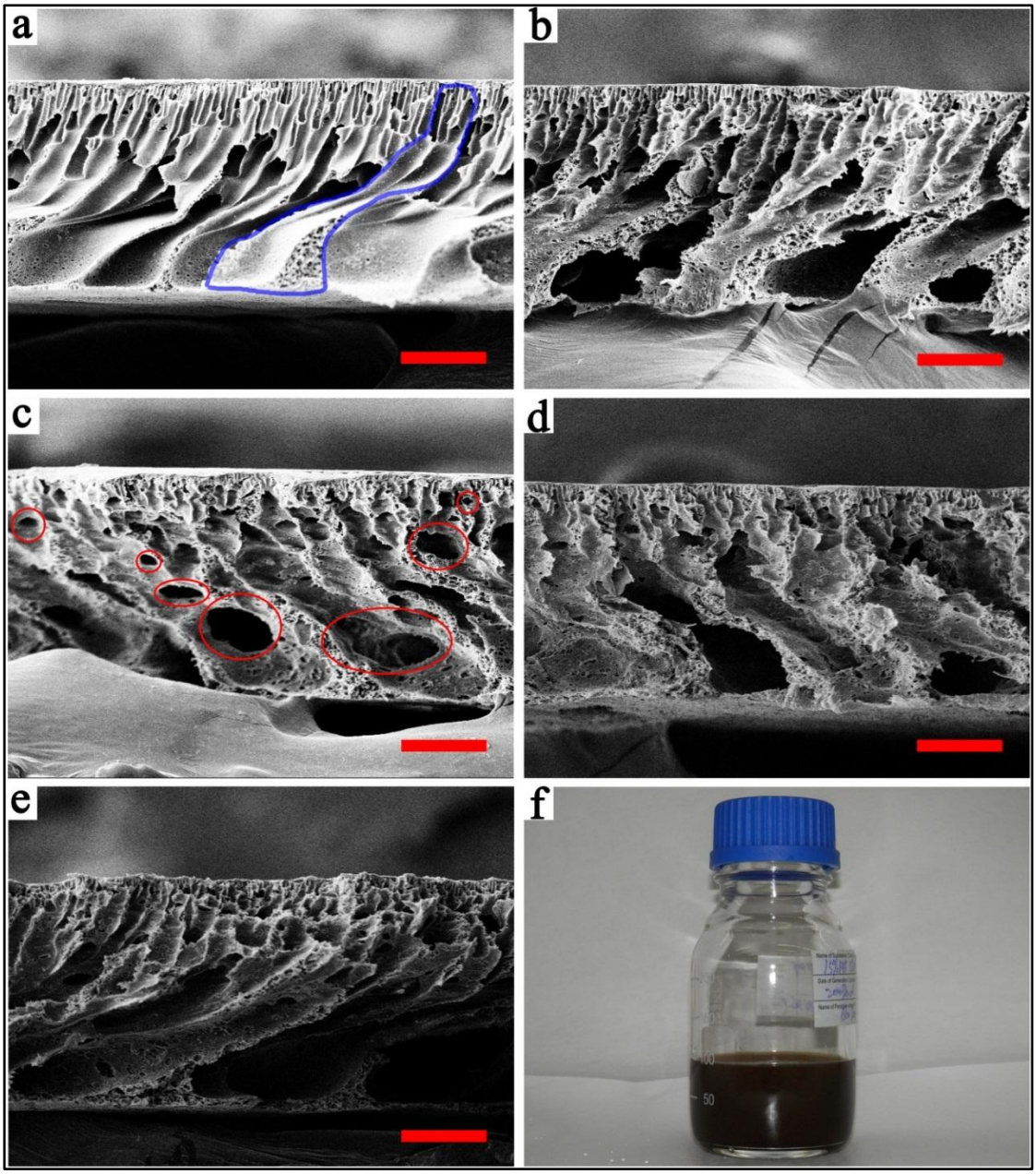

Figure 5.8 (a-e) Cross-section structure of as-synthesized GO\P nanocomposite support layers under different GO concentrations. (f) Optical photograph of GO incorporated nanocomposite dope solution, showing that GO nanosheets are uniformly dispersed to form a stable dope solution. The PES concentration is kept as 15 wt% in nanocomposite dope solution. Scale bar is 30 μm. Particularly, for Figure 5.8a, the light blue line exemplifies that no channels (along x or y axis) perforating cross-sectional plane is formed. For Figure 5.8c, the red circles give some typical examples of the GO induced new channels (along x or y axis) which are perforating the original z-axis channels (vertically from top to bottom in cross-sectional plane).

Figure 5.8 presents the effect of GO concentration on the interior pore structure of as-synthesized support layers. Figure 5.8a shows that the finger-like channels inside P support layer cross-section is connected only in one dimension (along z axis). The incorporation of GO nanosheets at relatively low concentration (0.10 ~ 0.20 wt%) can

already enlarge the width of such finger-like channels. But the qualitative change upon cross-sectional pore structure is achieved as GO concentration ≥ 0.30 wt% (Figure 5.8b). At GO concentration of 0.50 wt%, an optimized cross-section structure with pores interconnected in all three dimensions at tens of micrometer scale is produced (Figure 5.8c). The corresponding four significant changes in pore structure are emphasized in detail as follows.

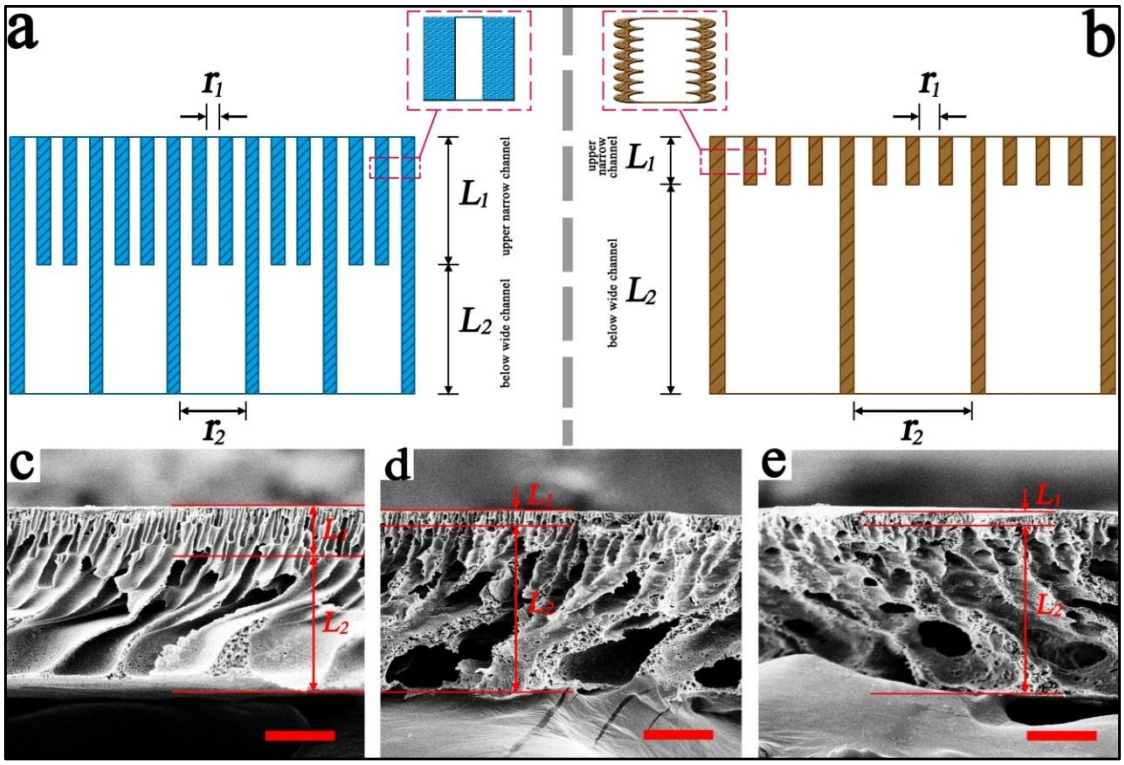

Figure 5.9 The definitions of upper narrow channel and below wide channel in cross-section plane (along z axis). (**a**) Schematic diagram of the cross-section fabricated by conventional phase inversion process. (**b**) Schematic diagram of the cross-section fabricated by GO assisted phase inversion process (the channels perforating cross-section are not depicted in Figure 5.9b). The enlarged views in dotted line frame of purple color contrast the structure of channel wall: the channel wall fabricated by GO assisted phase inversion process has curvaceous structure while that by conventional phase inversion process does not. (**c**) Support layer cross-section fabricated by conventional phase inversion process (corresponding to Figure 5.8a), scale bar 30 μm, wherein upper narrow channel length L_1 is 21.5 μm and below wide channel length L_2 is 59.0 μm. (**d**) Support layer cross-section fabricated by GO assisted phase inversion process (GO concentration of 0.30 wt%, corresponding to Figure 5.8b), scale bar 30 μm, wherein upper narrow channel length L_1 is 7.0 μm and below wide channel length L_2 is 71.3 μm. (**e**) Support layer cross-section fabricated by GO assisted phase inversion process (GO concentration of 0.50 wt%, corresponding to Figure 5.8c), scale bar 30 μm, wherein upper narrow channel length L_1 is 5.8 μm and below wide channel length L_2 is 72.9 μm.

Firstly, the length of upper narrow channels (located near the top surface) is shortened by >70% from ~21.5 μm to ~5.8 μm along with the increase of GO concentration from 0.00 wt% to 0.50 wt%. As illustrated in Figure 5.9, this study divides the channels in cross-section plane (along z axis) into two categories based upon their self-evident structural differences: the upper narrow channels with inner diameter (d_1) smaller than 5 μm (typically 0.5 ~ 4.5 μm), and the below wide channels with inner diameter (d_2) above 5 μm (typically 6.0 ~ 45.0 μm) which are grown bigger along z axis towards bottom.

Secondly, channel width is enlarged by ~1.0 times for both upper narrow channel and below wide channel. In detail, d_1 is enlarged from 1.0 ± 0.5 μm of P support layer to 2.2 ± 0.6 μm of GO\P support layer (0.5 wt% GO concentration) and d_2 is enlarged from 20 ± 6 μm of P support layer to 40 ± 9 μm of GO\P support layer. The total resistance to water permeation for upper narrow channel and below wide channel is the sum of each resistance. Because d_1 is much smaller than d_2, the resistance of upper narrow channel is far bigger than that of below wide channel. Therefore, the resistance of upper narrow channel dominates the total resistance of the two channels. This means GO assisted phase inversion can effectively reduce the total resistance of the two channels for the channel length of upper narrow channel is shortened and the widths of the two channels are enlarged. As a result, the entire channel structure constructed by GO assisted phase inversion becomes more advantageous to water permeation (even does not consider other changes in cross-sectional pore structure).

Thirdly, evident curvaceous structure is formed on the wall of channel, as also demonstrated in Figure 5.10. Noteworthily, to the best knowledge of the author, this characteristic transformation on channel wall structure is not revealed by all previous studies on the incorporation of GO into polymeric membrane (Wang & Lai, 2012; Lee *et al.*, 2013; Zhao *et al.*, 2013; Zinadini *et al.*, 2014; Park *et al.*, 2015; Wang *et al.*, 2015).

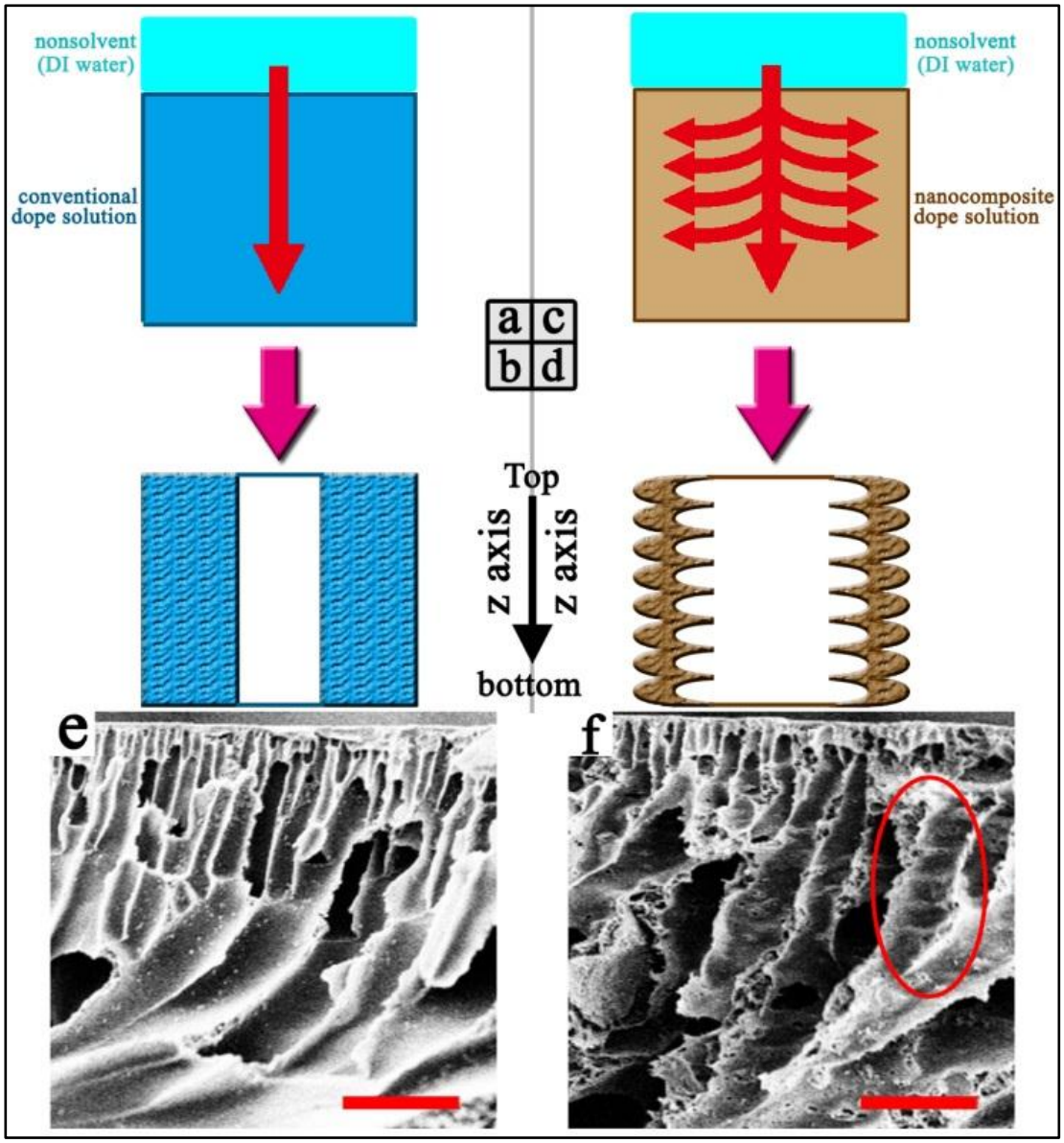

Figure 5.10 The formation of channel wall during phase inversion process. (**a**) Conventional phase inversion process, wherein the red arrow demonstrates the direction of viscous fingering. (**b**) Conventional phase inversion constructed channel wall is smooth and free of curvaceous structures. (**c**) GO assisted phase inversion process, wherein the red arrow demonstrates the direction of viscous fingering. (**d**) GO assisted phase inversion constructed channel has characteristic curvaceous wall structure. (**e**) Enlarged SEM image of conventional phase inversion constructed channel wall structure, scale bar 15 μm. (**f**) Enlarged SEM image of GO assisted phase inversion constructed channel wall structure (GO concentration is 0.50 wt%), wherein the red circle exemplifies the curvaceous structure on the channel wall, scale bar 15 μm.

Fourthly and most importantly, plenty of pores with sizes ranged from 3 ~ 30 μm emerge in the way of perforating the wall of z-axis channels and thus form the new channels perpendicular to cross-section plane (along both x and y axes), as highlighted by the red circles on Figure 5.8c. Enlarged FESEM image demonstrates that such

emerging x-axis (and y-axis) channels can be located as near as 7 μm from the top surface of support layer. For the first time, an entirely new support layer structure in terms of 3D pore interconnectivity at micrometer-scale is created owing to the incorporation of GO nanosheets, which is more favorable for the transportation of water molecules. Similar 3D interconnected porous support layer is also found at GO concentration of 0.75 wt% and 1.00 wt% (Figure 5.8d ~ 5.8e). Interestingly, at GO concentration of 1.00 wt%, these emerging channels grow in a tilt angle ~30 °deviated from x (or y) axis, probably because of the over high dope solution viscosity.

5.6.2. Effect of polymer concentration

To further verify the universality of GO's ability to prompt the formation of 3D interconnected porous support layer, the effect of polymer concentration and different solvents have also been investigated, with the corresponding results exhibited in Figure 5.11 and Figure 5.12, respectively.

The effect of polymer concentration on the formation of 3D interconnected porous support layer is shown in Figure 5.11. Particularly, GO induced new channels along x-axis (and y-axis) that perforate z-axis channels at micrometer scale are also found to be formed on the interior structure of support layer under polymer concentration of both 17.5 wt% and 20 wt%, as exemplified by the red circles on Figure 5.11d and 5.11f, respectively. In addition, another characteristic transformation on support layer pore structure *i.e.* the curvaceous channel wall structure is also observed on the interior channels of GO\P support layer at polymer concentration of 17.5 wt% and 20 wt%.

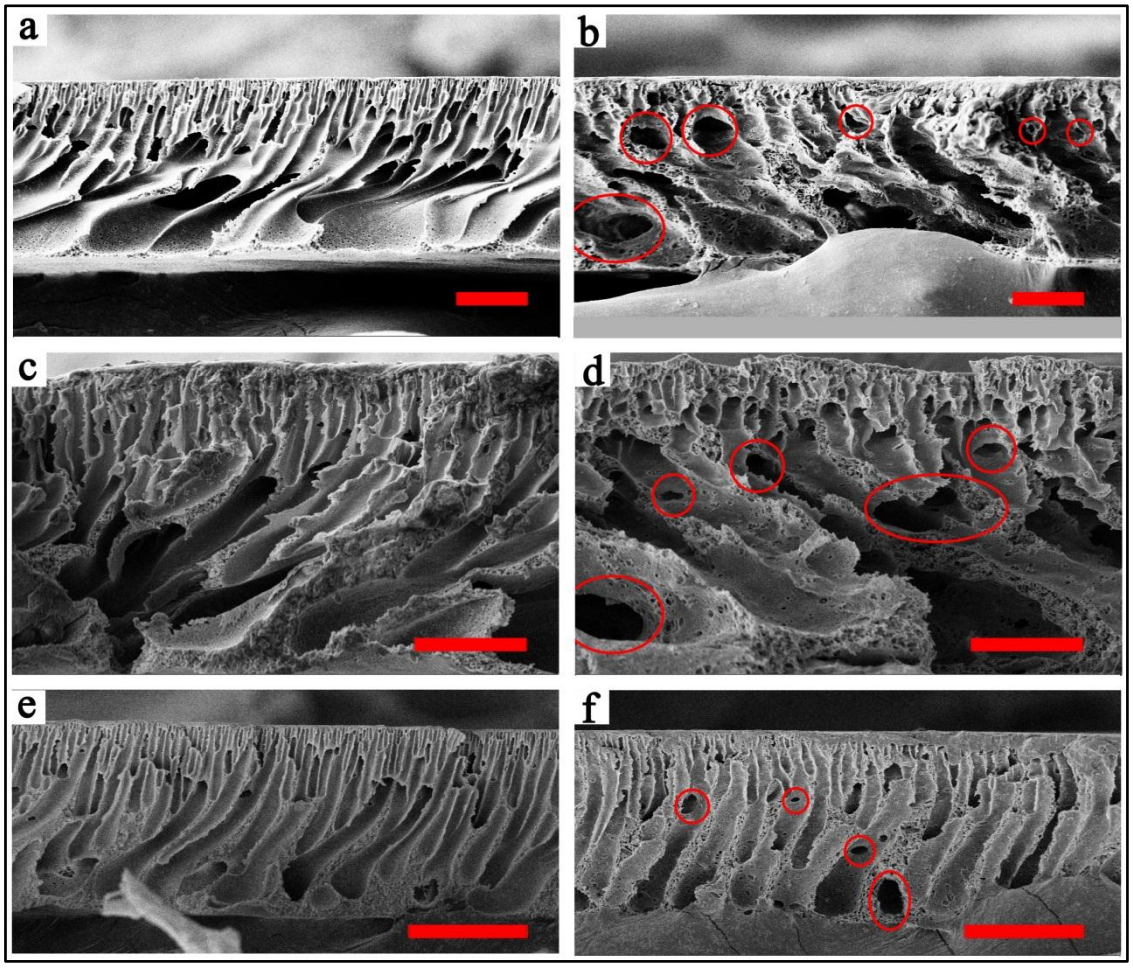

Figure 5.11 The effect of GO incorporation under different polymer concentrations. (**a**) 15 wt% PES, 0.00 wt% GO and 85 wt% DMF, scale bar, 30 μm. (**b**) 15 wt% PES, 0.50 wt% GO and 85 wt% DMF, scale bar, 30 μm. (**c**) 17.5 wt% PES, 0.00 wt% GO and 82.5 wt% DMF, scale bar, 30 μm. (**d**) 17.5 wt% PES, 0.50 wt% GO and 82 wt% DMF, scale bar, 30 μm. (**e**) 20 wt% PES, 0.00 wt% GO and 80 wt% DMF, scale bar, 30 μm. (**f**) 20 wt% PES, 0.50 wt% GO and 79.5 wt% DMF, scale bar, 50 μm. The red circles on Figure S10b,d,f highlight some typical new channels (along x or y axis) perforating z-axis channel.

However, it's worthy to note that the number density of these emerging x-axis (and y-axis) channels is decreased along with the increase of polymer concentration in nanocomposite dope solution from 15 wt% to 20 wt% as compared among Figure 5.11b, d and f. The relevant reason is elaborated as follows. The increase of polymer concentration leads to the increase in absolute viscosity of dope solution. And this increase in dope solution viscosity drives the entire interior pore structure of as-synthesized support layer to be transformed from finger-like to sponge-like. Such transformation is confirmed by the control groups as shown in Figure 5.11a, c and e, with the most noticeable evidence that the walls of z-axis channels grows thicker into sponge-like structure from support layer bottom surface. However, this transformation

towards sponge-like structure is unfavorable to the formation of emerging x-axis (and y-axis) channels, because the sponge-like interior structure provides bigger resistance to the perforation by the channeling along x (and y) axis. But it's necessary to point out that the incorporation of GO nanosheets under polymer concentration >15 wt% still renders as-synthesized nanocomposite support layers more advantageous to water transportation compared with their control support layer at the same polymer concentration. A typical example is to compare the structure of GO\P support layer and P support layer at polymer concentration of 20 wt% as shown in Figure 5.11e and Figure 5.11f, wherein the incorporation of GO nanosheets at 0.5 wt% concentration in dope solution is able to enlarge the width of z-axis channels and make their sponge-like channel walls significantly thinner and more porous.

In short, the incorporation of GO nanosheets can prompt the formation of 3D interconnected porous structure for as-synthesized support layer under a wide range of polymer concentration (at least from 15 wt% to 20 wt%). Furthermore, 15 wt% is the most beneficial polymer concentration among all examined concentrations to construct such 3D interconnected porous support layer with high number density of emerging x-axis (and y-axis) channels at micrometer scale.

5.6.3. Effect of different solvents

The effect of different solvents on the formation of 3D interconnected porous support layer is shown in Figure 5.12. As exemplified by the red circles on Figure 5.12d and Figure 5.12f, GO induced new channels along x-axis (and y-axis) that perforate z-axis channels at micrometer scale are also formed with DMAc or NMP as the solvent, separately. Meanwhile, the curvaceous channel wall structure is also observed on the interior channels of GO\P support layer when DMAc or NMP is used as the solvent. In addition, channel width also gets enlarged due to the incorporation of GO nanosheets, especially using DMF or NMP as indicated by Figure 5.12b,f.

As displayed in Figure 5.12a,c,e, the interior pore structure of as-synthesized control support layers differentiates from each other when using different solvents (PES concentration is kept as 17.5 wt%). This is because the stability of polymer in certain solvent is different from that in another solvent (polymer-solvent interaction parameter

is different) and the compatibility between nonsolvent and certain solvent is different from that between nonsolvent and another solvent (solvent-nonsolvent interaction parameter is different). These differences will affect the phase behavior of polymer/solvent/nonsolvent ternary system and thus generate different pore structure of support layer (van de Witte *et al.*, 1996).

The incorporation of GO nanosheets in polymer dope solution renders the demixing process even more complicated. Figure 5.12b,d,f indicates that the number density of the emerging x-axis (and y-axis) channels that perforate z-axis channel is highest using DMF as solvent and lowest using NMP as solvent. The relevant explanations are given as follows. This study has observed that the solubility of as-synthesized GO nanosheets is highest in DMF while lowest in NMP (GO nanosheet is polar while the polarity of solvents follows the order of DMF > DMAc > NMP). Hence the distribution of GO nanosheets in polymer dope solution is more homogeneous using DMF as solvent than using NMP as solvent. As a result, more homogenous distribution of GO nanosheets increases the number of GO containing micro region in nanocomposite dope solution and thus generates GO induced x-axis (and y-axis) channels in bigger number density.

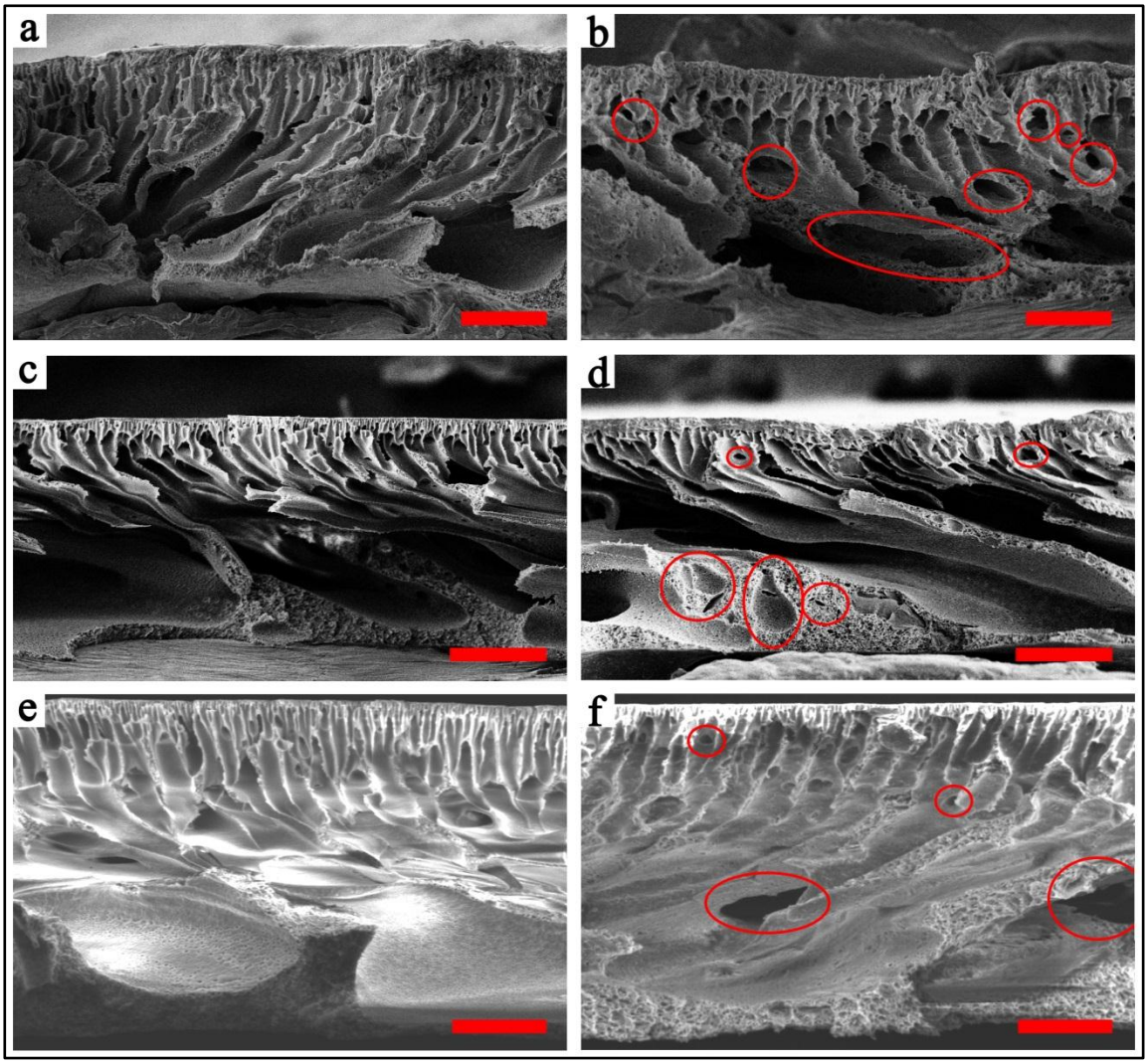

Figure 5.12 The effect of GO incorporation under different solvents. (**a**) 17.5 wt% PES, 0.00 wt% GO and 82.5 wt% DMF, scale bar, 30 μm. (**b**) 17.5 wt% PES, 0.50 wt% GO and 82 wt% DMF, scale bar, 30 μm. (**c**) 17.5 wt% PES, 0.00 wt% GO and 82.5 wt% DMAc, scale bar, 40 μm. (**d**) 17.5 wt% PES, 0.50 wt% GO and 82 wt% DMAc, scale bar, 40 μm. (**e**) 17.5 wt% PES, 0.00 wt% GO and 82.5 wt% NMP, scale bar, 20 μm. (**f**) 17.5 wt% PES, 0.50 wt% GO and 82 wt% NMP, scale bar, 20 μm. The red circles on Figure S11b,d,f highlight some typical new channels (along x or y axis) perforating z-axis channel.

In short, the incorporation of GO nanosheets can prompt the formation of 3D interconnected porous structure for as-synthesized support layer with different solvents including DMF, DMAc and NMP. DMF is the best of the three to construct such 3D interconnected porous support layer with high number density of emerging x-axis (and y-axis) channels at micrometer scale. Moreover, the universality of GO's ability to prompt the formation of 3D interconnected porous support layer has been verified in different GO concentrations, polymer concentrations and solvents.

5.7 Proposed mechanism on the formation of 3D pore interconnected support layer structure

Figure 5.13 illustrates the mechanism on the formation of 3D interconnected porous support layer from the perspective of viscous fingering. Viscous fingering characterizes the phenomenon that less viscous fluid (nonsolvent, DI water here) is injected displacing more viscous fluid (solvent) driven by viscosity difference at the interface between the two fluids (Wang & Lai, 2012). For the film cast from conventional polymer dope solution (GO concentration of 0.00 wt%), viscosity difference only exists along z axis at the interface between solvent and nonsolvent (Figure 5.13a-2). Therefore, finger-like channels only grow along z axis from top to bottom (Figure 5.13a-3, 5.13a-4). As a result, the channel inside support layer is connected only in one dimension.

In contrast, for the film cast from GO incorporated nanocomposite dope solution (*e.g.* GO concentration of 0.50 wt%), viscosity difference also exists along x axis and y axis between GO containing region and GO absent region (Figure 5.13b-2). As z axis finger-like channels grow near to GO containing region, the viscosity difference at the interface between nonsolvent and GO containing region is even bigger than that between nonsolvent and GO absent region. Moreover, GO's high affinity with water molecules (*i.e.* superhydrophilicity) also attracts the in-flow of DI water to be directed towards the GO containing region. This bigger viscosity difference, coupled with the attraction of water molecules to GO nanosheets, is able to drive fingering displacement direction to be spread from original one dimension (z axis) to all three dimensions (x, y, z axes). As a result, 3D interconnected porous interior structure is formed by GO assisted phase inversion (Figure 5.13b-3, 5.13b-4). Meanwhile, this GO induced regional viscosity differences along x and y axes also explain the formation of curvaceous channel wall structure, which is illustrated in Figure 5.10a~d.

Moreover, two points need to be emphasized here. One point is that this 3D pore interconnectivity relies on the beauty of GO's 2D structure. The nanometer-sized thickness of GO sheets ensures their stable distribution in dope solution while the micrometer-sized graphitic plane guarantees the spread of fingering direction and thus creates the emerging perpendicular channels in tens of micrometers' size. Quite

differently, the published studies that employ zero dimensional (*e.g.* SiO_2, zeolite, TiO_2, *etc.*) or one dimensional (*e.g.* carbon nanotube) nanomaterial as the ingredient in phase inversion dope solution never obtain such 3D interconnected porous structure in the polymeric membrane (support layer) (Qiu *et al.*, 2009; Majeed *et al.*, 2012; Amini *et al.*, 2013; Ma *et al.*, 2013; Emadzadeh *et al.*, 2014b; Khalid *et al.*, 2015). The other point is that GO induced 3D fingering is an optimized result based upon the systematic search of dope solution composition as demonstrated by this study. This is because both the concentration of GO nanosheets and the concentration of polymer are critical parameters that can influence the effect of GO induced regional viscosity difference. Hence an overhigh GO concentration would result in excessive viscosity that retards fingering displacement and thus shapes entire interior pore structure towards sponge-like.

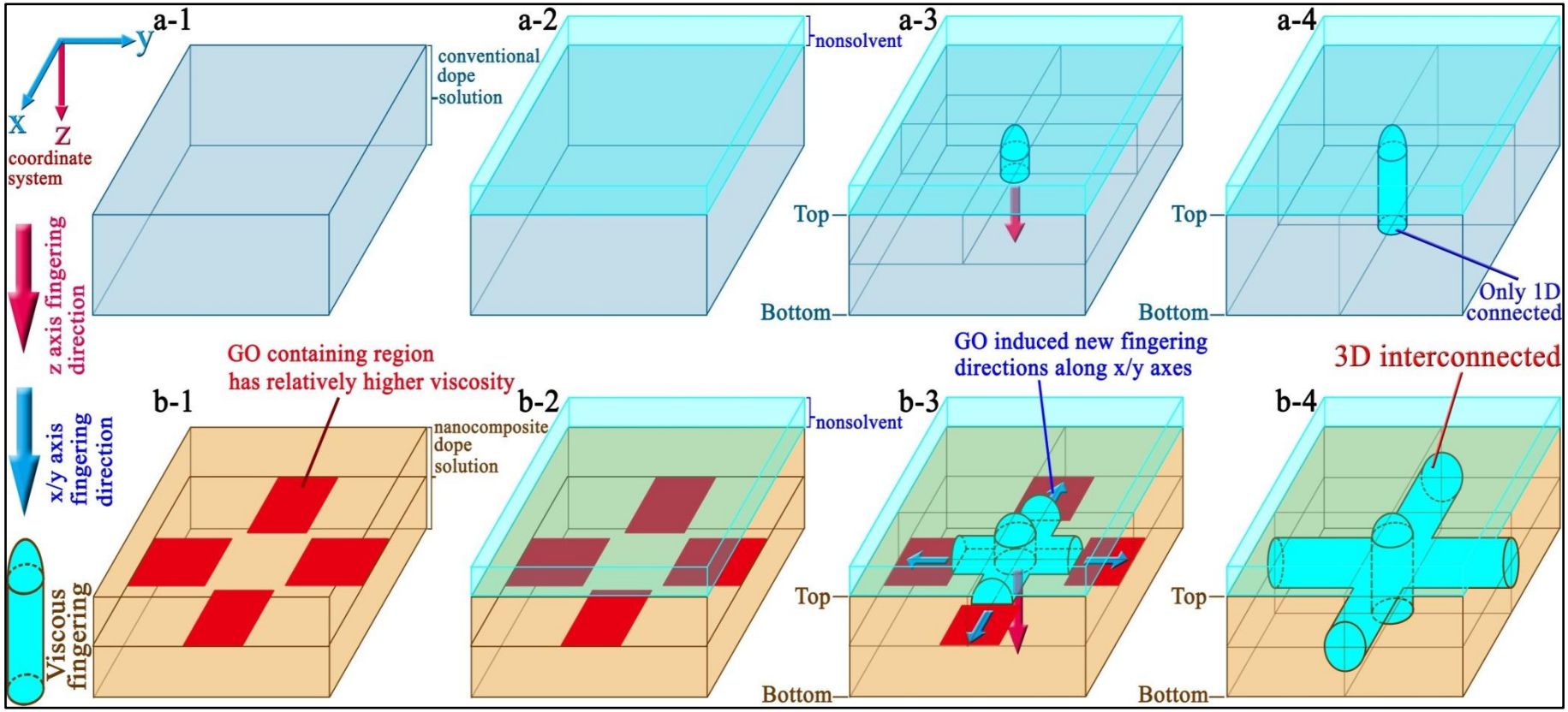

Figure 5.13 Comparison on viscous fingering between conventional phase inversion and GO assisted phase inversion. (**a**) Conventional phase inversion, wherein (**a-1**) the film is cast from conventional polymer dope solution and (**a-2**) immersed in the nonsolvent; (**a-3**) viscosity difference only exists in z-axis direction between nonsolvent and dope solution, which drives viscous fingering merely along z axis; (**a-4**) finger-like channel is connected in only one dimension. (**b**) GO assisted phase inversion, wherein (**b-1**) the film is cast from nanocomposite dope solution and (**b-2**) immersed in the nonsolvent; (**b-3**) as viscous fingering grows to the area near GO containing region, the existence of GO generates new viscosity differences at the interface between itself and nonsolvent, which leads to the spread of fingering direction from original one dimension (z axis) to three dimensions (x, y and z axes); (**b-4**) finger-like channels are connected in all three dimensions to form 3D interconnected porous support layer structure.

5.8. Minimization of FO internal concentration polarization (ICP)

5.8.1. Structures and properties of GO\P-H nanocomposite FO membrane

Thin film nanocomposite (TFNC) GO\P-H FO membrane is further synthesized through dip-coating the GO\P support layer in chemically crosslinked hydrogel (PVA) solution. The crosslinking procedure utilizes the optimized parameters including crosslinking agent, hydrogel molecular weight, hydrogel concentration, crosslinking degree and coating time *etc.* that have been already revealed in Chapter 3. The properties and structures of as-synthesized GO\P-H nanocomposite FO membrane are presented in Figure 5.14 ~ Figure 5.15.

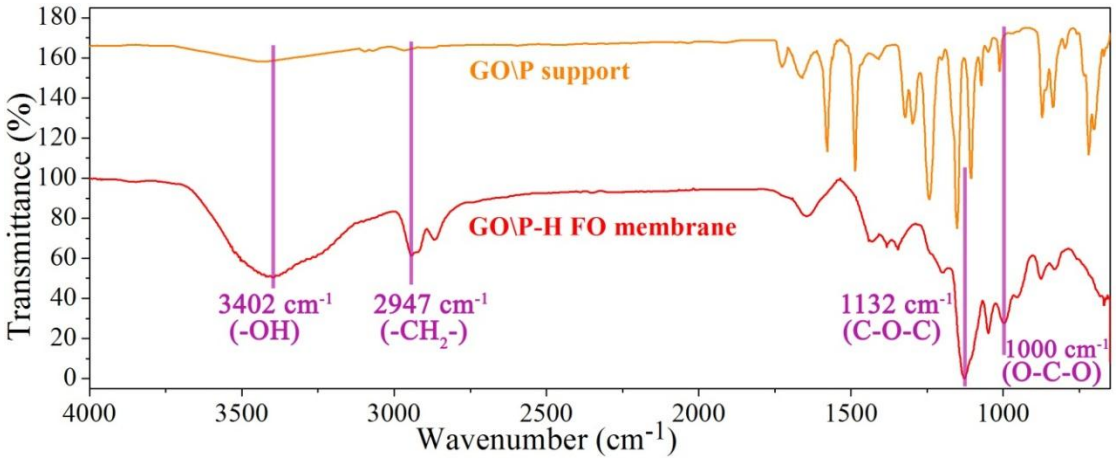

Figure 5.14 ATR-FTIR spectra of as-synthesized GO\P support layer and GO\P-H FO membrane.

Figure 5.14 compares the ATR-FTIR spectra between as-synthesized GO\P support layer and GO\P-H FO membrane. As elaborated previously in section 5.4, the IR spectrum of GO\P nanocomposite support layer has the characteristic bands originated from both PES (7 bands: 1578 cm^{-1}, 1487 cm^{-1}, 1325 cm^{-1}, 1300 cm^{-1}, 1244 cm^{-1}, 1153 cm^{-1} and 1107 cm^{-1} *etc.*) and GO nanosheets (3 bands: 3400 cm^{-1}, 1733 cm^{-1}, and 1627 cm^{-1} *etc.*). After the dip-coating of chemically crosslinked hydrogel macromolecule, significant transformations on FTIR spectrum are noted as follows. Firstly, the signal of IR band located near 3400 cm^{-1}, which corresponds to the stretching vibrations of hydroxyl groups, gets enhanced by ~1 order of magnitude with the peak position slightly red-shifted from 3400 cm^{-1} to 3402 cm^{-1}. This is because the number density of free hydroxyl group in crosslinked hydrogel macromolecules is much higher than that in GO\P nanocomposite support layer. Secondly, except the IR band at 3400 cm^{-1}, the other nine characteristic IR bands of GO\P support layer get weakened with certain

traces left on the IR spectrum of GO\P-H FO membrane. Thirdly and most importantly, several new IR bands that originate from hydrogel selective layer emerge on the spectrum of GO\P-H FO membrane including (1) the IR band at 2947 cm^{-1} that signifies the C-H asymmetric stretching vibration of alkyl groups ($-CH_2-$) in the skeleton of hydrogel macromolecule (PVA), (2) the IR band at 1132 cm^{-1} that represents the stretching vibration of C-O-C group in the acetal bridge of chemically crosslinked hydrogel macromolecules (see the illustration for molecular structure of acetal bridge in Figure 3.1), and (3) the IR band at 1102 cm^{-1} that symbolizes the stretching vibration of O-C-O group in the acetal bridge (Destaye *et al.*, 2013). Therefore, the IR bands at 1132 cm^{-1} and 1102 cm^{-1} can be considered as the characteristic bands of as-crosslinked hydrogel selective layer because they are absent from the IR spectrum of GO\P nanocomposite support layer and also indicative of the successful aldolization of aldehyde group (-CHO) of crosslinking agent (glutaraldehyde) with hydroxyl group (-OH) of hydrogel macromolecule (PVA).

In short, the above FTIR analysis not only substantiates the successful crosslinking between hydrogel macromolecule and crosslinking agent but also reveals that as-crosslinked hydrogel selective layer dominates the top surface chemical properties of as-synthesized GO\P-H FO membrane.

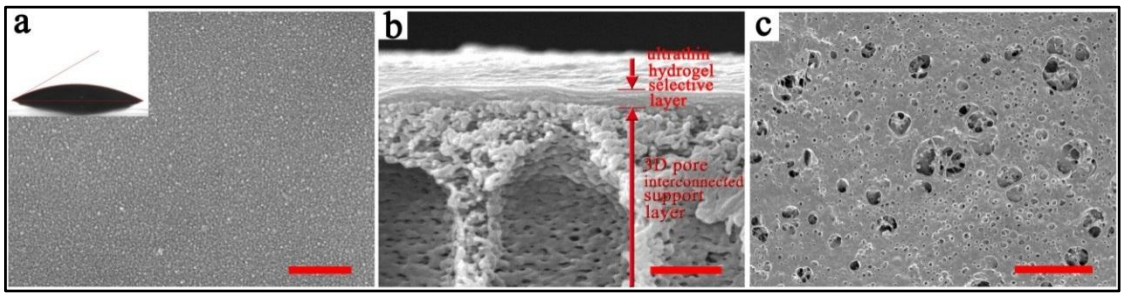

Figure 5.15 Structures of as-synthesized GO\P-H FO membranes. (**a**) FESEM image on top surface, scale bar 200 nm (the inset is water contact angle of GO\P-H FO membrane). (**b**) Enlarged FESEM image on cross-section, scale bar 500 nm. (**c**) FESEM image on bottom surface, scale bar, 10 μm. For (**a-c**), nanocomposite dope solution contains 0.5 wt% GO, 15 wt% PES and 84.5 wt% DMF.

Figure 5.15 displays the structures of as-synthesized GO\P-H FO membrane. As shown in Figure 5.15a, GO\P-H FO membrane is similar with P-H FO membrane in the architecture of upmost surface that is formed by the assembly of ~10 nm nanograins. These nanograins of crosslinked hydrogel macromolecules constitute the orderly

arrays that make membrane surface structure to be compact and defect free at nanometer scale, which is promising to reject tiny inorganic ions in sub-nanometer size. This surface architecture also enables hydrogel selective layer to possess ultrasmooth topography, as average roughness (R_a) reduced from 30 nm of GO\P support layer to 7 ± 1.9 nm of GO\P-H FO membrane. Noteworthily, although GO\P nanocomposite support layer is evidently rougher than P support layer in topography as discussed previously in Figure 5.5a, the coating of hydrogel selective layer renders GO\P-H FO membrane to be similar with P-H FO membrane in topography: the R_a of GO\P-H FO membrane is slightly higher than that of P-H FO membrane (5 ± 1.3 nm) but in the same level of sub-10 nm.

Meanwhile, the top surface of GO\P-H FO membrane is highly hydrophilic, with the water contact angle reduced from 59 ° ± 5.0 ° of GO\P support layer (0.50 wt% GO) to as low as 28 ° ± 2.9 ° after dip-coating. It's also worthy to note that GO\P-H FO membrane is the same with P-H FO membrane in surface hydrophilicity. This result confirms that surface properties of GO\P-H FO membrane are dominated by the as-crosslinked hydrogel macromolecules. More importantly, as discussed previously in Chapter 2 on antifouling mechanism, the ultrasmooth topography and high hydrophilicity of as-synthesized GO\P-H FO membrane are advantageous properties to resisting fouling.

As exhibited in Figure 5.15b, enlarged FESEM image on the cross-section of GO\P-H FO membrane indicates that the hydrogel selective layer is immobilized on the top of GO\P support layer at an ultrathin thickness of 103 ± 10 nm. Hence, the entire cross-section of GO\P-H FO membrane consists of an ultrathin hydrogel selective layer on top of a micrometer-scale 3D interconnected porous support layer. Furthermore, the underneath GO\P support layer maintains its 3D interconnected porous structure, which means most of the as-crosslinked macromolecules are immobilized on the top surface during dip-coating process without penetrating the GO\P support layer. This is also evidenced by the FESEM image on the bottom surface of as-synthesized GO\P-H FO membrane (Figure 5.15c), which shows that the formation of hydrogel selective layer does not alter the morphology of support layer bottom surface.

In short, hydrogel selective layer is successfully immobilized onto the top surface of GO\P support layer in ultrathin thickness through dip-coating technique; and as-coated hydrogel selective layer endows GO\P-H nanocomposite FO membrane with smooth topography and high hydrophilicity.

5.8.2. FO water flux (J_W) and reverse salt flux (J_S) of GO\P-H FO membranes

FO performances in terms of water flux (J_W) and reverse salt flux (J_S) are systematically examined for both GO\P-H and P-H membranes, with the commercially available HTI membrane employed as the comparison. The relevant results are presented in Figure 5.16a~b.

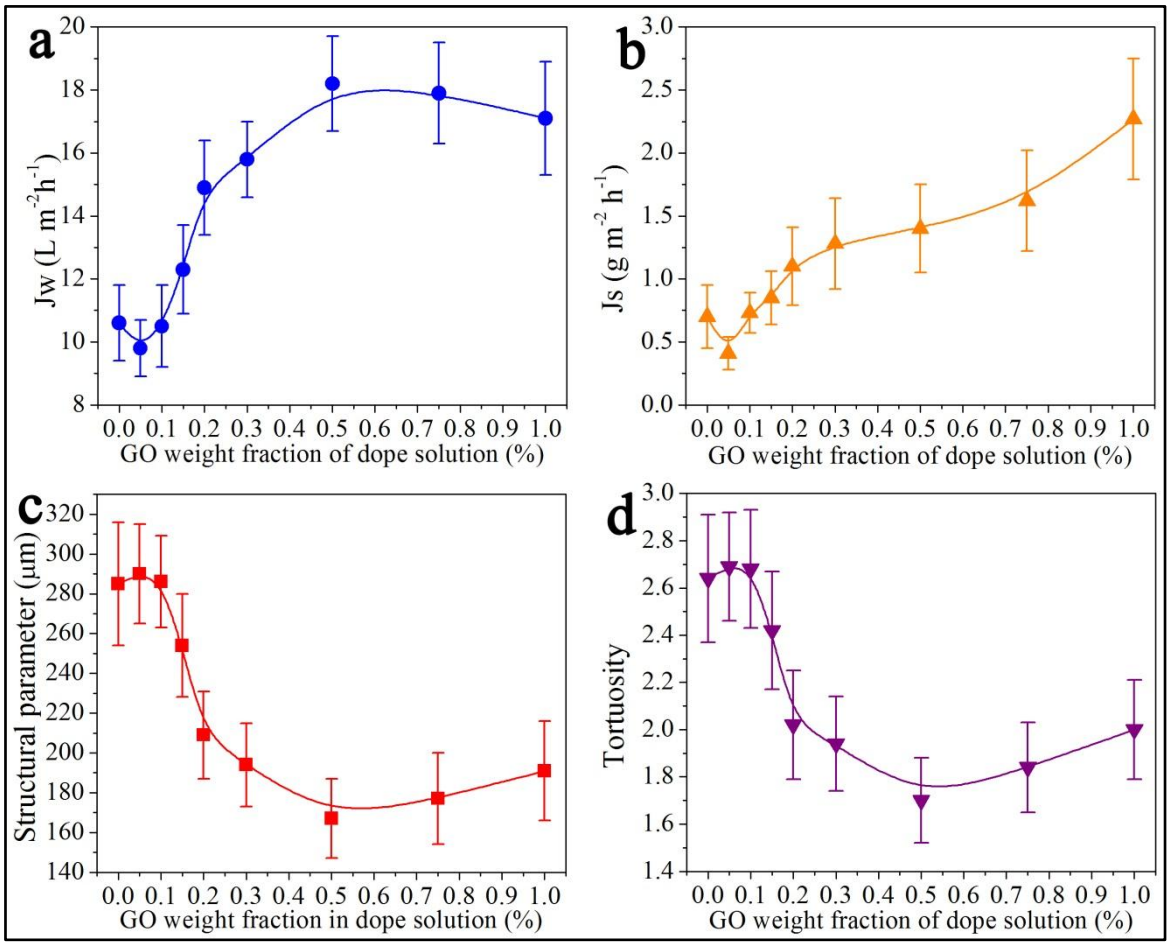

Figure 5.16 The influences of GO incorporation on FO membrane performances and structural parameter. (**a**) FO water flux (J_W). (**b**) FO reverse salt flux (J_S). (**c**) FO membrane structural parameter (S). (**d**) FO membrane support layer tortuosity (τ). The PES concentration is kept as 15 wt% in nanocomposite dope solution. The draw solution is 0.5 M Na_2SO_4 while feed solution is DI water. Membrane orientation is selective layer facing feed solution (FO mode).

The J_W values of as-synthesized FO membranes under different GO concentrations in the dope solutions that are used to fabricate support layer through phase inversion are shown in Figure 5.16a. And this J_W – GO concentration curve can be divided into three stages. Firstly, as GO concentration increased from 0.00 wt% to 0.05 wt%, the J_W of as-synthesized FO membranes undergoes a slight decrease from 10.6 ± 1.2 L m^{-2} h^{-1} to 9.8 ± 0.9 L m^{-2} h^{-1}. Secondly, as GO concentration further increased from 0.05 wt% to 0.50 wt%, the J_W of GO\P-H FO membranes is enhanced by 86% from 9.8 ± 0.9 L m^{-2} h^{-1} to 18.2 ± 1.5 L m^{-2} h^{-1}. Thirdly, as GO concentration further increased from 0.50 wt% to 1.00 wt%, the J_W turns to be reduced from 18.2 ± 1.5 L m^{-2} h^{-1} to 17.1 ± 1.8 L m^{-2} h^{-1}. Here two points are emphasized. One point is that the maximum J_W is obtained at GO concentration of 0.50 wt% that is corresponding to the optimized micrometer-scale 3D interconnected porous support layer structure, which is 72% higher than that of P-H FO membrane. This confirms the superiority of GO assisted phase inversion constructed 3D pore interconnected support layer structure over conventional phase inversion constructed 1D pore connected support layer structure in FO water flux. The other point is that GO\P-H FO membranes under all different GO concentrations outperform HTI membrane in terms of J_W value, with the maximum J_W value at GO concentration of 0.50 wt% reaching 2.8 times higher than that of HTI membrane (4.8 ± 0.7 L m^{-2} h^{-1}).

Meanwhile, the J_S values of as-synthesized FO membranes under different GO concentrations are shown in Figure 5.16b. The J_S – GO concentration curve can be divided into two stages. Firstly, as GO concentration increased from 0.00 wt% to 0.05 wt%, the J_S of as-synthesized FO membranes experiences a decrease from 0.7 ± 0.25 g m^{-2} h^{-1} to 0.43 ± 0.14 g m^{-2} h^{-1}. Secondly, as GO concentration further increased from 0.05 wt% to 1.00 wt%, the J_S of as-synthesized GO\P-H FO membranes is increased from 0.43 ± 0.14 g m^{-2} h^{-1} to 2.27 ± 0.48 g m^{-2} h^{-1}. The smallest J_S is at GO concentration of 0.05 wt%, which indicates as-synthesized GO\P-H FO membrane possesses a more compact selective layer structure that favors retarding the diffusion of solutes and thus leads to the corresponding decrease in J_W from GO concentration of 0.00 wt% to 0.05 wt%. Further elucidation is given as follows. The incorporation of GO nanosheets in support layer can generate two opposite effects upon the formation

of hydrogel selective layer. On one hand, the embedded GO nanosheets especially those near or on top surface of support layer can promote the interfacial electrostatic interactions between support layer top surface and crosslinked hydrogel macromolecules and thus facilitate hydrogel macromolecules to form the selective layer in more compact structure. On the other hand, as aforementioned in Figure 5.5 ~ 5.6, the incorporation of GO nanosheets can enlarge the surface pore sizes of as-synthesized support layer and thus increase the risk for the formation of sub-nanometer sized defects on hydrogel selective layer surface. The incorporation of GO at relatively low concentration of 0.05 wt% in dope solution does not generate any remarkable change upon pore structure of as-synthesized support layer. Hence, the promotion in interfacial electrostatic interactions dominates the effects induced by the embedment of GO nanosheets and thus facilitates the formation of a more compact hydrogel selective layer. As a result, both forward diffusion of water molecules and reverse diffusion of draw solute get retarded. However, above GO concentration of 0.05 wt%, the effect of surface pore size enlargement overwhelms the promotion in interfacial electrostatic interactions and thus facilitates the formation of a less compact selective layer structure. As a result, reverse salt leakage is increased for as-synthesized GO\P-H FO membranes. More importantly, this reveals that the controlling of GO concentration in polymer dope solution can influence to certain extent the structure and property of hydrogel selective layer which is subsequently constructed on the top surface of phase inversion constructed support layer.

It's necessary to highlight another two points here. One point is that the rejection of draw solute ions by as-synthesized GO\P-H nanocomposite membrane is not significantly compromised along with the increase of GO concentration from 0.05 wt% to 0.50 wt%, as listed in Table 5.3. However, the further increase of GO concentration from 0.50 wt% to 1.00 wt% results in the evident decrease in the rejection of draw solute (Na_2SO_4) from 93.5% to 92.2% and the significant exacerbation in reverse solute leakage from 1.4 $\pm$ 0.35 g m^{-2} h^{-1} to 2.27 $\pm$ 0.48 g m^{-2} h^{-1}. The other point is that GO\P-H FO membrane with optimized 3D interconnected porous support layer structure (GO concentration of 0.50 wt%) outclasses HTI membrane in terms of selectivity (J_W/J_S). The J_S of GO\P-H FO membrane at GO concentration of 0.50 wt% is 1.4 $\pm$ 0.35 g m^{-2} h^{-1}, which is comparable to the J_S of HTI membrane that is 1.35 $\pm$

0.33 g m^{-2} h^{-1}. Because the J_W of GO\P-H FO membrane at GO concentration of 0.50 wt% is 3.8 times as high as that of HTI membrane, the J_W/J_S f GO\P-H FO membrane at GO concentration of 0.50 wt% (13.0 ± 1.4 L g^{-1}) is 2.7 times higher than that of HTI FO membrane (3.56 ± 0.45 L g^{-1}).

Table 5.3 Intrinsic properties of commercial and as-synthesized FO membranes.

Membrane	Water Permeability ($L\ m^{-2}\ h^{-1}\ bar^{-1}$)	Rejection of Na_2SO_4(%)	Water flux in FO mode (J_W, $L\ m^{-2}\ h^{-1}$)	Reverse salt flux in FO mode (J_S, $g\ m^{-2}\ h^{-1}$)	Structural Parameter (S, μm)	Thickness (L, μm)	Porosity (ε, %)	Tortuosity (τ)
HTI	0.40 ± 0.07	97.0 ± 1.0	4.8 ± 0.7	1.35 ± 0.33	455 ± 43	52.5 ± 11	41.5 ± 2.8	3.65 ± 0.31
P-H	1.12 ± 0.10	95.2 ± 1.3	10.6 ± 1.2	0.70 ± 0.25	285 ± 31	88.6 ± 2.8	82.0 ± 2.5	2.64 ± 0.27
GO/P-H (0.05)	0.98 ± 0.09	96.0 ± 0.7	9.8 ± 0.9	0.41 ± 0.13	290 ± 25	88.6 ± 2.5	82.2 ± 2.7	2.69 ± 0.23
GO/P-H (0.10)	1.10 ± 0.08	95.0 ± 0.8	10.5 ± 1.3	0.73 ± 0.16	286 ± 23	88.2 ± 2.3	82.8 ± 3.1	2.68 ± 0.25
GO/P-H (0.20)	1.63 ± 0.13	94.1 ± 1.1	14.9 ± 1.5	1.1 ± 0.31	209 ± 22	86.4 ± 2.6	83.5 ± 1.9	2.02 ± 0.23
GO/P-H (0.30)	1.70 ± 0.15	93.8 ± 1.1	15.8 ± 1.2	1.28 ± 0.36	194 ± 21	84.1 ± 3.1	84.1 ± 2.5	1.94 ± 0.20
GO/P-H (0.50)	1.94 ± 0.17	93.5 ± 1.2	18.2 ± 1.5	1.4 ± 0.35	167 ± 20	83.0 ± 2.8	84.5 ± 2.8	1.70 ± 0.18
GO/P-H (0.75)	2.01 ± 0.15	93.0 ± 1.2	17.9 ± 1.6	1.62 ± 0.40	177 ± 23	81.8 ± 2.7	84.9 ± 2.9	1.84 ± 0.19
GO/P-H (1.00)	1.99 ± 0.14	92.2 ± 1.5	17.1 ± 1.8	2.27 ± 0.48	191 ± 25	81.3 ± 2.2	85.2 ± 2.6	2.00 ± 0.21

Note: the number inside brackets coming after "GO/P-H" indicates the weight fraction of GO to be incorporated in the nanocomposite dope solution.

5.8.3. The diminution in ICP owning to GO prompted support layer pore interconnectivity.

Based on the results of J_W and J_S as discussed in section 5.8.2, mathematical modeling of ICP is employed to investigate the impact on FO membrane structural parameter (S) by the incorporation of GO nanosheets. The relevant results are presented in Figure 5.16c~d, Figure 5.17~ Figure 5.18, and Table 5.3.

As displayed in Figure 5.16c, the change in S value of as-synthesized FO membranes along with the increase of GO concentration in phase inversion dope solution can be divided into three stages. Firstly, as GO concentration increased from 0.00 wt% to 0.10 wt%, no significant changes have been observed for the structural parameter of as-synthesized FO membranes with the S value stabilized around 287 ± 27 μm. Secondly and more importantly, as GO concentration further increased from 0.10 wt% to 0.50 wt%, the S value of as-synthesized GO\P-H FO membranes is reduced by 42% from 286 ± 23 μm to 167 ± 20 μm. Thirdly, along with the further increase in GO concentration from 0.50 wt% to 1.00 wt%, the S value of GO\P-H FO membranes turns to be increased from 167 ± 20 μm to 191 ± 25 μm. Undoubtedly, the minimum S value is achieved at GO concentration of 0.50 wt% (PES concentration is 15 wt%) that is corresponding to the optimized 3D interconnected porous support layer structure. Moreover, this minimum S value is 41.4% lower than the S value of P-H FO membrane and 63.2% lower than the S value of commercial HTI membrane (455 ± 43 μm), as listed in Table 5.2. Since ICP effect is positively correlated with S value, these results indicate that the ICP problem has been minimized through optimizing support layer pore structure to be 3D interconnected at micrometer-scale by the incorporation of GO nanosheets.

Furthermore, Table 5.3 reveals that the major contributor to the decrease in S value is the diminution of FO membrane tortuosity (τ). And Figure 5.16d shows that the change in τ value follows the similar trend with that of S value along with the increase of GO concentration. Firstly, the τ value of as-synthesized FO membranes stays around 2.67 ± 0.25 as GO concentration increased from 0.00 wt% to 0.10 wt%. Secondly and more importantly, the τ value of as-synthesized GO\P-H FO membranes undergoes a significant decrease from 2.68 ± 0.25 to 1.70 ± 0.18 along with the increase of GO

concentration from 0.10 wt% to 0.50 wt%. Thirdly, the τ value of GO\P-H FO membranes bounces back to 2.00 ± 0.21 as GO concentration further increased to 1.00 wt%. The minimum membrane tortuosity is also achieved at GO concentration of 0.50 wt%, which is 36% lower than that of as-synthesized P-H FO membrane (2.67 ± 0.25) and 54% lower than that of commercial HTI FO membrane (3.65 ± 0.31). These results demonstrate the advantage of GO assisted phase inversion technique over conventional phase inversion technique in the construction of low tortuosity support layer for FO membrane.

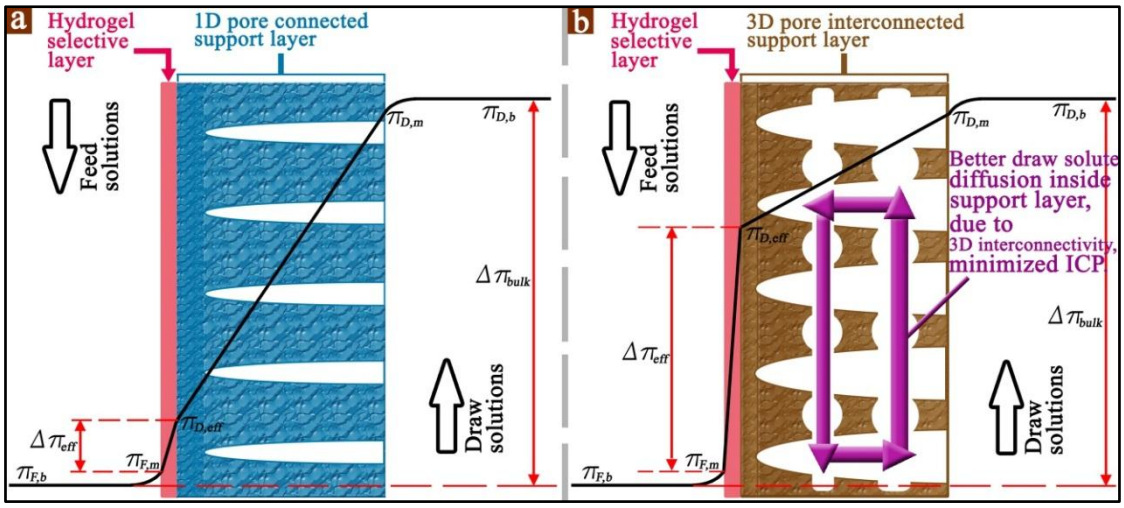

Figure 5.17 Internal concentration polarization profile across (a) 1D pore connected support layer and (b) 3D pore interconnected support layer.

This diminution in FO membrane tortuosity is attributed to the improvement in pore interconnectivity of support layer that facilitates the free transportation of water molecules in all three dimensions inside support layer and thus enables water molecules to find the shortest passage from top surface to bottom surface (along z axis). More importantly, accompanied by the free transportation of water molecules, the diffusion of draw solute inside support layer gets significantly enhanced especially in the directions perpendicular to cross-section plane (x and y axes). This will eliminate or to a large extent suppress the accumulation of draw solute within support layer interior micro regions otherwise takes place in traditional occluded pore structure (*e.g.* dead pores) that weakens the restoration of $\Delta\pi_{eff}$ by hindering compensated diffusion of draw solute. As a result, the ICP extent in 3D pore interconnected support layer is significantly diminished compared with that in conventional 1D pore connected support layer, as illustrated in Figure 5.17. This characterizes that GO assisted phase

inversion constructed micrometer-scale 3D interconnected porous support layer can effectively minimize ICP problem.

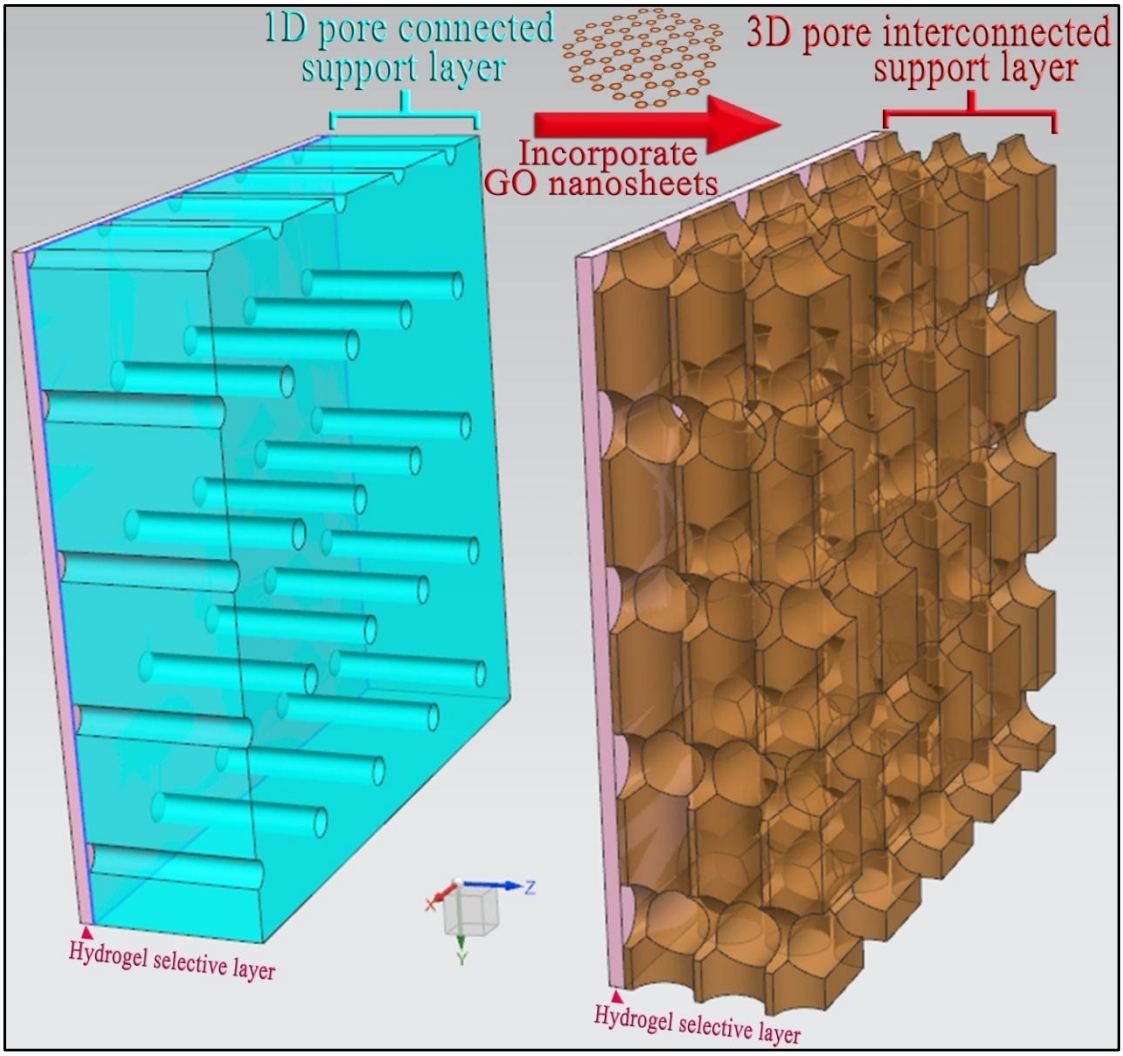

Figure 5.18 Illustration of the 3D pore interconnected support layer structure of GO\P-H nanocomposite FO membrane owning to the optimized incorporation of GO nanosheets.

In short, as illustrated in Figure 5.18, the incorporation of GO nanosheets can transform the interior pore structure of as-synthesized support layer from 1D connected to 3D interconnected. Moreover, this micrometer-scale 3D interconnected porous support layer has been demonstrated able to minimize the ICP problem and thus lead to high FO water flux.

5.9. Summary

In summary, it's the first time to demonstrate GO nanosheet's ability to transform the interior pore structure of support layer from conventionally 1D connected to 3D

interconnected, purposely for the synthesis of high water flux FO membrane. Important achievements are emphasized as follows.

Firstly, the incorporation of GO nanosheets modifies as-synthesized GO\P support layer to be more hydrophilic and negatively charged.

Secondly, the incorporation of GO nanosheets can enlarge the pore size of both top and bottom surfaces for as-synthesized GO\P support layer.

Thirdly and most importantly, the incorporation of GO nanosheets can generate a qualitative enhancement in the interior pore interconnectivity for as-synthesized GO\P support layer. Based upon systematic optimization of GO assisted phase inversion parameters including GO concentration, polymer concentration, solvent and so on, an entirely new support layer structure with its interior pores highly interconnected in all three dimensions at micrometer scale (3D interconnected porous support layer) can be created.

Fourthly, the formation mechanism of this 3D interconnected porous structure is discussed from the perspective of GO induced viscous fingering. Two points are worthy highlighted here: (1) GO induced viscosity difference serves as the driving force to prompt the spread of fingering directions from original one dimension to all three dimensions, and (2) GO's 2D structure characteristic guarantees channel growth in the emerging two dimensions (x and y axes) at micrometer-scale.

Fifthly, compared with conventional 1D pore connected support layer, this 3D pore interconnected support layer can enhance FO water flux (J_W) of as-synthesized membrane by 72% without significantly compromising its selectivity. Moreover, this 3D interconnected porous structure is proved able to effectively minimize ICP problem, as evidenced by the diminution in FO membrane structural parameter S value by as much as 41.4%. And the major contributor to the decrease in S value is the decrease of FO membrane support layer tortuosity (τ), which demonstrates that the incorporation of GO nanosheets can innovate FO membrane support layer structure in a smart way.

Sixthly, these outcomes demonstrate for the first time that micrometer-scale 3D interconnected porous support layer that is able to break the bottleneck of ICP can be achieved with dominant membrane manufacture processes *i.e.* phase inversion. As-demonstrated combination of cutting-edge nanotechnology with prevailed membrane manufacture process is expected to make a significant impetus to the industrialization of FO technology.

Finally, by clearing the last obstacle *i.e.* ICP caused low FO water flux issue, the door to investigate the response to fouling for as-synthesized nanocomposite FO membrane towards the final goal of treating challenging wastewater (*e.g.* highly saline and oily wastewater) with low fouling, high water flux, and high selectivity is openned.

CHAPTER 6 SIMULTANEOUS DESALINATION AND OIL/WATER SEPARATION BY AS-SYNTHESIZED NANOCOMPOSITE MEMBRANE THROUGH FO PROCESS

6.1. Introduction

As illustrated in the overview of this thesis (Figure 6.1), a special thin-film nanocomposite (TFNC) FO membrane (GO\P-H membrane) has been successfully synthesized based upon previous efforts carried out in Chapter 4 and Chapter 5. Particularly, the support layer of this TFNC FO membrane possesses a micrometer-scale 3D interconnected porous structure that is constructed by GO assisted phase inversion technology (Figure 6.1a,b). This 3D interconnected porous support layer contributes to the high FO J_W advantage which has been verified with DI water as feed solution. Furthermore, the hydrogel selective layer of this new FO membrane is synthesized through dip-coating technique (Figure 6.1c), which has demonstrated excellent rejections of tiny inorganic salt ions owning to its chemically-crosslinked molecular structure (Figure 6.1d). Moreover, this hydrogel selective layer also possesses high hydrophilicity that is expected to help resisting the fouling from oily pollutants (Figure 6.1e).

In this chapter, towards the final goal of this thesis, as-synthesized GO\P-H membrane is systematically examined for its potentiality to overcome the unprecedented challenge that is to separate hypersaline oil/water mixtures (*e.g.* shale gas wastewater *etc*.) with low fouling, high water flux, and high selectivity. Research activities are organized based upon the deliberate design as follows.

Firstly, FO performances in terms of water flux (J_W) and reverse salt flux (J_S) have been studied at high concentration of draw solute (feed solution is DI water) for GO\P-H membrane, with P-H membrane and HTI membrane as comparisons.

Secondly, the antifouling capability of GO\P-H membrane has been systematically examined with various salinity-free oil-in-water emulsions as FO feed solution.

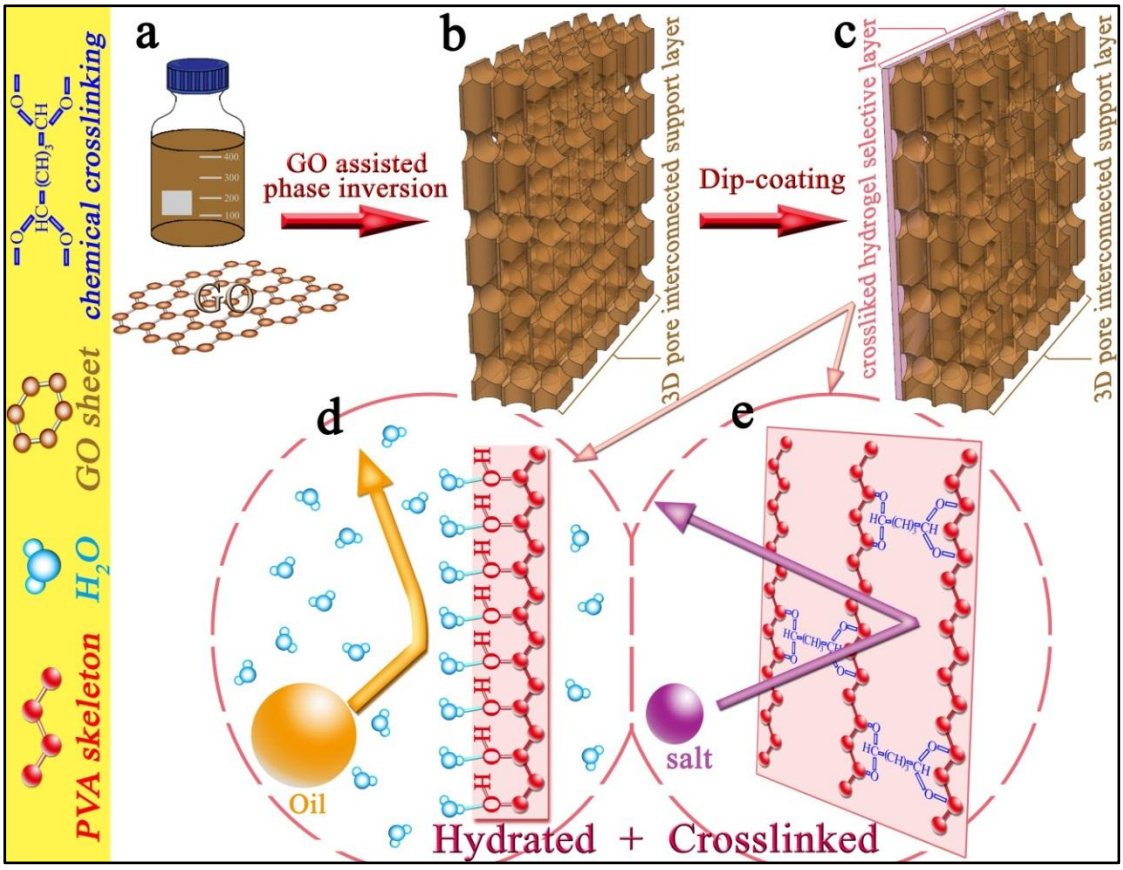

Figure 6.1 Illustration of the synthetic process and working mechanisms of GO\P-H nanocomposite FO membrane. (**a**) Graphene oxide (GO) nanosheets are prepared and homogeneously dispersed in the polymer (PES) dope solution. (**b**) GO\P nanocomposite support layer is cast by GO assisted phase inversion technique. (**c**) The hydrogel macromolecule (PVA) is chemically crosslinked and coated on the top surface of nanocomposite support layer to synthesize GO\P-H FO membrane. (**d**) The upmost surface of the hydrogel layer undergoes hydration in water to create an ultrathin water barrier that resists oil-fouling. (**e**) Simultaneously, the crosslinked structure of the hydrogel layer endows itself with the capability of rejecting salt ions efficiently. The molecular structures of the hydrated and crosslinked hydrogel layer are illustrated in (**d**) and (**e**), respectively.

Thirdly, the mechanisms on different membrane responses to oil-fouling during FO separation have been explored among GO\P-H membrane, P-H membrane and HTI membrane, including the impacts of membrane surface wettability and oil droplet size distribution. The above three investigations are designated to solidify the research basis on oil/water separation through FO process.

Fourthly and most importantly, a variety of saline oily wastewaters are employed as FO feed solution to investigate the ability of GO\P-H membrane to treat challenging wastewater. And the performances of all the three membranes are systematically compared on membrane fouling, water flux and salt rejections in detail.

Fifthly, important issues about water recovery and technical shackles on the separation of hypersaline oil/water emulsion through FO process have been discussed in a critical manner.

Last but not least, the significances and implications of this study on simultaneous desalination and oil/water separation of hypersaline emulsion have been carefully summarized.

To the best knowledge of the author, this is the first study that design, synthesize and examine the suitable membrane to purposely treat hypersaline oil-in-water emulsion through FO process.

Noteworthily, membrane orientation is fixed as selective layer facing feed solution (*i.e.* FO mode) throughout all FO running in this chapter. This setting is to follow the rationale that utilizes the functional layer of FO membrane to confront the challenge of fouling and thus avoid the choking of support layer pores otherwise intruded by foulants.

6.2. FO performance under high draw solute concentrations

Since the wastewaters that are eventually targeted at contain high concentration of salts besides high concentration of oily pollutants (*e.g.* shale gas wastewater contains salts with its total dissolved salinity even higher than that of seawater), the draw solution should be more concentrated (hypertonic) than the wastewater to provide sufficient osmotic difference as the driving force for FO process. Therefore, membrane performances in terms of water flux (J_W) and reverse salt flux (J_S) under high concentration of draw solute are investigated first in order to solidify the ground work (DI water is feed solution).

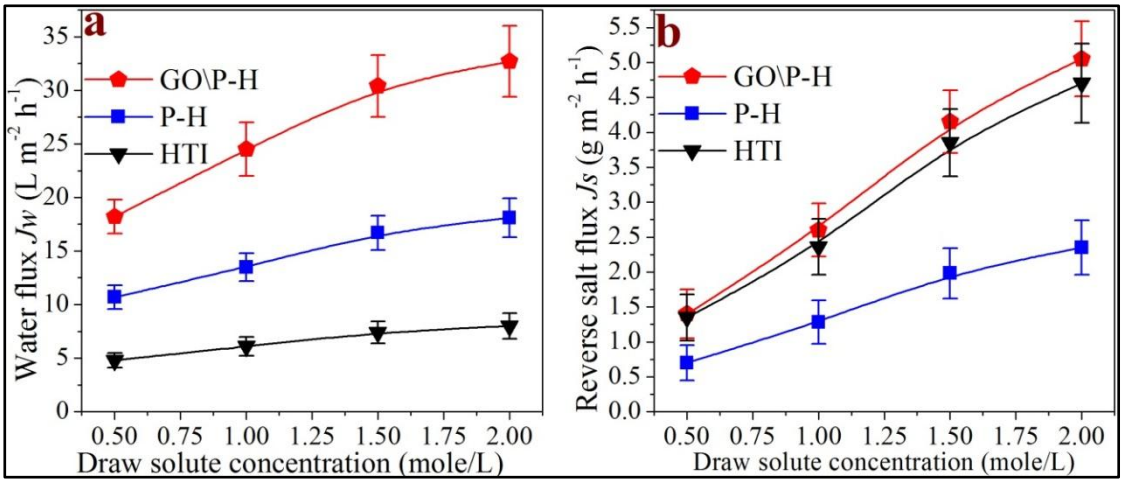

Figure 6.2 FO water flux (J_W) and reverse salt flux (J_S) of GO\P-H, P-H and HTI membranes under different draw solute concentrations. Membrane orientation is selective layer facing feed solution (FO mode). Draw solute is Na_2SO_4 and feed solution is DI water.

Figure 6.2 presents the J_W and J_S of as-synthesized hydrogel FO membranes under different concentrations of draw solute (Na_2SO_4) with HTI FO membrane as the comparison. Figure 6.2a shows that along with the increase of draw solute concentration from 0.50 M to 2.00 M, the J_W is increased monotonously for all the three membranes in different ranges: (1) from 18.2 ± 1.6 L m^{-2} h^{-1} to 32.7 ± 3.3 L m^{-2} h^{-1} for GO\P-H FO membrane, (2) from 10.7 ± 1.1 L m^{-2} h^{-1} to 18.1 ± 1.8 L m^{-2} h^{-1} for P-H FO membrane, and (3) from 4.8 ± 0.7 L m^{-2} h^{-1} to only 8.0 ± 1.2 L m^{-2} h^{-1} for HTI FO membrane. These results verify the advantage in high water flux for GO\P-H FO membrane over other membranes under high concentration of draw solute.

Figure 2b shows that as draw solute concentration increased from 0.50 M to 2.00 M, the J_S is also increased monotonously (1) from 1.40 ± 0.35 g m^{-2} h^{-1} to 5.05 ± 0.54 g m^{-2} h^{-1} for GO\P-H FO membrane, (2) from 0.71 ± 0.25 g m^{-2} h^{-1} to 2.35 ± 0.40 g m^{-2} h^{-1} for P-H FO membrane, and (3) from 1.35 ± 0.33 g m^{-2} h^{-1} to 4.7 ± 0.57 g m^{-2} h^{-1} for HTI FO membrane. It's clear that under different concentrations of draw solute, the J_S of GO\P-H membrane is slightly higher than that of HTI membrane with the exceeding ratio less than 10%. This indicates that GO\P-H membrane outperforms HTI membrane in membrane selectivity (J_W/J_S) under high draw solute concentration because the J_W of GO\P-H membrane is ~4 times as high as that of HTI membrane. Taking account of that the increase in J_W is not as remarkable as that in J_S along with the elevation of draw solution concentration from 1.5 M to 2.0 M, draw solute

concentration of 1.5 M is selected for the following investigations.

6.3. Evaluation of membrane antifouling property

It's believed that FO process provides a unique scenario to investigate the susceptibility of salt-rejecting membrane to certain foulants, because fouling associated with hydraulic pressure is minimized or negligible. In order to enrich the fundamental studies on membrane fouling under oil-polluted wastewaters, the effects of oil concentration, surfactant/oil ratio and different oil kinds are systematically investigated. In this section a variety of salinity-free oil-in-water emulsions are employed as the feed solution to rule out the interference of salinity, which will functions as the basis for the further explorations. Besides, it's worthy to note that the experimental settings in this study guarantee the membrane to truly confront the oil concentration as high as designated and thus validate the significances of research activities, as stated previously in section 3.9.2 of Chapter 3.

6.3.1. Effect of oil concentration

For the purpose of excluding the possibility that the existence of surfactant complicates the factor analysis on membrane fouling, surfactant-free emulsions made of one specific kind of oil (vegetable oil) are employed at first to study the effect of oil concentration. Figure 6.3a, b shows that along with the increase of oil concentration, membrane fouling is exacerbated and hence water recovery at the given operation time (360 min separation fed by emulsion during the FO cycle) is reduced; more importantly, under all circumstances compared with commercially available HTI FO membrane, as-synthesized nanocomposite GO\P-H FO membrane achieves better fouling-mitigation in terms of lower flux reduction ratio (*FRR*).

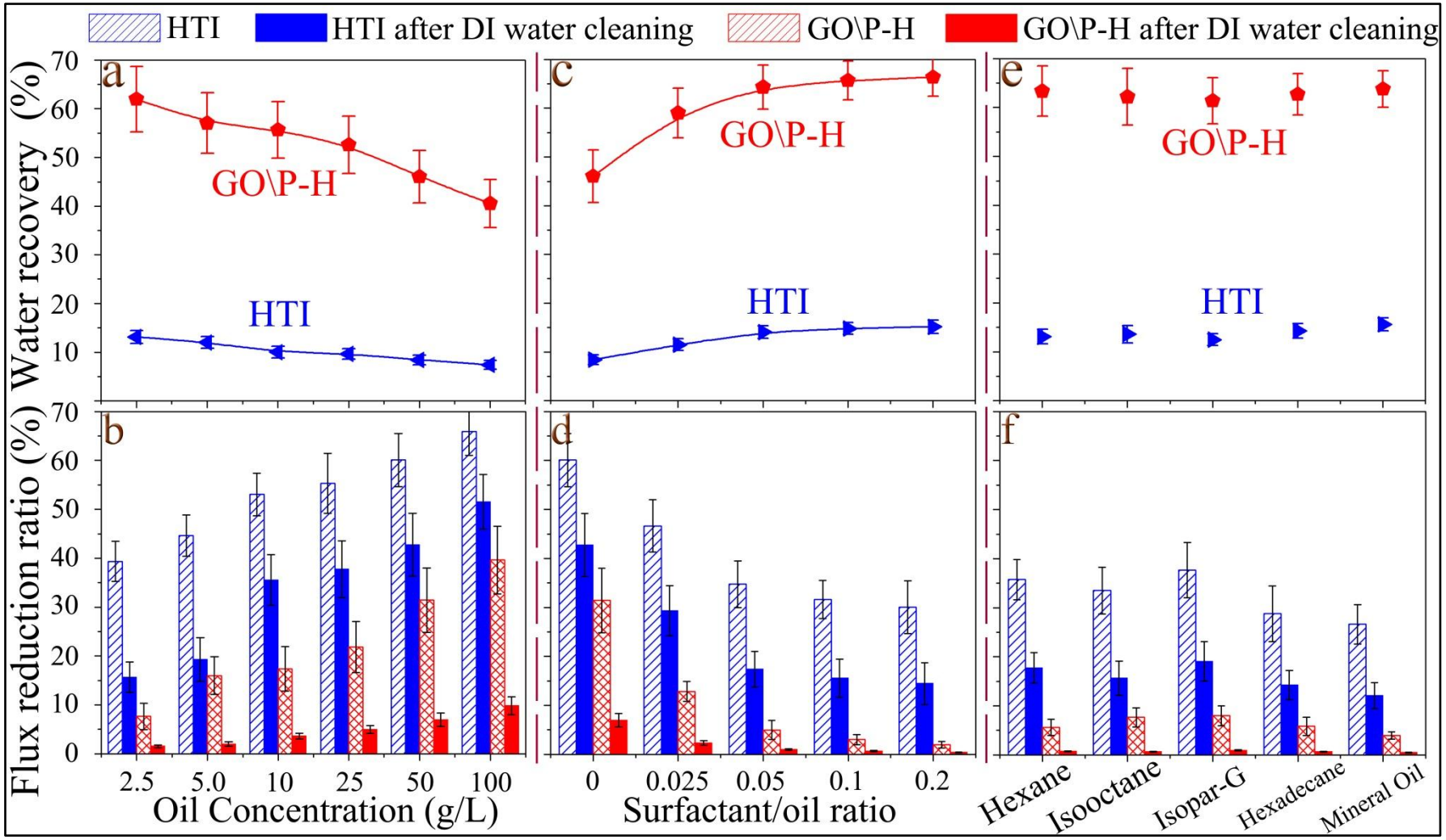

Figure 6.3 Water recoveries and flux reduction ratios of GO\P-H and HTI FO membranes. (**a**, **b**) Effect of oil concentrations (Surfactant concentration is zero). (**c**, **d**) Effect of surfactant/oil ratios (Oil concentration is 50 g/L). (**e**, **f**) Effect of different kinds of oils (Oil concentration is 25 g/L and surfactant/oil ratio is 0.05). Draw solution is 1.5 M Na_2SO_4. FRR_f and water recovery are recorded at the 360th min of "oil-fouling" stage.

In particular, GO\P-H FO membrane is >50% lower than HTI FO membrane in FRR_f (*FRR* in "oil-fouling stage") under 2.5~50 g/L oil concentrations. Even fed with ultrahigh oil concentration like 100 g/L, the FRR_f of GO\P-H membrane is 39.6% ± 6.8%, still 40% lower than the FRR_f of HTI membrane that is 65.9% ± 4.9%. Correspondingly, under oil concentration of 100 g/L, GO\P-H membrane achieves 41% ± 4.8% water recovery, surpassing HTI membrane that attains only 7.4% ± 0.9% water recovery. Furthermore, most of the J_W losses can be recovered for GO\P-H FO membrane through *in-situ* washing by DI water, leading to its FRR_c (*FRR* in "post-cleaning stage") ranged from 1.5% ± 0.3% to 9.8% ± 1.8%. On the contrary, the DI water cleaning effect for HTI FO membrane is poor, resulting in much higher FRR_c that is ranged from 15.7% ± 3.1% to 51.6% ± 5.6%.

In short, GO\P-H membrane demonstrates remarkably better antifouling capability than HTI membrane during FO separation of surfactant-free oil-in-water emulsions under a wide range of oil concentrations.

6.3.2. Effect of surfactant/oil ratio

In order to investigate membrane fouling under emulsions stabilized by surfactant, Triton X-100 (surfactant) is added into vegetable oil-in-water emulsion to prepare the feed solution of different surfactant/oil ratios, with oil concentration kept as 50 g/L. Figure 6.3c,d shows that as surfactant/oil ratio increased, fouling is mitigated and hence water recovery is restored; furthermore, the superiorities in fouling-mitigation and water recovery of GO\P-H membrane are strengthened over HTI membrane. The FRR_f of HTI membrane is reduced from 60.1% ± 5.5% to 34.8% ± 4.8% along with the increase of surfactant/oil ratio from 0.00 to 0.05. However, the further increase of surfactant/oil ratio from 0.05 to 0.20 is ineffective to continue such remarkable diminution in membrane fouling, with FRR_f and FRR_c of HTI membrane stabilized around 30.1% ± 5.0% and 14.5% ± 4.3%, respectively. On the contrary, the FRR_f of GO\P-H FO membrane is reduced steadily from 31.4% ± 6.5% to 5.0% ± 1.9% as surfactant/oil ration increased from 0.00 to 0.05. Above surfactant/oil ratio of 0.05, fouling of GO\P-H FO membrane is negligible, for the FRR_f of GO\P-H membrane is reduced to < 3.0% ± 1.0% accompanied by approximately zero FRR_c. Consequently, as surfactant/oil ratio ≥ 0.05%, GO\P-H FO membrane achieves above 64.3% ± 4.5%

water recovery, surpassing HTI FO membrane that obtains only 14.1% ± 1.4% water recovery.

In short, the advantages of high antifouling capability and high water recovery of GO\P-H membrane over HTI membrane are enhanced as surfactant employed to stabilize oil-in-water emulsions.

6.3.3. Effect of different kinds of oil

To substantiate the universality of GO\P-H membrane's excellent antifouling capability, petroleum oils of different carbon atoms in molecule are selected to prepare emulsions with oil concentration and surfactant/oil ratio fixed as 25 g/L and 0.05, respectively. Figure 6.3e,f demonstrates that there is no obvious correlation between carbon atoms in molecule and membrane fouling extent as expected. Particularly, Figure 6.3f shows that GO\P-H FO membrane exhibits ultralow fouling extents under emulsions from different kinds of oil with its FRR_f ranged from 3.9% ± 0.8% to 8.0% ± 2.2% accompanied by <1.0 ± 0.1% FRR_c. On the contrary, HTI FO membrane suffers much severer losses of water flux with its FRR_f ranged from 26.7% ± 3.7% to 37.7% ± 5.6% accompanied by its FRR_c ranged from 12.1% ± 2.7% to 19.1% ± 4.1%, respectively. Consequently, in terms of water recovery HTI membrane (~15% ± 1.7%) is outclassed by GO\P-H membrane (~64% ± 5.5%) when investigated with emulsions prepared from different petroleum oils.

In short, GO\P-H membrane demonstrates considerably higher antifouling-capability and water recovery when separating surfactant-stabilized oil-in-water emulsions prepared from different kinds of oil.

6.3.4. Effect of different washing chemicals

Furthermore, the effect of different washing chemicals on FRR_c has also been studied with the relevant results displayed in Figure 6.4. The employment of sodium dodecyl sulfate (SDS, 0.1 wt% aqueous solution) as the detergent can wash out considerable amounts of oil-fouling and thus further reduce FRR_c. In detail, when DI water is replaced by SDS aqueous solution in washing stage, the FRR_c at 10 g/L surfactant-free emulsion is reduced from 35.6% ± 4.5% to 8.9% ± 1.1% for HTI membrane, and

reduced from 3.6% ± 0.6% to 0.3% ± 0.05% for GO\P-H membrane. Along with the elevation of oil concentration from 10 g/L to 100 g/L, the FRR_c using SDS as the washing solution is increased from 8.9% ± 1.1% to 16.5% ± 2.7% for HTI membrane, and increased from 0.3% ± 0.05% to 0.5% ± 0.1% for GO\P-H membrane. It's clear that the FRR_c under ultrahigh oil concentration of 100 g/L is negligible for GO\P-H membrane with SDS as washing chemical. This indicates that most of the oil-fouling is reversible when using GO\P-H membrane to separate oil-in-water emulsion through FO process.

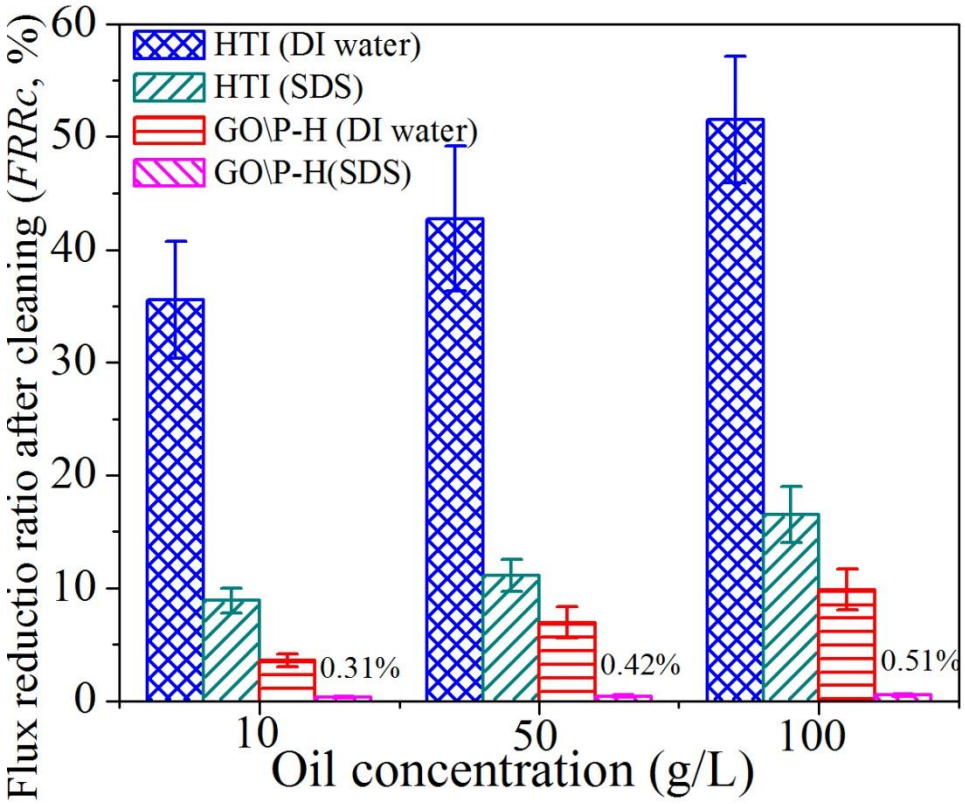

Figure 6.4 Flux reduction ratios (FRR_c) after DI water or SDS cleaning. Note that the pink columns, which refer to the FRR_c values of GO\P-H FO membrane after the cleaning using SDS aqueous solution, appear approximately invisible in the diagram. This is because their values are much smaller (< 0.6%) compared with other columns. Draw solution is 1.5 M Na_2SO_4 and feed solutions are surfactant-free oil-in-water emulsions. The concentration of SDS in its aqueous solution is 0.1 wt%.

On the contrary, 9% ~ 17% of J_W of HTI membrane remains lost even after washed by SDS aqueous solution, which indicates that HTI membrane suffers considerable irreversible fouling by oily pollutants when separating oil-in-water emulsion through FO process. Taking account of that the FRR_c is sufficiently low for GO\P-H FO membrane using merely DI water as the washing fluid, this study employs DI water

other than any harsh chemicals/detergents to clean membrane surface for the following investigations, in order to elongate membrane life and prevent any secondary pollution.

In short, almost all of the oil-fouling can be reversible for GO\P-H membrane while considerable part of the oil-fouling is irreversible for HTI membrane when separating oil-in-water emulsion through FO process after cleaning by SDS aqueous solution.

6.4. The mechanism on different membrane responses to oil-fouling

6.4.1. The relationship between oil-fouling and membrane wettability

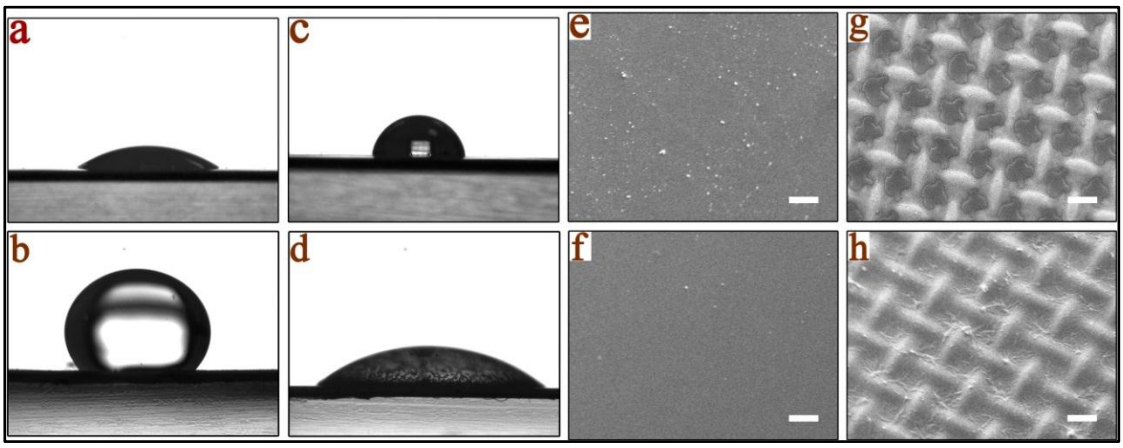

Figure 6.5 The relationship between oil-fouling of membrane and membrane's wettability. (**a**) Water contact angle and (**b**) underwater oil contact angle of GO\P-H FO membrane, respectively. (**c**) Water contact angle and (**d**) underwater oil contact angle of HTI FO membrane, respectively. (**e**) SEM image of GO\P-H membrane surface after oil-fouling test and (**f**) SEM image of GO\P-H membrane surface after *in-situ* cleaning by DI water, respectively (scale bar, 100 μm; the feed solution is surfactant-free emulsion with oil concentration of 25 g/L). (**g**) SEM image of HTI FO membrane surface after oil-fouling test and (**f**) SEM image of HTI membrane surface after *in-situ* cleaning by DI water, respectively (scale bar, 100 μm; the feed solution is surfactant-free emulsion with oil concentration of 25 g/L, which is exactly the same with that used for GO\P-H membrane). Please note in this thesis that all the contact angle data are recorded at the initial moment (0^{th} second) when the probe liquid fully wet solid surface, as briefed in Chapter 3.

The exceptional anti-fouling capability of GO\P-H FO membrane under various oil/water emulsions can be principally attributed to its superior surface wettability. GO\P-H membrane surface is highly hydrophilic and underwater oleophobic, with its water contact angle in air as low as $31 \pm 2.8°$ (Figure 6.5a) and its underwater oil contact angle as high as $141 \pm 4.3°$ (Figure 6.5b). This is because the hydrogel

selective layer undergoes hydration in aqueous environment and thus endows itself with strong oil-repellency that leads to high antifouling property (as depicted previously in Figure 6.1d). On the contrary, HTI membrane surface is weak in hydrophilicity and strong in underwater oleophilicity, with its water contact angle as high as $87 \pm 4.1°$ (Figure 6.5c) and its underwater oil contact angle as low as $35 \pm 5.7°$ (Figure 6.5d). The strong affinity of HTI membrane surface for oil induces the adsorption of oily pollutants from the feed solutions (oil-in-water emulsions) during FO separation process.

As the result of different surface wettability, GO\P-H membrane demonstrates distinct response to oil-fouling from HTI membrane when separating oil-in-water emulsion through FO process. In detail, only a small amount of oil aggregates is able to settle on GO\P-H membrane surface during "oil-fouling stage" (Figure 6.5e). The loose attachment between hydrogel selective layer and oily foulant renders most of these oil aggregates flushed away through *in-situ* washing even merely using DI water (Figure 6.5f). This is consistent with the high recovery of J_W (ultralow FRR_c) after *in-situ* cleaning for GO\P-H membrane as discussed previously in section 6.2.

On the contrary, the oil adsorbed from feed emulsion covers almost all the effective surface area of HTI membrane and further agglomerates into ~10 μm thick cake layer at the concave parts (Figure 6.5g), wherein the hydraulic flow is lacking in shear force to remove this oil cake. What's even worse, the strong adhesion of oily foulant to HTI membrane surface makes *in-situ* washing only able to extrude part of this cake layer and hence leave an oil film stuck on membrane surface (Figure 6.5h). This explains the poor restoration of water flux (high FRR_c) after *in-situ* washing for HTI FO membrane as aforementioned.

In short, high underwater oleophobicity of GO\P-H membrane surface leads to its low membrane fouling when separating oil-in-water emulsion through FO process.

6.4.2. The correlation between membrane fouling and oil droplet size distribution

6.4.2.1. The impacts of surfactant/oil ratio and oil concentration on oil droplet size distribution

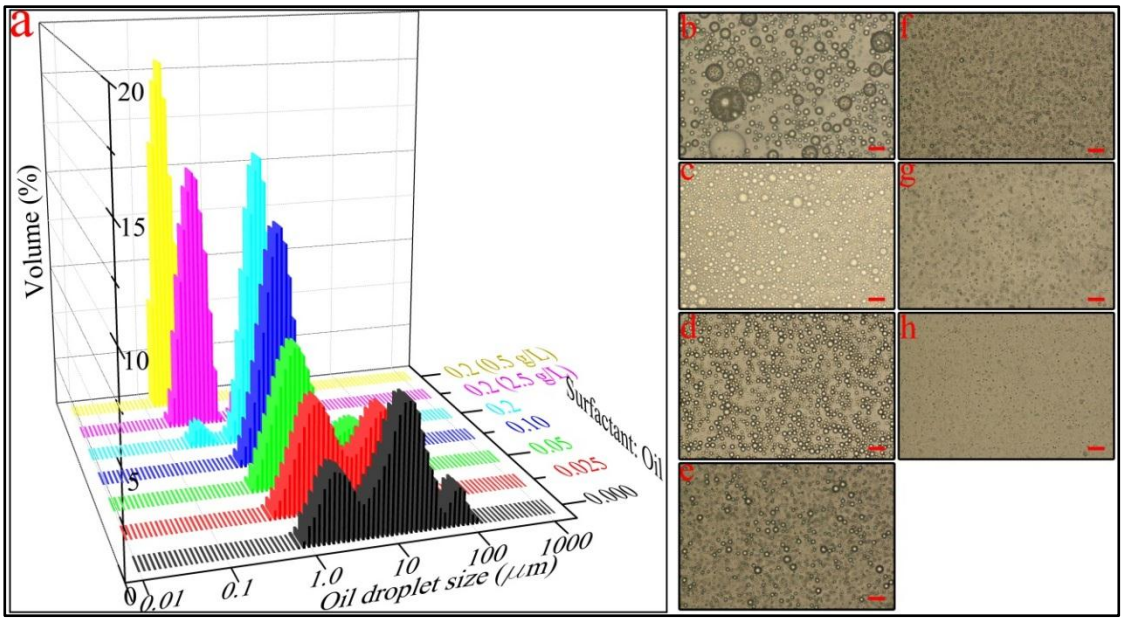

Figure 6.6 Oil droplet size distributions under different surfactant/oil ratios and different oil concentrations. (**a**) Dynamic light scattering (DLS) analysis results of oil droplet size distribution under different surfactant/oil ratios and oil concentrations. (**b**-**h**) Optical microscopic images of salinity-free oil-in-water emulsions (scale bar, 50 μm), wherein (**b**-**f**) oil concentration is 50 g/L and surfactant/oil ratios are (**b**) 0.000, (**c**) 0.025, (**d**) 0.05, (**e**) 0.1, (**f**) 0.2, respectively; (**g**-**h**) surfactant/oil ratio is 0.2 and oil concentrations are (**g**) 2.5 and (**h**) 0.5 g/L, respectively. The details of oil droplet size distributions are elaborated in Table 6.1.

Towards further understanding other factors that also influence membrane response to oil-fouling, dynamic light scattering (DLS) and optical microscope are used to examine oil droplet size distributions. In order to analyze particle (droplet) size distribution from the perspective of statistics, the parameter mass median diameter d_{50} that refers to the particle (oil droplet) diameter at the cumulative mass proportion of 50% is utilized here. This is because d_{50} can be regarded as the average particle size to represent the distribution in a simplified way.

Figure 6.6 presents the DLS and optical microscope characterization results for one specific kind of oil (vegetable oil), with the detailed peak assignments of their oil droplet size distributions listed in Table 6.1. These results elucidate that for the same kind of oil, oil droplet size distribution is determined by both surfactant/oil ratio and

oil concentration. The d_{50} of emulsion in oil concentration of 50 g/L is reduced from 10.5 μm to 2.55 μm along with the increase of surfactant/oil ratio from 0.00 to 0.05. However, the further increase of surfactant/oil ratio from 0.05 to 0.20 only reduces the d_{50} slightly from 2.55 μm to 1.76 μm. This indicates that it's not effective to control major size distribution of oil droplets below 1.0 μm only through increasing surfactant concentration, because the oil concentration is too high to avoid the agglomeration of submicrometer sized droplets. Therefore, submicrometer-sized emulsions are purposely prepared by reducing the oil concentration to 2.5 and 0.5 g/L while keeping surfactant/oil ratio as 0.2. As a result, the d_{50} is reduced to 0.41 μm for 2.5 g/L emulsion and 0.21 μm for 0.5 g/L emulsion, respectively.

Table 6.1 Details of oil droplet size distributions as shown in Figure 6.6

Surfactant/oil ratio	Oil concentration (g/L)	Peak positions on droplet size distribution	Optical Microscopy
0.000	50	a minor peak at 69.2 μm (volume 1.84%), a major peak at 13.2 μm (volume 6.04%), a minor peak at 1.93 μm (volume 3.30%).	Fig. 6.6b
0.025	50	a major peak at 15.1 μm (volume 4.59%), a major peak at 2.19 μm (volume 5.27%).	Fig. 6.6c
0.050	50	a minor peak at 11.5 μm (volume 2.70%), a major peak at 1.91 μm (volume 6.79%).	Fig. 6.6d
0.10	50	a major peak at 2.18 μm (volume 11.59%).	Fig. 6.6e
0.20	50	a major peak at 1.90 μm (volume 14.26%), a minor peak at 275 nm (volume 1.03%)	Fig. 6.6f
0.20	2.5	a minor peak at 1.90 μm (volume 1.6%), a major peak at 363 nm (volume 13.11%).	Fig. 6.6g
0.20	0.5	a main peak at 209 nm (volume 18.08%).	Fig. 6.6h

In short, the increase of surfactant/oil ratio can narrow oil droplet distribution towards smaller size, however, such effectiveness is limited within the scope of micrometer-sized emulsions; and to obtain the submicrometer-sized emulsions, oil concentration must be controlled under a reasonable level (*e.g.* ≤2.5 g/L in this study).

6.4.2.2. The impacts of different oil kinds on oil droplet size distribution

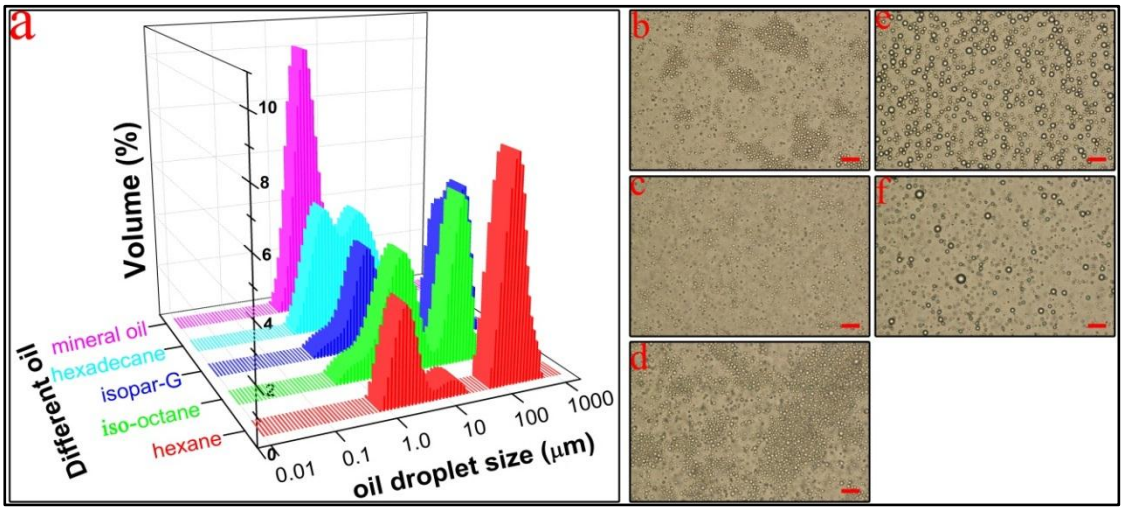

Figure 6.7 Oil droplet size distributions of different kinds of oil. (**a**) Dynamic light scattering (DLS) analysis results of oil droplet size distributions under different kinds of oil. (**b**-**f**) Optical microscopic images of salinity-free emulsions prepared from different kinds of oils (scale bar, 50 μm; oil concentration is 25 g/L and surfactant/oil ratios is 0.05), wherein (**b**) *n*-hexane, (**c**) iso-octane, (**d**) isopar-G, (**e**) *n*-hexadecane, and (**f**) mineral oil, respectively. The details of oil droplet size distributions are elaborated in Table 6.2.

Table 6.2 Details of oil droplet size distributions as shown in in Figure 6.7

Different oil	Oil concentration (Surfactant/oil ratio)	Peak positions on droplet size distribution	Optical Microscopy
n-hexane	25 g/L (0.05)	a major peak at 138.0 μm (volume 7.89%), a minor peak at 11.48 μm (volume 0.60%), a major peak at 1.91 μm (volume 3.44%).	Fig. 6.7b
Iso-octane (Trimethylpentane)	25 g/L (0.05)	a major peak at 69.2 μm (volume 5.98%), a major peak at 5.75 μm (volume 4.27%).	Fig. 6.7c
Isopar-G	25 g/L (0.05)	a major peak at 316 μm (volume 5.57%) a major peak at 158 μm (volume 4.91%), a major peak at 4.37 μm (volume 3.75%).	Fig. 6.7d
n-hexadecane	25 g/L (0.05)	a major peak at 10.0 μm (volume 4.35%), a major peak at 2.19 μm (volume 4.63%).	Fig. 6.7e
Mineral oil	25 g/L (0.05)	a major peak at 2.51 μm (volume 10.80%).	Fig. 6.7f

Figure 6.7 exhibits the DLS and optical microscope characterization results for different kinds of petroleum oil, with the detailed peak assignments of their oil droplet size distributions enumerated in Table 6.2. These results exhibit that among different

petroleum oils, most droplets of iso-octane (Figure 6.7c), hexadecane (Figure 6.7e) and mineral oil (Figure 6.7f) remain detached in single droplet form with their sizes ranged from 2 ~ 10 μm. However, the oil droplets of hexane (Figure 6.7b) and isopar-G (Figure 6.7d) cohere into macroaggregates as large as 100~500 μm. As a result, the d_{50} values are 2.3 μm for mineral oil, 5.0 μm for *n*-hexadecane, and 11.8 μm for iso-octane, respectively; while for the macroaggregate formed emulsion, the d_{50} values are relatively much bigger: 103.5 μm for *n*-hexane and 122.7 μm for isopar-G. In short, there exist considerable differences in terms of oil droplet size distribution among the emulsions prepared from different kinds of petroleum oil.

6.4.2.3. Correlating oil droplet size distribution with membrane fouling mathematically

Based upon these characterization results on oil droplet size distribution, mathematical fittings between oil droplet size distribution in terms of d_{50} and the FO fouling extent in terms of FRR_f are systematically analyzed for both GO\P-H and HTI FO membranes under different scenarios, with the important results displayed in Figure 6.8.

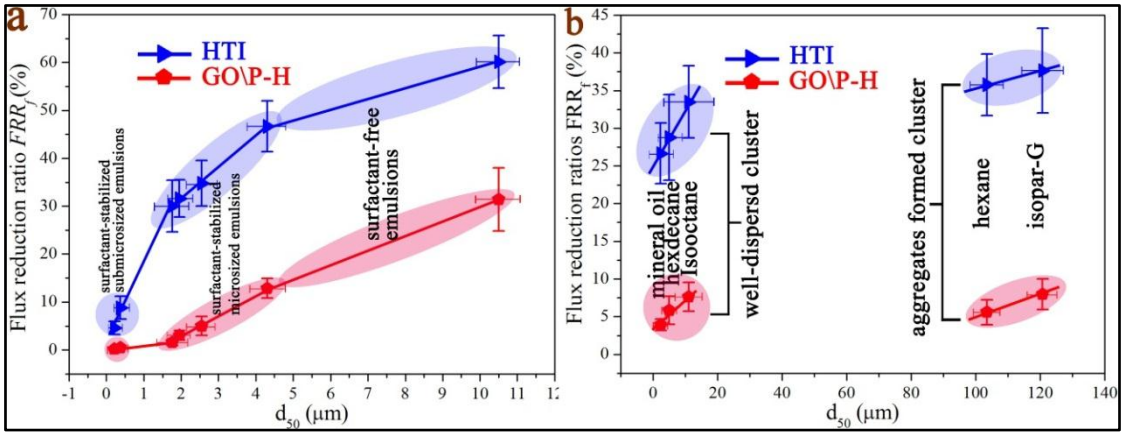

Figure 6.8 The correlations between oil-fouling of membrane and oil droplet size distribution. (**a**) Water flux reduction ratio (FRR_f) as a function of average oil droplet size (d_{50}) for the same kind of oil (The oil is vegetable oil). (**b**) Water flux reduction ratio (FRR_f) as a function of average oil droplet size (d_{50}) under different kinds of petroleum oil (The oil concentration is 25 g/L and the surfactant/oil ratio is 0.05).

The data points on Figure 6.8a can be grouped into three clusters, which refer to surfactant-free emulsions, surfactant-stabilized microsized emulsions and surfactant-stabilized submicrosized emulsions, respectively. Two points need to be emphasized here. Firstly, for both GO\P-H and HTI FO membranes, the bigger d_{50} of

emulsion, the heavier FO fouling will be. This is because oil droplet in bigger size has larger surface area and hence enhances the attraction force by membrane surface towards the droplet (the membrane surface can be considered as a relative infinite 2D plane for oil droplet). Particularly, as the d_{50} controlled below 1 μm, the FRR_f of HTI FO membrane is reduced as low as 4.6% ± 1.4% ~ 8.8% ± 2.3% while the FRR_f of GO\P-H FO membrane is almost negligible (< 0.5% ± 0.07%). These results indicate that the split of oil droplets into smaller sizes may serve as an optional approach to mitigate membrane fouling when separating oil-in-water emulsions through FO process. Interestingly, the lowest fouling can be attained through controlling oil droplets under submicrometer-sized, though it is very difficult to do so especially under high oil concentration. Secondly and more importantly, it's found that strong linear correlation existing between d_{50} and FRR_f within each data group separately. However, the slope of linear fitting in each data group cannot be extrapolated to another group. Furthermore, the FRR_f-d_{50} curve slope of HTI membrane changes in much greater extents from one data group to the next group, compared with that of GO\P-H membrane. This indicates that the fouling of underwater oleophilic membrane (*e.g.* HTI membrane) is highly dependent on oil droplet size distribution and thus HTI membrane is more susceptible to oil droplet in larger size.

Meanwhile, Figure 6.8b demonstrates that for different kinds of petroleum oil, the data points of FRR_f can be grouped into two clusters based on the dispersibility of oil. One is named as "well-dispersed cluster", which refers to the emulsion prepared from mineral oil, *n*-hexadecane, and iso-octane. The other is named as "aggregates formed cluster", which refers to the emulsion prepared from isopar-G and hexane. Within each cluster, linear correlation between FRR_f and d_{50} is established for both GO\P-H and HTI FO membranes. However, regarding the correlation throughout the two clusters, HTI membrane and GO\P-H membrane exhibits different trends. Interestingly, the FRR_f of HTI FO membrane establishes the order as: isopar-G > hexane > iso-octane (2,2,4-trimethylpentane) > hexadecane > mineral oil, which is basically in conformity with the order of d_{50}. However, such conformity does not exist for GO\P-H membrane. For example, iso-octane (2,2,4-trimethylpentane) belongs to "well-dispersed" cluster because its oil droplets remains detached without aggregation in emulsion. But the FRR_f of iso-octane for GO\P-H membrane approaches or even exceeds those values

belongs to "aggregates formed cluster". These results imply that the factors other than physical size of oil droplet (*e.g.* chemical affinity between oil and surface as aforementioned in section 6.3.1) may also play significant roles in membrane fouling.

In short, mathematical fitting between d_{50} and FRR_f reveals the positive correlation between oil droplet size and membrane fouling during the separation of oil-in-water emulsion through FO process for one kind of oil. The differences in the trend of FRR_f under different oil kinds between GO\P-H and HTI membranes indicate that the factors other than oil droplet size could also influence membrane fouling.

6.5. Simultaneous desalination and oil/water separation

6.5.1. Effect of salinity on FO water flux (J_W) and membrane fouling (FRR_f)

In order to prepare highly saline and oily wastewater (here simulated shale gas wastewater) as FO feed solution, inorganic salts of different electrovalences namely NaCl, $MgSO_4$ and $Al_2(SO_4)_3$ are included in the hexadecane-in-water emulsions with total dissolved salts (TDS) ranged from 0 g L^{-1} to 260 g L^{-1} while oil concentration and surfactant/oil ratio fixed as 25 g/L and 0.05, respectively. Simultaneous desalination and oil/water separation by GO\P-H, P-H and HTI membranes are systematically investigated through FO process with 1.5 M Na_2SO_4 employed as draw solution. The important results are presented in Figure 6.9 ~ Figure 6.13 and Table 6.3.

Generally, GO\P-H membrane can achieve more than three times higher FO water flux (J_W) compared with HTI membrane when investigated with simulated shale gas wastewater. The solid lines on Figure 6.9a demonstrates that along with the increase in TDS of hexadecane-in-water emulsion from 0 g L^{-1} to 260 g L^{-1}, FO J_W values are lowered down almost linearly due to the diminution of osmotic driving force (the osmotic gradient between the bulk of feed solution and draw solution is decreased). As a result, the J_W is reduced from 30.5 $\pm$ 3.9 L m^{-2} h^{-1} to 3.5 $\pm$ 0.4 L m^{-2} h^{-1} for GO\P-H membrane, from 16.7 $\pm$ 2.0 L m^{-2} h^{-1} to 1.9 $\pm$ 0.3 L m^{-2} h^{-1} for P-H membrane, and from 7.4 $\pm$ 0.8 L m^{-2} h^{-1} to 0.6 $\pm$ 0.1 L m^{-2} h^{-1} for HTI membrane, respectively.

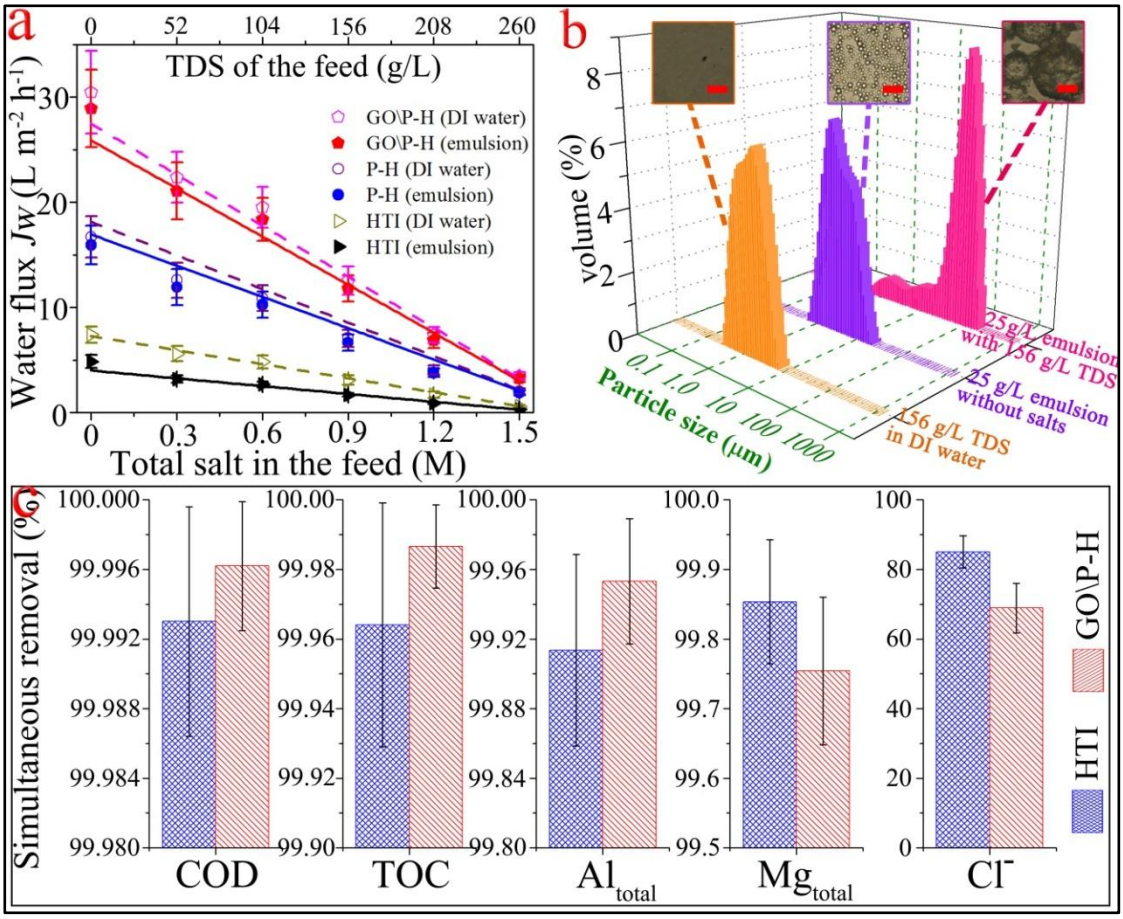

Figure 6.9 The study on simultaneously desalting and deoilling highly saline and oily wastewater (simulated shale gas wastewater). (**a**) Water flux of GO\P-H, P-H and HTI FO membranes as a function of salinity in feed solution (Draw solution is 1.5 M Na_2SO_4. Dotted lines represent the studies without oil, while solid lines represent the studies with surfactant-stabilized hexadecane-in-water emulsions). (**b**) Salt/oil particle size distributions in different feed solutions, wherein the peak observed for 156 g/L TDS in DI water is mainly ascribed to the colloids formed by $Al_2(SO_4)_3$. The inset figures are optical microscopic images of different feed solutions, scale bar, 50 μm. (**c**) Simultaneous removals of oil and salts from shale gas wastewater by GO\P-H and HTI FO membranes. Feed solution is hexadecane-in-water emulsion with 25 g/L oil concentration, 0.05 surfactant/oil ratio and 156 g/L total dissolved salinity (TDS). Draw solution is 1.5 M Na_2SO_4. Note the calculation of removal by FO process should consider the dilution of permeate in draw solution, as carried out in this thesis.

More importantly, at any particular TDS compared with HTI membrane, as-synthesized hydrogel FO membranes are smaller in the absolute value of J_W loss resulted from oil-fouling, which can be represented by the vertical distance between dash line and solid line of each membrane on Figure 6.9a. Because the J_W value of GO\P-H FO membrane fed by oil-free saline solution (*i.e.* baseline test as indicated by the dashed line on Figure 6.9a) is more than four times as high as that of HTI membrane, the FRR_f of GO\P-H FO membrane fed by the salinity-existed emulsions

should be smaller than one fourth as that of HTI membrane. This means that GO\P-H membrane maintains its remarkable antifouling advantage over HTI membrane despite the existence of salinity in emulsions.

The even severer fouling of HTI membrane during the treatment of shale gas wastewater can be attributed to two reasons. One reason is that salinity-induced agglomeration of oil droplets aggravates the fouling extent for underwater oleophilic surface. In reality, shale gas wastewater usually contains high concentrations of scale-forming constituents (Kargbo *et al.*, 2010), which can develop into colloids or precipitates (*e.g.* multi-valent cations like $Al_2(SO_4)_3$ can form colloids as indicated by the DLS peak observed for 156 g/L TDS in DI water on Figure 6.9b) and further trigger the aggregation of oil droplets. Correspondingly, both DLS and optical microscopy results confirm that the average oil droplet size (d_{50}) is increased from 3.0 μm to 67.3 μm as TDS of emulsion increased from 0 g L^{-1}L to 156 g L^{-1} (Figure 6.9b). Consequently, underwater oleophilic membrane *e.g.* HTI FO membrane suffers even severer loss of water permeability at higher feed salinity because it is more susceptible to oil droplet in larger size as revealed in section 6.3.3. The other reason can be cake enhanced osmotic pressure (CEOP) (Lee *et al.*, 2010a) arisen from the synergistic effect between salts and oil-fouling in feed solution on the surface of underwater oleophilic membrane (*e.g.* HTI membrane). In detail, on HTI membrane surface micrometer sized oil droplets can agglomerate through adsorption and further grow into a cake layer as thick as ~10 μm (as previously shown in Figure 6.5g). The diffusions of salt ions within as-built oil cake layer are significantly hindered. Therefore, in the feed side the TDS is accumulated to a much higher level at membrane surface than that of solution bulk, which dramatically undermines the effective osmotic driving force across HTI membrane. As a result, HTI membrane suffers heavier loss of J_W compared with salinity-free emulsion at the same oil concentration and surfactant/oil ratio.

On the contrary, for GO\P-H FO membrane the FRR_f of shale gas wastewater (7.9% ± 1.3%) is slightly higher than that of salinity-free emulsion (6.1% ± 1.0%) at the same oil concentration and surfactant/oil ratio. This indicates that superior antifouling

property of as-synthesized hydrogel selective layer is robust even under oil-in-water emulsions of high salinity.

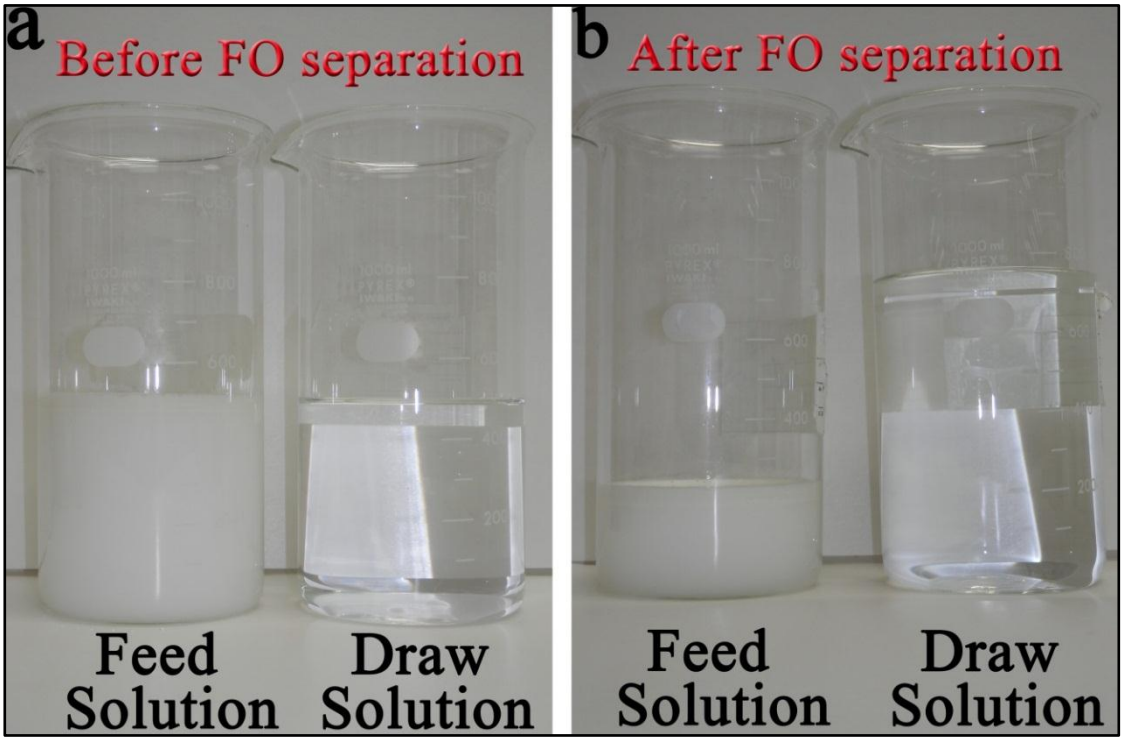

Figure 6.10 Optical photographs of feed and draw solutions for simultaneously desalting and deoilling shale gas wastewater by GO\P-H FO membrane. Draw solution is 1.5 M Na_2SO_4. Feed solution is surfactant-stabilized hexadecane-in-water emulsion with 25 g/L oil concentration, 0.05 surfactant/oil ratio and 156 g/L TDS, which is used as simulated shale gas wastewater. (a) Before the "oil-fouling stage" of FO running. (b) At the end of "oil-fouling stage" of FO running.

Furthermore, clean water can be obtained as a result of simultaneously desalting and deoilling shale gas wastewater by GO\P-H membrane through FO process, as displayed in Figure 6.10. Table 6.3 exemplifies water quality analysis results of both feed and draw solutions at the end of "oil-fouling stage", based upon which simultaneous removals of oil and ions by FO process are calculated according to equation 3.10 and shown in Figure 6.9c. Both GO\P-H and HTI FO membranes can reach >99.99% removal of COD and >99.9% removal of TOC, indicating all organic pollutants including both oil and surfactant in simulated shale gas wastewater are rejected. More importantly, GO\P-H membrane outperforms HTI membrane in oil removal, which is mainly attributed to the strong underwater oil-repellency of as-synthesized hydrogel selective layer. Simultaneously, GO\P-H FO membrane also demonstrates ~99.95% removal of total Al and ~99.75% removal of total Mg, which is

slightly higher than or comparable to that of HTI membrane, respectively. In addition, GO\P-H membrane can achieve ~70% removal of Cl^-. Though the removal of monovalent ions of GO\P-H membrane is lower than that of HTI membrane (~85% removal of Cl^-), this result confirms that chemically-crosslinked hydrogel selective layer (at *TCLD* of 30% here) is able to reach NF to RO selectivity.

In short, GO\P-H membrane demonstrates the advantage of high water flux and low membrane fouling over HTI membrane when simultaneously desalting and deoilling oil-in-water emulsion of high salinity through FO process.

Table 6.3 Water quality analysis results of feed and draw solutions at the end of "oil-fouling stage" (400th min) for the treatment of simulated shale gas wastewater

Parameter	HTI feed solution	HTI draw solution	GO\P-H feed solution	GO\P-H draw solution
COD (mg/L)	75,502 ± 4,314	0.5 ± 0.2	120,236 ± 6,010	0.5 ± 0.1
TOC (mg/L)	9,419 ± 566	0.30 ± 0.05	15,283 ± 928	0.18 ± 0.04
$(Al^{3+})_{total}$ (mg/L)	16,814 ± 2,068	0.53 ± 0.06	20,335 ± 2,745	1.02 ± 0.14
$(Mg^{2+})_{total}$ (mg/L)	7,853 ± 709	0.88 ± 0.13	9,033 ± 838	3.75 ± 0.53
Cl^- (mg/L)	10,973 ± 924	75.5 ± 9.1	12,590 ± 1,217	516 ± 42
Turbidity (NTU)	>99,999	0.125 ± 0.02	>99,999	0.130 ± 0.015
Color (hazen)	1,780 ± 43	0.000	2,135 ± 65	0.000
Conductivity(mS/cm)	54.5 ± 1.3	117.3 ± 1.1	57.8 ± 1.4	112.5 ± 2.5
Temperature (℃)	23.5 ± 0.3	23.5 ± 0.3	23.5 ± 0.3	23.5 ± 0.3

Note: Draw solution is 1.5 M Na_2SO_4. Feed solution is surfactant-stabilized hexadecane-in-water emulsion with 25 g/L oil concentration, 0.05 surfactant/oil ratio and 156 g/L TDS, which is used as simulated shale gas wastewater. Because GO\P-H membrane achieves much higher water recovery than HTI membrane at the given operation time (*e.g.* 360 min), the concentration of pollutant in the draw solution confronted by GO\P-H FO membrane is higher than that confronted by HTI FO membrane at the end of "oil-fouling" stage.

6.5.2. Comparison on *Jw*-time curve

In order to further understand how the existence of salts in emulsion complicates membrane fouling, J_W - time functions under both salinity-free emulsions (including surfactant-free emulsion as well as surfactant-stabilized emulsion) and simulated shale gas wastewater are systematically compared.

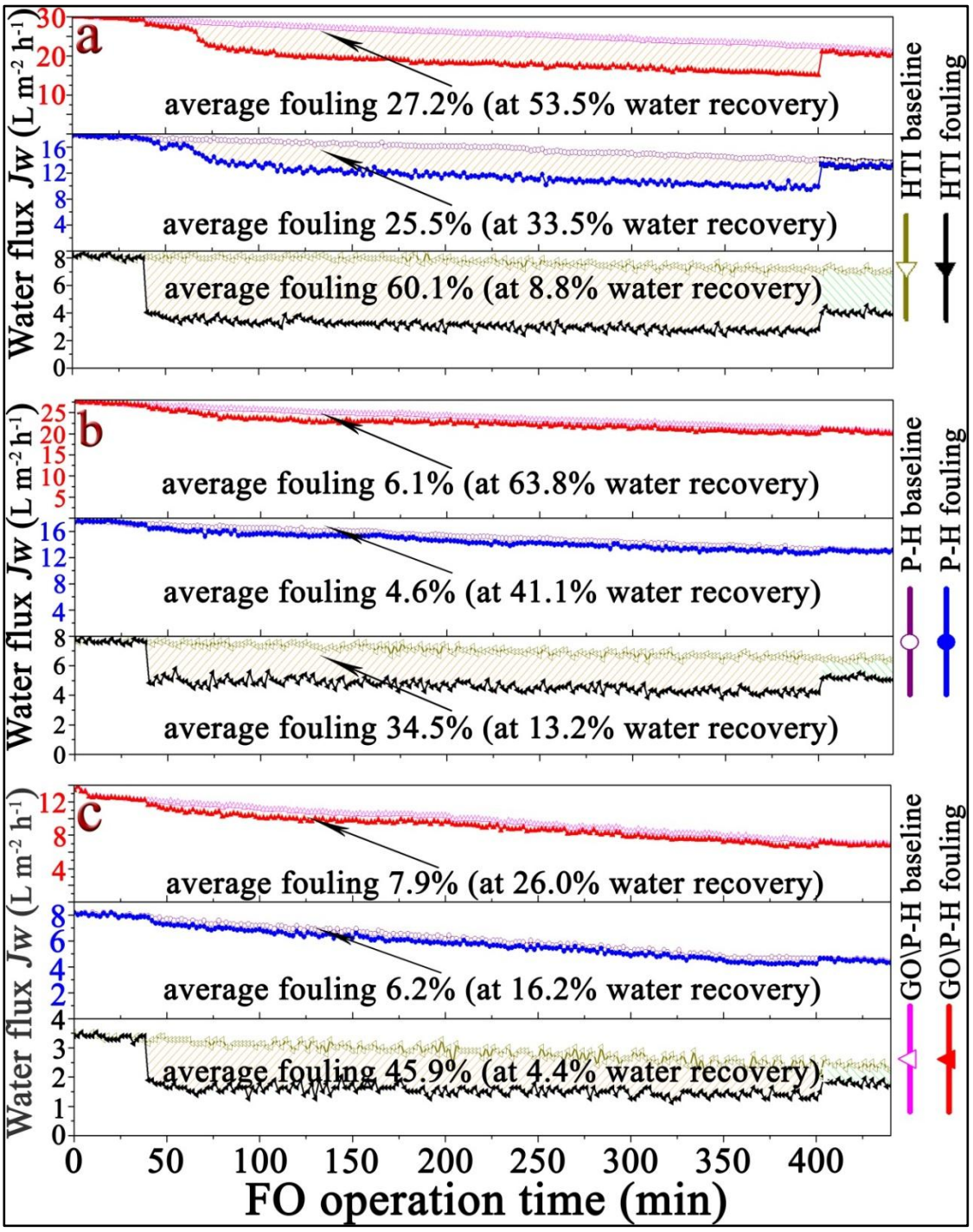

Figure 6.11 Systematic investigations on J_W - time functions under salinity-free emulsions and shale gas wastewater. Draw solution is 1.5 M Na_2SO_4. (a) Feed solution is DI water for "baseline running", while surfactant-free 25 g/L hexadecane-in-water emulsion with 0 g/L TDS for "fouling running". (b) Feed solution is DI water for "baseline running", while surfactant-stabilized 25 g/L hexadecane-in-water emulsion with 0.05 surfactant/oil ratio and 0 g/L TDS for "fouling running". (c) Feed solution is 156 g/L TDS in DI water for "baseline running", while surfactant-stabilized 25 g/L hexadecane-in-water emulsion with 0.05 surfactant/oil ratio and 156 g/L TDS for "fouling running", which is designed as shale gas wastewater. The shadow area indicates *FRR*.

Figure 6.11 exemplifies typical J_W – time curves under various oil-in-water emulsions for GO\P-H, P-H and HTI FO membranes for the comparison. Four points need to be highlighted here. Firstly, the decrease slope in J_W curves during the "baseline running" fed by saline aqueous solution (*e.g.* 156 g L^{-1} TDS, Figure 6.11c) is much steeper than that fed by DI water (Figure 6.11a, b) for all the three FO membranes. This is because as water molecules permeate through FO membrane from feed solution to draw solution, the water volume is decreased in feed solution while increased in draw solution (batch-type test mode employed here). As a result, the draw solution becomes less concentrated due to this osmotic dilution. This is the main contributor to the decrease of J_W value along with operation time during the "baseline running" fed by DI water. However, as feed solution also contains inorganic salts especially in a considerable level as demonstrated in Figure 6.11c, water permeation leads to the osmotic concentration of feed solution. And this osmotic concentration of feed solution accelerates the decrease in osmotic gradient between feed and draw solution bulks (apparent osmotic driving force). As a result, the J_W value of "base running" fed by saline aqueous solution will take a steeper decrease for all the three FO membranes.

Secondly, when comparing the J_W – time curve of "fouling running" among the three FO membranes, it's evident that HTI membrane suffers a sudden drop of J_W by 35%~60% once being fed with oil-in-water emulsions (within the first 10 min of "oil-fouling stage"), indicating its underwater oleophilic property. In contrast, the J_W values of as-synthesized hydrogel FO membranes (both P-H and GO\P-H FO membranes) take a ~45 min slow decline at much smaller rates before reaching stabilization, disclosing their superior anti-fouling capabilities.

Thirdly, under each kind of feed emulsion, the FRR_f of GO\P-H FO membrane is slightly higher than that of P-H FO membrane. For example, when using salinity-free hexadecane-in-water emulsion (25 g L^{-1} oil concentration and 0.05 surfactant/oil ratio) as feed solution, the FRR_f is 6.1% for GO\P-H membrane while 4.6% for P-H membrane. When using hypersaline hexadecane-in-water emulsion (25 g L^{-1} oil concentration, 0.05 surfactant/oil ratio and 156 g L^{-1} TDS) as feed solution, the FRR_f is 7.9% for GO\P-H membrane while 6.2% for P-H membrane. The relatively higher

FRR_f encountered by GO\P-H membrane is probably because the incorporation of GO nanosheets shapes the topography of support layer to be rougher and thus slightly increase the surface roughness of subsequently coated hydrogel selective layer (as aforementioned in section 5.8.1 of Chapter 5). However, it's worthy to emphasize that because the J_W in 'baseline running' of GO\P-H membrane is remarkably higher than that of P-H membrane owing to the GO induced transformation of support layer pore structure from 1D to 3D, the absolute J_W value in 'fouling running' of GO\P-H membrane is more than 60% higher than that of P-H membrane.

Fourthly and most importantly, the water recovery follows the trend of GO/P-H membrane > P-H membrane > HTI membrane. The superiority in high water recovery for as-synthesized hydrogel FO membranes is ascribed to their much higher water fluxes and better antifouling capabilities compared with HTI membrane.

In short, the advantage in high water flux and high water recovery of GO\P-H membrane when separating various oil-in-water emulsions have been demonstrated with typical *Jw* - time function in fullest detail.

6.5.3. Long term operation figure

For the purpose of verifying the stability of GO/P-H membrane's advantage in high water flux over HTI membrane during simultaneous desalination and oil/water separation through FO process, relatively long term operation results of 20 FO cycles are compared in Figure 6.12.

As shown by the red line on Figure 6.12, GO\P-H membrane is able to maintain the high J_W during long term operation with its FRR_f ranged from 6.3% to 10.3%. More importantly, the FRR_c values of GO\P-H membrane remain smaller than 1.3% after 20 FO cycles' operation. Therefore, almost all the J_W loss during fouling stage is recovered by *in situ* DI water cleaning and thus the J_W is maintained at high level throughout long term separation.

On the contrary, as shown by the blue line on Figure 6.12, HTI membrane suffers much severer loss in J_W at each "oil-fouling stage", with its FRR_f gradually increased

from 45.9% ~ 61.6% along with operation time. What's even worse, the oil-fouling of HTI membrane that cannot be reversible by *in-situ* DI water cleaning is aggravated along with the increase in FO cycle number. Noteworthily, an evident decrease of normalized water flux from 67.5% to 60.0% in "post-cleaning stage" has been observed in 11^{th} ~ 20^{th} FO cycles. This is possibly because more amount of oil-foulants are left stuck on HTI membrane surface along with operation time in spite of the routine cleaning in each FO cycle. Taking account of that HTI membrane is outclassed by GO\P-H membrane in both water flux and antifouling capability, these results reveal GO\P-H membrane's overwhelming advantage over HTI membrane in the economic feasibility for long term operation.

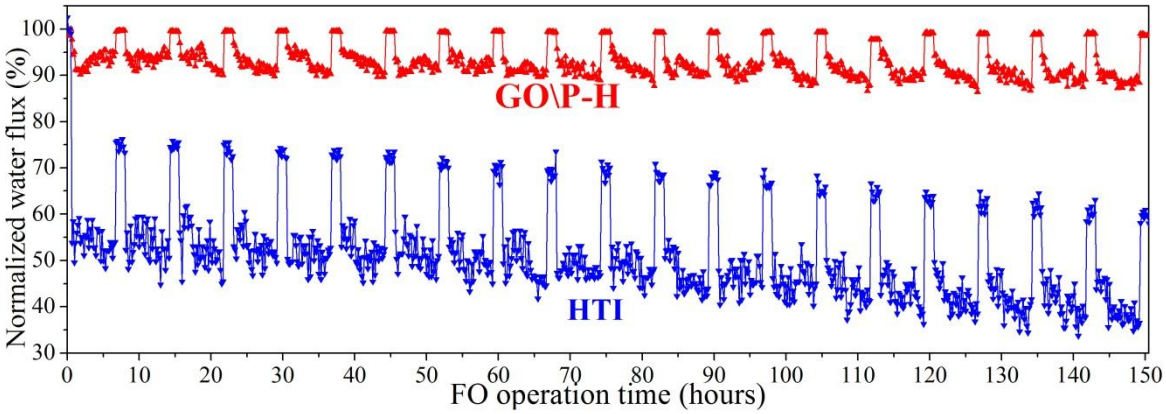

Figure 6.12 Long term FO operation results of synthesized GO\P-H and commercial HTI membranes. Draw solution is 1.5 M Na_2SO_4. Feed solution is surfactant-stabilized hexadecane-in-water emulsion with 25 g/L oil concentration, 0.05 surfactant/oil ratio and 156 g/L TDS, which is used as simulated shale gas wastewater. At the beginning of each FO cycle, new batches of feed and draws solutes are employed.

In short, long term FO separation results confirm that GO\P-H membrane's superior antifouling capability is durable.

6.6. Critical discussions on simultaneous desalination and oil/water separation

6.6.1. Critical discussion on the water recovery of hypersaline oil/water emulsions

As exemplified in Figure 6.11, the water recovery fed by shale gas wastewater is considerably lower than that fed by salinity-free emulsion at the same oil concentration and surfactant/oil ratio for all the three membranes. This is because hypersaline emulsions (*e.g.* shale gas wastewater) contain not only high contents of oils but also high concentrations of salts. For example, the total dissolved salts (TDS) concentration

of shale gas wastewater can be higher than that of seawater (Gregory *et al.*, 2011). It is the high salt concentration that makes the achievement of high water recovery to be very challenging for the treatment of highly saline and oily wastewater.

In this chapter, as-synthesized GO\P-H nanocomposite membrane has delivered on the promise to address this issue. 45% ± 4.8% water recovery has been attained by GO\P-H FO membrane before reaching osmotic balance between feed and draw solutions (feed solution is 25 g/L hexadecane-in-water emulsion with 0.05 surfactant/oil ratio and 156 g/L TDS; draw solution is 1.5 M Na_2SO_4). And the theoretically maximum water recovery is estimated to be 60%~70% under batch-type operation mode utilized here.

Moreover, water recovery is interlinked with many other factors including membrane fouling, salt rejection, energy cost, discharge options and so on in salt-rejecting membrane processes. In practical application, membrane desalination processes are often operated at the water recovery lower than the theoretically maximum value for system optimization purpose. Taking seawater RO desalination as a comparison, excessively high water recovery would cause many unfavorable results including uneconomical energy input, aggravated membrane fouling, poor salt rejection *etc*. Therefore, ~50% water recovery is usually employed in practical seawater RO desalination based upon optimum configuration in energy design (Greenlee *et al.*, 2009). This is the rationale why the water recovery (~45%) achieved by GO\P-H membrane during the treatment of shale gas wastewater with TDS higher than seawater is already good for practical application. In addition, even higher water recovery can be attained through combing this FO process with a downstream draw solute reconcentration process or using more concentrated draw solution (e.g. 2~5 M $MgCl_2$), for theoretically maximum water recovery is elevated owing to the increase in the osmotic gradient between draw and feed solution bulks.

6.6.2. Breaking the technical shackles on membrane separation of hypersaline oil/water emulsions

The major technical shackle on the implementation of membrane technology to treat hypersaline oil/water emulsions (*e.g.* shale gas wastewater) is the lack of a membrane

that can simultaneously have two functions: oil-repellency and salt-rejection. Conventional salt-rejecting membranes (such as polyamide RO and FO membrane) are hydrophobic (oleophilic), which results in severe membrane fouling during oil/water separation. This study reveals that certain crosslinked hydrogels can serve as the bifunctional selective layer that possesses both oil-repelling and salt-rejecting properties. On one hand, the upmost surface of the hydrogel selective layer undergoes hydration in water and bonds water molecules tightly to create an ultrathin water barrier. And this water barrier can repel oil adhesion because of dehydration entropic effect (Chen *et al.*, 2010; Magin *et al.*, 2010) and thus lead to low membrane fouling. More interestingly, as-synthesized hydrogel FO membranes exhibit robust resistance to salinity-induced fouling aggravation under hypersaline oil/water emulsions. On the other hand, the hydrogel polymer chains can be bridged through covalent-bonded chemical crosslinking. As a result, the synthesized hydrogel FO membranes also possess high rejections of inorganic ions as well as emulsified oil droplets.

Besides, the incorporation of GO nanosheets plays a crucial role to enhance water flux of as-synthesized hydrogel FO membrane through transforming the pore structure of support layer from 1D connected to 3D interconnected. As-demonstrated high water flux is essential to make this new FO membrane economically feasible for the practical treatment of hypersaline oil/water emulsions.

In short, as illustrated in Figure 6.13, GO\P-H FO membrane is capable of simultaneously desalting and deoilling hypersaline oil-in-water emulsion (*e.g.* shale gas wastewater) with its hydrogel selective layer rejecting all organic pollutants and most inorganic ions at low membrane fouling and its micrometer scale 3D interconnected porous support layer enabling forward transportation of water molecules at high flux.

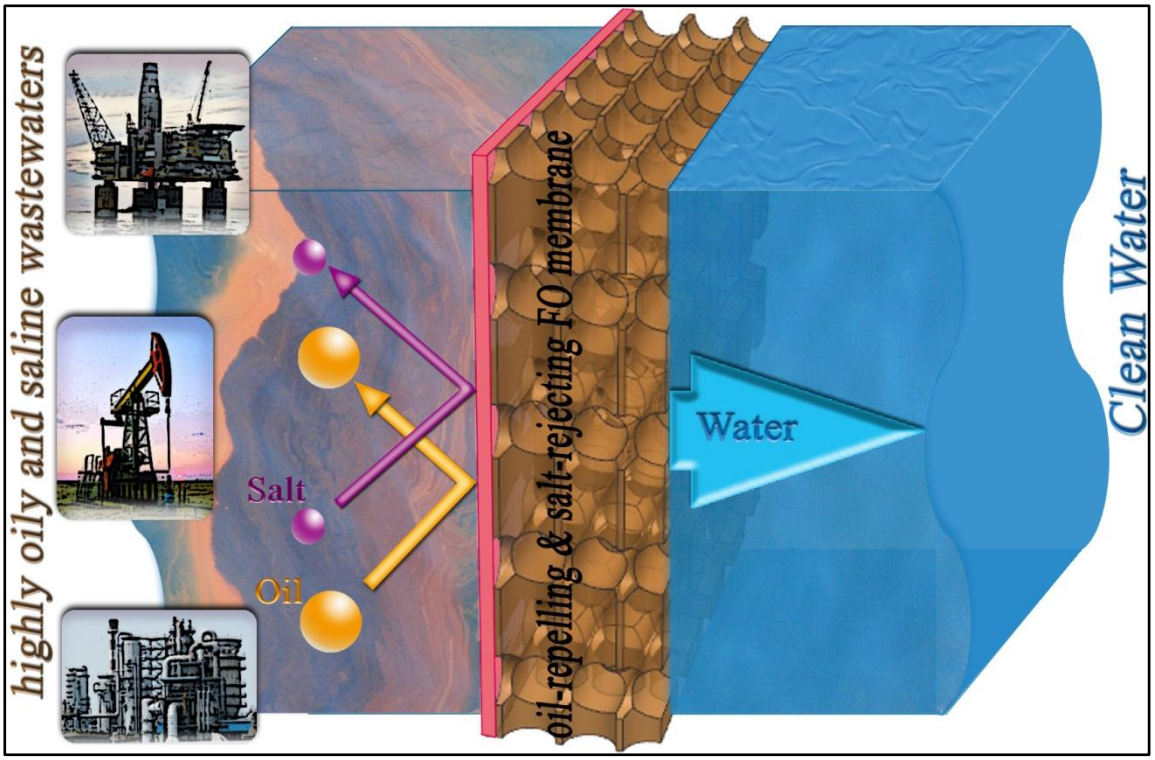

Figure 6.13 Illustration of simultaneous oil/water separation and desalination by GO/P-H FO membrane. The hydrogel selective layer of GO\P-H FO membrane (The pink colored ultrathin layer) can simultaneously reject salt ions with high selectivity owing to its crosslinked molecular structure and resist oil-fouling (low fouling) owning to its high underwater oleophobicity. Besides, the GO induced 3D pore interconnected support layer (brown colored layer) ensures GO\P-H FO membrane to achieve high water flux.

6.7. Summary

In summary, it is the first time to report a new membrane technology *i.e.* simultaneous desalination and oil/water separation purposely for the treatment of highly saline and oily wastewater. Here, a new nanocomposite membrane (GO\P-H membrane) is designed and synthesized to realize this special technology and investigated with hypersaline oil-in-water emulsions (*e.g.* shale gas wastewater) as feed solution. Important outcomes are highlighted as follows.

Firstly, systematic investigations with diverse salinity-free oil-in-water emulsions as FO feed solution have verified that as-synthesized GO\P-H FO membrane possesses remarkably superior antifouling capability over commercially available HTI FO membrane, with the water flux reduction ratio during "fouling stage" (FRR_f) of GO\P-H membrane > 40% lower than that of HTI membrane under all emulsions tested. Particularly, the employment of surfactant to stabilize emulsion (surfactant/oil

ratio ≥ 0.05) strengthens such antifouling advantage with the FRR_f of GO\P-H membrane reduced to < 5% while the FRR_f of HTI membrane remained as high as ~35%. In addition, fed by surfactant-stabilized emulsion, most of the oil-fouling can be reversible for GO\P-H membrane through *in-situ* washing even merely with DI water while 15%~30% loss of water flux (J_W) cannot be recovered for HTI membrane through the identical cleaning method.

Secondly, the mechanisms on distinct membrane responses to oil-fouling during FO process have been explored among as-synthesized hydrogel membranes (including P-H membrane and GO\P-H membrane) and HTI membrane. Based upon the fouling extents of hydrogel FO membranes considerably lower than that of HTI membrane, it's concluded that the surface wettability of membrane plays the dominant role in controlling FO fouling: the high underwater oleophobicity of as-synthesized hydrogel selective layers leads to their strong anti-oil-fouling capabilities. And based upon the fouling extent of P-H membrane always slightly lower than that of GO\P-H membrane, it's concluded that the smoother topography of membrane helps to further diminish FO fouling under similar surface wettability.

Thirdly, mathematical fittings on the correlation between FO fouling and oil droplet size distribution of emulsion has revealed that for emulsion made of the same oil kind, underwater oleophilic membrane *i.e.* HTI membrane is more dependent on oil droplet size distribution and suffers severer fouling along with the increase in average droplet size (d_{50}), while underwater oleophobic membrane *e.g.* GO\P-H membrane are more independent. In addition, the tentative correlation between FO fouling and oil droplet size distribution among emulsions made of different oil kinds has confirmed that membrane fouling is a complex result of factors more than the physical size of oil droplet.

Fourthly and most importantly, as-synthesized hydrogel membranes have been investigated with highly saline and oily wastewaters (simulated shale gas wastewaters) to examine its ability to separate salinity-containing oil-in-water emulsion. FO separation results show that GO\P-H membrane can simultaneously desalt and deoil hypersaline oil-in-water emulsion with more than three times higher water flux, higher

removal efficiencies for oil and salts (>99.9% for oil and >99.7% for multivalent ions), and significantly lower membrane fouling (>80% lower FRR_f) compared with HTI membrane. Furthermore, long term operation results demonstrate the overwhelmingly superior antifouling durability and better resistance to salinity induced fouling aggravation of GO\P-H membrane over HTI membrane.

Finally, these results point out a new direction for the design and synthesis of membrane to treat challenging wastewater (*e.g.* highly saline and oily wastewater) through FO process. More importantly, the final goal of this thesis *i.e.* the development of membrane's ability to address the treatment of highly saline and oily wastewater has been eventually accomplished by as-synthesized GO\P-H membrane with its hydrogel selective layer leading to low fouling and high selectivity and its 3D interconnected porous support layer endorsing high water flux during the separation of hypersaline emulsion through FO process.

CHAPTER 7 CONCLUSIONS AND RECOMMENDATIONS

7.1. Conclusions

To the best knowledge of the author, this thesis is the first study that develops the design rationale for a genuine FO membrane that is able to excel with challenging wastewater, the first study that investigates and further optimizes the capability of hydrogel macromolecule (PVA) as FO membrane selective layer, the first study that creates a 3D interconnected porous nanocomposite support layer with prevailed membrane manufacture process (*i.e.* phase inversion), and the first study that explores the feasibility to simultaneously desalinate and deoil highly saline and oily wastewater by as-synthesized nanocomposite membrane through FO process. This thesis is expected to provide a new direction for the design and synthesis of FO membrane and make a significant impetus to the industrialization of FO technology. Concluding remarks are drawn in the following four aspects with detail.

7.1.1. The design rationale for a genuine FO membrane

This study carefully analyzes the specialties of FO technology, for the purpose of establishing the correct notions that (1) FO-draw solution regeneration technology is not a low energy process, and (2) the production of freshwater or energy through FO process from brackish water or seawater is inferior to existing available technologies or even economically infeasible. The true future for FO technology is to cope with those challenging wastewaters (*e.g.* highly saline and/or highly oily wastewaters) that cannot be tackled by pressure-driven membrane processes (*e.g.* RO, NF, UF *etc.*). Therefore, a genuine FO membrane must simultaneously possess (1) high antifouling capability that should not but usually be neglected, (2) high water flux and (3) high selectivity, which enables itself to excel with the treatment of challenging wastewater. Such FO membrane should be designed as a thin film composite membrane, which empowers its selective layer and support layer to be fabricated in separate process towards each optimum structures and properties. Ideally, its selective layer should possess (1) integrated surface properties of superhydrophilicity (superoleophobicity), ultrasmooth topography, and electroneutrality to effectively resist fouling, (2) ultrathin thickness to favor high water permeability and (3) high rejection of tiny ionic draw solutes to minimize reverse salt leakage. Meanwhile, its support layer should possess

high interconnectivity of interior pores in three dimensions at micrometer scale that is able to break the internal concentration polarization (ICP) bottleneck on FO and thus achieve high water flux. Furthermore, the technical routes to attain its selective layer and support layer should both be compatible with affordable membrane manufacture processes, which will guarantee the scale-up production of this membrane. As-developed design rationales in this study serve as the important guidelines for the following membrane synthesis including the innovations on both selective layer and support layer.

7.1.2. Crosslinked hydrogel selective layer leading to low fouling and high selectivity

Hydrogel selective layer in ultrathin thickness around 100 nm has been successfully synthesized through dip-coating technique. The immobilization of this hydrogel selective layer has been investigated from the perspective of irreversible adsorption in order to optimize the functions of as-synthesized selective layer.

This study has revealed that chemical crosslinking plays the key role in tuning the physical structures and chemical properties of as-synthesized hydrogel selective layer. Uncrosslinked hydrogel macromolecule is found not suitable to be used as selective layer due to its poor rejection of common ionic draw solutes. The best crosslinking agent is identified as glutaraldehyde. The optimum crosslinking degree is determined as *TCLD* of 30%, at which as-synthesized hydrogel selective layer is endowed with not only high selectivity but also high hydrophilicity.

Furthermore, other important factors that also influence the formation and properties of as-synthesized hydrogel selective layer have also been optimized. The optimum molecular weight of hydrogel macromolecule (PVA) to construct this selective layer is found to be 93 kDa. The concentration of hydrogel aqueous solution has been optimized as 0.25 wt%. And the optimum time for the dip-coating process is demonstrated as 20 min. In addition, the best ionic draw solute to sustain FO process for this selective layer is Na_2SO_4.

Based upon all these optimized outcomes, as-synthesized hydrogel FO membrane with

conventional phase inversion constructed support layer (P-H membrane) demonstrates the evident advantages in high selectivity and high antifouling capability, with its J_W/J_S (feed solution is DI water) 2.4 times higher than that of commercially available HTI FO membrane (cellulose triacetate, woven). These achievements validate the ability of crosslinked hydrogel as FO membrane selective layer and pave the way towards the new FO membrane that is able to address the treatment of challenging wastewater (*e.g.* highly saline and oily wastewater).

7.1.3. GO induced 3D interconnected porous support layer leading to high water flux

Nanocomposite support layer (GO\P support layer) with highly interconnected interior pore structure is successfully fabricated through GO assisted phase inversion technique with the aim of breaking ICP bottleneck and thus enhancing FO water flux. The roles of GO nanosheets in the formation of GO\P support layer have been carefully studied.

This study has found the incorporation of GO nanosheets can modify as-synthesized nanocomposite support layer to be more hydrophilic and negatively charged, mainly due to the equipment of oxygen-containing functional groups on support layer. Furthermore, the incorporation of GO nanosheets can enlarge the pore size of both top and bottom surfaces for as-synthesized GO\P support layer.

Most importantly, for the first time hydrophilic 2D graphitic nanomaterial is demonstrated able to transform the interior pore structure of support layer from conventionally 1D connected to 3D interconnected. Based upon systematic optimization of GO assisted phase inversion parameters including GO concentration, polymer concentration, solvent and so on, an entirely new support layer structure with its interior pores highly interconnected in all three dimensions at micrometer scale has been created. The formation mechanism of this 3D interconnected porous support layer is ascribed to GO induced viscosity difference that triggers the spread of viscous displacement from original one direction to all three directions.

This 3D interconnected porous support layer is proved able to effectively minimize ICP problem, which is evidenced by the diminution in FO membrane structural

parameter *S* value by as much as 41.4%. As a result, this 3D pore interconnected support layer enhances FO water flux (J_W) of as-synthesized hydrogel membrane by 72% compared with conventional 1D pore connected support layer (feed solution is DI water). Therefore, a micrometer-scale 3D interconnected porous support layer able to break the ICP bottleneck is successfully fabricated with phase inversion technique for the first time. This also points out a new direction for the synthesis of thin-film composite FO membrane by leveraging the state-of-art nanotechnology. These achievements clear the last obstacle 'ICP caused low FO J_W issue" and thus open the door to the eventual investigation on the treatment of highly saline and oily wastewater.

7.1.4. Simultaneous desalination and oil/water separation by as-synthesized nanocomposite membrane through FO process

The new membrane technology *i.e.* simultaneous desalination and oil/water separation is proposed for the first time purposely to solve the difficulties brought by highly saline and oily wastewater. The capability of as-synthesized nanocomposite membrane (GO\P-H membrane) to realize this new technology through FO process is systematically investigated with various oil-in-water emulsions as feed solution.

It's confirmed that GO\P-H membrane possesses remarkably superior antifouling capability over HTI membrane under all oil-in-water emulsions tested in FO process (membrane orientation is selective layer facing feed solution *i.e.* FO mode). Noteworthily, most of the oil-fouling can be reversible for GO\P-H membrane through *in-situ* washing with DI water while a considerably higher part of J_W loss cannot be recovered for HTI membrane through the identical cleaning method.

The analysis on the distinct membrane response to oil-fouling between hydrogel membranes and HTI membrane has revealed that FO fouling is determined by many factors including both chemical affinity between oil and membrane surface and physical size of oil droplet. Particularly, Membrane wettability plays a key role in controlling oil-fouling and the high underwater oleophobicity of as-synthesized hydrogel selective layers leads to their stronger anti-fouling capabilities. Besides, mathematical fittings on the correlation between FO fouling and oil droplet size

distribution of emulsion has demonstrated that underwater oleophobic membrane *e.g.* GO\P-H membrane is more independent on oil droplet size distribution of feed solution while underwater oleophilic membrane *i.e.* HTI membrane is less independent and suffers severer fouling along with the increase of average oil droplet size (d_{50}).

Most importantly, GO\P-H membrane has been systematically investigated for its ability to fulfill simultaneous desalination and oil/water separation with a variety of saline oily-polluted wastewaters (simulated shale gas wastewaters) as FO feed solution. The separation results show that GO\P-H membrane can simultaneously desalinate and deoil hypersaline oil-in-water emulsion with more than three times higher water flux, higher removal efficiencies for oil and salts (>99.9% for oil and >99.7% for multivalent ions), and significantly lower membrane fouling (>80% lower FRR_f) compared with HTI membrane. And further FO operation results display the overwhelmingly superior resistance to salinity induced fouling aggravation and long-term antifouling durability of GO\P-H membrane over HTI membrane.

Finally, these results point out a new direction for the design and synthesis of FO membrane. And the final goal of this study that is to address the treatment of challenging wastewater (*e.g.* highly saline and oily wastewater) has been eventually accomplished by a deliberately designed nanocomposite membrane *i.e.* GO\P-H membrane whose hydrogel selective layer leads to low fouling as well high selectivity and 3D interconnected porous support layer contributes to high water flux during the separation of hypersaline oil-in-water emulsion through FO process.

7.2. Recommendations

This study has developed a new nanocomposite membrane with hydrogel selective layer on top of GO induced 3D interconnected porous support layer that is able to desalinate and deoil hypersaline oil-in-water emulsion through FO process with low fouling, high water flux, and high selectivity. Based upon the outcomes achieved in this thesis, further explorations are recommended to carry out but not confined with the following aspects, in order to advance this nanocomposite membrane towards practical applications especially in environmental engineering and industrial processes.

7.2.1. Scale-up investigations

The investigations on as-synthesized GO\P-H nanocomposite membrane at pilot-scale FO process for the separation of hypersaline oil-in-water emulsion are recommended to be conducted before moving ahead to full-scale experiments. Viewed in the way of the author, the experiments at the pilot-scale are suggested to be directed towards the optimization of FO system as follows. Firstly, the operation mode needs to be upgraded from batch-type employed in this thesis to continuous-type that is more frequently used in industry. Particularly, the optimum interval to wash membrane is one of most interesting topics to be studied in order to keep GO\P-H membrane at good performance under long-term continuous operation. It's significant to optimize the ratio of washing interval to wastewater filtration time in terms of long term operation cost. Therefore, in the pilot-scale research, a new real-time control system is recommended to be built, which can investigate the washing interval by control the valve of feed tubings according to adjustable program. Besides, the method to regenerate the draw solution is also recommended to be considered in the pilot-scale project. It's necessary to point out different draw solutes have different requirements on the specific instrument to reconcentrate the draw solution. For example, multivalent ionic salts such as Na_2SO_4, $MgCl_2$ need RO or high performance NF equipment for the recycling, while thermolytic draw solute such as NH_4HCO_3 need heating instrument to separate draw solute from produced water for further reuse. Secondly, longer operation time in terms of months needs to be conducted for the purpose of prudent validation. It's very important to find out whether the performance of GO\P-H membrane can be sustained in the acceptable level when experiencing months of continuous operation. Thirdly and most importantly, the most favorable water recovery should be searched out during pilot-scale experimental work in order to optimize the entire FO system in terms of economic feasibility and operational sustainability, as partially discussed in section 6.6.1.

Noteworthily, the solid basis towards pilot-scale investigations is to synthesize this new FO membrane in larger size *i.e.* the lateral sizes of membrane sheet in meter scale. Fortunately, all the technologies employed to fabricate this new FO membrane (GO assisted phase inversion technology and dip-coating technology) is compatible with currently prevalent membrane manufacture processes and can be used in these

manufacture processes directly. Therefore, this is expected to facilitate the industrialization of this new membrane technology to a great extent as the result of the deliberate research design at the very beginning by this thesis.

7.2.2. Actual hypersaline oil/water mixtures

Nature can be mimicked but hardly replaced. The simple but most straightforward way to test this new membrane in order to propel it towards practical application is nothing other than examining its performance with actual highly saline and oily wastewater as FO feed solution. So the future studies are recommended to use real oil/water mixtures such as real shale gas wastewater, real onshore oil & gas produced water, actual oil spilled seawater instead of their simulated counterparts as the feed solution to run the FO process. This is because the components other than oil and salts contained in actual saline oil/water mixtures (*e.g.* hardness, alkalinity, barium, bromide, iron, *etc.*) may also have impacts on FO performance especially on water flux and membrane fouling. Besides, the influences of temperature, pH and other parameters are also worthy to be investigated. Taking this into account, the pilot-scale membrane setup shall be constructed at the site of oil/gas exploration field if possible, so as to avoid the changes in water quality due to long-distance transportation of water sample. Particularly, because the specific quality of produced wastewater from oil/gas exploration projects can vary from site to site, a detailed list of quality analysis on the raw water as well as the permeate of applied pilot-scale FO process will be important to provide a rational evaluation on the performance of this new nanocomposite FO membrane.

REFERENCES

Aaberg, R.J. (2003). "Osmotic power: A new and powerful renewable energy source?", ReFocus, **4**(6), 48-50.

Achilli, A., Cath, T.Y. and Childress, A.E. (2009a). "Power generation with pressure retarded osmosis: An experimental and theoretical investigation", Journal of Membrane Science, **343**(1-2), 42-52.

Achilli, A., Cath, T.Y., Marchand, E.A. and Childress, A.E. (2009b). "The forward osmosis membrane bioreactor: A low fouling alternative to MBR processes", Desalination, **239**(1-3), 10-21.

Achilli, A., Cath, T.Y. and Childress, A.E. (2010). "Selection of inorganic-based draw solutions for forward osmosis applications", Journal of Membrane Science, **364**(1-2), 233-241.

Achilli, A. and Childress, A.E. (2010). "Pressure retarded osmosis: From the vision of Sidney Loeb to the first prototype installation - Review", Desalination, **261**(3), 205-211.

Akther, N., Sodiq, A., Giwa, A., Daer, S., Arafat, H.A. and Hasan, S.W. (2015). "Recent advancements in forward osmosis desalination: A review", Chemical Engineering Journal, **281**, 502-522.

Aldhous, P. (2003). "The world's forgotten crisis - Over a billion people cannot get clean water, and things are getting worse", Nature, **422**(6929), 251-251.

Altaee, A. and Hilal, N. (2014). "Dual-stage forward osmosis/pressure retarded osmosis process for hypersaline solutions and fracking wastewater treatment", Desalination, **350**, 79-85.

Alturki, A., McDonald, J., Khan, S.J., Hai, F.I., Price, W.E. and Nghiem, L.D. (2012). "Performance of a novel osmotic membrane bioreactor (OMBR) system: Flux stability and removal of trace organics", Bioresource Technology, **113**, 201-206.

Amini, M., Jahanshahi, M. and Rahimpour, A. (2013). "Synthesis of novel thin film nanocomposite (TFN) forward osmosis membranes using functionalized multi-walled carbon nanotubes", Journal of Membrane Science, **435**, 233-241.

An, Q.F., Li, F., Ji, Y.L. and Chen, H.L. (2011). "Influence of polyvinyl alcohol on the surface morphology, separation and anti-fouling performance of the composite polyamide nanofiltration membranes", Journal of Membrane Science, **367**(1-2), 158-165.

Bai, H.W., Liu, Z.Y. and Sun, D.D. (2011). "Highly water soluble and recovered dextran coated Fe3O4 magnetic nanoparticles for brackish water desalination", Separation and Purification Technology, **81**(3), 392-399.

Baier, R.E. (2006). "Surface behaviour of biomaterials: The theta surface for

biocompatibility", Journal of Materials Science-Materials in Medicine, **17**(11), 1057-1062.

Baker, M.I., Walsh, S.P., Schwartz, Z. and Boyan, B.D. (2012). "A review of polyvinyl alcohol and its uses in cartilage and orthopedic applications", Journal of Biomedical Materials Research Part B-Applied Biomaterials, **100B**(5), 1451-1457.

Bamaga, O.A., Yokochi, A., Zabara, B. and Babaqi, A.S. (2011). "Hybrid FO/RO desalination system: Preliminary assessment of osmotic energy recovery and designs of new FO membrane module configurations", Desalination, **268**(1-3), 163-169.

Barnaby, W. (2009). "Do nations go to war over water?", Nature, **458**(7236), 282-283.

Batchelder, G.W. (1965). "Process for the demineralization of water", US Patent 3,171,799.

Beaudry, E.G. and Lampi, K.A. (1990). "Membrane technology for direct osmosis concentration of fruit juices", Food Technology, **44**(6), 121-121.

Belfer, S., Fainshtain, R., Purinson, Y., Gilron, J., Nystrom, M. and Manttari, M. (2004). "Modification of NF membrane properties by in situ redox initiated graft polymerization with hydrophilic monomers", Journal of Membrane Science, **239**(1), 55-64.

Biberdorf, C. (2004). "Filter in a pouch", The Warrior, **3**.

Blandin, G., Verliefde, A.D., Tang, C.Y.Y., Childress, A.E. and Le-Clech, P. (2013). "Validation of assisted forward osmosis (AFO) process: Impact of hydraulic pressure", Journal of Membrane Science, **447**, 1-11.

Bolto, B., Tran, T., Hoang, M. and Xie, Z.L. (2009). "Crosslinked poly(vinyl alcohol) membranes", Progress in Polymer Science, **34**(9), 969-981.

Bonn, D., Eggers, J., Indekeu, J., Meunier, J. and Rolley, E. (2009). "Wetting and spreading", Reviews of Modern Physics, **81**(2), 739-805.

Bourzac, K. (2013). "Water: the flow of technology", Nature, **501**(7468), S4-S6.

Bowen, S.E. and Balster, R.L. (1998). "The effects of inhaled isoparaffins on locomotor activity and operant performance in mice", Pharmacology Biochemistry and Behavior, **61**(3), 271-280.

Bui, N.N. and McCutcheon, J.R. (2013). "Hydrophilic nanofibers as new supports for thin film composite membranes for engineered osmosis", Environmental Science & Technology, **47**(3), 1761-1769.

Butler, E., Silva, A., Horton, K., Rom, Z., Chwatko, M., Havasov, A. and McCutcheon, J.R. (2013). "Point of use water treatment with forward osmosis for emergency relief", Desalination, **312**, 23-30.

Cadotte, J.E., Petersen, R.J., Larson, R.E. and Erickson, E.E. (1980). "New thin-film composite seawater reverse osmosis membrane ", Desalination, **32**(1-3), 25-31.

Cao, X.X., Huang, X., Liang, P., Xiao, K., Zhou, Y.J., Zhang, X.Y. and Logan, B.E. (2009). "A new method for water desalination using microbial desalination cells", Environmental Science & Technology, **43**(18), 7148-7152.

Castrillon, S.R.V., Lu, X.L., Shaffer, D.L. and Elimelech, M. (2014). "Amine enrichment and poly(ethylene glycol) (PEG) surface modification of thin-film composite forward osmosis membranes for organic fouling control", Journal of Membrane Science, **450**, 331-339.

Cath, T.Y., Adams, D. and Childress, A.E. (2005a). "Membrane contactor processes for wastewater reclamation in space II. Combined direct osmosis, osmotic distillation, and membrane distillation for treatment of metabolic wastewater", Journal of Membrane Science, **257**(1-2), 111-119.

Cath, T.Y., Adams, V.D., Childress, A.E., Gormly, S.J. and Flynn, M.T. (2005b). "Progress in the development of direct osmotic concentration wastewater recovery process for advanced life support system", Proceedings of the 35th International Conference on Environmental System (ICES), Rome, Italy.

Cath, T.Y., Gormly, S., Beaudry, E.G., Flynn, M.T., Adams, V.D. and Childress, A.E. (2005c). "Membrane contactor processes for wastewater reclamation in space Part I. Direct osmotic concentration as pretreatment for reverse osmosis", Journal of Membrane Science, **257**(1-2), 85-98.

Cath, T.Y., Childress, A.E. and Elimelech, M. (2006). "Forward osmosis: Principles, applications, and recent developments", Journal of Membrane Science, **281**(1-2), 70-87.

Cath, T.Y. (2010). "Osmotically and thermally driven membrane processes for enhancement of water recovery in desalination processes", Desalination and Water Treatment, **15**(1-3), 279-286.

Chen, P.C. and Xu, Z.K. (2013). "Mineral-coated polymer membranes with superhydrophilicity and underwater superoleophobicity for effective oil/water separation", Scientific Reports, **3**.

Chen, S.F., Li, L.Y., Zhao, C. and Zheng, J. (2010). "Surface hydration: principles and applications toward low-fouling/nonfouling biomaterials", Polymer, **51**(23), 5283-5293.

Chiellini, E., Corti, A., D'Antone, S. and Solaro, R. (2003). "Biodegradation of poly (vinyl alcohol) based materials", Progress in Polymer Science, **28**(6), 963-1014.

Chou, S.R., Shi, L., Wang, R., Tang, C.Y.Y., Qiu, C.Q. and Fane, A.G. (2010). "Characteristics and potential applications of a novel forward osmosis hollow fiber membrane", Desalination, **261**(3), 365-372.

Chow, J., Kopp, R.J. and Portney, P.R. (2003). "Energy resources and global development", Science, **302**(5650), 1528-1531.

Chung, T.S., Zhang, S., Wang, K.Y., Su, J.C. and Ling, M.M. (2012). "Forward osmosis processes: Yesterday, today and tomorrow", Desalination, **287**, 78-81.

Coday, B.D. and Cath, T.Y. (2014). "Forward osmosis: Novel desalination of produced water and fracturing flowback", Journal American Water Works Association, **106**(2), 37-38.

Cooper, A.R. and Vanderveer, D.S. (1979). "Characterization of ultrafiltration membranes by polymer transport measurements", Separation Science and Technology, **14**(6), 551-556.

Cornelissen, E.R., Harmsen, D., de Korte, K.F., Ruiken, C.J., Qin, J.J., Oo, H. and Wessels, L.P. (2008). "Membrane fouling and process performance of forward osmosis membranes on activated sludge", Journal of Membrane Science, **319**(1-2), 158-168.

Dabelstein, W., Reglitzky, A., Schütze, A. and Reders, K. (2007). "Automotive fuels", Ullmann's Encyclopedia of Industrial Chemistry.

Dalla Rosa, M. and Giroux, F. (2001). "Osmotic treatments (OT) and problems related to the solution management", Journal of Food Engineering, **49**(2-3), 223-236.

DeMerlis, C.C. and Schoneker, D.R. (2003). "Review of the oral toxicity of polyvinyl alcohol (PVA)", Food and Chemical Toxicology, **41**(3), 319-326.

Destaye, A.G., Lin, C.K. and Lee, C.K. (2013). "Glutaraldehyde vapor cross-linked nanofibrous PVA mat with in situ formed silver nanoparticles", Acs Applied Materials & Interfaces, **5**(11), 4745-4752.

Dova, M.I., Petrotos, K.B. and Lazarides, H.N. (2007). "On the direct osmotic concentration of liquid foods. Part I: Impact of process parameters on process performance", Journal of Food Engineering, **78**(2), 422-430.

Dreyer, D.R., Todd, A.D. and Bielawski, C.W. (2014). "Harnessing the chemistry of graphene oxide", Chemical Society Reviews, **43**(15), 5288-5301.

Duong, P.H.H., Zuo, J. and Chung, T.S. (2013). "Highly crosslinked layer-by-layer polyelectrolyte FO membranes: Understanding effects of salt concentration and deposition time on FO performance", Journal of Membrane Science, **427**, 411-421.

Duong, P.H.H. and Chung, T.S. (2014). "Application of thin film composite membranes with forward osmosis technology for the separation of emulsified oil-water", Journal of Membrane Science, **452**, 117-126.

Duong, P.H.H., Chung, T.S., Wei, S. and Irish, L. (2014). "Highly permeable double-skinned forward osmosis membranes for anti-fouling in the emulsified oil-water separation process", Environmental Science & Technology, **48**(8), 4537-4545.

Elimelech, M., Zhu, X.H., Childress, A.E. and Hong, S.K. (1997). "Role of membrane surface morphology in colloidal fouling of cellulose acetate and composite aromatic polyamide reverse osmosis membranes", Journal of Membrane Science, **127**(1), 101-109.

Elimelech, M. (2007). "Yale constructs forward osmosis desalination pilot plant", Membrane Technology, **2007**(1), 7-8.

Elimelech, M. and Phillip, W.A. (2011). "The future of seawater desalination: energy, technology, and the environment", Science, **333**(6043), 712-717.

Emadzadeh, D., Lau, W.J., Matsuura, T., Hilal, N. and Ismail, A.F. (2014a). "The potential of thin film nanocomposite membrane in reducing organic fouling in forward osmosis process", Desalination, **348**, 82-88.

Emadzadeh, D., Lau, W.J., Matsuura, T., Ismail, A.F. and Rahbari-Sisakht, M. (2014b). "Synthesis and characterization of thin film nanocomposite forward osmosis membrane with hydrophilic nanocomposite support to reduce internal concentration polarization", Journal of Membrane Science, **449**, 74-85.

Feeley, T.J., Skone, T.J., Stlegel, G.J., McNemar, A., Nemeth, M., Schimmoller, B., Murph, J.T. and Manfredo, L. (2008). "Water: A critical resource in the thermoelectric power industry", Energy, **33**(1), 1-11.

Flanagan, M.F. and Escobar, I.C. (2013). "Novel charged and hydrophilized polybenzimidazole (PBI) membranes for forward osmosis", Journal of Membrane Science, **434**, 85-92.

Flemming, H.C. (2002). "Biofouling in water systems - cases, causes and countermeasures", Applied Microbiology and Biotechnology, **59**(6), 629-640.

Frank, B.S. (1972). "Desalination of sea water", US Patent 3,670,897.

Ganesh, B.M., Isloor, A.M. and Ismail, A.F. (2013). "Enhanced hydrophilicity and salt rejection study of graphene oxide-polysulfone mixed matrix membrane", Desalination, **313**, 199-207.

Ge, Z. and He, Z. (2012). "Effects of draw solutions and membrane conditions on electricity generation and water flux in osmotic microbial fuel cells", Bioresource Technology, **109**, 70-76.

Ge, Z., Ping, Q.Y., Xiao, L. and He, Z. (2013). "Reducing effluent discharge and recovering bioenergy in an osmotic microbial fuel cell treating domestic wastewater", Desalination, **312**, 52-59.

Geim, A.K. and Novoselov, K.S. (2007). "The rise of graphene", Nature Materials, **6**(3), 183-191.

Geise, G.M., Lee, H.S., Miller, D.J., Freeman, B.D., McGrath, J.E. and Paul, D.R. (2010). "Water Purification by Membranes: The Role of Polymer Science", Journal of Polymer Science Part B-Polymer Physics, **48**(15), 1685-1718.

Ghanbari, M., Emadzadeh, D., Lau, W.J., Matsuura, T., Davoody, M. and Ismail, A.F. (2015). "Super hydrophilic TiO_2/HNT nanocomposites as a new approach for fabrication of high performance thin film nanocomposite membranes for FO application", Desalination, **371**, 104-114.

Ghosh, A.K., Jeong, B.H., Huang, X.F. and Hoek, E.M.V. (2008). "Impacts of reaction and curing conditions on polyamide composite reverse osmosis membrane properties", Journal of Membrane Science, **311**(1-2), 34-45.

Gilron, J., Belfer, S., Vaisanen, P. and Nystrom, M. (2001). "Effects of surface modification on antifouling and performance properties of reverse osmosis membranes", Desalination, **140**(2), 167-179.

Gohil, J.M. and Ray, P. (2009). "Polyvinyl alcohol as the barrier layer in thin film composite nanofiltration membranes: Preparation, characterization, and performance evaluation", Journal of Colloid and Interface Science, **338**(1), 121-127.

Goosen, M.F.A., Sablani, S.S., Ai-Hinai, H., Ai-Obeidani, S., Al-Belushi, R. and Jackson, D. (2004). "Fouling of reverse osmosis and ultrafiltration membranes: A critical review", Separation Science and Technology, **39**(10), 2261-2297.

Gray, G.T., McCutcheon, J.R. and Elimelech, M. (2006). "Internal concentration polarization in forward osmosis: role of membrane orientation", Desalination, **197**(1-3), 1-8.

Greenlee, L.F., Lawler, D.F., Freeman, B.D., Marrot, B. and Moulin, P. (2009). "Reverse osmosis desalination: water sources, technology, and today's challenges", Water Research, **43**(9), 2317-2348.

Gregory, K.B., Vidic, R.D. and Dzombak, D.A. (2011). "Water management challenges associated with the production of shale gas by hydraulic fracturing", Elements, **7**(3), 181-186.

Han, G., Chung, T.S., Toriida, M. and Tamai, S. (2012a). "Thin-film composite forward osmosis membranes with novel hydrophilic supports for desalination", Journal of Membrane Science, **423**, 543-555.

Han, G., Zhang, S., Li, X., Widjojo, N. and Chung, T.S. (2012b). "Thin film composite forward osmosis membranes based on polydopamine modified polysulfone substrates with enhancements in both water flux and salt rejection", Chemical Engineering Science, **80**, 219-231.

Han, Y., Xu, Z. and Gao, C. (2013). "Ultrathin graphene nanofiltration membrane for water purification", Advanced Functional Materials, **23**(29), 3693-3700.

Herrlich, S., Spieth, S., Messner, S. and Zengerle, R. (2012). "Osmotic micropumps for drug delivery", Advanced Drug Delivery Reviews, **64**(14), 1617-1627.

Herrwerth, S., Eck, W., Reinhardt, S. and Grunze, M. (2003). "Factors that determine the protein resistance of oligoether self-assembled monolayers - Internal hydrophilicity, terminal hydrophilicity, and lateral packing density", Journal of the American Chemical Society, **125**(31), 9359-9366.

Hightower, M. and Pierce, S.A. (2008). "The energy challenge", Nature, **452**(7185), 285-286.

Hilal, N., Al-Khatib, L., Atkin, B.P., Kochkodan, V. and Potapchenko, N. (2003). "Photochemical modification of membrane surfaces for (bio)fouling reduction: a nano-scale study using AFM", Desalination, **158**(1-3), 65-72.

Holloway, R.W., Childress, A.E., Dennett, K.E. and Cath, T.Y. (2007). "Forward

osmosis for concentration of anaerobic digester centrate", Water Research, **41**(17), 4005-4014.

Hook, M. and Tang, X. (2013). "Depletion of fossil fuels and anthropogenic climate change-A review", Energy Policy, **52**, 797-809.

Hoover, L.A., Phillip, W.A., Tiraferri, A., Yip, N.Y. and Elimelech, M. (2011). "Forward with Osmosis: emerging applications for greater sustainability", Environmental Science & Technology, **45**(23), 9824-9830.

Hoover, L.A., Schiffman, J.D. and Elimelech, M. (2013). "Nanofibers in thin-film composite membrane support layers: Enabling expanded application of forward and pressure retarded osmosis", Desalination, **308**, 73-81.

Howell, D. and Behrends, B. (2006). "A review of surface roughness in antifouling coatings illustrating the importance of cutoff length", Biofouling, **22**(6), 401-410.

Huang, L.W. and McCutcheon, J.R. (2015). "Impact of support layer pore size on performance of thin film composite membranes for forward osmosis", Journal of Membrane Science, **483**, 25-33.

Huang, M.H., Chen, Y.S., Huang, C.H., Sun, P.Z. and Crittenden, J. (2015). "Rejection and adsorption of trace pharmaceuticals by coating a forward osmosis membrane with TiO2", Chemical Engineering Journal, **279**, 904-911.

Hummers, W.S. and Offeman, R.E. (1958). "Preparation of graphitic oxide", Journal of the American Chemical Society, **80**(6), 1339-1339.

Hurwitz, G., Guillen, G.R. and Hoek, E.M.V. (2010). "Probing polyamide membrane surface charge, zeta potential, wettability, and hydrophilicity with contact angle measurements", Journal of Membrane Science, **349**(1-2), 349-357.

Immelman, E., Bezuidenhout, D., Sanderson, R.D., Jacobs, E.P. and Vanreenen, A.J. (1993). "Poly(vinyl alcohol) gel sublayers for reverse osmosis membrane. 3. insolubilization by cross-linking with potassium peroxydisulfate", Desalination, **94**(2), 115-132.

Ismail, A.F., Padaki, M., Hilal, N., Matsuura, T. and Lau, W.J. (2015). "Thin film composite membrane - Recent development and future potential", Desalination, **356**, 140-148.

Jeon, S.I., Lee, J.H., Andrade, J.D. and Degennes, P.G. (1991). "Protein surface interactions in the presence of polyethylene oxide 1. simplified theory ", Journal of Colloid and Interface Science, **142**(1), 149-158.

Jiao, B., Cassano, A. and Drioli, E. (2004). "Recent advances on membrane processes for the concentration of fruit juices: a review", Journal of Food Engineering, **63**(3), 303-324.

Jin, X., Huang, X.F. and Hoek, E.M.V. (2009). "Role of specific ion interactions in seawater RO membrane fouling by alginic acid", Environmental Science & Technology, **43**(10), 3580-3587.

Jin, X., Tang, C.Y., Gu, Y.S., She, Q.H. and Qi, S.R. (2011). "Boric acid permeation in forward osmosis membrane processes: modeling, experiments, and implications", Environmental Science & Technology, **45**(6), 2323-2330.

Joseph, N., Ahmadiannamini, P., Hoogenboom, R. and Vankelecom, I.F.J. (2014). "Layer-by-layer preparation of polyelectrolyte multilayer membranes for separation", Polymer Chemistry, **5**(6), 1817-1831.

Kang, G.D. and Cao, Y.M. (2012). "Development of antifouling reverse osmosis membranes for water treatment: A review", Water Research, **46**(3), 584-600.

Karakulski, K., Gryta, M. and Morawski, A. (2002). "Membrane processes used for potable water quality improvement", Desalination, **145**(1-3), 315-319.

Kargbo, D.M., Wilhelm, R.G. and Campbell, D.J. (2010). "Natural gas plays in the marcellus shale: challenges and potential opportunities", Environmental Science & Technology, **44**(15), 5679-5684.

Kessler, J.O. and Moody, C.D. (1976). "Drinking water from sea water by forward osmosis", Desalination, **18**(3), 297-306.

Khalid, A., Al-Juhani, A.A., Al-Hamouz, O.C., Laoui, T., Khan, Z. and Atieh, M.A. (2015). "Preparation and properties of nanocomposite polysulfone/multi-walled carbon nanotubes membranes for desalination", Desalination, **367**, 134-144.

Kim, J.J., Chung, J.S., Kang, H., Yu, Y.A., Choi, W.J., Kim, H.J. and Lee, J.C. (2014). "Thermo-responsive copolymers with ionic group as novel draw solutes for forward osmosis processes", Macromolecular Research, **22**(9), 963-970.

Kjeldsen, P., Barlaz, M.A., Rooker, A.P., Baun, A., Ledin, A. and Christensen, T.H. (2002). "Present and long-term composition of MSW landfill leachate: A review", Critical Reviews in Environmental Science and Technology, **32**(4), 297-336.

Klaysom, C., Cath, T.Y., Depuydt, T. and Vankelecom, I.F.J. (2013). "Forward and pressure retarded osmosis: potential solutions for global challenges in energy and water supply", Chemical Society Reviews, **42**(16), 6959-6989.

Kozlov, M., Quarmyne, M., Chen, W. and McCarthy, T.J. (2003). "Adsorption of poly(vinyl alcohol) onto hydrophobic substrates. A general approach for hydrophilizing and chemically activating surfaces", Macromolecules, **36**(16), 6054-6059.

Kramer, E.M. and Myers, D.R. (2013). "Osmosis is not driven by water dilution", Trends in plant science, **18**(4), 195-197.

Kravath, R.E. and Davis, J.A. (1975). "Desalination of sea water by direct osmosis ", Desalination, **16**(2), 151-155.

Krishnamoorthy, K., Veerapandian, M., Yun, K. and Kim, S.J. (2013). "The Chemical and structural analysis of graphene oxide with different degrees of oxidation", Carbon, **53**, 38-49.

Lang, K., Chowdhury, G., Matsuura, T. and Sourirajan, S. (1994). "Reverse osmosis performance of modified polyvinyl alcohol thin-film composite membranes ", Journal of Colloid and Interface Science, **166**(1), 239-244.

Lang, K., Matsuura, T., Chowdhury, G. and Sourirajan, S. (1995). "Preparation and testing polyvinyl alcohol composite membranes for reverse osmosis ", Canadian Journal of Chemical Engineering, **73**(5), 686-692.

Lang, K., Sourirajan, S., Matsuura, T. and Chowdhury, G. (1996). "A study on the preparation of polyvinyl alcohol thin-film composite membranes and reverse osmosis testing", Desalination, **104**(3), 185-196.

Lattemann, S. and Hopner, T. (2008). "Environmental impact and impact assessment of seawater desalination", Desalination, **220**(1-3), 1-15.

Lay, W.C.L., Zhang, Q.Y., Zhang, J.S., McDougald, D., Tang, C.Y., Wang, R., Liu, Y. and Fane, A.G. (2012). "Effect of Pharmaceuticals on the Performance of a Novel Osmotic Membrane Bioreactor (OMBR)", Separation Science and Technology, **47**(4), 543-554.

Lee, C.C. and Lee, J. (2014). "Temperature-Sensitive Polymers Adhered on FO Membrane as Drawing Agents", Polymer-Korea, **38**(5), 626-631.

Lee, J., Chae, H.R., Won, Y.J., Lee, K., Lee, C.H., Lee, H.H., Kim, I.C. and Lee, J.M. (2013). "Graphene oxide nanoplatelets composite membrane with hydrophilic and antifouling properties for wastewater treatment", Journal of Membrane Science, **448**, 223-230.

Lee, J.Y., She, Q.H., Huo, F.W. and Tang, C.Y.Y. (2015). "Metal-organic framework-based porous matrix membranes for improving mass transfer in forward osmosis membranes", Journal of Membrane Science, **492**, 392-399.

Lee, K.L., Baker, R.W. and Lonsdale, H.K. (1981a). "Membranes for power generation by pressure-retarded osmosis ", Journal of Membrane Science, **8**(2), 141-171.

Lee, K.L., Baker, R.W. and Lonsdale, H.K. (1981b). "Membranes for power-generation by pressure-retarded osmosis", Journal of Membrane Science, **8**(2), 141-171.

Lee, K.P., Arnot, T.C. and Mattia, D. (2011). "A review of reverse osmosis membrane materials for desalination-Development to date and future potential", Journal of Membrane Science, **370**(1-2), 1-22.

Lee, S., Boo, C., Elimelech, M. and Hong, S. (2010a). "Comparison of fouling behavior in forward osmosis (FO) and reverse osmosis (RO)", Journal of Membrane Science, **365**(1-2), 34-39.

Lee, W., Ahn, C.H., Hong, S., Kim, S., Lee, S., Baek, Y. and Yoon, J. (2010b). "Evaluation of surface properties of reverse osmosis membranes on the initial biofouling stages under no filtration condition", Journal of Membrane Science, **351**(1-2), 112-122.

Li, D., Zhang, X.Y., Yao, J.F., Simon, G.P. and Wang, H.T. (2011). "Stimuli-responsive polymer hydrogels as a new class of draw agent for forward osmosis desalination", Chemical Communications, **47**(6), 1710-1712.

Li, G.Z., Cheng, G., Xue, H., Chen, S.F., Zhang, F.B. and Jiang, S.Y. (2008). "Ultra low fouling zwitterionic polymers with a biomimetic adhesive group", Biomaterials, **29**(35), 4592-4597.

Li, X., Wang, K.Y., Helmer, B. and Chung, T.S. (2012a). "Thin-film composite membranes and formation mechanism of thin-film layers on hydrophilic cellulose acetate propionate substrates for forward osmosis processes", Industrial & Engineering Chemistry Research, **51**(30), 10039-10050.

Li, X.M., Zhao, B.L., Wang, Z.W., Xie, M., Song, J.F., Nghiem, L.D., He, T., Yang, C., Li, C.X. and Chen, G. (2014). "Water reclamation from shale gas drilling flow-back fluid using a novel forward osmosis-vacuum membrane distillation hybrid system", Water Science and Technology, **69**(5), 1036-1044.

Li, Z.Y., Yangali-Quintanilla, V., Valladares-Linares, R., Li, Q.Y., Zhan, T. and Amy, G. (2012b). "Flux patterns and membrane fouling propensity during desalination of seawater by forward osmosis", Water Research, **46**(1), 195-204.

Ling, M.M., Wang, K.Y. and Chung, T.S. (2010). "Highly water-soluble magnetic nanoparticles as novel draw solutes in forward osmosis for water reuse", Industrial & Engineering Chemistry Research, **49**(12), 5869-5876.

Ling, M.M. and Chung, T.S. (2011). "Desalination process using super hydrophilic nanoparticles via forward osmosis integrated with ultrafiltration regeneration", Desalination, **278**(1-3), 194-202.

Liu, C., Fang, W.X., Chou, S.R., Shi, L., Fane, A.G. and Wang, R. (2013). "Fabrication of layer-by-layer assembled FO hollow fiber membranes and their performances using low concentration draw solutions", Desalination, **308**, 147-153.

Liu, M.H., Chen, Q., Wang, L.Z., Yu, S.C. and Gao, C.J. (2015a). "Improving fouling resistance and chlorine stability of aromatic polyamide thin-film composite RO membrane by surface grafting of polyvinyl alcohol (PVA)", Desalination, **367**, 11-20.

Liu, X. and Ng, H.Y. (2015). "Fabrication of layered silica-polysulfone mixed matrix substrate membrane for enhancing performance of thin-film composite forward osmosis membrane", Journal of Membrane Science, **481**, 148-163.

Liu, Y.Q., Zhang, Y.L., Fu, X.Y. and Sun, H.B. (2015b). "Bioinspired underwater superoleophobic membrane based on a graphene oxide coated wire mesh for efficient oil/water separation", Acs Applied Materials & Interfaces, **7**(37), 20930-20936.

Liu, Z.Y., Bai, H.W., Lee, J. and Sun, D.D. (2011). "A low-energy forward osmosis process to produce drinking water", Energy & Environmental Science, **4**(7), 2582-2585.

Loeb, S. and Sourirajan, S. (1962). "Sea water demineralization by means of an osmotic membrane", Advances in Chemistry, **38**(9), 117-132.

Loeb, S. (1975). "Osmotic power plants", Science, **189**(4203), 654-655.

Loeb, S. (1976). "Production of energy from concentrated brines by pressure-retarded osmosis 1. preliminary technical and economic correlations. ", Journal of Membrane Science, **1**(1), 49-63.

Loeb, S., Vanhessen, F. and Shahaf, D. (1976). "Production of energy from concentrated brine by pressur retarded osmosis 2. experimental results and projected energy costs", Journal of Membrane Science, **1**(3), 249-269.

Loeb, S., Titelman, L., Korngold, E. and Freiman, J. (1997). "Effect of porous support fabric on osmosis through a Loeb-Sourirajan type asymmetric membrane", Journal of Membrane Science, **129**(2), 243-249.

Loeb, S. (1998). "Energy production at the Dead Sea by pressure-retarded osmosis: challenge or chimera?", Desalination, **120**(3), 247-262.

Louie, J.S., Pinnau, I., Ciobanu, I., Ishida, K.P., Ng, A. and Reinhard, M. (2006). "Effects of polyether-polyamide block copolymer coating on performance and fouling of reverse osmosis membranes", Journal of Membrane Science, **280**(1-2), 762-770.

Lu, X.L., Castrillon, S.R.V., Shaffer, D.L., Ma, J. and Elimelech, M. (2013). "In situ surface chemical modification of thin-film composite forward osmosis membranes for enhanced organic fouling resistance", Environmental Science & Technology, **47**(21), 12219-12228.

Lu, X.L., Chavez, L.H.A., Castrillon, S.R.V., Ma, J. and Elimelech, M. (2015). "Influence of active layer and support layer surface structures on organic fouling propensity of thin-film composite forward osmosis membranes", Environmental Science & Technology, **49**(3), 1436-1444.

Luo, L., Wang, P., Zhang, S., Han, G. and Chung, T.S. (2014). "Novel thin-film composite tri-bore hollow fiber membrane fabrication for forward osmosis", Journal of Membrane Science, **461**, 28-38.

Ma, N., Wei, J., Liao, R.H. and Tang, C.Y.Y. (2012). "Zeolite-polyamide thin film nanocomposite membranes: Towards enhanced performance for forward osmosis", Journal of Membrane Science, **405**, 149-157.

Ma, N., Wei, J., Qi, S.R., Zhao, Y., Gao, Y.B. and Tang, C.Y.Y. (2013). "Nanocomposite substrates for controlling internal concentration polarization in forward osmosis membranes", Journal of Membrane Science, **441**, 54-62.

Ma, X.L., Su, Y.L., Sun, Q., Wang, Y.Q. and Jiang, Z.Y. (2007). "Enhancing the antifouling property of polyethersulfone ultrafiltration membranes through surface adsorption-crosslinking of poly(vinyl alcohol)", Journal of Membrane Science, **300**(1-2), 71-78.

Magin, C.M., Cooper, S.P. and Brennan, A.B. (2010). "Non-toxic antifouling strategies", Materials Today, **13**(4), 36-44.

Majeed, S., Fierro, D., Buhr, K., Wind, J., Du, B., Boschetti-De-Fierro, A. and Abetz, V.

(2012). "Multi-walled carbon nanotubes (MWCNTs) mixed polyacrylonitrile (PAN) ultrafiltration membranes", Journal of Membrane Science, **403**, 101-109.

Marcano, D.C., Kosynkin, D.V., Berlin, J.M., Sinitskii, A., Sun, Z.Z., Slesarev, A., Alemany, L.B., Lu, W. and Tour, J.M. (2010). "Improved synthesis of graphene oxide", Acs Nano, **4**(8), 4806-4814.

Marshall, A.D., Munro, P.A. and Tragardh, G. (1993). "The effect of protein fouling in microfiltration and ultrafiltration on permeate flux, protenin retention and selectivity: A literature review", Desalination, **91**(1), 65-108.

McAloney, R.A. and Goh, M.C. (1999). "In situ investigations of polyelectrolyte film formation by second harmonic generation", Journal of Physical Chemistry B, **103**(49), 10729-10732.

McCormick, P., Pellegrino, J., Mantovani, F. and Sarti, G. (2008). "Water, salt, and ethanol diffusion through membranes for water recovery by forward (direct) osmosis processes", Journal of Membrane Science, **325**(1), 467-478.

McCutcheon, J.R., McGinnis, R.L. and Elimelech, M. (2005). "A novel ammonia-carbon dioxide forward (direct) osmosis desalination process", Desalination, **174**(1), 1-11.

McCutcheon, J.R. and Elimelech, M. (2006). "Influence of concentrative and dilutive internal concentration polarization on flux behavior in forward osmosis", Journal of Membrane Science, **284**(1-2), 237-247.

McCutcheon, J.R., McGinnis, R.L. and Elimelech, M. (2006). "Desalination by ammonia-carbon dioxide forward osmosis: Influence of draw and feed solution concentrations on process performance", Journal of Membrane Science, **278**(1-2), 114-123.

McCutcheon, J.R. and Elimelech, M. (2007). "Modeling water flux in forward osmosis: Implications for improved membrane design", Aiche Journal, **53**(7), 1736-1744.

McGinnis, R.L. (2002). "Osmotic desalination process", US patent 6,391,205,B1.

McGinnis, R.L. and Elimelech, M. (2008). "Global challenges in energy and water supply: the promise of engineered osmosis", Environmental Science & Technology, **42**(23), 8625-8629.

McGovern, R.K. and Lienhard, J.H. (2014). "On the potential of forward osmosis to energetically outperform reverse osmosis desalination", Journal of Membrane Science, **469**, 245-250.

Mehta, G.D. and Loeb, S. (1978). "Internal polarization in the porous substructure of a semipermeable membrane under pressure retarded osmosis", Journal of Membrane Science, **4**(2), 261-265.

Mi, B.X. and Elimelech, M. (2010). "Gypsum scaling and cleaning in forward osmosis: measurements and mechanisms", Environmental Science & Technology, **44**(6), 2022-2028.

Miao, X.L. and Wu, Q.Y. (2006). "Biodiesel production from heterotrophic microalgal oil", Bioresource Technology, **97**(6), 841-846.

Michaels, A.S. (1980). "Analysis and prediction of sieving curves for ultrafiltration membranes - a universal correlation? ", Separation Science and Technology, **15**(6), 1305-1322.

Montgomery, M.A. and Elimelech, M. (2007). "Water and sanitation in developing countries: Including health in the equation", Environmental Science & Technology, **41**(1), 17-24.

Moody, C.D. and Kessler, J.O. (1976). "Foward osmosis extractors ", Desalination, **18**(3), 283-295.

Mulder, M. 1996. Basic principles of membrane technology. Springer Science & Business Media.

Nayak, C.A. and Rastogi, N.K. (2010). "Forward osmosis for the concentration of anthocyanin from Garcinia indica Choisy", Separation and Purification Technology, **71**(2), 144-151.

Nguyen, A., Azari, S. and Zou, L.D. (2013). "Coating zwitterionic amino acid L-DOPA to increase fouling resistance of forward osmosis membrane", Desalination, **312**, 82-87.

Niksefat, N., Jahanshahi, M. and Rahimpour, A. (2014). "The effect of SiO_2 nanoparticles on morphology and performance of thin film composite membranes for forward osmosis application", Desalination, **343**, 140-146.

Norberg, D., Hong, S., Taylor, J. and Zhao, Y. (2007). "Surface characterization and performance evaluation of commercial fouling resistant low-pressure RO membranes", Desalination, **202**(1-3), 45-52.

Novoselov, K.S., Jiang, D., Schedin, F., Booth, T.J., Khotkevich, V.V., Morozov, S.V. and Geim, A.K. (2005). "Two-dimensional atomic crystals", Proceedings of the National Academy of Sciences of the United States of America, **102**(30), 10451-10453.

Nunes, S.P., Sforca, M.L. and Peinemann, K.V. (1995). "Dense hydrophilic composite membranes for ultrafiltration", Journal of Membrane Science, **106**(1-2), 49-56.

Ong, R.C., Chung, T.S., de Wit, J.S. and Helmer, B.J. (2015). "Novel cellulose ester substrates for high performance flat-sheet thin-film composite (TFC) forward osmosis (FO) membranes", Journal of Membrane Science, **473**, 63-71.

Ostuni, E., Chapman, R.G., Holmlin, R.E., Takayama, S. and Whitesides, G.M. (2001). "A survey of structure-property relationships of surfaces that resist the adsorption of protein", Langmuir, **17**(18), 5605-5620.

Parisi, M., Dorr, R.A., Ozu, M. and Toriano, R. (2007). "From membrane pores to aquaporins: 50 years measuring water fluxes", Journal of Biological Physics, **33**(5-6), 331-343.

Park, M.J., Phuntsho, S., He, T., Nisola, G.M., Tijing, L.D., Li, X.M., Chen, G., Chung, W.J. and Shon, H.K. (2015). "Graphene oxide incorporated polysulfone substrate for the fabrication of flat-sheet thin-film composite forward osmosis membranes", Journal of Membrane Science, **493**, 496-507.

Parsegian, V.A., Rand, R.P. and Rau, D.C. (2000). "Osmotic stress, crowding, preferential hydration, and binding: A comparison of perspectives", Proceedings of the National Academy of Sciences of the United States of America, **97**(8), 3987-3992.

Pattle, R.E. (1954). "Production of electric power by mixing fresh and salt water in hydroelectric pile ", Nature, **174**(4431), 660-660.

Peng, F.B., Huang, X.F., Jawor, A. and Hoek, E.M.V. (2010). "Transport, structural, and interfacial properties of poly (vinyl alcohol)-polysulfone composite nanofiltration membranes", Journal of Membrane Science, **353**(1-2), 169-176.

Peng, F.B., Jiang, Z.Y. and Hoek, E.M.V. (2011). "Tuning the molecular structure, separation performance and interfacial properties of poly(vinyl alcohol)-polysulfone interfacial composite membranes", Journal of Membrane Science, **368**(1-2), 26-33.

Petrotos, K.B. and Lazarides, H.N. (2001). "Osmotic concentration of liquid foods", Journal of Food Engineering, **49**(2-3), 201-206.

Petrotos, K.B., Tsiadi, A.V., Poirazis, E., Papadopoulos, D., Petropakis, H. and Gkoutsidis, P. (2010). "A description of a flat geometry direct osmotic concentrator to concentrate tomato juice at ambient temperature and low pressure", Journal of Food Engineering, **97**(2), 235-242.

Phillip, W.A., Yong, J.S. and Elimelech, M. (2010). "Reverse draw solute permeation in forward osmosis: modeling and experiments", Environmental Science & Technology, **44**(13), 5170-5176.

Phuntsho, S., Shon, H.K., Hong, S., Lee, S. and Vigneswaran, S. (2011). "A novel low energy fertilizer driven forward osmosis desalination for direct fertigation: Evaluating the performance of fertilizer draw solutions", Journal of Membrane Science, **375**(1-2), 172-181.

Post, J.W., Veerman, J., Hamelers, H.V.M., Euverink, G.J.W., Metz, S.J., Nymeijer, K. and Buisman, C.J.N. (2007). "Salinity-gradient power: Evaluation of pressure-retarded osmosis and reverse electrodialysis", Journal of Membrane Science, **288**(1-2), 218-230.

Puguan, J.M.C., Kim, H.S., Lee, K.J. and Kim, H. (2014). "Low internal concentration polarization in forward osmosis membranes with hydrophilic crosslinked PVA nanofibers as porous support layer", Desalination, **336**, 24-31.

Qi, S.R., Qiu, C.Q. and Tang, C.Y.Y. (2011). "Synthesis and characterization of novel forward osmosis membranes based on layer-by-layer assembly", Environmental Science & Technology, **45**(12), 5201-5208.

Qi, S.R., Li, W.Y., Zhao, Y., Ma, N., Wei, J., Chin, T.W. and Tang, C.Y.Y. (2012). "Influence of the properties of layer-by-layer active layers on forward osmosis

performance", Journal of Membrane Science, **423**, 536-542.

Qin, J.J., Oo, M.H., Kekre, K.A. and Liberman, B. (2010). "Development of novel backwash cleaning technique for reverse osmosis in reclamation of secondary effluent", Journal of Membrane Science, **346**(1), 8-14.

Qiu, C.Q., Qi, S.R. and Tang, C.Y.Y. (2011). "Synthesis of high flux forward osmosis membranes by chemically crosslinked layer-by-layer polyelectrolytes", Journal of Membrane Science, **381**(1-2), 74-80.

Qiu, S., Wu, L.G., Pan, X.J., Zhang, L., Chen, H.L. and Gao, C.J. (2009). "Preparation and properties of functionalized carbon nanotube/PSF blend ultrafiltration membranes", Journal of Membrane Science, **342**(1-2), 165-172.

Ramon, G., Agnon, Y. and Dosoretz, C. (2010). "Dynamics of an osmotic backwash cycle", Journal of Membrane Science, **364**(1-2), 157-166.

Rosenhahn, A., Schilp, S., Kreuzer, H.J. and Grunze, M. (2010). "The role of "inert" surface chemistry in marine biofouling prevention", Physical Chemistry Chemical Physics, **12**(17), 4275-4286.

Sagiv, A. and Semiat, R. (2005). "Backwash of RO spiral wound membranes", Desalination, **179**(1-3), 1-9.

Sairam, M., Sereewatthanawut, E., Li, K., Bismarck, A. and Livingston, A.G. (2011). "Method for the preparation of cellulose acetate flat sheet composite membranes for forward osmosis-Desalination using MgSO4 draw solution", Desalination, **273**(2-3), 299-307.

Sareen, R., Jain, N. and Kumar, D. (2012). "An Insight to Osmotic Drug Delivery", Current Drug Delivery, **9**(3), 285-296.

Sarkar, A., Carver, P.I., Zhang, T., Merrington, A., Bruza, K.J., Rousseau, J.L., Keinath, S.E. and Dvornic, P.R. (2010). "Dendrimer-based coatings for surface modification of polyamide reverse osmosis membranes", Journal of Membrane Science, **349**(1-2), 421-428.

Schiermeier, Q. (2008a). "Water: A long dry summer", Nature, **452**(7185), 270-273.

Schiermeier, Q. (2008b). "Purification with a pinch of salt", Nature, **452**(7185), 260-261.

Segal, M. (2009). "Selling graphene by the ton", Nature Nanotechnology, **4**(10), 611-613.

Seidel, A. and Elimelech, M. (2002). "Coupling between chemical and physical interactions in natural organic matter (NOM) fouling of nanofiltration membranes: implications for fouling control", Journal of Membrane Science, **203**(1-2), 245-255.

Service, R.F. (2006). "Desalination freshens up", Science, **313**(5790), 1088-1090.

Setiawan, L., Wang, R., Li, K. and Fane, A.G. (2011). "Fabrication of novel

poly(amide-imide) forward osmosis hollow fiber membranes with a positively charged nanofiltration-like selective layer", Journal of Membrane Science, **369**(1-2), 196-205.

Setiawan, L., Wang, R., Tan, S.H., Shi, L. and Fane, A.G. (2013). "Fabrication of poly(amide-imide)-polyethersulfone dual layer hollow fiber membranes applied in forward osmosis by combined polyelectrolyte cross-linking and depositions", Desalination, **312**, 99-106.

Shaffer, D.L., Werber, J.R., Jaramillo, H., Lin, S.H. and Elimelech, M. (2015). "Forward osmosis: Where are we now?", Desalination, **356**, 271-284.

Shannon, M.A., Bohn, P.W., Elimelech, M., Georgiadis, J.G., Marinas, B.J. and Mayes, A.M. (2008). "Science and technology for water purification in the coming decades", Nature, **452**(7185), 301-310.

She, Q.H., Wang, R., Fane, A.G. and Tang, C.Y.Y. (2016). "Membrane fouling in osmotically driven membrane processes: A review", Journal of Membrane Science, **499**, 201-233.

Shen, Y.X., Zhao, W.T., Xiao, K. and Huang, X. (2010). "A systematic insight into fouling propensity of soluble microbial products in membrane bioreactors based on hydrophobic interaction and size exclusion", Journal of Membrane Science, **346**(1), 187-193.

Singer, E. (2004). "New technologies deliver in treating neurological diseases", Nature Medicine, **10**(12), 1267-1267.

Singh, S., Khulbe, K.C., Matsuura, T. and Ramamurthy, P. (1998). "Membrane characterization by solute transport and atomic force microscopy", Journal of Membrane Science, **142**(1), 111-127.

Skilhagen, S.E., Dugstad, J.E. and Aaberg, R.J. (2008). "Osmotic power - power production based on the osmotic pressure difference between waters with varying salt gradients", Desalination, **220**(1-3), 476-482.

Slaughter, B.V., Khurshid, S.S., Fisher, O.Z., Khademhosseini, A. and Peppas, N.A. (2009). "Hydrogels in regenerative medicine", Advanced Materials, **21**(32-33), 3307-3329.

Song, X.X., Liu, Z.Y. and Sun, D.D. (2011). "Nano gives the answer: breaking the bottleneck of internal concentration polarization with a nanofiber composite forward osmosis membrane for a high water production rate", Advanced Materials, **23**(29), 3256-2260.

Song, X.X., Liu, Z.Y. and Sun, D.D. (2013). "Energy recovery from concentrated seawater brine by thin-film nanofiber composite pressure retarded osmosis membranes with high power density", Energy & Environmental Science, **6**(4), 1199-1210.

Straub, A.P., Deshmukh, A. and Elimelech, M. (2016). "Pressure-retarded osmosis for power generation from salinity gradients: is it viable?", Energy & Environmental Science, **9**(1), 31-48.

Su, J.C., Yang, Q., Teo, J.F. and Chung, T.S. (2010). "Cellulose acetate nanofiltration hollow fiber membranes for forward osmosis processes", Journal of Membrane Science, **355**(1-2), 36-44.

Su, J.C., Chung, T.S., Helmer, B.J. and de Wit, J.S. (2012). "Enhanced double-skinned FO membranes with inner dense layer for wastewater treatment and macromolecule recycle using Sucrose as draw solute", Journal of Membrane Science, **396**, 92-100.

Su, Y.C., Lin, L.W. and Pisano, A.P. (2002). "A water-powered osmotic microactuator", Journal of Microelectromechanical Systems, **11**(6), 736-742.

Subramani, A., Badruzzaman, M., Oppenheimer, J. and Jacangelo, J.G. (2011). "Energy minimization strategies and renewable energy utilization for desalination: A review", Water Research, **45**(5), 1907-1920.

Sukitpaneenit, P. and Chung, T.S. (2012). "High performance thin-film composite forward osmosis hollow fiber membranes with macrovoid-free and highly porous structure for sustainable water production", Environmental Science & Technology, **46**(13), 7358-7365.

Tan, C.H. and Ng, H.Y. (2010). "A novel hybrid forward osmosis - nanofiltration (FO-NF) process for seawater desalination: Draw solution selection and system configuration", Desalination and Water Treatment, **13**(1-3), 356-361.

Tang, C.Y.Y., She, Q.H., Lay, W.C.L., Wang, R. and Fane, A.G. (2010). "Coupled effects of internal concentration polarization and fouling on flux behavior of forward osmosis membranes during humic acid filtration", Journal of Membrane Science, **354**(1-2), 123-133.

Tang, W.L. and Ng, H.Y. (2008). "Concentration of brine by forward osmosis: Performance and influence of membrane structure", Desalination, **224**(1-3), 143-153.

Tian, E.L., Zhou, H., Ren, Y.W., Mirza, Z.A., Wang, X.Z. and Xiong, S.W. (2014). "Novel design of hydrophobic/hydrophilic interpenetrating network composite nanofibers for the support layer of forward osmosis membrane", Desalination, **347**, 207-214.

Tiraferri, A., Yip, N.Y., Phillip, W.A., Schiffman, J.D. and Elimelech, M. (2011). "Relating performance of thin-film composite forward osmosis membranes to support layer formation and structure", Journal of Membrane Science, **367**(1-2), 340-352.

Tiraferri, A., Kang, Y., Giannelis, E.P. and Elimelech, M. (2012). "Superhydrophilic thin-film composite forward osmosis membranes for organic fouling control: fouling behavior and antifouling mechanisms", Environmental Science & Technology, **46**(20), 11135-11144.

Ulbricht, M. and Riedel, M. (1998). "Ultrafiltration membrane surfaces with grafted polymer 'tentacles': preparation, characterization and application for covalent protein binding", Biomaterials, **19**(14), 1229-1237.

United Nations World Water Assessment Program. 2003. The world water development report 1: water for People, water for Life, UNESCO: Paris, France.

Vaisocherova, H., Yang, W., Zhang, Z., Cao, Z.Q., Cheng, G., Piliarik, M., Homola, J. and Jiang, S.Y. (2008). "Ultralow fouling and functionalizable surface chemistry based on a zwitterionic polymer enabling sensitive and specific protein detection in undiluted blood plasma", Analytical Chemistry, **80**(20), 7894-7901.

van't Hoff, J.H. (1995). "The role of osmotic-pressure in the analogy between solutions and gases (reprinted from zeitschrift für physikalische chemie, vol 1, page 481, 1887)", Journal of Membrane Science, **100**(1), 39-44.

van de Witte, P., Dijkstra, P.J., van den Berg, J.W.A. and Feijen, J. (1996). "Phase separation processes in polymer solutions in relation to membrane formation", Journal of Membrane Science, **117**(1-2), 1-31.

Verma, R.K., Mishra, B. and Garg, S. (2000). "Osmotically controlled oral drug delivery", Drug Development and Industrial Pharmacy, **26**(7), 695-708.

Verma, R.K., Krishna, D.M. and Garg, S. (2002). "Formulation aspects in the development of osmotically controlled oral drug delivery systems", Journal of Controlled Release, **79**(1-3), 7-27.

Visvanathan, C., Ben Aim, R. and Parameshwaran, K. (2000). "Membrane separation bioreactors for wastewater treatment", Critical Reviews in Environmental Science and Technology, **30**(1), 1-48.

Vrijenhoek, E.M., Hong, S. and Elimelech, M. (2001). "Influence of membrane surface properties on initial rate of colloidal fouling of reverse osmosis and nanofiltration membranes", Journal of Membrane Science, **188**(1), 115-128.

Wang, B. and Lai, Z.P. (2012). "Finger-like voids induced by viscous fingering during phase inversion of alumina/PES/NMP suspensions", Journal of Membrane Science, **405**, 275-283.

Wang, H.L., Chung, T.S. and Tong, Y.W. (2013). "Study on water transport through a mechanically robust Aquaporin Z biomimetic membrane", Journal of Membrane Science, **445**, 47-52.

Wang, K.Y., Yang, Q., Chung, T.S. and Rajagopalan, R. (2009). "Enhanced forward osmosis from chemically modified polybenzimidazole (PBI) nanofiltration hollow fiber membranes with a thin wall", Chemical Engineering Science, **64**(7), 1577-1584.

Wang, K.Y., Ong, R.C. and Chung, T.S. (2010a). "Double-skinned forward osmosis membranes for reducing internal concentration polarization within the porous sublayer", Industrial & Engineering Chemistry Research, **49**(10), 4824-4831.

Wang, K.Y., Teoh, M.M., Nugroho, A. and Chung, T.S. (2011). "Integrated forward osmosis-membrane distillation (FO-MD) hybrid system for the concentration of protein solutions", Chemical Engineering Science, **66**(11), 2421-2430.

Wang, K.Y., Chung, T.S. and Amy, G. (2012a). "Developing thin-film-composite forward osmosis membranes on the PES/SPSf substrate through interfacial polymerization", Aiche Journal, **58**(3), 770-781.

Wang, R., Shi, L., Tang, C.Y.Y., Chou, S.R., Qiu, C. and Fane, A.G. (2010b). "Characterization of novel forward osmosis hollow fiber membranes", Journal of Membrane Science, **355**(1-2), 158-167.

Wang, X.H., Chang, V.W.C. and Tang, C.Y.Y. (2016). "Osmotic membrane bioreactor (OMBR) technology for wastewater treatment and reclamation: Advances, challenges, and prospects for the future", Journal of Membrane Science, **504**, 113-132.

Wang, Y.Q., Ou, R.W., Wang, H.T. and Xu, T.W. (2015). "Graphene oxide modified graphitic carbon nitride as a modifier for thin film composite forward osmosis membrane", Journal of Membrane Science, **475**, 281-289.

Wang, Z.H., Yu, H.R., Xia, J.F., Zhang, F.F., Li, F., Xia, Y.Z. and Li, Y.H. (2012b). "Novel GO-blended PVDF ultrafiltration membranes", Desalination, **299**, 50-54.

Wei, J., Qiu, C.Q., Tang, C.Y.Y., Wang, R. and Fane, A.G. (2011). "Synthesis and characterization of flat-sheet thin film composite forward osmosis membranes", Journal of Membrane Science, **372**(1-2), 292-302.

Wei, Y.M., Xu, Z.L., Qusay, F.A. and Wu, K. (2005). "Polvvinvl alcohol/polysulfone (PVA/PSF) hollow fiber composite membranes for pervaporation separation of ethanol/water solution", Journal of Applied Polymer Science, **98**(1), 247-254.

Wei, Y.S., Van Houten, R.T., Borger, A.R., Eikelboom, D.H. and Fan, Y.B. (2003). "Minimization of excess sludge production for biological wastewater treatment", Water Research, **37**(18), 4453-4467.

Weis, C., Odermatt, E.K., Kressler, J., Funke, Z., Wehner, T. and Freytag, D. (2004). "Poly(vinyl alcohol) membranes for adhesion prevention", Journal of Biomedical Materials Research Part B-Applied Biomaterials, **70B**(2), 191-202.

Werner, C.M., Logan, B.E., Saikaly, P.E. and Amy, G.L. (2013). "Wastewater treatment, energy recovery and desalination using a forward osmosis membrane in an air-cathode microbial osmotic fuel cell", Journal of Membrane Science, **428**, 116-122.

Widjojo, N., Chung, T.S., Weber, M., Maletzko, C. and Warzelhan, V. (2011). "The role of sulphonated polymer and macrovoid-free structure in the support layer for thin-film composite (TFC) forward osmosis (FO) membranes", Journal of Membrane Science, **383**(1-2), 214-223.

Wilbert, M.C., Pellegrino, J. and Zydney, A. (1998). "Bench-scale testing of surfactant-modified reverse osmosis/nanofiltration membranes", Desalination, **115**(1), 15-32.

Wiley, P.E., Campbell, J.E. and McKuin, B. (2011). "Production of biodiesel and biogas from algae: a review of process train options", Water Environment Research, **83**(4), 326-338.

Wilson, A.D. and Stewart, F.F. (2013). "Deriving osmotic pressures of draw solutes used in osmotically driven membrane processes", Journal of Membrane Science, **431**, 205-211.

Wrolstad, R.E., McDaniel, M.R., Durst, R.W., Micheals, N., Lampi, K.A. and Beaudry, E.G. (1993). "Composition and sensory characterization of red raspberry juice concentrated by direct osmosis or evaporation ", Journal of Food Science, **58**(3), 633-637.

Xiao, D.Z., Tang, C.Y.Y., Zhang, J.S., Lay, W.C.L., Wang, R. and Fane, A.G. (2011). "Modeling salt accumulation in osmotic membrane bioreactors: Implications for FO membrane selection and system operation", Journal of Membrane Science, **366**(1-2), 314-324.

Xu, G.R., Wang, J.N. and Li, C.J. (2013). "Strategies for improving the performance of the polyamide thin film composite (PA-TFC) reverse osmosis (RO) membranes: Surface modifications and nanoparticles incorporations", Desalination, **328**, 83-100.

Xu, Z.W., Zhang, J.G., Shan, M.J., Li, Y.L., Li, B.D., Niu, J.R., Zhou, B.M. and Qian, X.M. (2014). "Organosilane-functionalized graphene oxide for enhanced antifouling and mechanical properties of polyvinylidene fluoride ultrafiltration membranes", Journal of Membrane Science, **458**, 1-13.

Xue, Z.X., Wang, S.T., Lin, L., Chen, L., Liu, M.J., Feng, L. and Jiang, L. (2011). "A novel superhydrophilic and underwater superoleophobic hydrogel-coated mesh for oil/water separation", Advanced Materials, **23**(37), 4270-4273.

Yamagiwa, K., Kobayashi, H., Ohkawa, A. and Onodera, M. (1993). "Membrane fouling in ultrafiltration of hydrophobic nonionic surfactant", Journal of Chemical Engineering of Japan, **26**(1), 13-18.

Yang, Q., Wang, K.Y. and Chung, T.S. (2009a). "Dual-layer hollow fibers with enhanced flux as novel forward osmosis membranes for water production", Environmental Science & Technology, **43**(8), 2800-2805.

Yang, Q., Wang, K.Y. and Chung, T.S. (2009b). "A novel dual-layer forward osmosis membrane for protein enrichment and concentration", Separation and Purification Technology, **69**(3), 269-274.

Yang, Q., Lei, J., Sun, D.D. and Chen, D. (2016). "Forward Osmosis Membranes for Water Reclamation", Separation and Purification Reviews, **45**(2), 93-107.

Yangali-Quintanilla, V., Li, Z.Y., Valladares, R., Li, Q.Y. and Amy, G. (2011). "Indirect desalination of Red Sea water with forward osmosis and low pressure reverse osmosis for water reuse", Desalination, **280**(1-3), 160-166.

Yap, W.J., Zhang, J.S., Lay, W.C.L., Cao, B., Fane, A.G. and Liu, Y. (2012). "State of the art of osmotic membrane bioreactors for water reclamation", Bioresource Technology, **122**, 217-222.

Yasukawa, M., Mishima, S., Shibuya, M., Saeki, D., Takahashi, T., Miyoshi, T. and Matsuyama, H. (2015). "Preparation of a forward osmosis membrane using a highly porous polyketone microfiltration membrane as a novel support", Journal of Membrane Science, **487**, 51-59.

Yen, S.K., Haja, F.M., Su, M.L., Wang, K.Y. and Chung, T.S. (2010). "Study of draw

solutes using 2-methylimidazole-based compounds in forward osmosis", Journal of Membrane Science, **364**(1-2), 242-252.

Yip, N.Y., Tiraferri, A., Phillip, W.A., Schiffman, J.D. and Elimelech, M. (2010). "High performance thin-film composite forward osmosis membrane", Environmental Science & Technology, **44**(10), 3812-3818.

Yip, N.Y., Tiraferri, A., Phillip, W.A., Schiffrnan, J.D., Hoover, L.A., Kim, Y.C. and Elimelech, M. (2011). "Thin-film composite pressure retarded osmosis membranes for sustainable power generation from salinity gradients", Environmental Science & Technology, **45**(10), 4360-4369.

Yokozeki, A. (2006). "Osmotic pressures studied using a simple equation-of-state and its applications", Applied Energy, **83**(1), 15-41.

York, R., Thiel, R. and Beaudry, E. 1999. Full-scale experience of direct osmosis concentration applied to leachate management. *Proceedings of the Seventh International Waste Management and Landfill Symposium (Sardinia'99), S. Margherita di Pula, Cagliari, Sardinia, Italy*.

Yu, H.Y., Xie, Y., Hu, M.X., Wang, J.L., Wang, S.Y. and Xu, Z.K. (2005). "Surface modification of polypropylene microporous membrane to improve its antifouling property in MBR: CO_2 plasma treatment", Journal of Membrane Science, **254**(1-2), 219-227.

Yu, H.Y., Kang, Y., Liu, Y.L. and Mi, B.X. (2014). "Grafting polyzwitterions onto polyamide by click chemistry and nucleophilic substitution on nitrogen: A novel approach to enhance membrane fouling resistance", Journal of Membrane Science, **449**, 50-57.

Zeman, L.J. and Zydney, A.L. 1996. Microfiltration and ultrafiltration: principles and applications. M. Dekker.

Zeng, J.W. and Guo, Z.G. (2014). "Superhydrophilic and underwater superoleophobic MFI zeolite-coated film for oil/water separation", Colloids and Surfaces a-Physicochemical and Engineering Aspects, **444**, 283-288.

Zhang, C.H., Yang, F.L., Wang, W.J. and Chen, B. (2008). "Preparation and characterization of hydrophilic modification of polypropylene non-woven fabric by dip-coating PVA (polyvinyl alcohol)", Separation and Purification Technology, **61**(3), 276-286.

Zhang, F., Brastad, K.S. and He, Z. (2011). "Integrating forward osmosis into microbial fuel cells for wastewater treatment, water extraction and bioelectricity generation", Environmental Science & Technology, **45**(15), 6690-6696.

Zhang, F., Zhang, W.B., Shi, Z., Wang, D., Jin, J. and Jiang, L. (2013). "Nanowire-haired inorganic membranes with superhydrophilicity and underwater ultralow adhesive superoleophobicity for high-efficiency oil/water separation", Advanced Materials, **25**(30), 4192-4198.

Zhang, H.M., Ma, Y.J., Jiang, T., Zhang, G.Y. and Yang, F.L. (2012a). "Influence of

activated sludge properties on flux behavior in osmosis membrane bioreactor (OMBR)", Journal of Membrane Science, **390**, 270-276.

Zhang, J.S., Loong, W.L.C., Chou, S.R., Tang, C.Y., Wang, R. and Fane, A.G. (2012b). "Membrane biofouling and scaling in forward osmosis membrane bioreactor", Journal of Membrane Science, **403**, 8-14.

Zhang, S., Wang, K.Y., Chung, T.S., Chen, H.M., Jean, Y.C. and Amy, G. (2010). "Well-constructed cellulose acetate membranes for forward osmosis: Minimized internal concentration polarization with an ultra-thin selective layer", Journal of Membrane Science, **360**(1-2), 522-535.

Zhang, W.B., Zhu, Y.Z., Liu, X., Wang, D., Li, J.Y., Jiang, L. and Jin, J. (2014). "Salt-induced fabrication of superhydrophilic and underwater superoleophobic PAA-g-PVDF membranes for effective separation of oil-in-water emulsions", Angewandte Chemie-International Edition, **53**(3), 856-860.

Zhao, H.Y., Wu, L.G., Zhou, Z.J., Zhang, L. and Chen, H.L. (2013). "Improving the antifouling property of polysulfone ultrafiltration membrane by incorporation of isocyanate-treated graphene oxide", Physical Chemistry Chemical Physics, **15**(23), 9084-9092.

Zhao, S.A.F. and Zou, L.D. (2011). "Relating solution physicochemical properties to internal concentration polarization in forward osmosis", Journal of Membrane Science, **379**(1-2), 459-467.

Zhao, S.F., Zou, L.D. and Mulcahy, D. (2012). "Brackish water desalination by a hybrid forward osmosis-nanofiltration system using divalent draw solute", Desalination, **284**, 175-181.

Zhao, Y.H., Wee, K.H. and Bai, R. (2010). "Highly hydrophilic and low-protein-fouling polypropylene membrane prepared by surface modification with sulfobetaine-based zwitterionic polymer through a combined surface polymerization method", Journal of Membrane Science, **362**(1-2), 326-333.

Zhu, H.T., Zhang, L.Q., Wen, X.H. and Huang, X. (2012). "Feasibility of applying forward osmosis to the simultaneous thickening, digestion, and direct dewatering of waste activated sludge", Bioresource Technology, **113**, 207-213.

Zhu, X.H. and Elimelech, M. (1997). "Colloidal fouling of reverse osmosis membranes: measurements and fouling mechanisms", Environmental Science & Technology, **31**(12), 3654-3662.

Zhu, Y.W., Murali, S., Cai, W.W., Li, X.S., Suk, J.W., Potts, J.R. and Ruoff, R.S. (2010). "Graphene and graphene oxide: synthesis, properties, and applications", Advanced Materials, **22**(35), 3906-3924.

Zinadini, S., Zinatizadeh, A.A., Rahimi, M., Vatanpour, V. and Zangeneh, H. (2014). "Preparation of a novel antifouling mixed matrix PES membrane by embedding graphene oxide nanoplates", Journal of Membrane Science, **453**, 292-301.

Zou, L., Vidalis, I., Steele, D., Michelmore, A., Low, S.P. and Verberk, J. (2011).

"Surface hydrophilic modification of RO membranes by plasma polymerization for low organic fouling", Journal of Membrane Science, **369**(1-2), 420-428.

Zou, S., Wang, Y.N., Wicaksana, F., Aung, T., Wong, P.C.Y., Fane, A.G. and Tang, C.Y. (2013). "Direct microscopic observation of forward osmosis membrane fouling by microalgae: Critical flux and the role of operational conditions", Journal of Membrane Science, **436**, 174-185.